Electrochemical Composite Membranes based on Intrinsically Conducting Polymers

Synthesis and Characterization

Asif Ali Qaiser

A thesis submitted in fulfilment of the requirements for the degree of Doctor of Philosophy in Engineering, The University of Auckland, 2010.

Abstract

Membranes based on intrinsically conducting polymers (ICPs) have been employed in various membrane processes such as gas separation, pervaporation, nanofiltration and electrodialysis. The change in the membrane morphology, hydrophilicity, and ion exchange behaviour based on the oxidation state and doping levels of ICP have been used to enhance permeability and selectivity. In this thesis, a highly permeable membrane with high selectivity was developed by depositing polyaniline (PANI) on the pore walls of a microporous base membrane without blocking the pores. The layering of positively charged polyaniline originates electrolyte polarisation in the pores and permselectivity is achieved by the electrostatic screening of permeating ions through the membrane.

Polyaniline (PANI) was deposited on mixed-cellulose ester (ME) microporous membranes by using various in situ chemical oxidative polymerization techniques. These include solution-phase polymerization, vapour-phase polymerization and diaphragmatic polymerization in a two-compartment cell. The composite membranes were characterized by scanning electron microscopy (SEM), gravimetric PANI content measurement, Fourier-transform infrared (FTIR-ATR) spectroscopy and x-ray photoelectron spectroscopy (XPS). The solution-phase and vapour-phase polymerizations yielded PANI layering on the surface of the base membrane whereas PANI was deposited on the pore walls of the membrane by using the two-compartment cell technique. FTIR and XPS results showed PANI deposition in its emeraldine salt state and Cl^- doping was polymerization time dependent. XPS quantified the extent of PANI layering at the surface that was polymerization time dependent. The solution-phase polymerization yielded an incomplete surface layering as compared to the vapour-phase polymerization. Surface and trans-membrane electrical conductivities were measured by using four-point micro probe and two- point probe techniques, respectively. These conductivities showed dependence on PANI deposition site and extent in the membranes.

Electrochemical characterization of the composite membranes was conducted by using electrochemical impedance spectroscopy (EIS) and transport numbers measurements. EIS data were analysed by using equivalent circuit modelling technique. The results showed the dependence of charge transport resistance of the membranes on PANI deposition site, extent and doping levels. In-pore PANI deposition in the membranes showed several orders of magnitude lower levels of resistance and higher capacitance due to the polarisation of pore electrolyte. In addition, the low values of diffusional resistance and high capacitance indicate

anion-coupled charge transport in the membrane through PANI polaron/bipolaron transitions. The composite membranes with PANI layering only at the surface or undoped PANI showed higher diffusional resistance and low capacitance due to slow electronic/ionic diffusion inside the bulk membrane.

Transport numbers of counter-ions in the composite membranes showed high anion selectivity at low pH (in HCl) as compared to the membranes at high pH (~12). The transport numbers showed the weak dependence on PANI deposition site and levels.

Acknowledgements

I would like to express my special gratitude to Associate Professor Margaret Hyland, my main supervisor, for her guidance, support and encouragement during my PhD studies at the University. In fact, she always has been accommodative to me in spite of her busy schedules and facilitated my work and living here in every aspect. I am also thankful to Dr. Darrell Patterson, my co-supervisor for his time-to-time discussions and evaluation of my work. His appreciation always remained a source of encouragement to me. I am also thankful to Associate Professor Allen Easteal and Neil Edmonds for providing me the electrochemical testing facilities at the Tamaki campus. The discussions with Allen Easteal also contributed towards my better understanding of the conducting polymers.

I want to thank Michael Wadsworth (Chemistry) and his team for the fabrication of the two-compartment permeation cells. Many thanks go to Catherine Hobbis for her help in SEM, Dr. Colin Doyle for XPS analysis and Michel Nieuwoudt (Chemistry) for FTIR spectroscopy. I would like to specially acknowledge the help of Stephen Cawley (CACM) in the electrochemical characterizations of the membranes.

I applaud the patience and cooperation of my wife and the kids (Abeeha, Abdullah and Saad) during my tough PhD schedules; indeed they have been a wonderful source of inspiration for me. At the last but not the least, my parents, whose sincere wishes and prayers always paved the way to success in my life.

Table of Contents

List of Figures

List of Tables

List of Abbreviations and Symbols

$\hat{V}$, Î	phasor representation of voltage and current, respectively.
A^-	doping anion
a	activity coefficient
A	area
A^o	angstrom
ac	alternating current
APS	ammonium persulphate
asym.	asymmetric
At.	Atomic
BE	binding energy
c	concentration
C	capacitance
CA	cellulose acetate
C_d	double layer capacitance
cm	centimetre
CPE	constant phase element
CPS	counts per second
CSA	camphursulphonic acid
D	diffusion coefficient
d	distance
DBSA	dodecylbenzesulphonic acid
dc	direct current
DMF	dimethylformamide
DMFC	direct methanol fuel cell
e^-	electron

EDS	electron-dispersive-spectroscopy
EIS	electrochemical impedance spectroscopy
EMI	electromagnetic interference
E^o	standard electrode potential
eV	electron volts
f	linear frequency
F	Faraday
FTIT-ATR	fourier -transform infrared-attenuated total reflectance
g	gram
g_{ct}	frequency-dependent charge transfer resistance
h	hour
HIPS	high-impact polystyrene
I	current
i	current
ICP	intrinsically conducting polymer
Im	imaginary
I_o	current amplitude
j	$\sqrt{-1}$
k	conductivity
m-	meta
m	meter
m	milli (10^{-3})
M	mole
ME	mixed-ester membrane
MF	microfiltration
min	minutes
min	minutes
MWCO	molecular weight cut off
NC	nitrocellulose

NF	nanofiltration
NHE	neutral hydrogen electrode
nm	nanometer
NMP	N-methylpyrrolidone
o-	ortho
OSN	organic solvent nanofiltration
p-	para
P	permeability
P(%)	percentage permselectivity
PAAc	polyacrylic acid
PAc	polyaceytelene
PANI	polyaniline
PCB	printed circuit board
PE	polyethylene
PEEK	polyether-ether ketone
PEMFC	polymer-electrolyte-membrane-fuel cell
Ph	phenyl
PPY	polypyrrole
PTFE	polytetraflouroethene
pTSA	p-toluenesulphonic acid
PV	pervaporation
PVA	polyvinyl acetate
PVDF	polyvinyldiflouride
PVTMS	polyvinyl trimethylsilane
q	charge
R	resistance
R_{ct}	charge transfer resistance
Re	real
Redox	reduction-oxidation

r.m.s	root-mean-squared
RO	reverse osmosis
s	seconds
S	siemen
S	solubility
SDS	sodium dodecylsulphate
SEM	scanning electron microscopy
SPEEK	sulphonated polyether-ether ketone
SPEEKK	sulphonated polyether-ether ketone ketone
sym.	symmetric
t	thickness
T	transmittance
$t_{coun,}$ t_{co},	transport number of counter- and co-ion, respectively.
TCPB	three-component polymer blend
THF	tetra-hydrofurane
UF	ultrafiltration
V	volts
V_o	voltage amplitude (volts)
vs.	versus
W	Warburg impedance
wt	weight
X_c	reactance
XPS	x-ray photoelectron spectroscopy
Z	impedance
Z', Z"	real and imaginary component of impedance, respectively.
α	dispersion index
λ	wave length
Ω	resistance
ρ	resistivity

υ	wave number
ϕ	phase angle
φ	potential
ω	angular frequency
χ^2	"chi-square value" for EIS model fitting

Chapter One

Introduction

1.1 Membrane Separation Processes and their Limitations

Separation processes such as distillation, gas separation, liquid-liquid extraction and leaching are the integral part of a process industry where these processes are employed for raw material and product purification. These processes involve phase change and transference of various species across different phases and by virtue of their nature, have inherent phase equilibrium limitations. In addition, these processes are highly energy intensive due to inter-phase conversion e.g., generation of vapour phase in distillation. Membrane based separation processes are comparatively new in the field of separation and have many advantages such as non-equilibrium transference across the phases and involvement of single phase streams in most cases with an efficient energy utilization [1].

Membrane separation processes can be classified based on the retention (rejection) size of the particles (or molecules) in the permeation process [2]. The pressure-driven processes are classified into, by decreasing retention size, microfiltration (MF), ultrafiltration (UF), nanofiltration (NF), reverse osmosis (RO) and pervaporation (PV). Microfiltration membranes are used as pre-filters where suspended solids and long-chain biomolecules are retained by a sieving action [3]. On the lower extreme, reverse osmosis is used to remove dissolved salts from the water whereas short-chain solvent molecules can be separated in pervaporation process. The governing mechanism in these membranes is shifted from size-exclusion in MF, UF and NF to a solution-diffusion process in RO and PV. Size-exclusion phenomenon is based on the sieving effects of the membranes whereas in the solution-diffusion mechanism, separation is achieved by the difference in the solvating tendency of the permeating species in the membrane structure and diffusion rate in the bulk membrane. On the other hand, charged membranes are employed in the processes where separation is achieved by the interaction of permeating species (i.e. electrolyte) with the fixed charges of an ion exchange membrane. Depending on the polarity of the embedded ionic charges in the membrane structure, counter-ions are permeated through the ion exchange membrane whereas electrostatic repulsive force excludes co-ions. Ion exchange based processes include electrodialysis, dialysis and membrane electrolysis. An electric current is applied across the

stack of alternatively arranged cation- and anion exchange membranes in electrodialysis whereas the concentration gradient across an ion exchange membrane acts as the driving force in dialysis. Electrolysis is used in the production of salts and alkalis by an electrochemical decomposition reaction such as in chlor-alkali process.

Permeation flux and selectivity (i.e. preferred permeation of one species over others in a feed mixture) are the major concerns in any membrane based separation process along with the initial fixed capital investment and process economy. The permeation and selectivity are inversely related to each other and usually a trade off is sought to make the process economical [4]. To recover the dissolved salts and molecules from solutions or to separate a mixture of charged or neutral solvent molecules, homogeneous (dense) membranes (pore size < 0.2 nm) are used in NF, RO and PV and in ion exchange membrane based processes [3]. Because of the non-porous and insulating nature of these membranes, either a pressure as high as > 80 bar or high electrical potential (in the case of electrodialysis) has to be employed to get an economical selectivity and permeation rate. In addition, the increased cost of a membrane to withstand high pressures and other capital costs make these processes highly expensive. The development of an asymmetric membrane where a thin dense layer at the surface of a thick microporous support serves as a barrier film lowers the operating pressure by maintaining the high permeation rate. In these membranes, the microporous support contributes to the structural strength of the membrane and the dense surface layer yields selectivity. However, to achieve a thin dense layer is still a technical challenge for membrane scientists. Further, this technique cannot be adopted in ion exchange membranes processes due to significantly lower selectivity of the process [3, 4].

1.2 Application of ICPs in Membrane Separation

Intrinsically conducting polymers (ICPs) are used in membrane separation processes mainly due to their high electrical conductivity, the electrochemical activity and switchability between various oxidation and doping states [5]. Pristine ICP or ICP-modified composite membranes are used in various membrane separation processes such as gas separation, pervaporation and electrochemical-based separation processes [6, 7]. These include films and membranes of pristine PANI and PANI blends with other polymers (e.g. polyimide), polypyrrole and substituted poly(N-methyl)pyrrole, and poly(3-methyl thiophene) specifically for gas separation and pervaporation processes. ICPs assume various oxidation and doping states and each of the oxidation states has a characteristic morphology due to the

absorption or desorption of doping anions. Generally, ICPs have a compact film structure in their lower oxidation state (i.e. reduced state) whereas more 'loose' structures are assigned to the higher oxidation states. This variation in ICP morphology has been used in size-exclusion based gas separation and nanofiltration applications. Pervaporation is based on the solution-diffusion type interaction of permeating species with membrane skeleton. The electrochemical activity of ICPs enhances the solvent-polymer interaction in pervaporation that results in a significant increase in the selectivity. In ion exchange membrane processes, either ion exchange properties of an oxidized/doped ICP or steric hindrance of undoped ICP influences the selectivity and permeation rate of the base membrane. Because of the switchability of ICP in various oxidation states, dynamically controllable permeation membranes are started to be developed where permselectivity (i.e. permeation of an ion relative to other ions of similar polarity) was changed *in situ* by the application of electrical potential [8-10]. In addition, ICPs have also been utilized in non-membrane applications where barrier properties of ICPs play significant role. These applications include ICP coatings for corrosion resistance, chemical, electrochemical and biological sensors, modified electrodes e.g., in fuel cell to enhance the catalytic activity, and responsive packaging [11, 12].

Pristine ICP or ICP composite membranes are synthesized by using various techniques and processes including the processes that are used in conventional membrane synthesis. These techniques include solution blending and subsequent film casting, electrochemical and chemical oxidative polymerization to form a free-standing or electrode-deposited film and *in situ* polymerization on various base membranes [6].

ICPs have many issues that limit their synthesis and application in various fields. These include low solubility in the common solvents and poor mechanical properties. ICPs in their doped oxidized form are insoluble and infusible so processing of ICPs in a free-standing film form is very difficult. Usually ICPs in their undoped form are soluble in various strong solvents from which films can be cast. For example, emeraldine polyaniline (PANI) is soluble in N-methylpyrrolidone (NMP) and films have been cast by either phase inversion or thermal evaporation processes from PANI solutions. As-cast films are brittle in nature with low elongation-to-break values. To overcome the mechanical limitations of pristine ICPs films, blends and composites of ICPs with the conventional polymers have been developed by using various synthesis techniques. These techniques either disperse ICP in the bulk of the other polymer or deposit it at the surface of the template.

In this thesis, Polyaniline (PANI) has been used as the ICP component of the composite membranes due to its high electrical conductivity (up to ~10^2 $S.cm^{-1}$) , doping/undoping cycling by pH change in addition to the redox switchability, good environmental and solution stability and aqueous based clean synthesis chemistry [6, 13-15]. Membrane separation processes are based on the interaction of permeating species with the membrane skeleton and for PANI membranes, it depends on the oxidation and doping states of PANI in the composite membranes. Furthermore, the interaction is physical, chemical and/or electrochemical in nature and depends on the free volume, hydrophilicity, ion exchange behaviour, high H^+ conductivity and solubility (swelling) of PANI in a particular gas (i.e., CO_2) in gas separation, pervaporation and ion exchange applications. However, the dense nature of pristine or PANI composite films reduces the permeation rate in membrane separation processes. To achieve high permeation fluxes, ultrathin PANI films have been deposited on microporous support to form asymmetric membranes which yield high permeability and selectivity in pressure-driven processes such as gas separation and pervaporation [16]. Casting of a defect-free ultrathin PANI film and attachment to the support membrane is a highly challenging process with poor reproducibility. On the other hand, electrochemical polymerization yields defect-free coherent film at the surface of the electrode. The insulating nature of the most support membranes limits the application of electrochemical polymerization at industrial scale along with the poor economy of the process [6, 13].

Microporous membranes are used in pressure-driven filtration of microorganisms and other micro-sized particles based on size-exclusion principle. To develop highly permeable novel membranes, the pore surface of microporous membranes may be functionalized by depositing the functional materials where the permeation of the electrolyte takes place under the influence of induced electrostatic and steric interactions. By this pore functionalization, micro-sized pores affect the permeation of ions flowing through the membrane. The pore functionalization reduces the filtration pressure as compared to that in ultrafiltration and nanofiltration processes with acceptable levels of selectivity and permeability. Various materials such as metal and carbon nanotubules, polymeric dendrites and polyaminoacids have been deposited inside the pores of microporous base membranes [4, 17-25]. These pore-deposited membranes are different from the electrolyte-pore-filled membranes used as the separators in rechargeable batteries [26, 27]. In the latter case, pores of the base membrane are completely filled with an electrolyte (e.g., gel phase) that acts as ion exchange medium

for the mobile ions (e.g. Li^+ ions). Contrary to this, in the former case, either a metal was layered on the pore walls of the base membrane or polymer chains were anchored at the pore surface via single point covalent bonding. This pore functionalization increased the hydrodynamic resistance to the flow of the electrolyte. Gold was deposited as nanotubules inside the pores of microporous polycarbonate membrane by electroless plating process [24]. Switchable cation- or anion exchange behaviour has been studied depending on the polarity of the externally induced charge on the membrane by the application of an electrical potential. Carbon nanotubules were deposited in microporous alumina filter by chemical vapour deposition method yielding carbon nanotubules running throughout the membrane cross section [25]. These tubules were surface-functionalized with carboxylic acid moieties that were hydrolysed depending on pH of the surrounding environment. Due to the anionic charge of the carboxylate ions, these membranes behaved as cation-exchange membranes and solvent (water) passed through in the direction of cations diffusion in electrodialysis. This process is called electroosmotic flow and has been studied as a function of the pH of the electrolyte solution. Responsive membranes were developed by immobilizing polyaminoacids in the pores of microporous cellulose membranes [4, 17, 18]. The base membrane had lamellar porous structure (Figure 1.1) and polyaminoacids were immobilized inside the pores of these membranes. During the permeation studies, the acid chains were dissociated into protons and long-chain anions at high pH that resulted in the development of electrostatic charge and change in the morphology of the polymer chains inside the pores. Permselectivity was achieved due the electrostatic interaction and steric hindrance of the ionized polymeric chains in the pores.

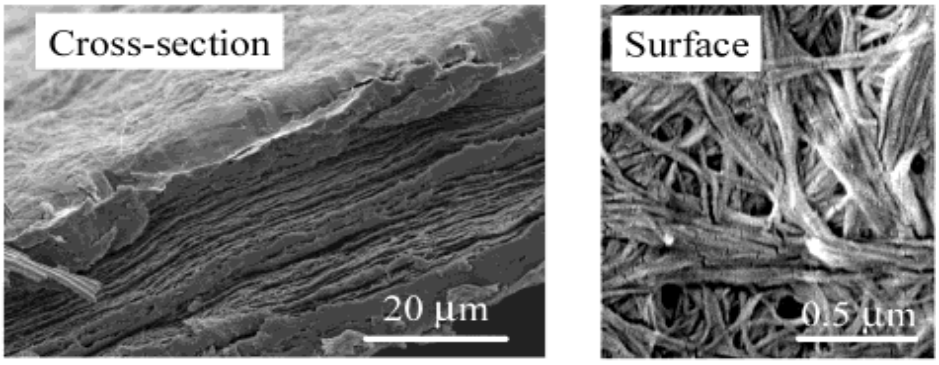

	Pore size (µm)	Thickness (µm)
Cellulosic Support	0.05 – 0.21	127 – 270

Figure 1.1: *Base microporous cellulose membrane for polyaminoacids immobilization [17].*

Microporous base membranes were also modified with ICPs to get the selectivity between different ions at the maximum permeation rate. The ICP was coated on the base microporous support by using various polymerization techniques such as electrochemical and *in situ* chemical polymerization. Polycarbonate microporous membrane was made electrically conductive by sputter-coating gold on the membrane surface and then PANI was coated on the base membrane by electrochemical polymerization of aniline [10]. The reduction of pore size from 1000 nm to 0.1-0.2 nm indicated compact PANI layering at the membrane surface. Electrically controlled permeation studies of electrolytes were conducted by applying direct redox potentials to the membrane that changed the layer morphology upon the oxidation-reduction transition of PANI. Polypyrrole (PPY) and PANI were deposited on the base microporous polyethylene (PE) membrane by *in situ* chemical polymerization of the monomers [19, 20, 28]. PPY was coated by vapour phase polymerization where PE membrane was, initially, soaked in an oxidant ($FeCl_3$) solution and then polymerized with the gaseous pyrrole. PANI was deposited by *in situ* solution phase polymerization by dipping PE membrane in a polymerizing solution of aniline chloride (monomer) and the oxidant (ammonium persulphate). In another study [19], PE membrane was treated, initially, with ethanol to convert it into a hydrophilic film and, subsequently, PANI was deposited by the solution-phase polymerization. The dependence of electronic conductivity on the membrane orientation (surface versus trans-membrane) showed PPY and PANI deposition mainly at the surface with comparatively six to seven orders of magnitude lower trans-membrane conductivity values (e.g., 0.8 $S.cm^{-1}$ at surface versus $1.1x10^{-6}$ $S.cm^{-1}$ trans-membrane conductivity). Electrolytic conductivity studies revealed that improving the hydrophilicity of otherwise hydrophobic PE membranes, increased aqueous electrolyte flow through the membranes. It was concluded that incomplete PANI deposition within the pores of base PE membrane, for the case of initial treatment with ethanol, increased the diffusion coefficients of HCl and NaOH in the composite membranes. Apparently, it can be explained in terms of the swelling of films and improvement in hydrophilicity by ethanol treatment. All these composite membranes have a common structure of ICP layering at the surface of the base microporous membrane [20, 28].

PANI has different film morphologies and ion exchange behaviour depending on its oxidation state and the dopant anion (Please see Figure 2.4 on Page 16). Leucoemeraldine has more compact film morphology as compared to emeraldine salt. Emeraldine in doped form gives rise to an anion exchange character due to the positive charge on its molecular chains

but if doped with a long-chain (immobilized) dopant, PANI behaves as a cation-exchanger. If PANI can be layered on the pore walls of a microporous membrane without complete pore blockage, permeation of electrolyte through the membrane can be controlled by the electrostatic interaction with pore walls. This interaction includes an ion exchange reaction between PANI chains and permeating ions and the development of a kinetic boundary layer in the pores. The electrostatic charge state of PANI within the pores can be changed by doping/undoping of the PANI layers at low and high pH, respectively. In addition to these electrostatic charge based permselectivity control, electroosmotic flow can be affected by the change in the morphology of the deposited PANI layer in the pores depending on the oxidation/reduction state and/ or doping/undoping levels. The challenge to develop an effective porous composite membrane is twofold: depositing ICP on the insulating base membrane to yield electrochemically active composite membrane and controlling the deposition on the pore walls to allow a maximum permeation rate at the reasonably good selectivity.

1.3 Research Objectives and Strategy

The main objective of this thesis is to develop PANI composite membranes for electrochemical based separation processes such as electrodialysis, diffusion dialysis and electro-kinetic based separations. The development involves the synthesis and characterization of the membranes along with the elaboration of electronic and ionic transport characteristics of the membranes. In diffusion dialysis, charge-based separation is achieved under the concentration gradient across the ion exchange membrane whereas electrical potential gradient is applied in electrodialysis. In electro-kinetic based separations, an electrolyte solution flows under an applied electrical potential across a porous charged membrane and the separation is achieved depending upon the electrostatic interaction in the pores of the membrane. In order to get a better permselectivity along with a high permeation rate, PANI deposition inside the pores of base membrane has been targeted in this research. The effects of PANI deposition site and intercalation levels on the conduction mechanism of the composite membranes have been elaborated in order to assess the real advantage of in-pore PANI deposition. Furthermore, because membrane/electrolyte interface plays an important role in electrochemical separation processes, quantification of PANI deposition levels at the surface and its oxidation/doping states was conducted by using x-ray photoelectron spectroscopy (XPS).

This work involves the experimentation and discussion on the following aspects of the synthesis and chemical and electrochemical characterizations of PANI composite membranes.

1. Effects of the various chemical polymerization techniques on PANI deposition site, extent, oxidation state and doping levels on the base microporous membrane.

2. Quantification of PANI deposition extent, oxidation state and doping levels at the membrane surface by using XPS.

3. Characterization of the electronic and ionic transport properties of the composite membranes using various electrochemical techniques such as electrochemical impedance spectroscopy and membrane potentials as a function of the morphology of the composite membranes and PANI doping state.

1.4 Thesis Structure

The thesis discusses synthesis, characterization and testing of PANI composite membranes. Chapter Two includes the characteristic properties of ICPs and their application in various fields based on these properties. Their unique redox chemistry and electrical conduction mechanism have also been elaborated in this chapter. In the last section of the chapter, the literature on PANI based membranes has been extensively reviewed with the focus on the synthesis techniques and resultant membrane performance.

Chapter Three discusses the experimental techniques used for the synthesis and characterization of PANI composite membranes in the present study. A detailed experimental account on membrane synthesis is given with a basic introduction of the employed characterization techniques. The details of the characterization techniques such as x-ray photoelectron spectroscopy and electrochemical impedance spectroscopy are included in the subsequent relevant chapters.

Chapter Four includes results and discussion on the effect of chemical polymerization techniques on PANI deposition in the base membrane. It includes a detailed discussion on the composite membrane morphology as studied by scanning electron microscopy (SEM) and its influence on the various properties of the resultant membranes. Characterization of PANI composite membranes by FTIR-ATR, XPS and electrical conductivity measurement have been discussed in detail.

Chapter Five covers the evaluation of the electrochemical performance of the developed composite membranes. The modelling of the electronic and ionic transport processes of the membranes by using electrochemical impedance spectroscopy (EIS) have been presented. In addition, membrane potential studies have been included.

Chapter Six includes the conclusions of the thesis and potential applications of the developed membranes.

Chapter Two

Intrinsically Conducting Polymers (ICPs) and ICP based Membranes

2.1 Intrinsically Conducting Polymers (ICPs): Properties and Applications

Intrinsically conducting polymers (ICPs) are a class of organic polymers with conjugated molecular chain structure which imparts special properties to the material such as high level of electrical conductivity which is comparable to metals and semiconductors in some cases. In the late 1970s, Shirakawa, MacDiarmid and Heeger reported the metal-like electrical conductivity of polyacetylene (PAc) [29, 30], and since then, the field of ICPs including the syntheses, characterization, application and device fabrication has grown tremendously with the advent of many new ICPs and modified ICPs structures. The basic building block of the structure of some commonly studied ICPs are shown in Figure 2.1 and the common levels of electrical conductivity are shown in Figure 2.2 [31, 32].

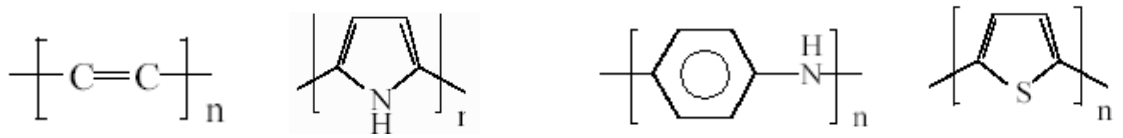

Polyacetylene Polypyrrole Polyaniline Polythiophene

***Figure 2.1 :**. Molecular structures of common ICPs.*

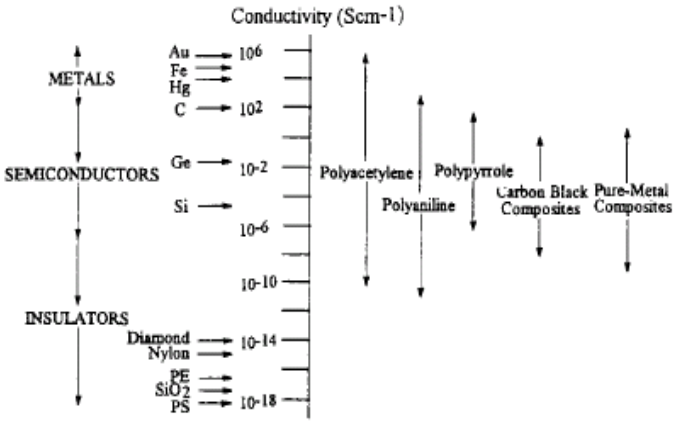

Figure 2.2: *Electrical conductivity levels of various ICPs [33].*

ICPs show a wide spectrum of electrical conductivities which range from insulating to highly conducting depending on the oxidation and doping state of the ICP, in addition to its base chemical structure. ICPs are oxidized by oxidation-reduction reactions, chemically and electrochemically by the treatment with a redox agent and application of an electrical potential, respectively. Oxidation of ICPs generally increases the electrical conductivity level where an anion is incorporated to balance the positive charge of the oxidized chain. This process is called doping and affects the electrical conductivity in a similar manner to the doping in semiconductors. The doping/undoping cycle of polypyrrole is shown in Figure 2.3. In this particular case, polypyrrole is excited to its oxidation potential in an electrolyte containing doping anions (A^-). An electron is removed from the polymer chain with the simultaneous incorporation of negatively charged doping anion (A^-) which results in a drastic change in the properties. The oxidation and doping state of an ICP can be adjusted either by changing the doping level during their syntheses or in a chemical or electrochemical doping process involving an already polymerized ICP.

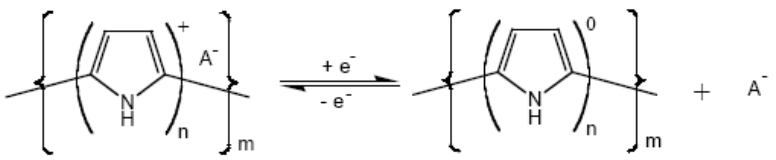

Figure 2.3: *Doping/undoping process of polypyrrole [15].*

In addition to the high electrical conductivity, ICPs have gained special attention due to their other useful properties associated with π-electron conjugation such as electromagnetic

shielding, barrier properties in coatings, electro-catalysis etc. These properties depend on the oxidation and doping states of ICPs and can be tailored by either chemical or electrochemical oxidation. The particular application of an ICP depends on the specific level of the property of interest or the combination of the various useful properties as shown in Table 1.1[15].

Table 2.1: Property change and potential applications of ICPs [15]

ICP Property	Typical change	Application
Electrical Conductivity	10^{-7}-10^{3} S.cm^{-1}	Electronic circuits, Electrostatic and EMI shielding, Sensors
Swelling	~ 10%	Artificial muscles and actuators
Electrochromatic	300-nm shift in absorbance	Displays, Smart windows
Ion permeability	0-10^{-8} mol cm^{-2} s^{-1}	Membranes, Responsive packaging

Intrinsically conducting polymers are synthesized by using various techniques such as electrochemical and chemical oxidative polymerization, enzyme catalysed polymerization and photochemical initiated polymerization. Among the employed techniques, electrochemical and chemical oxidative polymerization are the most common because of the better control and reproducibility in the chemistry of the ICP [15, 34]. In electrochemical polymerization, ICP is synthesized under an anodic (positive) potential that oxidizes the monomer on the electrode surface. The deposition is conducted either by the application of a cyclic voltage where deposition extent is controlled by the number of cycles or under potentiostatic/galvanostatic mode in which applied voltage/current density controls the deposition extent (i.e., film thickness on electrode). In the chemical oxidative polymerization, monomer is oxidized in the presence of an oxidant (e.g., ammonium persulphate or $FeCl_3$).

In spite of their useful properties and tremendous application potential, ICPs have issues such as intractability, poor mechanical properties (e.g., brittleness) and poor environmental stability. ICP composites with conventional polymers have been developed to overcome these problems [35]. ICPs are insoluble in their conducting doped state but in most of the cases

these show some solubility in strong solvents (e.g., N-Methylpyrrolidone (NMP)) in undoped state. Due to this solubility, ICP are blended with other conventional polymers to form conducting composites. In addition to solution blending, other techniques such as *in situ* polymerization of monomer in the stabilized dispersions of base polymer (e.g. latexes), polymerization in the solid polymer matrix and melt processing (e.g., extrusion) have been widely investigated in ICP composites technology [36]. An improvement in mechanical and environmental properties is achieved in ICP composites but with the decreasing electrical conductivity. Due to the processing limitations of ICPs, implantation or deposition of ICPs on the solid structures has been more focused where activity of the ICPs can be maintained along with the benefits of the basic inert matrix/structure.

Intrinsically conducting polymers have a tremendous application potential due to their high electrical conductivities, tuneable ionic conductivity and electrochemical activity coupled with their low materials cost, ease of processing in aqueous and organic solutions and low specific weight. The applications of ICPs can be classified into the areas where either electronic conductivity or its redox-ability is utilized. In the first class of the applications, an ICP does not change its oxidation state such as in electrostatic and electromagnetic shielding, components of a printed circuit board (PCB) etc. In the second, the redox switchability of ICPs is used such as in electrochromic displays, sensors, membranes, drug release systems, corrosion inhibition and electromechanical actuators [12]. In the following section, some representative applications from the both groups are discussed to illustrate the functional utilization of ICPs, including conductivity dependent applications and beyond.

Electrostatic dissipation and electronics. As the progress has been made in the fabrication of small-sized electronic components and devices such as microchips, the danger of the damage caused by the sudden build up of an electrostatic charge at the surface during storage and transportation has also become significant. ICPs deposition on the packaging films yields surface resistivity values in the range 10^3-10^9 ohm.cm^{-2} that can discharge the surface charge very quickly and protect the electronic component. Various types of ICPs such as polyaniline and polythiophene have been used by processing them in the film form with self or secondary doping processes [11, 37]. Another similar application based on the conductivity of ICPs and their processability is electromagnetic interference (EMI) shielding in which ICPs either absorb or transmit electromagnetic rays without reflecting then significantly [38]. In microelectronic systems, ICPs have found applications mainly due to their ease in processing

such as lithographic patterning and coating in the holes in PCBs which are drilled to host various circuit components [39].

Sensors. The application of intrinsically conducting polymers in sensors technology is based on the electroactivity in the switching process of an ICP between different oxidation states. Other factors such as the high level of electronic conductivity to transmit the sensed signal and biocompatibility widen the application spectrum. The application ranges from detecting and measuring anions, metal cations, chemicals (e.g. ammonia) and biological species such as proteins etc. [40-42]. The target component changes either conductivity or capacitance of ICP that can be calibrated to quantify the detected species [43, 44]. In addition to these chemical or biological sensors, physical sensors such as strain gauges have also been developed where the change in electronic conductivity by the change in dimensions has been employed [15].

Charge Storage. During the oxidation of ICPs, the backbone chains acquire positive charge and anions are incorporated to balance the charge as shown below.

$$P + zA^- + xS \longrightarrow P^{z+}A^-_z(S)_x + ze^-$$

Where P, A^-, S and e^- denote neutral ICP chain, anion, solvent and electron, respectively and z and x denote the stoichiometric coefficients. This process is highly reversible with very fast reaction rates [12]. These charging-discharging characteristics are used in the charge storage applications such as rechargeable batteries and super-capacitors. In rechargeable batteries, ICP is used as a cathode with Li electrode as a working anode. Recently such batteries have been developed where anode, cathode and electrolytes all are assembled using intrinsically conducting polymers [15, 45, 46]. A considerably higher charge density can be achieved as compared to other rechargeable batteries in the commercial use such as Nickel-cadmium cell etc.

Super-capacitors are charge storage devices that have capacitance as high as 30 $F.cm^{-3}$ and these can discharge in a very short period in the applications such as starting pulse for electric cars etc. Redox capacitance of ICPs has been exploited to acquire such high charge storage density [12, 34, 35].

Corrosion inhibition. The corrosion of active metals such as steel, aluminium and copper is controlled either by coating a thin layer of ICP on the metal surface or incorporating ICP particles (~20 μm) in conventional anti-corrosion paints [47]. A thin protective coating of

ICP is achieved either by electrochemical deposition or by *in situ* chemical polymerization by dip coat method. The exact nature of ICP corrosion inhibition process is not fully clear yet and various mechanisms have been proposed such as ICP working as a sacrificial layer, formation of protective oxide layer during oxidation state change and shifting of the oxidation potential of the metal on the higher (passive) side.

Drug release systems. Redox switching of ICPs involves movement of anions and solvent molecules in or out of the film. Using drug molecules as either anions or solvent makes it possible to release (or capture) the drugs by the electrochemical switching of ICPs. Controlled release applications of therapeutic drugs etc. have been investigated by many researchers by either soaking ICP films or encapsulating target molecules within the ICP film [34, 48, 49].

2.2 Polyaniline (PANI)-A Promising ICP

Polyaniline has been the most widely used ICP due to its high electrical conductivity, environmental stability and low materials and synthesis costs. Furthermore, the aqueous-phase aniline polymerization does not pose the problems such as high solvent cost and disposal [13, 15]. PANI has unique chemistry by virtue of its pH dependent protonation/deprotonation in addition to the common electrochemical oxidation-reduction switchability. Based on the above mentioned factors, PANI was chosen as the ICP component of the composite membranes in the present study.

2.2.1 Redox Switchability

Polyaniline has three unique oxidation states (leucoemeraldine, emeraldine and pernigraniline). In addition, the nitrogen in PANI molecular chain can be doped by treating with acids and a nitrogen base salt is formed. This acid doping is different from the protonation of other ICPs where radical cation is formed with the positive charge on ICP repeat unit [50]. As a result, PANI can exist in six unique oxidation and doping states with characteristic properties associated with each of these states. The redox and doping transformation of PANI are shown in Figure 2.4.

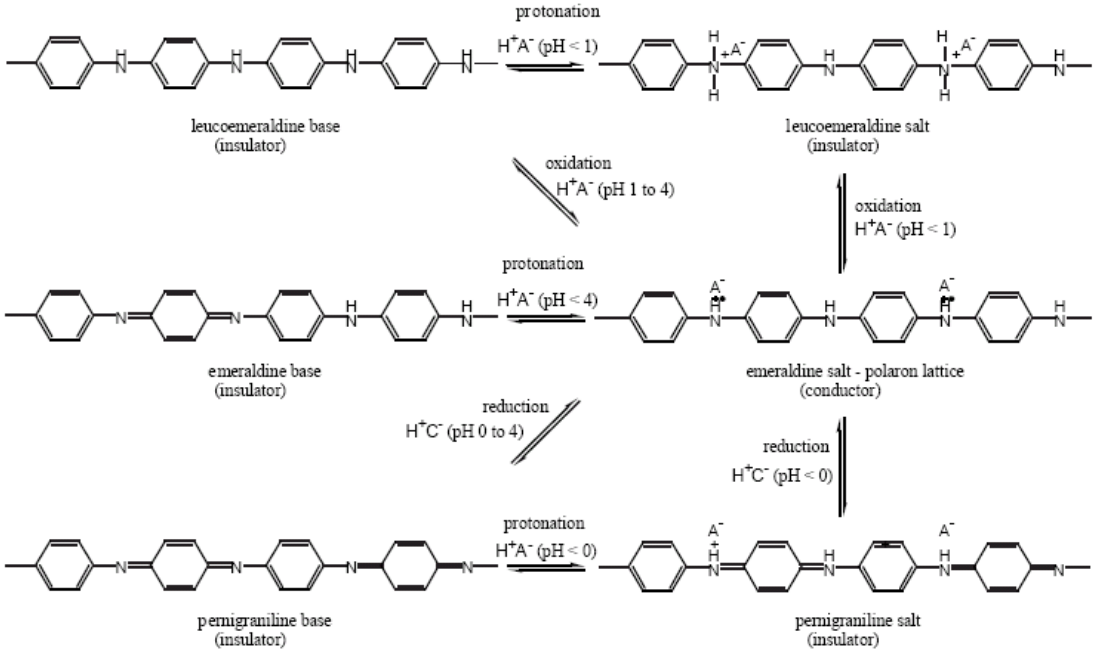

Figure 2.4: *Transformation of PANI into various states by oxidation/reduction and doping/undoping processes [15].*

Polyaniline is synthesized as half-oxidized emeraldine salt by electrochemical and chemical polymerization processes. PANI shows electrochromatic properties so each state can be distinguished by its characteristic colour. Emeraldine salt (doped) PANI is highly conductive with dark green colour. Emeraldine salt can be readily undoped to emeraldine base (bluish-purple) by dipping in a high pH solution (e.g., NaOH solution). Once undoped, PANI cannot be further switched, electrochemically, due to the loss of electroactivity at pH > 3. Emeraldine salt is converted either chemically (by adding strong oxidation or reducing agents) or electrochemically to either the fully reduced leucoemeraldine form or fully oxidized pernigraniline form. The fully oxidized or reduced forms can also be doped or undoped depending on the solution pH. Leucoemeraldine has yellowish-green whereas pernigraniline has violet colour and both forms are highly insulating. The electrochemical switchability of PANI is shown in Figure 2.5 where a cyclic voltammogram of PANI layer on a porous alumina electrode in 0.5 M H_2SO_4 is shown.

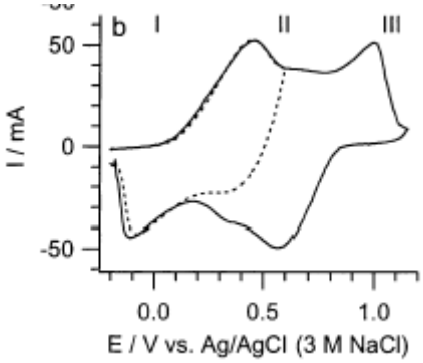

Figure 2.5: *Cyclic voltammogram of polyaniline film.* The regions I, II and III represent leucoemeraldine, emeraldine and pernigraniline states of PANI film, respectively *[8]*.

The oxidation states of PANI are marked as regions in the diagram whereas the peaks show state transformation points. The broader regions between the oxidation-reduction peaks signify an increase in the doping level in a single oxidation state. The transformation potentials are, 0.45 V (vs. Ag/AgCl) for leucoemeraldine to emeraldine, and 0.9 V for emeraldine to pernigraniline. Beyond the oxidation peak of the highest oxidation state, further increase in the potential introduces additional peak for the redox transformation of the degradation products of PANI (i.e. benzoquinone → hydroquinone). In addition to the change in electrical conductivity and electrochromism, the solvent incorporation associated with the ingress of doping anions results in film swelling. The span of electrochemical window shown in Figure 2.5 depends on many factors such as the nature of electrode material and nature of doping anion. Contrary to polypyrrole and polythiophene, involvement of nitrogen heteroatom in the repeat units of PANI results in the significant changes in the morphology of the film.

2.2.2 Mechanism of Electronic Conduction

The mechanism of electronic conduction is unique in PANI due to p-type doping as well as protonation of the chain nitrogen. Although the high level of electronic conductivity in emeraldine salt is well known phenomenon, still there are on-going debates on the molecular mechanisms involved in the charge transport in the PANI films and membranes [51].

Electronic conductivity of PANI depends on its oxidation state (i.e. imine/amine ratio) and doping level. Protonation at low pH and simultaneous anion doping in emeraldine salt generates a bipolaron structure which is thermodynamically stable, as shown in the following figure [15].

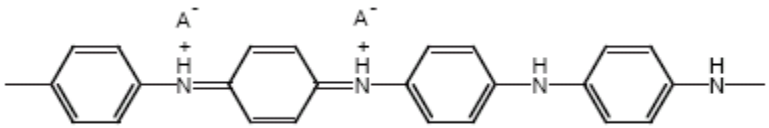

Figure 2.6: *Bipolaron structure of polyaniline [15].*

However, the defects in the local molecular chains and increased strain geometry of the polymer chains destabilize the structure and convert it into a resonance structure of a delocalized polaron PANI (Figure 2.7).

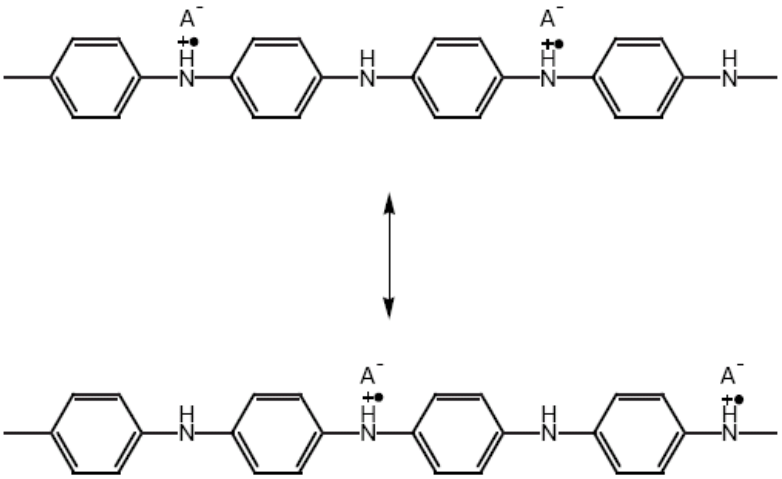

Figure 2.7: *Resonance structure of delocalized polaron in PANI [15].*

The oxidizing dopant (A^-) originates free radical and spinless positive charge on PANI backbone that are in equilibrium with each other through the local resonance. On further oxidation, the free radical is removed and the structure is converted into bipolaron again. Although bipolaron structure exists in PANI, but it is believed that polarons are responsible for the electronic charge transport in the bulk polymer. In addition to the polaron-bipolaron transitions in conjugated structure, inter-chain hopping is also involved in the charge transport mechanism [51].

The protonation and oxidation of PANI nitrogen make polymer chains highly sensitive and responsive to external stimuli as compared to other ICPs, for example polypyrrole, where positive charge is distributed on the whole repeat unit. The morphology of PANI film changes from the highly compact in leucoemeraldine to the open-pore in pernigraniline. This leads to a better control in the membrane applications where permeation can be changed.

2.3 An Overview of Membrane Separation Processes

Membrane separation processes can be classified based on the driving force for the separation and also classified with respect to the size of the species/molecules that are being separated [1]. The driving force based classification includes pressure driven membrane processes, charge based membrane separation and tuneable separation based on functional membranes.

2.3.1 Pressure-driven Membrane Separation

Membrane based processes in which separation is achieved by applying pressure on the feed side (or vacuum on the permeate side) are further subdivided into filtration and solution-diffusion based processes such as pervaporation etc. [2]. Microfiltration, ultrafiltration and nanofiltration are included in the first type where size-exclusion is the governing mechanism. Microfiltration processes are used for filtering the colloids and suspensions such as pre-filtration step in the water treatment ultrafiltration process or for the retention of proteins from the biochemical and biological solutions. The typical particulate (or macromolecule) retention size ranges from 50 nm to 5 μm [3]. Ultrafiltration membranes are used to retain solids, bacteria and microorganisms with the smaller size range (5 to 50 nm) as compared to the microfiltration. In the both processes, membranes with open-pore structure are used which allow solvent to pass through the membrane along with soluble solids. Nanofiltration membranes have non-porous dense surface layer on a microporous support and these are termed as asymmetric membranes. These membranes have pore size range of 1 to 10 nm and are used to separate the small organic molecules and multivalent ions from the solutions. Presently nanofiltration membranes are also employed in organic solvent separation.

Contrary to these size-exclusion based filtration processes, reverse osmosis (RO), gas separation and pervaporation are based on the dissolution of feed in the membrane phase at the surface (i.e. membrane swelling) and then diffusion through the bulk with desorption on the permeate side. The separation arises from the difference in the solution affinity at the surface coupled with the difference in the diffusion rates of various feed components in the bulk. These solution-diffusion based pressure-driven processes are used to separate the species at molecular level. Reverse osmosis is commonly used in desalination process where salts from the sea water are removed to produce drinking water. Another important application of RO process is in renal dialysis. Gas separation is used to separate various gaseous mixtures such as hydrogen recovery from reformer gas or oxygen separation from

nitrogen from air. Pervaporation is used to separate azeotropes that are otherwise very difficult and expensive to be purified by the conventional separation processes due to the close boiling points of the components. In pervaporation, slightly positive pressure is applied on the feed side while species are desorbed by the vaporizing at the permeate side under high vacuum. Difference in the vapour pressure of a component at the feed and permeate side is the driving force in this process. The classification and applications of membrane based processes are shown in Figure 2.8.

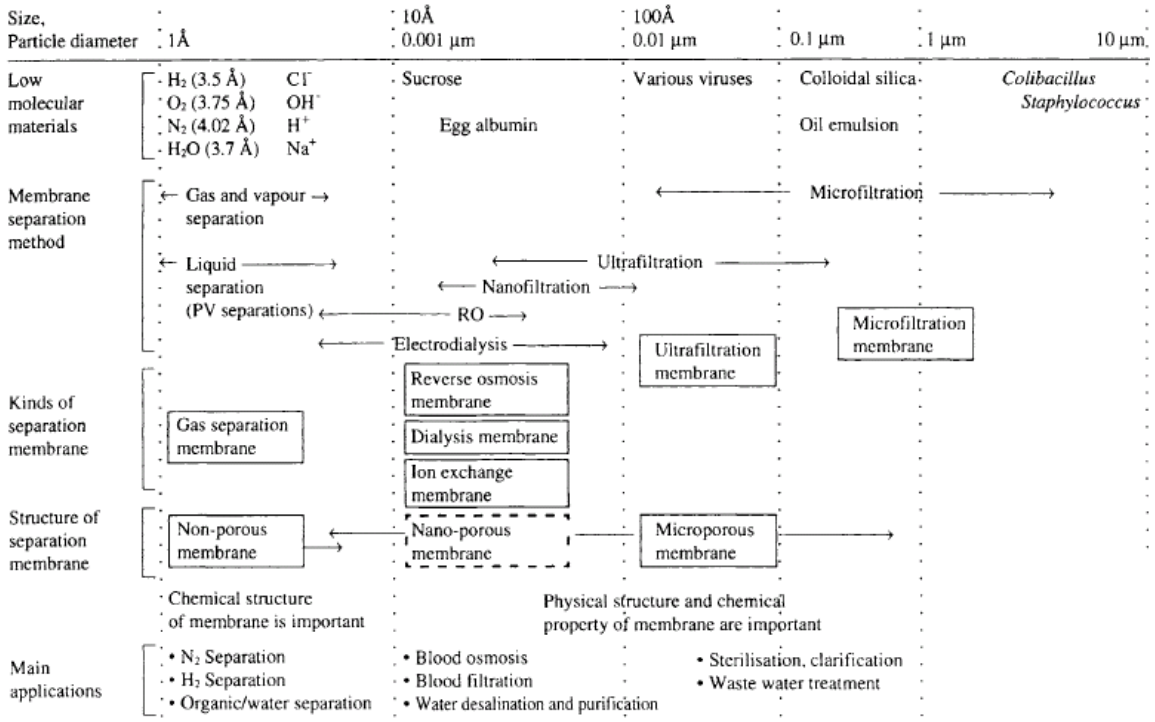

Figure 2.8: *Classification of membrane based separation processes [3].*

Various types of membranes with a variety of materials have been used in pressure-driven processes. Symmetric and asymmetric membrane structures are used in which properties do not vary throughout the cross section of the membrane in the first type whereas a skin (surface layer), porous or non-porous, is produced on the microporous support, in the second type, which differs in the properties from the support material [52]. Symmetric membranes are mostly used in the microfiltration applications whereas asymmetric membranes are used in other pressure-driven membrane processes. Thin but dense layers are desirable in the processes dealing with the low molecular weight separations such as nanofiltration, RO, gas separation and pervaporation in order to decrease the operating pressure for a reasonable

permeation flux. A wide variety of materials such as ceramics (e.g.α-alumina, titania), polymers (cellulose, polyamide, polypropylene), and glasses are used. Among these, the polymers are most common membrane materials due to their low materials and manufacturing costs and better mechanical properties. Various fabrication techniques such as sintering in the ceramics and phase inversion for the polymeric membranes have been used on commercial scale. Membranes are assembled in various configurations (modules) to achieve the compactness such as shell and tube and spiral-wound membrane modules.

2.3.2 Charge based Membrane Separation

Interaction of charged molecules with the fixed charges of the dense membrane is the basis of ion exchange membrane processes. Fixed charge groups such as sulfonic acid (cation-exchange) and quaternary ammonium salts (anion exchange) are incorporated in the inert membrane matrix such as perflourinated olefins to synthesize the homogeneous ion exchange membranes. Depending on the polarity of the fixed charges, the oppositely charged cations or anions from the solution are exchanged through the membranes (counter-ions) whereas co-ions of similar polarity are blocked. Ion exchange membranes are utilized in the various processes which can be classified into following three categories [53].

1. Electrodialysis, Donnan dialysis
2. Membrane electrolysis
3. Fuel cells

In the first type, separation is achieved by the application of either electrical potential difference (in electrodialysis) or concentration difference (dialysis) as driving force. The typical applications include desalination of seawater and milk whey by electrodialysis. Membrane electrolysis involves water hydrolysis in membrane phase such as the production of acids or sodium hydroxide in chlor-alkali processes. Fuel cells utilize selective transport of charged species across an ion exchange membrane to produce electrical energy by the reactions at the electrodes.

2.4 Polyaniline based Membranes

Sairam et al. [6] discussed various synthesis techniques of PANI composite membranes and classified these membranes depending on their applications in various membrane separation processes such as gas separation, pervaporation and electrodialysis. In the following text, PANI based membranes have been classified according to various synthesis techniques that yield specific membrane morphologies suitable for a particular separation process. An extensive literature review has been included to highlight the various synthesis techniques for PANI membranes and their effects on the membrane morphology that ultimately affects the application properties. Figure 2.9 illustrates the various components of the literature review and their relevance with the present research. In section 2.4.4, the inferences drawn from the literature review are summarized along with the directions for the present research.

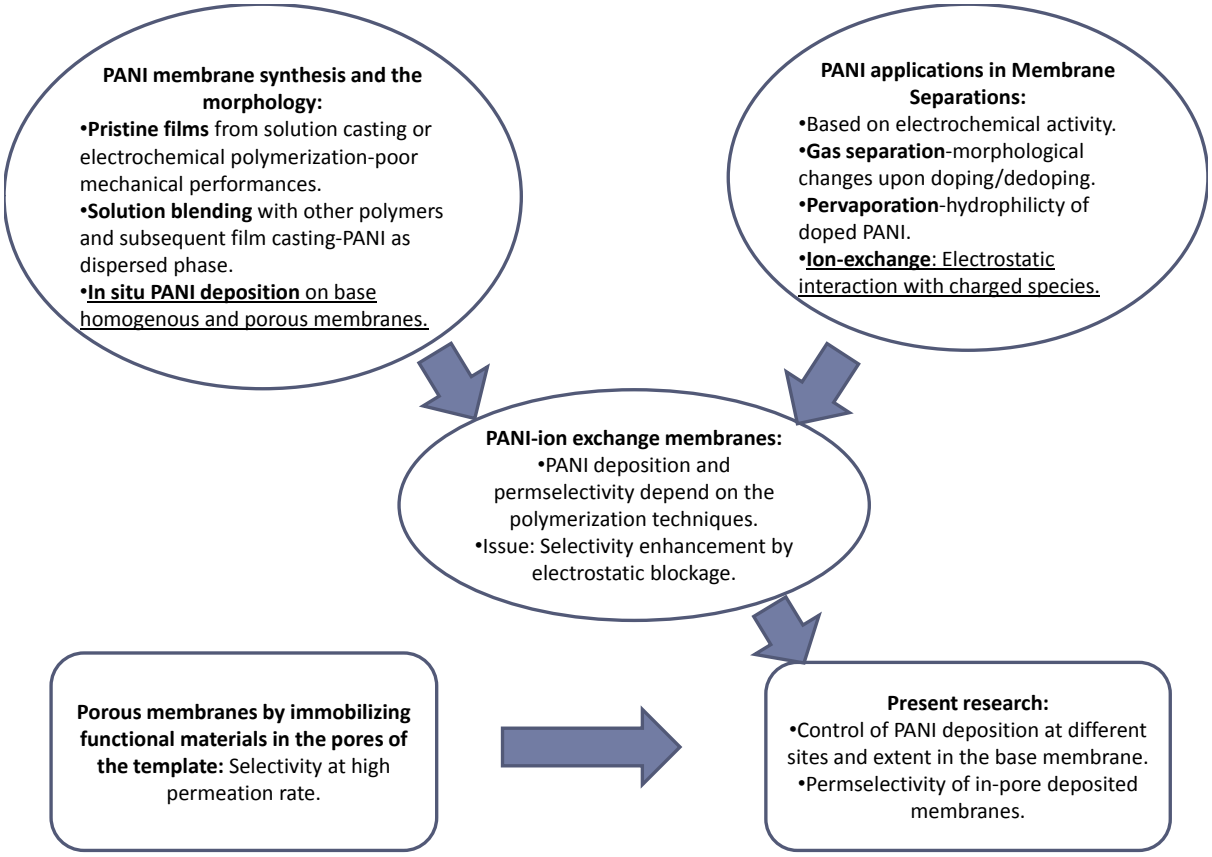

Figure 2.9: *Pictorial representation of the inferences of the literature review and its relation with the thesis.*

2.4.1 Pristine PANI Membranes

Pristine PANI membranes have been mainly used as dense membranes in gas separation and nanofiltration processes. In a typical synthesis process, undoped films are cast from a PANI solution and then aged at high temperature (~120 ^{o}C). These membranes are doped, undoped and then redoped in low and high pH solutions to achieve the final doping level. The changes in membrane morphology from ICP doping and gas-polaron interaction in the membrane phase are used for the separation of gaseous mixture in a gas separation process. Diffusivity and solubility have been evaluated which give permeability of the gases as follows [54]:

$$P=D \times S \tag{2.1}$$

where P is permeation rate ($\frac{cm^3.cm}{cm^2.s.cmHg}$), D is diffusion coefficient ($\frac{cm^2}{s}$) and S is solubility coefficient ($\frac{cm^3}{cm^3.cmHg}$).

Chang et al. [54, 55] have demonstrated the ability of solution-cast PANI films doped with HCl for the separation of various gases such as H_2, CO_2, O_2, N_2 and CH_4. Bare and ring-substituted PANI such as methoxy- and ethoxy-polyaniline films were cast by using undoped PANI solutions. Diffusion coefficients and permeation rates were evaluated by gas permeation experiments in which feed was introduced under vacuum on the up-stream side of the membrane and permeate was collected at higher vacuum on the down-stream side. These PANI membranes showed high but temperature dependent values of the diffusion coefficient (~ 10^{10} $\frac{cm^2}{s}$) and permeation rate (~10^{11} $\frac{cm^3.cm}{cm^2.s.cmHg}$). The diffusion coefficients have been correlated with the size of permeating gas molecules whereas the solubility coefficients showed dependence on the critical temperature (i.e. boiling point) of the gases.

The effects of insulator-conductor transition of PANI films on gas solubility and diffusivity have been studied [56]. The variations in permeabilities have been correlated to the degree of doping of a free-standing PANI membrane. Andreson et al. [57] correlated an increased selectivity of the various gas pairs such as He/N_2, N_2/H_2, O_2/N_2 to the morphological changes associated with the doping of PANI membranes. PANI membranes were doped at various levels by changing acid concentration and it was elaborated that a precise control on the selectivity could be achieved.

Kang et al. [58, 59] have studied O_2 transport in a free-standing PANI membrane which was cast from the PANI solution in NMP. As-cast films were cycled between fully doped and undoped states in order to realize a maximum morphology change. Undoped membranes were redoped again by using various concentrations of HCl. The high O_2 permeability was attributed to O_2-polaron interaction in PANI membrane. However, a decline in O_2 permeability on increasing acid concentration (higher doping level) was explained in terms of decrease in free volume of PANI chains. This free volume was measured on excessive doping by using x-ray diffraction (d-spacing).

Conklin et al. [60] have elaborated the effects of doping with anhydrous (gaseous) dopants on the gas separation properties of PANI membranes. These membranes were doped with gaseous halides using HCl, HBr, HI and HF and then undoped by gaseous ammonia. The higher content of the residual halide dopant was found as compared to halide levels from doping and undoping processes conducted in aqueous phase. Low permeability values were recorded due to the decrease in free volume in the membrane phase by the presence of doping anion.

To elucidate the effects of doping state of PANI on the solubility of various gases and their permeation rates, solubility isotherms of various gases of doped, undoped and redoped PANI have been constructed [61]. The linear isotherm for N_2 sorption was modelled with Henry's law whereas O_2, CO_2 and CH_4 showed complex absorption behaviour attributed to the presence of molecular spacing within polymer chains due to a non-equilibrium chain conformation.

Wang et al. [62] have investigated the temperature dependence of the permeability and selectivity of H_2, N_2, O_2 and CH_4 through emeraldine base PANI films which were cast from 20 % PANI-NMP solution. The activation energies of the permeation and solubility have been estimated. It was concluded that the permeability of all the gases increased whereas the selectivity decreased by increasing the temperature.

Pervaporation process is used mainly to separate liquids that form azeotropes and cannot be separated by a simple distillation. To separate these liquid mixtures, an additional separating component is added in azeotropic distillation that makes the process more energy intensive due to the additional removal of the separating component from the products. The high selectivity of PANI membranes can be used to separate the components of an azeotropic mixture, economically.

Ball et al. [63-65] studied the pervaporation of ethanol-water and carboxylic acid (e.g., acetic acid, propionic acid)-water binary solutions using PANI membranes. Permeation studies were conducted by using various PANI doping levels at different temperatures. Dense and defect-free PANI membranes were prepared using a solution casting technique from PANI-NMP solution. In acetic acid-water pervaporation, a high selectivity but with a low flux has been observed using doped PANI film [64]. This was attributed to the large water diffusivity in hydrophilic doped PANI films. Undoped PANI membranes showed the high permeation flux but with low separation factors. Temperature increases flux by orders of magnitude in undoped PANI membranes. Permeabilities and diffusion coefficients of water, alcohols and carboxylic acids were evaluated using doped and undoped PANI membranes in pervaporation process [65]. Undoped PANI yielded lower fluxes with smaller diffusion coefficients as compared to HCl doped PANI membranes. A high selectivity was observed in the latter case where fully doped PANI showed a negligible permeation of the longer molecule alcohols (propanol) and carboxylic acids. In these experiments, the issue of dopant (Cl^-) washout was observed which resulted in a declining pervaporation flux over time. The higher water diffusivity was observed in ethanol-water pervaporation using undoped PANI membrane (selectivity > 1000), however with a low permeation flux [63]. Doping improved the flux at the cost of selectivity where dopant loss was also observed. Dopant immobilization by the incorporation of a long-chain dopant such as polyacrylic acid and polyamic acid showed sustained permeation rates as compared to HCl. In another study on carboxylic acid-water separation by pervaporation, the higher selectivity based on water diffusion was recorded in doped PANI as compared to the diffusion in undoped PANI films. This high water diffusion was attributed to the higher hydrophilicity of doped PANI. In addition to doping/undoping, the effects of molecular chain length of carboxylic acid on the permeation rate were studied. In these membranes, the doped PANI almost completely blocked the permeation of longer molecular chain acid (acetic acid, propionic acid) as compared to the short-chain formic acid. Furthermore, changing PANI membrane structure from a symmetric dense membrane to an asymmetric membrane with the same thickness has shown a significant increase in the permeation flux.

Kaner et al. [66] demonstrated the ability of chiral PANI membranes for gas separation, pervaporation and enantiomers separation. For gas separation and pervaporation processes, the effects of doping and undoping on the permeation of N_2 and O_2 and separation of carboxylic acid-water mixtures have been elaborated. In gas separation, removal of dopant

anion increased the free volume between molecular chains, which resulted in increased permeation rates. Long-chain carboxylic acids showed smaller permeabilities as compared to short-chain acid such as formic acid. Chiral PANI films were synthesized by blending either (S+) or (R-) camphorsulfonic acid (CSA) with undoped PANI in NMP and subsequent casting on a glass plate. Circular dichromism studies showed that both (S+) and R(-) films had chiral activity and these were the exact mirror image of each other. The undoped form of CSA-PANI films were used in chiral recognition experiments using L-phenylaniline absorption on PANI films.

Cross-linked asymmetric PANI membranes were employed in the nanofiltration of various organic solvents such as ethyl acetate, acetonitrile and acetone [67, 68]. In these studies, the excellent stability of the cross-linked PANI membranes has been utilized in strong solvent environment and high temperature conditions. Asymmetric PANI membranes have been prepared by phase inversion by dissolving emeraldine base in a mixed solvent system comprising NMP and 4-methyl pepridine. Treatment with alkaline solution yielded selective nanofiltration channels in the membranes. In order to enhance the structural integrity, the membranes were cross-likened either by the thermal cross-linking of the nitrogen sites of acid doped PANI or by the chemical cross-linking with the help of chemical cross-linkers, α,α'-dichloro-*p*-xylene and glutaraldehyde (Figure 2.10). Nanofiltration performance of these membranes was studied using molecular weight cut-off (MWCO) method in which styrene oligomers of different molecular weights were filtered by using a dead-end filtration set-up. The membranes showed MWCO values in the range of 150-250 g/mol, demonstrating these as successful nanofiltration membranes. These membranes were doped by treating with various organic acids such as maleic, phthalic and camphorsulfonic acid. Subsequent leaching of the acid moieties by the treatment with an alkali yielded nano-scale channels for the filtration. The filtration experiments were conducted at higher temperatures to take the advantage of the higher permeation flux at elevated temperatures (70 ^{o}C for chemically cross-linked and 150 ^{o}C for thermally cross-linked membranes). Excellent chemical and high temperature stability with sharp rejection in a narrow molecular weight range suggest that these membranes are suitable for organic solvent nanofiltration (OSN) applications.

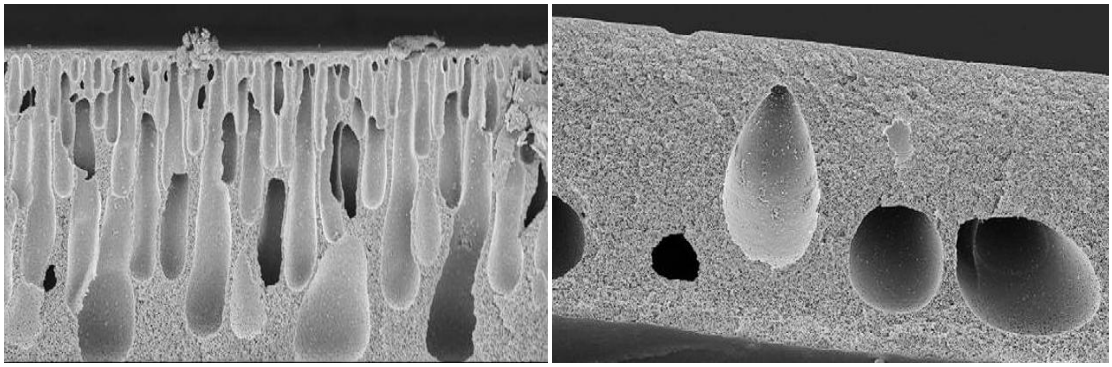

Figure 2.10: *SEM images of PANI membranes (a) untreated PANI and (b) cross-linked PANI membranes [67].*

In addition to the application of PANI in conventional membrane separation processes, the direct use of its electronic conductivity and electroactivity in the processes such as H^+ and ionic conduction for trans-membrane redox reactions and fuel cell applications have been demonstrated.

Electrochemical impedance spectroscopy (EIS) technique has been used to study the ion transport across PANI membranes. In EIS, a dynamic (sinusoidal) electrical input (potential or current) displaces the system from its electrochemical equilibrium position and the resultant output signal gives rise the conduction mechanism in the membrane. In these studies, membranes separated various electrolyte solutions in a two-compartment cell and input signal was applied using a set of working-counter electrode whereas a pair of reference electrodes (e.g. Ag/AgCl) recorded output. Deslouis et al. [69, 70] have modelled the transport of chloride ion and polaron by Nernst-Planck type model where different co-ions (cations for doped PANI) affected the transport parameters. Also the effects of pH on EIS behaviour of PANI have been elaborated with doping as most influential factor [70]. Ion exchange behaviour (anion exchange in acid doped PANI) has been studied by measuring the transport numbers of various acids with different anions (HCl, H_2SO_4) [71]. The exchangeability of pristine PANI membranes approach to that of an ideal ion exchange membrane that excludes the co-ions completely).

Wen and Kocherginsky have studied H^+ and anion transport across pristine PANI membranes and its dependence on the doping level of the membrane. Aniline was polymerized by the chemical oxidative method and PANI membranes were cast from a PANI-NMP solution (Figure 2.11). The trans-membrane potential was recorded in a two-compartment cell where the membrane separated “donor’ HCl solution in one compartment from the acceptor KCl

buffer in the second compartment. Undoped PANI membrane was permeable to H^+ but it completely restricted anion transport. Both anion and H^+ diffused through the membrane in the doped state [72].

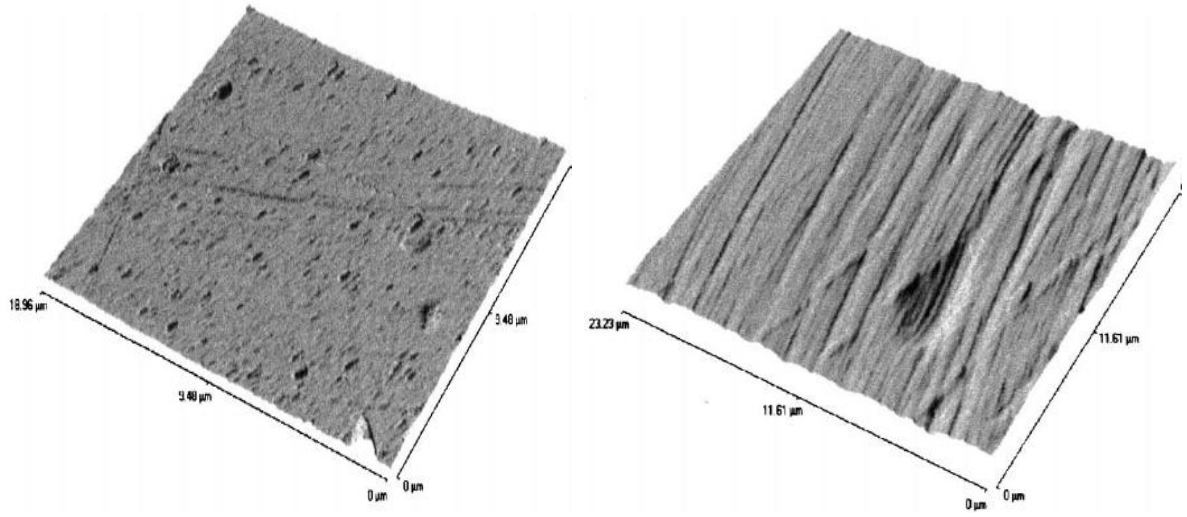

Figure 2.11: *AFM images of (a) undoped and (b) doped PANI membranes [7].*

In another study, H^+ transport across the membrane was studied by using a two-compartment cell where H^+ flux reached its study-state value after a long time (400 min) and this time lag was dependent on H^+ ions concentration on the donor side [73]. It was also observed that H^+ transport did not follow the Fick's (first) law of steady state diffusion. A multistep mechanism for coupled H^+/anion has been postulated that explained H^+ transport in the PANI membrane in terms of accompanied morphological and doping level changes with the progression of H^+ transport (Figure 2.12).

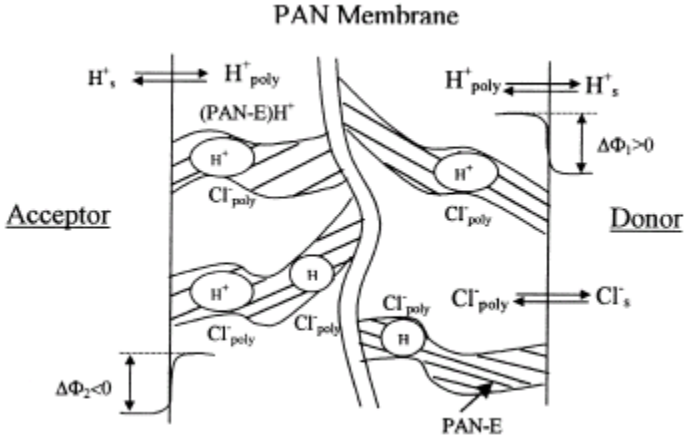

Figure 2.12: *Mechanism of H^+ transport coupled with the anion through undoped PANI membrane. Φ_1 and Φ_2 represent Donnan potentials at the interface [73].*

During the transport through the membrane, H^+ interacts with imine nitrogen by the proton-doping reaction and as the result PANI molecular chains become highly anion selective. Protons are blocked in the membrane and anions move through the doped PANI layers with the progress of coupled H^+ doping and anion transport. The difference of ionic mobility promotes charge separation in the membrane and Donnan potential is established at the solution/membrane interfaces due the selective anion transport. Anion movement through PANI membrane occurs under both concentration gradient and Donnan potential thus deviating from the linear Fickian diffusion behaviour.

Kocherginsky and Wang proposed a redox reaction mechanism across PANI membrane without direct contact of oxidizing and reducing species [74-77]. In these experiments, solution cast PANI membranes have been used which were doped either by HCl or by camphorsulfonic acid (CSA). The membranes separated $FeCl_3$ + HCl solution in one compartment of a two-compartment cell and ascorbic acid (HA) + HCl solution in another compartment. Due to the electronic conductivity of doped PANI, Fe^{3+} was reduced to Fe^{2+} by the transference of electrons from ascorbic acid that was oxidized by the following reaction.

$$H_2A \rightarrow 2H^+ + A + 2e^-$$

It was proposed that the electron transference across the membrane occurs in three steps: electrons reduce imine PANI sites to amine at the solution/membrane interface on the ascorbic acid side, electron transport through the membranes balanced by the counter-transport of coupled H^+/anion and then electron transference to Fe^{3+} solution from membrane interface. The mechanism is depicted in Figure 2.13.

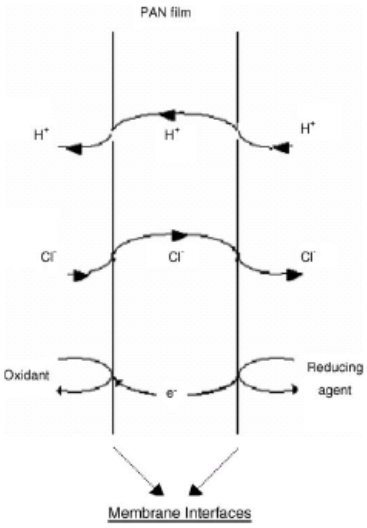

Figure 2.13: *Coupled counter transport of electron and anion, and co-transport of electron and proton through PANI membrane [76].*

Doping of PANI membrane with immobilized dopant (CSA) showed the higher electron transport rates at neutral solution pH as compared to HCl doped PANI films.

Treptow et al. [78] studied proton conductivity of doped PANI membranes for the potential application in polymer-electrolyte-membrane-fuel cell (PEMFC) to fulfil the requirement of high proton conductivity across the proton exchange membrane. Solution cast PANI membranes with inorganic acid doping were employed as proton exchange membrane. Various membrane transport processes were identified by using EIS for the estimation of various electrochemical parameters. These PANI membranes showed proton conductivity half in the magnitude as compared to a commercial ion exchange membrane (Nafion®). The leach-out of a low molecular weight anion was attributed to the decline in membrane performance.

Highly electrically conductive PANI has p-phenylenediamine polymer chain structure which is targeted during synthesis mainly due to the high environmental stability of the isomer. Linear chain m-PANI has been synthesized from the polymerization of m-phnylenediamine and films have been cast by using tetrahydrofurane (THF) as a solvent [79]. These H_3PO_4 doped films have been studied for their proton conduction in PEMFC fuel cell application. The high H^+ conductivity at elevated temperature and low humidity conditions was observed.

The most of the commercial membranes such as Nafion® lose their protonic conductivity in these harsh conditions.

Mirmohseni et al. [80] showed adaptive permeation control by a solution cast PANI film that separated an acid solution from pure water in a two-compartment cell. High proton transport rates were observed through doped PANI membranes. Application of a negative (i.e. reducing) potential (with reference to Ag/AgCl reference electrode) to the membrane reduced emeraldine PANI to leucoemeraldine that blocked H^+ transport completely.

In another study, Mirmohseni and Saeedi have demonstrated the dynamically controllable permeation of various anions through PANI membranes by the application of an external electrical potential [81]. The membranes showed high selectivity in the dialysis process for various acid pairs such as H_2SO_4/H_3PO_4 and HNO_3/H_2SO_4. Electrodialysis studies showed high permeation flux with a low selectivity between various acids. Application of a positive potential to the membrane in electro-dynamic mode drastically increased the selectivity.

The typical applications of pure PANI membranes are based on the dense nature and the electrochemical activity of the films. Gas separation by using PANI membranes is based on the steric hindrance of the PANI molecular chains that can be controlled by altering the doping state of the membrane. In the pervaporation of azeotropic mixtures, the hydrophilicity of doped PANI and the steric hindrance caused by the doping anion to the long-chain organic acids were used. In the non conventional applications, the high proton conduction of doped PANI arising from its inherent charge transport properties was used for trans-membrane redox reaction.

The application of pristine PANI in membrane applications has issues and limitations. The poor mechanical properties specifically the brittleness has been emerged as the challenge for PANI applications in the high-pressure processes. Secondly, because doped PANI is intractable in most of the solvents, the free-standing films are cast from undoped PANI solutions. The reproducibility of the post-casting doping of PANI has remained always a question as the doping levels depend strongly on many factors. In fact, only the doping-undoping and redoping cycle showed the maximum levels of anion incorporation. The loss of the doping anion during high-pressure gas separation and high-vacuum pervaporation processes is another technical challenge. The dopant loss reduces the performance of the membrane by reducing the active membrane component. However, the selective leach-out of the dopant was used to develop nano-channel membranes for organic solvent separation. To

improve the mechanical properties and avoiding the dopant leach-out, PANI blends with other polymers were developed which are discussed in the following sections.

2.4.2 Membranes based on PANI Blends

PANI blends with conventional polymers have been developed to achieve the better mechanical and environmental stability in various applications where electrical and electroactive properties of PANI were used as an active component. In membrane technology, PANI blends have been developed and used for gas separation, pervaporation and ion exchange applications. Various synthesis methods have been used including solution blending and subsequent membrane casting, fibre-spinning, melt blending and film forming and dispersion of PANI particles and nanofibres in host polymer matrices.

PANI-polyacrylic acid (PAAc) composite membranes were synthesized by dissolving PANI and PAAc in NMP and then casting and drying under vacuum at 120^{o}C [82]. In these composite membranes, PAAc behaved as a long-chain dopant attached with doped PANI chains. Pervaporation of water-isopropanol mixtures was trialled by using the membranes of varying PAAc concentration. The increase in PAAc content enhanced the permeating flux and water selectivity due to the strong water interaction with doped PANI chains. Beyond 30 wt % level of PAAc in PANI where PANI was at its maximum doping level, the flux started decreasing. Increasing iso-propanol concentration in the feed decreased the flux while maintaining the concentration of water > 85 % in permeate. X-ray diffraction studies revealed PANI interaction with PAAC chains in the composite membranes.

As discussed in the previous section, pristine PANI membranes in their doped state show very high selectivity (>1000 [65] versus typical values in the range of 1-12 for cellulose membranes [11]) for the separation of ethanol/water mixture in pervaporation. A declining membrane performance over time due to the leach-out of short-chain dopant from the membrane has been a serious issue in these applications. Ball et al. [63] developed PANI blends with polyamic and polyacrylic acids to prevent the loss of doping anion under high vacuum in pervaporation. The composite membranes were cast from 10 wt% solution of polyamic and polyacrylic acids, separately, in NMP and subsequently cured at an elevated temperature (110 ^{o}C) for 1 hour. High level of electrical conductivity of the composite membranes indicated the partial doping of PANI attributed to PANI interaction with polymeric dopant. These composite membranes showed a lower permeability and selectivity

in the pervaporation of 50% ethanol- 50% water mixture than that of an undoped pristine PANI but higher than that of an HCl doped PANI membrane. The hydrophilicity of partly doped PANI increased the permeability whereas an increase in the void fraction of the polymeric chains decreased the selectivity by allowing methanol to permeate through the membranes along with water. Polyacrylic acid modified membranes showed higher permeability but with a lower permselectivity than polyamic modified PANI membranes due to the superior dopability of polyacrylic acid. Membrane performance remained consistent over extended times during pervaporation that confirmed the immobilization of the long-chain dopant contrary to the loss of a small-chain dopant.

PANI-polyvinyl acetate (PVA) composite membranes were developed by *in situ* polymerizing aniline in 3 wt% PVA–water solution [83]. As the result of dispersion polymerization, PANI was distributed as nanoparticles in the PVA solution that was cast on a glass sheet and subsequently dried. These films were cross-linked by dipping them in glutaraldehyde solution for 10 hours. PVA-PANI nanocomposite membranes were employed in the pervaporation of water-isopropanol mixtures ranging in water concentration from 10-50 wt %. The highest selectivity was achieved with 10 wt% water feed but at a lower permeation flux than that of an unmodified PVA membrane. The higher selectivity was attributed to the change in PANI particulate morphology on doping which changed inter-chain distance of PVA cross-linked network.

Ultrafiltration membranes comprising polysulfone-PANI nanofibres were prepared by mixing PANI nanofibres (43 nm diameter) with polysulfone in different ratios and then film casting by phase inversion in a non-solvent [84]. PANI nanofibres migrated to the membrane surface that resulted in the conversion of hydrophobic polysulfone surface into the hydrophilic one, gradually, by increasing the PANI nanofibres mass percentage. An improvement in the water flux and membrane fouling was observed.

Hollow fibres of polyimide and polyimide-polyaniline were developed and studied for gas separation permeabilities and permselectivity by using various pure gases and gas pairs [85]. These hollow fibres were spun from a dope prepared by dissolving either polyimide or polyaniline and polyimide in NMP solvent. Fibres are extruded through spinneret die at 50 ^{o}C and coagulated in water bath. Polyimide-PANI hollow fibres showed enhanced permeabilities for He, N_2, O_2, CH_4 and H_2 due to the increase in free volume caused by the presence of short-chain PANI molecules in polyimide mass. The permselectivity of CH_4/CO_2 increased

significantly in the composite hollow fibre membrane as compared to bare polyimide fibres however it decreased for other gas pairs.

In another study, polyimide-PANI sheet membranes were prepared by the solution casting method [86]. After casting on a glass plate, these membranes were heat-treated at elevated temperatures with the formation of polyimide via imidization reaction (Figure 2.14). PANI in the composite membrane was doped with HCl, subsequently. A strong interaction between positively charged imine nitrogen in PANI and imide oxygen was suggested. This resulted in the higher permeabilities and separation factors for H_2, $N_{2,}$, O_2, CH_4 and CO_2 using 50/50 polyimide/PANI blend as compared to undoped PANI composite membranes. Pervaporation studies revealed higher permeation flux for water/acetic acid mixture with almost complete absorption of acid in the membranes. It was attributed to the additional PANI doping with polyamic acid in already HCl doped chains.

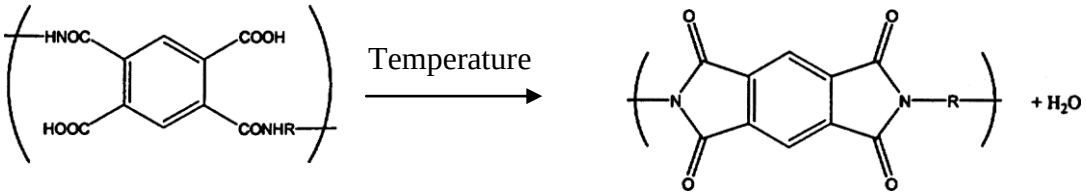

Figure 2.14: *A simple reaction scheme representing conversion of polyamic acid into polyimide.*

Permeation of sodium dodecylsulfate (SDS) through cellulose acetate (CA)/PANI blend membranes prepared by solution casting technique was studied [87]. Homogeneous CA/PANI films were cast by dissolving both components in tetrahydrofuran (THF) whereas formic acid was added to PANI, which resulted in PANI suspension in the solvent. Composite membranes were subsequently cast from this suspension. Permeation of water and sodium dodecylsulfate revealed the significant influence of free volume on the diffusion constants through the membranes. SDS permeation was affected by the micelle formation in the feed that occurred above a critical feed concentration. In addition, SDS interaction with the CA surface was observed. A strong interaction between CA and PANI was observed which influenced the diffusivity of SDS through the membranes.

PANI blends with other polymers have also been employed in ion exchange membrane processes. The exchangeability of the composite was based on either the ion exchange

properties of doped PANI or improvement in the properties of a conventional ion exchanger by PANI incorporation. High impact polystyrene (HIPS) and PANI composites were developed by blending and subsequently palletizing in a single screw extruder [88, 89]. Prior to the melt blending, PANI was doped by using various long-chain dopants such as dodecylbenzenesulfonic acid (DBSA), *p*-toluenesulfonic acid (pTSA) and camphorsulfonic acid (CSA). Composite membranes were synthesized by pressure moulding at 160 ^{o}C. Due to the immobilization of long-chain dopants, these PANI composite membranes behaved as cation-exchange membranes. The transport number of Zn^{2+} and corresponding monovalent and divalent anions were determined by using a three-compartment electrodialysis cell and these were compared with the transport numbers acquired by using a commercial cation-exchange Nafion® membrane. The cation transport numbers were comparable to that in Nafion® membrane in the case of PANI-CSA and PANI-pTSA whereas much lower transport numbers were recorded in PANI-DBSA blend. The size of the doping and permeating anions played an important role in the transport across the membranes. PANI-polyurethane composite membranes were prepared by solution casting method where PANI was doped with pTSA and CSA at different concentration [90-92]. Ion exchange performance was observed to be comparable with that of Nafion® membranes. Improved Zn^{2+} transport was observed by increasing the concentration of SO_3^- ions at high doping levels. In another study [93], electrodialysis performance of PANI-HIPS membranes prepared by two different methods was compared. These methods include mechanical mixing of PANI and HIPS in an extruder and subsequent heat-pressing to the films, and blending and film casting from a solution. Two different doping acids, TSA and CSA were used. Sodium and chloride ion transport through the membranes showed the influence of the preparation method and nature of doping acid on the electrodialysis performance of these cation-exchange membranes.

Sulfonated polyether-ether ketone (SPEEK) was blended with PANI to improve high temperature performance and lowering the methanol transport of SPPEK when employed as a proton-exchange membrane in direct methanol fuel cell (DMFC) [94]. At elevated temperatures, swelling and degradation of SPEEK warrants its maximum performance in DMFC. After incorporating PANI in SPEEK by solution casting method, high temperature stability and performance have been improved due to the interaction between PANI nitrogen with SPEEK sulfonate group. High proton conductivity was achieved by operating DMFC at a higher temperature. Similarly, hydrogen bonding between PANI nitrogen and SO_3^- group of solution blended sulfonated polyether-ether ketone ketone (SPEEKK) improved the proton

conductivity by suppressing the methanol cross-over in DMFC [95]. An improvement in the blend compatibility (i.e. homogeneity of the phases) by the incorporation of PANI resulted in the compact morphology of the membrane, which hampered the methanol permeation.

Pei et al. developed PANI composite membranes by incorporating PANI nanoparticles in the host matrix of a proton-exchange membrane made up of three-component polymer blend (TCPB) [96]. PANI particles were synthesized by using two different techniques that yielded nanoparticles with different shape and oxidation states. Emeraldine PANI particles at 2 wt% loading in the base matrix showed maximum proton-exchangeability.

Polymer gel electrolyte comprising poly(vinylidene fluoride-co-hexafluoropropylene) and lithium perchlorate ($LiClO_{4)}$ salt was modified by incorporating undoped PANI nanofibres in the membrane bulk by solution blending and subsequent film casting [97]. Undoped PANI nanofibres being electrical insulator did not contribute towards the ion exchange process but these increased the free volume of the dense polyelectrolyte film and facilitated ions transport through the composite membrane. Beyond a certain critical concentration, these PANI nanofibres formed insulating clusters and blocked the ion transport that had been facilitated by the strong ion exchange property of the base polyelectrolyte.

Blending of PANI with conventional polymers (either solution or melt blending) yielded membranes with improved mechanical properties due to the contribution of the properties from the blending constituents. In some cases, the cross linking of the base matrix polymer even yielded the composite membranes to be employed in more severe conditions. In addition, the blending with polyamic and polyacrylic acids could solve the problem of short-chain dopant leach-out in pervaporation applications. In fact, PANI dispersion in the base matrix affects the permeation properties not only due to the steric hindrance and change in the morphology on doping/undoping but its electrochemical activity also affects permselectivity. For example, hydrophilicity of doped PANI increased the permeation characteristics of water containing pervaporation feeds and the doping anion size changed counter-ion permeation in electrodialysis. However, the complete doping of embedded PANI particles in the host polymer matrix could not be achieved by conventional solution blending technique due to the limitation of doped PANI solubility. Secondly, the morphology of the composite membrane depends on the casting conditions and desirable morphologies cannot be easily achieved. For instance, the casting of an asymmetric membrane with a thin PANI film alone at the surface of the base porous membrane is very difficult to achieve. Due to

these limitations, *in situ* polymerization on template membranes has been trialled to get the advantages of full electrochemical activity of PANI, mechanical and environmental stability of the template and desirable morphology by selecting an appropriate template.

2.4.3 Composite Membranes based on *in situ* PANI Deposition

In the previous studies, PANI has been deposited on pre-fabricated membranes by *in situ* polymerization either to affect the ion transport properties of base membranes or as a thin barrier layer at the surface for size-based separations. Conventional ion exchange membranes such as Nafion$^{(R)}$ have been modified by *in situ* PANI deposition where PANI was deposited either as surface layer or inside the bulk of the homogenous membranes depending on the employed deposition technique. PANI deposition site and extent, and its oxidation and doping states affect ion transport through the base ion exchange membrane. PANI has also been deposited at the surface of base microporous membranes and synthesized composite membranes were investigated either for the gas separation or for ion diffusion properties. Both electrochemical and chemical oxidative polymerizations have been employed to deposit PANI on various types of substrate. Electrochemical polymerization has many limitations as compared to the chemical polymerization such as insulating nature of base membrane, and size limitations of the working electrodes etc. However, a more uniform PANI surface layering with controllable thickness can be achieved by this technique.

In non-electrochemical separation processes of PANI composite membranes by *in situ* PANI deposition, barrier properties of thin PANI layer are used whereas the base membrane serves as a support only by contributing towards the mechanical integrity of the composite membranes. In such membranes, high permeation flux can be achieved by integrating a reasonably thin PANI layer on the support microporous membrane. *In situ* PANI film deposition on solution cast base polyvinyltrimethylsilane (PVTMS) was obtained by using the borderline polymerization technique [98]. PVTMS film of 50 μm thickness was cast on cellophane support and then air dried. PANI was deposited from a reaction mixture of aniline and ammonium persulfate in HCl solution by a rotating flask that was almost touching the surface of PVTS film. SEM images of PVTMS-PANI membranes showed homogenous PANI film of 0.5-1 μm thickness at the surface. Gas permeabilities were evaluated for CO_2, N_2, O_2, CH_4, and He where selectivities were measured for CO_2/CH_4, He/N_2, He/CH_4, and O_2/N_2 pairs. Higher permeation fluxes for individual gases were achieved by using the composite membranes as compared to the pristine PANI membranes. The selectivity in a

particular gas pair depends on the doping state of PANI whereas doping/undoping cycling and nature of the doping acid showed negligible effects. In a similar study, a dense PANI film was prepared by the chemical oxidative polymerization and polystyrene solution was cast on an already formed PANI film. Evaporation of solvent (benzene) from polystyrene solution yielded a coherent and uniform film of polystyrene on PANI [99] . Permeabilities and selectivities of H_2, N_2 and O_2 as the function of PANI protonation and size of doping anion were investigated. An increase in protonation level decreased permeability and the subsequent degree of deprotonation increased the permeability coefficients without changing the selectivity of the gases. In a similar manner, PVDF was cast on an already polymerized and cured (at 125 ^oC for 4 hours) PANI film [100, 101]. Submicron PANI films (~ 0.8 μm) could be produced that adhered well to the base microporous support. PANI films showed selectivity comparable to the values already quoted in the literature and the permeability increased linearly by decreasing the film thickness. PANI-PVDF asymmetric membranes were prepared in a two-step method as mentioned above [16]. PVDF film was cast on the PANI films of different thickness approaching to submicron level (~ 0.4 μm). About five orders of magnitude higher permeabilities for various gases were observed by using ultrathin PANI layer on PVDF support membranes as compared to the permeabilities from undoped pristine PANI films. This high permeation rate was attributed to the high free volume in the first type of membranes due to highly ordered PANI layers (crystalline structure). The development the ordered structures can be attributed to the orientation effects in the film casting. Lee et al. [102] developed PANI-nylon composite membranes by attaching an already polymerized PANI film on microporous nylon filter by using solvent welding technique where both polymers were swelled by a common (NMP) solvent. Separation characteristics in terms of the selectivity for O_2/N_2 mixture were evaluated as the function of doping/undoping cycles and redoping time. High values of selectivity were observed for redoped membranes for two hours due to the d-space (free volume) values in the range of kinetic diameters of O_2 and N_2. To improve the antifouling property and water permeation rate through polysulfone membrane, PANI nanofibres were deposited at the membrane surface by filtering the already synthesized nanofibres through ultrafiltration polysulfone membrane [103]. Hydrophilicity of doped PANI increased the water permeability while maintaining the rejection performance of the base polysulfone membrane.

Thin PANI films for gas separation and pervaporation studies were developed by interfacial polymerization method [104]. Surface of a microporous alumina membrane (Anopore®) was

turned to hydrophobic by treating with substituted silanes (e.g. hexadecyltrichlorosilane) and then these membranes were held between the two compartments of a polymerization cell. One compartment contained oxidant solution whereas monomer vapours were generated in the second compartment that diffused through the membrane yielding a thin surface PANI film. Pervaporation data on methanol-methylterbutylether system showed preferred methanol diffusion due to the greater interaction with PANI modified membranes.

Microporous ceramic discs were modified with polyaniline to study the acid diffusion rates through composite membranes [105]. Polyaniline was intercalated inside the pores of the ceramic disc by using a two-compartment cell where PANI was formed in bulk membrane by the counter-diffusion of aniline and oxidant (APS) through the membrane. These composite membranes were used to study the acid diffusion rates by measuring the time constant (time required to attain 63.8 % of the steady state value) in a two-compartment diffusion cell. It was observed that PANI intercalation obstructed the acid diffusion whereas doped PANI promoted the proton diffusion over the undoped PANI inside the ceramic discs.

Protein immobilization and the stability of the activity over time on PANI-polypropylene membranes were elaborated [106]. Commercial polypropylene membranes were modified with PANI by *in situ* chemical polymerization by dipping the base membrane in a polymerizing solution of monomer and oxidant that resulted in a PANI film on the base membrane surface.

Cation-exchange membranes were modified by depositing PANI either on both faces or on a single face of the base membrane [107]. In the double-sided coating, aniline chloride (monomer) was exchanged with sulfonate groups of the membrane and then polymerized with ammonium persulfate. Single-face coating was achieved by polymerizing aniline, selectively, on a single side of the membrane. Transport behaviour of various cations (Na^+, Ca^{2+}, Mg^{2+}) have been studied using the two-compartment cell under electrodialysis conditions (under constant current density). From these experiments, diffusion coefficients and permselectivity were calculated. Cations were excluded from the membrane by the electrostatic repulsion offered by the positive charge on doped emeraldine PANI chains. The difference in the repulsive forces on monovalent (Na^+) and bivalent (e.g. Ca^{2+}) cations gave rise to the permselectivity in PANI modified cation-exchange membrane. Higher oxidation state of PANI (pernigraniline) remained ineffective regarding permselectivity because of its

neutral molecular chains that did not participate in the ion exchange process of the membrane.

Sulfonated polystyrene and Nafion® cation-exchange membranes were modified with PANI by *in situ* chemical oxidative deposition to alter the permselectivity of the membranes [108-110]. Base membranes were modified by using two-compartment cell technique in which two-step method as mentioned above yielded single-face PANI deposition whereas the lower oxidant (ammonium persulfate) concentration deposited PANI within the bulk membrane. The deposited PANI layer decreased ion exchange capacity of the base membrane due to the negative charge neutralization by cationic PANI molecular chains. Chemical state of PANI at the surface was characterized by XPS and it was shown that polymerization for more than one hour degraded the surface PANI to benzoquinone, a hydrolysis product of PANI. The PANI surface layer blocked the passage of the bivalent cations through the composite membrane whereas an enhanced proton diffusion was observed due to the presence of doped PANI layer. For prolonged in-bulk polymerization, PANI formed an insulating cluster blocking the transport of both monovalent (protons) and bivalent cations.

PANI was deposited on perflourinated sulfocationic membranes by the two-compartment cell technique and the effects of PANI intercalation on the permselectivity and electro-osmotic water flow were elaborated [111]. Protonic conductivities were measured by EIS whereas permselectivity was evaluated by measuring the transport numbers of various cations with common anions in a two-compartment cell. Electro-osmotic water flow occurs under the concentration gradient of a salt solution in the compartments of a diffusion cell when ion concentration changed due to electrodialysis process. In these membranes, both protonic conductivity and the electro-osmotic flow depended on polymerization time in the two-compartment cell. At a five-hour aniline polymerization, higher proton conductivity and a low water flow have been observed as compared to the thirty-hour polymerization due to pernigraniline formation. PANI intercalation did not affect the cation transport number in the composite membranes.

Cation- and anion exchange membranes were modified with PANI which was deposited on the single face of an ion exchange membrane to study the exchange or blocking behaviour of PANI layer [112]. Base membranes were modified by *in situ* chemical polymerization of aniline in a two-compartment cell where, for cation-exchange membrane, first anilinium ions were exchanged with H^+ ions of the membranes and then surface adsorbed anilinium was

polymerized by reacting with oxidant (ammonium persulfate). For anion exchange membranes, the reverse sequence was used. Different permselectivities for different cations and anions have been observed in cation- and anion exchange modified membranes respectively, mainly depending on the electrostatic interaction of PANI chains with the permeating ions and blocking behaviour of PANI due to electrostatic repulsion.

Perflourinated sulfonate cation-exchange membranes were modified by PANI using either a two-compartment cell or solution-dip polymerization technique [113-117]. These studies discuss the various aspects of the modification of the base ion exchange membrane and the transport mechanisms in bare and PANI modified membranes. The reaction rate of aniline polymerization depended on the oxidant concentration ($FeCl_3$ in this case) and on the degree of saturation of anilinium ions. Ion transport studies of bare membranes have been conducted in its acidic (H^+) and neutral form (Na^+). It was observed that proton hopping and ion diffusion phenomena played important roles in the transport processes. PANI deposition in the bulk membrane enhanced the proton transport due to the presence of emeraldine PANI but hindered the ionic diffusion transport.

Cation-exchange membrane that are used as polymer electrolyte membranes in fuel cells have been modified with PANI for various reasons which include enhancing the high temperature membrane stability, improvement in proton conduction at low humidity conditions, blocking the transport of uncharged species and lowering the electro-osmotic flow [95, 118]. Usually a thin layer at the surface of the base ion exchange membrane serves the purpose that can be achieved by *in situ* chemical oxidative polymerization of aniline. A good example is the Direct Methanol Fuel Cell (DMFC) where an enhanced proton conductivity is required with the lowest possible methanol transport under concentration gradient or electro-osmotic flow conditions [119]. PANI being highly conductive for protons in its emeraldine doped state has been employed and the studies on the performance of PANI modified ion exchange membranes have been conducted.

PEEK (polyether-ether ketone) was sulfonated by dissolving in sulfuric acid and subsequently membranes were cast by using SPEEK solution (10 w/v %) in DMF (dimethylformamide) [118]. PANI was deposited on a single face of the membrane in the two-compartment cell by using $FeCl_3$ as an oxidant. Composite membranes have been characterized for their proton conduction by evaluating the transport number of H^+ by measuring the membrane potential in a two-compartment permeation cell. Methanol

permeation was also measured from a 15% v/v % methanol-water solution. The proton conductivities and methanol diffusion decreased in these composite membranes due to the layering of doped PANI at the surface as compared to the bare SPEEK or Nafion® membranes. This blocking ability increased by increasing the PANI film density at the longer polymerization times.

Effects of PANI oxidation state on proton conduction and methanol permeation were studied when commercial Nafion® were modified with PANI by using a two-step solution dip method of *in situ* aniline polymerization [120]. Either surface deposited PANI in emeraldine salt form was reduced to the lower oxidation state by exposing to phenyl hydrazine solution or a fully oxidized PANI (pernigraniline) was achieved by early terminating the polymerization reaction. In the chemical oxidative polymerization, pernigraniline is formed initially which is subsequently reduced to emeraldine form. It was observed that layering of emeraldine salt increased proton conductivity of the base membrane and decreased the methanol permeation as compared to the other oxidation forms of PANI. FTIR characterization showed an interaction between the PANI chains and sulfonic acid groups of the base membrane that altered the morphology of the base membrane affecting the transport properties.

Power output from membrane electrode assemblies for DMFC using bare Nafion® and Nafion-PANI membranes were compared where latter type of membranes was achieved by *in situ* chemical polymerization [121]. Composite membranes showed higher power densities as compared to the bare membranes at normal operating temperatures and high methanol concentrations. It was observed that PANI deposition reduced methanol cross over in the fuel cell resulting in higher efficiency. Yang et al. [122] observed high proton conductivity of Nafion-PANI composite membranes at low humidity conditions where normally bare Nafion almost loses all of its proton conductivity. PANI was deposited on base membrane by *in situ* chemical oxidative technique in its emeraldine state. The unique proton conduction mechanism of protonated amine was responsible for the high conductivity at the low humidity conditions.

Nafion®-polyaniline-silica composite membranes were prepared by depositing PANI on the surface of silica particles embedded in Nafion® membranes by *in situ* chemical deposition [119]. PANI enhanced the stability of the base membrane as Nafion modified membranes retained their crystalline nature at higher methanol concentration in the feed to achieve high

power output. Undoped PANI reduced the methanol permeation at the cost of lower proton conduction.

PVDF microporous membrane (pore size: 0.22 μm) were modified with PANI and its various derivatives such as poly (n-ethylaniline), poly (n-methylaniline) and poly (o-anisidine) by solution dip method in which base membrane were dipped in a polymerizing solution of aniline [123] . Hydrophilicity and water up-take of the PVDF membranes were increased by the PANI deposition. Cation-exchange properties of PANI and its derivatives doped with long-chain naphthelensulfonic acid were used in Donnan dialysis in water treatment process. High cation rejection was observed with Ca^{2+} recovery approached to up to 30 %.

Polyaniline was coated by *in situ* chemical polymerization on the cellulose acetate films blended with different plasticizers [124, 125]. Various effects of the plasticization with triphenyl phosphate such as change in morphology and increase in the electronic conductivity were studied. PANI composite membranes were used in AuI_2 absorption by using the ion exchange properties of surface coated PANI film.

Blinova et al. [126] elaborated the mechanism of PANI deposition on microporous cellulosic tubing (regenerated cellulose) by *in situ* oxidative chemical deposition. The tubing was filled with monomer and it was dipped in a beaker carrying ammonium persulfate (oxidant). PANI was deposited on the monomer facing side of the tubing that showed oxidant diffusion to the monomer side only, without aniline transport to the other side. Once PANI film was formed, initially, subsequent polymerization took place by coupled electron-proton transport across the conducting PANI layer without a direct contact of monomer and oxidant. A trans-membrane redox reaction facilitated by PANI layer without direct contact of reacting species was proposed.

PANI deposition on various membrane substrates by *in situ* electrochemical polymerization has limitations of low electrical conductivity of base membrane as it acts as anode in a two- or three-electrode electrochemical step. The base membrane has to be made reasonably electronically conductive by attaching a conducting material such as metal or carbon on at least one side of the membrane. This limits the size and materials of base membrane for electrochemical modification. On the other hand, controlled aniline polymerization in the form of defect free film can be achieved on the base substrate.

Electrochemical polymerization of aniline on polyethylene-propylene copolymer dense membranes which had been surface grafted with polyacrylic acid (PAAc) and sulfonated in order to make these membranes functional and hydrophilic was conducted as shown by the scheme in Figure 2.15 [127].

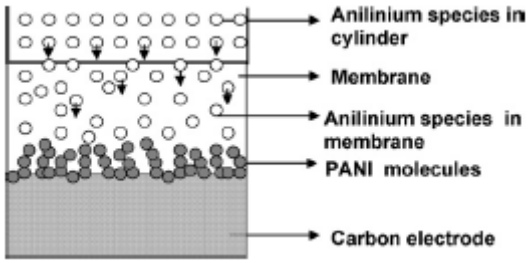

Figure 2.15: *Mechanism of electrochemical polymerization of aniline on FEP-g-PAAc-SO_3H membrane [127].*

In the experimental set-up, a cation-exchange membrane was placed on a carbon paper (anode) which supports a cylinder containing 25 ml aniline solution with a carbon cathode immersed in it. Electrochemical deposition started from the anode side of the membrane and progressed through the membrane bulk towards cathode side. Potentiostatic conditions were maintained so PANI deposition extent depended on polymerization time. Leakage of bivalent Zn^{2+} ions under electrodialysis increased by the increase in the polymerization time of aniline showing an improvement in permselectivity with deposited PANI on the base membrane.

Anion exchange membranes were modified with PANI by electrochemical polymerization method [128]. Base ion exchange membranes were made conductive by adhering carbon paste and electro-polymerization was conducted in a three-electrode cell by cyclic voltammetry. Deposited carbon paste was removed by solvent washing before conducting the electrochemical permeation experiments on the composite membranes. Coupled proton transport with anion (NO_3^-) permeation was observed due to the deposited PANI layer.

Shimizu et al. compared the ionic conductivities and methanol permeability of Nafion®-PANI composite membranes prepared either by electrochemical or chemical *in situ* polymerization [129] . It was shown that chemically deposited PANI showed better performance as compared to that of electrochemically deposited for the applications in DMFC.

A thin film of PANI was formed, electrochemically, on microporous alumina which had been made conductive by depositing a gold layer on one side of the membrane [8] . The composite

membrane was used in electrochemically modulated permselectivity studies where the potential of membrane was controlled, *in situ*, in a three-electrode configuration in a two-compartment permeation cell. Permeation of neutral phenol and negatively charged 4-hydroxybezenesulfonate were studied by changing the oxidation state of the PANI film on the base membrane. The permeation of both probe molecules was explained in terms of membrane morphology and electrostatic interaction of PANI in a particular oxidation state. Emeraldine salt state showed the highest permeation levels due to open pore morphology of the film and cationic charge on PANI chains. PANI degradation via hydrolysis at high anodic potentials was also observed.

2.5 Inferences from the Literature Review and Direction for the Present Research

A quick overview on the early developments (starting from late 1980s) of PANI based membranes concludes the following.

- PANI was used extensively in the membrane research due to its simple (clean) chemistry, environmental stability and acid/base dopability. This combination makes PANI a unique ICP among the developed ones.
- Pristine PANI membranes were trialled for more conventional gas separation and pervaporation processes by using switchability in morphology, hydrophilicity and electrochemical interaction on doping/undoping. Mostly solution casting technique was used for the membrane fabrication. High selectivities, particularly in the pervaporation due to acid/water interaction with doped PANI was observed but low permeabilities remained a big concern.
- Ion exchange applications of PANI membranes were studied where switchability in ion exchangeability was recorded. However, as the major part of the work, ion exchange properties were explored in the modified electrode geometry for sensors application (not discussed in this thesis).

Some critical issues associated with pristine PANI membranes restricted their wide spread use in various applications. These include insolubility of doped PANI in most of the solvents, poor mechanical properties of as-cast films and loss of low molecular weight dopant,

especially in pervaporation process. This leads to the blending of other polymers with PANI for the free-standing films fabrication.

PANI blends, at least partially, solved the problems of dopant loss and poor mechanical properties but the control on PANI oxidation/doping state remained a challenge. In addition, the poor dispersion of PANI in the membrane bulk limited the effectiveness of PANI as an active (functional) membrane component. Although the selectivities in gas separation and pervaporation were increased but the thick dense membranes yielded low fluxes (permeabilities). In the ion exchange applications of PANI blends, polystyrene-PANI membranes were formed by melt extrusion and subsequent pressure moulding. These membranes were tested as ion exchange membrane in electrodialysis process. However, the dependence of cation-exchangeability on the size of long-chain dopant suggested that polystyrene just contributed towards the structural integrity.

In the recent past, modification of various types of template with *in situ* polymerization of aniline has emerged as a promising technique for the synthesis of PANI composites and composite membranes. In conventional gas separation type size-exclusion applications, thin PANI layers have been deposited on the base, particularly, porous membranes. These asymmetric type composite membranes enhanced permeabilities at reasonable selectivity levels. However, the fabrication of ultrathin PANI films remained a challenge.

The various synthesis techniques of pristine PANI and PANI composite membranes have been discussed to elucidate the effects of the synthesis conditions on membrane morphology and resultant membrane properties. To develop a PANI composite membrane for the potential electrochemical applications, PANI-ion exchange composite membranes have been specifically focused in this thesis [107-129]. The deposition of PANI either on the surface or in the bulk of a conventional ion exchange membrane has been investigated for several reasons. These include improving the permselectivity of the conventional ion exchange membranes, PANI deposition as a surface layer to restrict the methanol cross over in a fuel cell and improving the ion exchangeability of the membranes at high temperature and low humidity conditions in the fuel cell. In the most of these studies, homogenous ion exchange membranes were modified by depositing PANI by *in situ* chemical polymerization. To get a thin PANI surface layer, a few studies have focused on the electrochemical polymerization too. In the modification of homogenous ion exchange membranes, two aspects have been focused:

1. Exclusion of co-ions due to the presence of a positively charged PANI layer at the membrane surface (e.g. blockage of cations in PANI modified cation-exchange membranes. The exclusion depends on the valence number of the cation due to the variation in the electrostatic force.

2. Effects of PANI deposition site on the permselectivity. PANI was deposited either as the surface layer or inside the membrane bulk by altering the contacting patterns of the reactants. It was observed that incorporation of PANI in the membrane bulk restricted the permeation of big-sized counter-ions and improved the selectivity.

3. Effects of PANI oxidation/doping state on the permeation of protons (H^+) and other cations. Doped PANI enhanced the transportation of proton over other cations.

However, these studies cover only the limited scope probably due to their focus on the commercial cation-exchange membranes for electrodialysis and fuel cell applications. Cation-exchange membranes were used in the most of the cases with only a few studies on anion exchange membranes. The base membranes had already very high exchangeability (transport numbers ~0.92) and PANI deposition only improved the permselectivity by its steric hindrance. In some cases, PANI even reduced the exchangeability of the base membrane by reacting with the anion functionalities in the membranes. In addition, the permeabilities did not change and these were depended on the current density across the ion exchange membranes in electrodialysis cell.

To address the issue of reduced permeation flux in dense homogenous membranes, synthesis of porous PANI composite membranes has been proposed in this thesis. The separation in these membranes takes place by the development of an electro-kinetic double layer inside the pores. The charge density of this double layer can be increased either by doping the PANI layer on the pore walls or by directly applying an electrical potential to the membrane. Therefore, contrary to the conventional homogenous ion exchange membranes, charge transportation takes place, predominately, through the pore electrolyte though transportation in the polymer phase is not completely eliminated. Microporous membranes modified with long-chain polyaminoacids showed pore controlled permeation in the pressure driven filtration processes.

As mentioned in Introduction of the thesis, a few earlier studies discussed in-pore PANI deposition on the base microporous membranes. These include PANI deposition on the base

porous polyethylene membranes [19, 20, 28] and in-pore PANI deposition on the ceramic microporous filters [105]. However, a critical analysis of the earlier studies suggests that PANI was mainly coated on the surface of the base membranes as also evidenced by other studies under the similar conditions. PANI was coated inside the pores of the ceramic discs by using the two-compartment cell technique. Acid diffusion studies showed irregular PANI deposition inside the membranes. None of the above-mentioned studies has systematically evaluated the effects of various experimental conditions such as polymerization technique, time, concentration and nature of the oxidants on the PANI deposition site, extent and oxidation/doping state.

In this thesis, a systematic study on the control of PANI deposition site in the base membrane and intercalation levels using various *in situ* polymerization techniques and conditions is presented. Oxidation state and doping levels were quantified by detailed x-ray photoelectron spectroscopy analysis of the composite membranes. Electrochemical performance of the membranes was evaluated by studying the charge transport and charge transfer characteristics using electrochemical impedance spectroscopy (EIS) and transport number measurements. Electronic and ionic transportation properties were correlated with the PANI deposition site and extent depending on the *in situ* chemical polymerization technique.

Chapter Three

Experimental Methods

The focus of this research has been the investigation of the effects of various techniques of aniline chemical polymerization on PANI deposition on the base membrane and characterization of the electrochemical performance of the resultant composite membranes. The experimental methods involve various techniques of *in situ* chemical oxidative polymerization of aniline on microporous base membranes and the characterization techniques pertaining to the chemical state determination and electrochemical performance evaluation of the composite membranes.

Description of materials and synthesis methods are included in this chapter along with the introduction of the employed chemical and electrochemical characterization techniques. The detailed discussion on x-ray photoelectron spectroscopy (XPS) and electrochemical impedance spectroscopy (EIS) are included in the following chapters where the characterization results are discussed.

3.1 Synthesis of PANI Composite Membranes

3.1.1 Materials

Mixed cellulose ester membranes (Millipore®, pore size: 0.22 μm, thickness: 150 μm) were used as the base membranes which have been modified with polyaniline by *in situ* chemical polymerization. Cellulose acetate membranes (Whatman®, pore size: 0.45 μm, thickness: 115 μm) have been used for support and comparison purpose only. Aniline (Sigma-Aldrich), ammonium persulfate (Univar), HCl (Merck), $FeCl_3.6H_2O$ (Scientific Supplies) were all of reagent grade and used as received. Aniline was stored under dark and the long-term exposure to the atmosphere has been avoided in order to prevent oligomer formation and degradation in the presence of light and air. All solutions were prepared in highly purified (18MΩ) water obtained from ELGA (Maxima Ultra) purifier system.

3.1.2 PANI Deposition on the base Membrane

Prior to the investigation of the effects of various parameters such as polymerization time involved in the composite membranes synthesis, a series of preliminary experiments were performed which served as the basis for the selection of the polymerization techniques and tailoring the parameters involved in these techniques. In these preliminary screening types of experiments, two types of the base microporous membranes, hydrophobic polytetraflouroethylene (PTFE) and hydrophilic mixed cellulose ester (a blend of cellulose nitrate and cellulose acetate in 75:25 ratio) were used in the following techniques of the chemical polymerization of aniline.

1. **Solution-dip polymerization:** In this single-step method, the base membranes were dipped in a reacting mixture of aniline and oxidant (either ammonium persulfate or $FeCl_3$) of various concentrations and for various times. In the two-step dipping, base membrane was treated, first with aniline solution and then dipped in an oxidant solution.

2. **Vapour-phase polymerization:** Base membrane was first soaked either with monomer (aniline) or with oxidant (APS) solution and then held in a closed reagent bottle where the vapours of the other reactant were generated by heating the solution (at 60-70 ^{o}C) over a hot plate. The treatment of APS-soaked membrane with aniline vapours distorted the base ME membranes so for all subsequent vapour-phase polymerizations, base membranes were soaked in aniline and treated with APS vapours.

3. **Filtration-through deposition:** In-pore PANI deposition was achieved by driving the reagents through the membrane pores under pressure (vacuum). Both single- or two-step polymerization techniques have been used where aniline polymerization mixture was pressure-filtered through the membrane in the former technique whereas one of the reactants passed through the membrane followed by the other in the latter one.

In these techniques, various combinations of the experimental conditions were employed and PANI deposition site and state (identified by the characteristic colour of various forms of PANI) were recorded. The following conclusions were drawn from these preliminary experiments.

1. Hydrophilic mixed ester membranes showed better adhesion of PANI layer on the surface as compared to the hydrophobic PTFE membranes probably due to the presence of hydrogen bonding between PANI and ME. It implies that hydrophilic functionality of the substrate promotes an on-substrate deposition in competition with the homo-polymerization of the monomer in the solution.

2. Concentration effects were minimal on the PANI deposition site and on the uniformity of surface coverage on the base membranes. Furthermore, the extent of the surface coverage could be controlled by manipulating aniline polymerization time.

3. Aniline polymerization using APS as oxidant yielded large quantity of PANI both in the solution and on the substrate as compared to $FeCl_3$ based polymerization due to the higher reaction rate constant of APS. Furthermore, PANI degradation was observed (blackish brown colour that followed dark green emeraldine PANI) in this case after about 20 minutes polymerization at the employed concentrations.

4. Contacting pattern of the reactants in the polymerization had influenced the PANI deposition site in the base membranes as evidenced from the filtration-through technique which yielded in-bulk deposition with PANI deposition inside the pores whereas solution-phase polymerization yielded PANI layer on the membrane surface.

Based on the observation of the preliminary experimentation, it was decided to employ solution (dip)-phase, vapour-phase and diaphragmatic type polymerization using a two-compartment cell. Because of the important role of the physical processes involved in the heterogeneous chemical reaction of PANI deposition on the substrate such as diffusion and adsorption, and due to the functionality of mixed cellulose ester membranes, it was anticipated that PANI could be deposited on the pore walls of the membranes by using the two-compartment cell polymerization.

For all the employed techniques, except for vapour-phase polymerization, aniline (0.8M), ammonium persulfate (0.3M) and $FeCl_3.6H_2O$ (0.3M) were prepared in 0.4M HCl aqueous solution. For the vapour-phase polymerization, APS (0.3M) was dissolved in 3M HCl solution. Solution-phase and two-compartment cell polymerizations were conducted at room temperature.

In the solution-phase PANI deposition, base membranes were dipped, for various times, in a polymerizing mixture of aniline and oxidant (APS or $FeCl_3$).

In the vapour-phase deposition, ME membranes were first soaked in an aniline solution and then held in a saturated oxidant vapour atmosphere. APS vapours were generated by heating the oxidant solution at 60-70 ^{o}C in a closed vessel.

In the two-compartment cell technique, the cell was composed of two identical compartments each of 150 ml capacity (Figure 3.1). Both compartments were joined together with membrane as the separating wall (exposed area= 4.5 cm^2) by using a sealing O-ring. Aniline and oxidant solutions were allowed to counter-diffuse, simultaneously, through the membrane. Various combinations of aniline, oxidant and acid (HCl) in both compartments were used to alter the PANI deposition site.

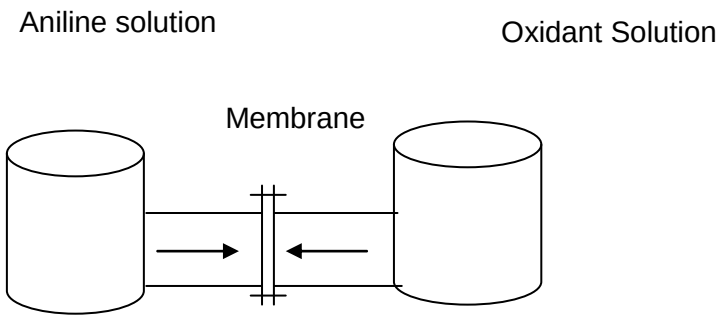

Figure 3.1: *Schematics of aniline polymerization in a two-compartment cell.*

After the polymerization reaction in all the techniques for predetermined times, composite membranes were dipped in 1M HCl solution for more than 24 hours to achieve the complete protonation and doping of PANI in the membranes. A few PANI particles, grown from the homopolymerization in the solution, adhered to the membrane surface. These were successfully wiped-off by using a soft blotting paper.

3.2 Characterization Techniques

3.2.1 Scanning Electron Microscopy (SEM)

Morphology of the membranes was studied by capturing the scanning electron micrographs. SEM is based on electron microscopy where electrons are impinged on the sample in an evacuated chamber and the resultant electrons are analysed to capture the morphology of the sample. The morphology of the membranes was captured using either an environmental SEM (ESEM, FEI Quanta 200F) or a field emission SEM (Philips XL30S FEG) both equipped

with EDS (energy-dispersive-spectroscopy) detectors. Membrane samples were mounted on the sample stud by using a double-sided conductive tape.

3.2.2 PANI Intercalation Levels Measurements

PANI deposition levels in the base membranes were measured by using the gravimetric technique. Membranes were dried in desiccators for more than 7 days and then weighed. The PANI intercalation levels were calculated by measuring weight difference between modified and bare ME membranes.

3.2.3 Electronic Conductivity Measurement

Electrical conductivity of PANI composite membranes was measured by using two- and four-point measurement techniques. For these measurements, all membranes were dessicator-dried for more than three days. Two-point technique was used for surface and trans-membrane conductivities. A high impedance multimeter was used to measure the conductivity that with-draws a negligible current. Contact resistance was reduced by applying silver paste at the electrode contact points on the membranes. For surface conductivity, both electrodes were placed at the surface whereas for trans-membrane (through) conductivity, these were placed across the membrane. The measured electronic resistance was converted to the conductivity by using the following relationship.

$$k = \frac{1}{\rho} = \frac{d}{RA} \tag{3.1}$$

where k is the conductivity (S. cm^{-1} or $ohm^{-1}.cm^{-1}$), ρ is resistivity (ohm. cm), R is resistance (ohm), A is the area (width x thickness) and d is the distance between the two measurement points.

Two-point conductivity measurement method has inherent limitations that affect the accuracy of the conductivity values. These limitations include contact resistance losses and polarization effects due to the same electrode being used as the current source and voltage measurement. Although two-point data for ICPs conductivity have been quoted in the literature, these have been used only for comparative study in this thesis. To compare the conductivity values with the widespread published data on PANI, a standard co-linear four-point method was used. The set-up consists of four equally spaced microprobe electrodes and

a high impedance multimeter is used for the supply of current and voltage measurement. Two outer electrodes supply the current whereas the two inner electrodes measure the voltage drop. The resistivity is defined as:

$$\rho = \frac{\pi}{2}.\frac{V}{I}.t.k \tag{3.2}$$

where ρ is resistivity, V and I are the measured voltage and supplied current, respectively, t is membrane thickness and k is a correction factor based on the ratio of electrodes spacing to the sample diameter. Separate electrodes for current supply and voltage measurement eliminate the contact polarization problem encountered in the simpler two-point conductivity measurement technique.

3.2.4 Fourier-transform (FTIR) Infrared Spectroscopy

FTIR spectroscopy is a vibrational spectroscopy technique where the infrared light is absorbed at the characteristic frequencies by the chemical functionalities of the sample resulting in the stretch or bending of the chemical bonds in the material [130]. The frequencies in FTIR are represented in the units of wave number (ν) which is defined as the number of waves per unit length (cm^{-1}). Wave number is inversely proportional to the wave length i.e.

$$\upsilon = \frac{10^4}{\lambda} \tag{3.3}$$

where λ is wave length in μm.

A sample in the form of solid, liquid or gas is placed in the path of an incident infrared light beam and absorption is measured in terms of transmittance which is the ratio of the intensity of transmitted rays to the intensity of the incident rays at a particular wave number. FTIR results are presented as spectrum with wave number on the x-axis and transmittance on the y-axis. In some cases, absorbance is plotted on the y-axis instead of transmittance, which is defined as:

$$A = -log\frac{1}{T} \tag{3.4}$$

where A is absorbance and T is transmittance. Transmittance shows linear change from 0-100% whereas absorbance shows logarithmic change from 0-infinity. Most commonly, the wave number on x-axis spans in the mid infrared range from 4000-400 cm^{-1}.

For the analysis of solid organic compounds, a small quantity of the compound is dispersed in a highly transparent salt (i.e. KBr) and a thin pellet is formed by the hydraulic pressing. This pellet is held perpendicular in the path of infrared beam where KBr acts as a transparent window material. However, for more thick and opaque films and membranes, attenuated-total-reflectance (ATR) technique is used. ATR is based on the fact that all the incident light is reflected back when it enters from a denser medium of higher refractive index to a lesser dense medium of lower refractive index with the incident angle higher than the critical angle. In ATR, sample is placed in the close contact with a crystal of zinc selenide, diamond or germanium, and infrared light when impinged on the sample, penetrates into sample (up to ~ 10 μm) before reflected back. There is no sample preparation involved in ATR technique, which adds to the advantages of the technique. The major disadvantage is that it yields only surface and sub-surface information without much bulk penetration.

For the present work, infrared spectroscopy was conducted by FTIR-ATR (Thermo Nicolet 8700) using Ge and diamond (for cellulose acetate membranes) crystals as backgrounds. Prior to the analysis of the spectra, each spectrum was corrected by fitting an appropriate base line and ATR background subtraction by the processing software.

3.2.5 X-ray Photoelectron Spectroscopy (XPS)

XPS is a surface characterization technique (penetration ~20 nm depth) which is used for the quantification of elements and chemical functionalities present on the surface of the sample [131]. XPS is based on photoelectron emission phenomenon where the irradiation of the sample with x-rays results in the ejection of electrons (photoelectrons) from the core (inner) level of the atom. These photoelectrons are detected by using energy dispersive detector where photoelectrons are detected by resolving these according to their kinetic energies and number of photoelectron in each kinetic energy range is measured. The kinetic energy of the electrons gives information about the parent atom and the number of photoelectron gives the abundance of a particular atom in the sample. Kinetic energy (K.E.) of the emitted photoelectron is correlated with the energy of the incident x-ray photon by the following equation.

$$K.E. = h\nu - B.E - \varphi \quad (3.5)$$

Where h is Planck's constant ($6.62\ 10^{-34}$ J. s) and ν is the frequency of the x-ray and φ is the work function. Binding energy (B.E) represents the difference in energy of ionized and neutral atom.

XPS results are shown as spectra in which abscissa shows B.E (in electron volts, eV) and ordinate shows normally photoelectron intensity (counts per second: CPS). Monochromatic x-ray is generated depending upon the source; MgKα (1253.6 eV) and AlKα (1486.6 eV) are the most common in XPS. XPS is conducted under high vacuum (< 10^{-8} Torr residual pressure) to avoid the interference of photoelectron emission from the ionization of air atoms.

The amount of the elements is quantified by peaks intensity on a characteristics B.E in XPS spectra. In addition to the elemental detection and quantification, XPS also yields information about the chemical environment of a particular element where a small shift in B.E characterizes the charge state of the atom due to the presence and interaction of surrounding heteroatom. Positive charge in the higher oxidation states of an atom shifts B.E energy on higher side on eV scale. Chemical shift is used to study the presence of various chemical functionalities on the surface.

For the XPS characterization in the present work, survey level spectra of each membrane sample have been recorded in 0-1000 eV range followed by the core level spectra for C, N, O Cl, and S elements depending upon the chemistry of the sample. XPS spectra were obtained on an AXIS Ultra DLD (Kratos Analytical Ltd.). Membrane samples were mounted on a standard sample holder using double-sided adhesive tape. Survey and core level spectra were obtained with Al Kα monochromatic x-ray source (1486.6 eV). The X-ray power supply was operated at 15 kV and 10 mA. The residual pressure in the analysis chamber during scans was kept below 10^{-8} Torr. XPS spectra of the membranes were analysed using CasaXPS software (version 2.3.15). Component peaks were fitted with reference to the binding energy of neutral (adventitious) carbon at 284.6 eV. The peak area ratios for various elements were corrected by experimentally determined instrumental sensitivity factors in the survey spectra. Core level C 1s, N 1s and Cl 2p spectra, after (Shirley) background subtraction, were curve-resolved using a Gaussian line shape with Lorentzian broadening function. Cl 2p spectra were resolved into Cl $2p_{3/2}$ and Cl $2p_{1/2}$ doublets, which are about 1.6 eV apart. Deconvolution was conducted by keeping approximately equal full-width half maxima (FWHM) for all the

components. For the illustration purpose, a spectrum of PANI-ME membrane that has been resolved into various components without background subtraction is shown in Figure 3.2.

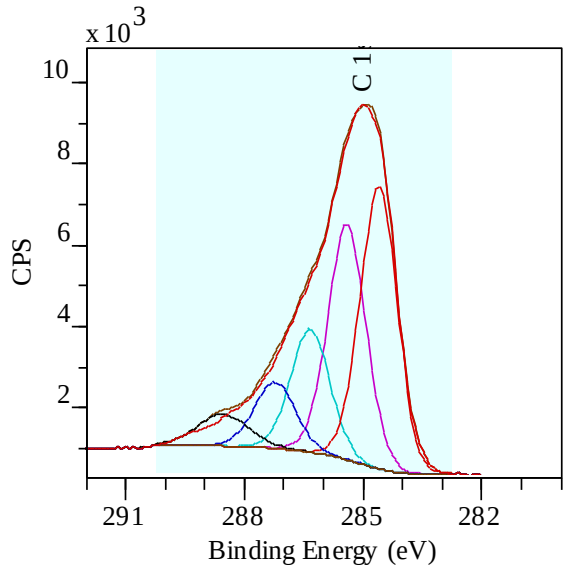

Figure 3.2: *XPS core level spectrum of a PANI-ME membrane showing Shirley background subtraction.*

3.2.6 Electrochemical Impedance Spectroscopy (EIS)

(An overview of EIS is presented here whereas the detail of the methods used are given in Chapter Five).

Electrochemical impedance spectroscopy (EIS) is a useful technique to study the interfacial transfer and bulk transport processes of membranes and films in electrochemical cells. A sinusoidal input signal of small amplitude is applied to the sample to displace it slightly from its electrochemical equilibrium state and the sinusoidal response is measured [132]. In potentiostatic EIS, electrical potential perturbation is applied whereas in galvanostatic EIS, electrical current is applied. For a given potentiostatic input signal v (V)

$$v = V_o \, sin(\omega t) \tag{3.6}$$

where V_o is potential amplitude (V), ω is angular frequency (radian. s^{-1}) i.e. $\omega=2\pi f$ (f: cycle. s^{-1}). The response is sinusoidal current (i) that is given by

$$i = I_o \sin(\omega t + \phi) \tag{3.7}$$

where I_o is the amplitude (A) of current wave i and ϕ is lag/lead angle. For a pure resistance, $\phi = 0$ and the response current is in-phase whereas for a pure capacitance, $\phi=\pi/2$ radians (90^o) and response is totally out of phase. The practical systems are mixed-resistance-capacitance so ϕ varies between 0-90^o depending upon the relative contribution of the two elements. The leading current (i.e. negative ϕ), in the response indicates inductance. Because of the existence of both real and imaginary components of the response, instead of an in-phase resistance, a complex resistance called impedance is used that is defined as Z(w) = $\frac{i(\omega)}{v(\omega)}$. Impedance is modelled as an element consists of a pure resistance and a pure capacitance connected in series so the impedance is given by

$$Z(\omega) = R - \frac{j}{\omega C} \tag{3.8}$$

where R is resistance (ohm) and C is the capacitance (F) which introduces imaginary component in the response. Generally, impedance is represented as a combination of real and imaginary components.

$$Z(\omega) = Z_{\mathrm{Re}\,al} - Z_{\mathrm{Im}\,aginary} \tag{3.9}$$

The imaginary component of the impedance in this R-C series element is called capacitor's reactance, $X_c = \frac{1}{\omega C}$. The electrochemical systems such as electrodes, films and membranes can be modelled as the combination of various electrical elements such as resistor, capacitor and inductor. Impedance shows real and imaginary components depending upon the number of constituent basic elements and their arrangement in the electrochemical model of the electrochemical systems.

EIS results are presented either as Nyquist or Bode diagrams (Figure 3.3). In Nyquist diagram imaginary versus real components of impedance are plotted. Bode plot comprises two sub-plots i.e., impedance amplitude and phase angles (ϕ) versus frequency. The transference processes taking place at the membrane/electrolyte interface and transportation of ions (and polarons in the case of PANI) in the membrane bulk are analysed by studying EIS data either in Nyquist or in Bode forms, each of which gives advantage over other in some specific circumstances.

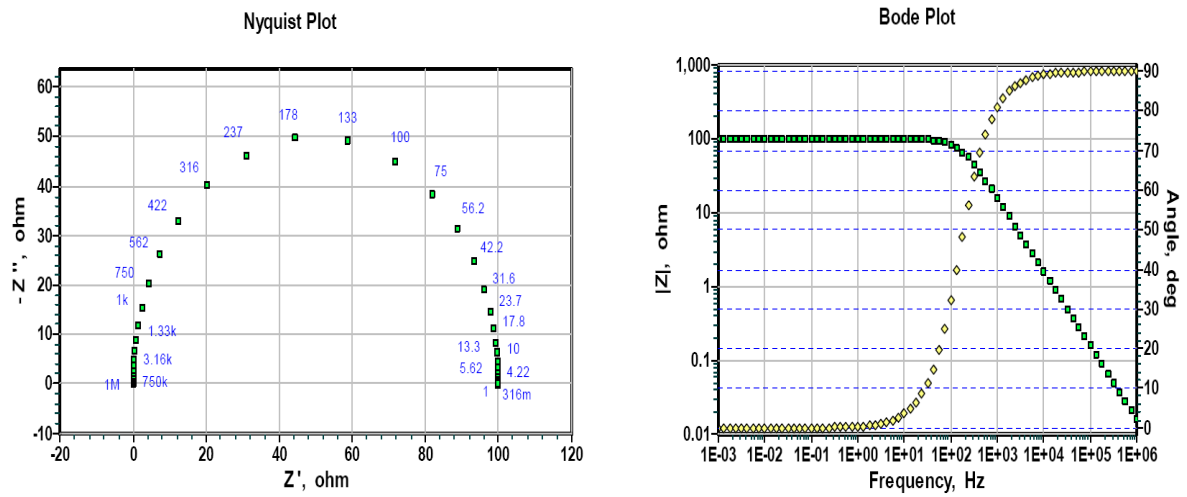

Figure 3.3: *Typical representation of EIS data (a) Nyquist and (b) Bode (b) plot (Note: These plots are generated by using ZSimpWin® Software).*

EIS of the PANI composite membranes in this research has been conducted by using two types of electrochemical configurations:

1. The electrolyte-soaked membranes are sandwiched between two electrode plates (0.636 cm^2).

2. PANI composite membranes were interposed between the two compartments of a permeation cell with Pt electrodes adhering to the both surfaces of the membranes whereas each compartment was filled with electrolyte (0.636 cm^2).

Moreover, each membrane was equilibrated both in 1M HCl, (PH < 1), water (pH~6) or 1M $CaCl_2$ (pH~12) solution, separately, to investigate the effects of doping state of PANI on the charge transport properties of the composite membranes. A number of composite membranes synthesized by using various polymerization techniques were employed in EIS studies to investigate the effects of various PANI deposition sites on the electrochemical characteristics of the membranes. The experimental conditions are summarized in Table 3.1.Please note that unmodified ME membranes in HCl, water and $CaCl_2$ were also tested to observe the EIS behaviour of the base membrane.

EIS was conducted in potentiostatic mode by the application of a small-amplitude of potential. The input signal was supplied and response was measured by using VersaSTAT3 Potentiostat (PAR Inc. U.S.A). EIS results have been analysed by fitting the equivalent

circuits that consist of various elements each approximate the resistance and capacitance in the physical electrochemical systems. ZSimpWin® electrochemical analysis software from Princeton Applied Research Inc. (PAR, U.S.A) has been used. The quality of the model fitting was assessed by the chi-squared (χ^2) value.

Table 3.1: Summary of the EIS experimental conditions

Polymerization technique	Polymerization time (Membrane identification)	Electrolyte	Electrochemical cell configuration
Solution-phase	1. 6 h (ME, Poly, Fe, 6h) 2. 22 h (ME, Poly, Fe, 22h)	HCl Water $CaCl_2$(pH~12)	1. Soaked membranes between two gold discs 2. 2-Pt wires attached with the membrane with electrolyte bathing.
Two-compartment cell	1. 2 h (ME, P1, Fe, 2h) 2. 6 h (ME, P1, Fe, 6h) 3. 22 h (ME, P1, Fe, 22h)	HCl Water $CaCl_2$(pH~12)	1. Soaked membranes between two gold discs 2. 2-Pt wires attached with the membrane with electrolyte bathing.
Vapour-phase	Soaked in aniline for 2.5 h and then polymerized for ~10 min. (ME,AN2.5,Vap)	HCl Water $CaCl_2$(pH~12)	1. Soaked membranes between two gold discs 2. 2-Pt wires attached with the membrane with electrolyte bathing.

Note. For membranes identification, please see Nomenclature (section 3.3).

3.2.7 Transport Number Measurements

Ionic transport through PANI composite membranes were studied by conducting the linear polarization experiments in the two-compartment permeation cell where membrane was interposed between the two-compartments of a permeation cell. A cell with each

compartment capacity of 80 ml was used and the ionic flux passed through a 1.7 cm^2 membrane cross section perpendicular to the flow. Linear polarization was performed in two-electrode configuration where Ag/Ag reversible electrodes were used for electrical potential input and current measurement. An electrical potential range -1000 to +1000 mV was traversed by using VersaSTAT3 Potentiostat (PAR Inc. U.S.A). Solutions of $CaCl_2$ and HCl were used for high and low pH behaviour with different concentrations in both compartments of the cell. The concentration was fixed 1M in one compartment whereas it was changed from 1 to 0.001 M, logarithmically, in the second compartment. Before each measurement, asymmetric potential of Ag/AgCl electrode pair was recorded which remained < 3 mV throughout the experiment.

3.3 Nomenclature

A descriptive nomenclature has been used for PANI composite membranes in this thesis. This includes base membrane (ME: mixed cellulose ester, CA: cellulose acetate), polymerization technique (Poly: solution-phase, Vap: vapour-phase, P1: two-compartment cell) and polymerization time (h, min or 'm', d (days)). The oxidant is specified by (Fe: $FeCl_3$, APS: ammonium persulfate) wherever required. In some places, an aniline-soaking time in the vapour-phase polymerization is also specified by AN (h)). An example is given, below, elaborating the used nomenclature system.

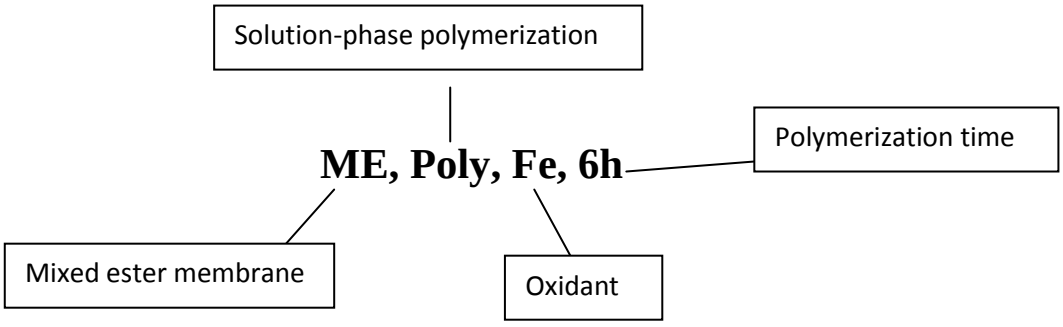

Chapter Four

Control of PANI Deposition Site and Extent in the Composite Membranes

4.1 Introduction

PANI deposition levels and its oxidation and doping states on a substrate are varied depending on the chemical nature of the substrate and conditions of *in situ* polymerization. Chemical oxidative polymerization of aniline is conducted, normally, in the presence of organic or inorganic acids such as HCl, H_2SO_4, H_3PO_4 and p-toluene sulfonic acid (pTSA). These acids are mainly incorporated in the reaction mixture to catalyse the oxidative polymerization reaction but the acid anion also dopes PANI chains along with the anion dopant from other reacting species (i.e. HSO_3^- from APS). Due to the high oxidation potential of the oxidant and low pH of the reaction medium, PANI is formed as emeraldine salt. The extent of aniline polymerization in the bulk polymerization depends on the reactants concentrations and polymerization time in addition to the nature of the oxidant [15, 50, 133, 134]. However, in the presence of a substrate, the deposition site and extent also depend on the chemical nature of the substrate and the various physical processes involved in the heterogeneous chemical reaction in the presence of functional substrate [13, 135-137].

A few groups have investigated the effects of various polymerization conditions on the PANI deposition site and its oxidation states on commercial ion exchange membranes. The PANI intercalation site in the base membrane affects the selectivity of the electrolyte through the membrane. Tan et. al. [109, 138] studied the effects of various oxidants on the PANI deposition site on base polystyrene-sulfonic acid membranes. The membranes were modified by the two-compartment cell polymerization technique where single step (simultaneous counter diffusion of monomer and oxidant) and two-step (addition of monomer and oxidant solutions in succession) polymerizations have been employed. A thin PANI layer was deposited on the oxidant-facing side of the membrane when APS was used as an oxidant whereas by using $FeCl_3$, PANI was deposited in the bulk membrane instead of surface layering. The sulfonate groups of polystyrene-sulfonate base membrane hindered the passage

of negatively charged $S_2O_8^{2-}$ species (generated from the decomposition of APS) by Donnan exclusion, which resulted in the diffusion of only anilinium ions ($C_6H_5NH_3^+$) to the oxidant-facing side of the two-compartment cell. In the case of $FeCl_3$ as oxidant, both positively charged oxidant (Fe^{3+}) and anilinium ions counter diffused simultaneously which resulted in aniline polymerization in the bulk membrane. Permeation studies of Zinc (Zn^{2+}) using these composite membranes showed that PANI layer on the surface of the base membrane blocked the bivalent cation transport over the proton transport as compared to the unmodified membrane.

In another study, Blinova et al. [126] elaborated the mechanism of PANI layering on the face of a microporous cellulosic dialysis tubing under diaphragmatic (i.e. monomer and oxidant counter-diffused across the membrane) polymerization condition. PANI was deposited on the monomer-facing side of the tubing as the result of chemical polymerization of aniline hydrochloride with ammonium persulfate (APS). A mechanism was proposed according to which monomer was polymerized by the simultaneous transference of electrons and protons across the deposited PANI layer without directly contacting the reactants. In the earlier studies, PANI deposition site was controlled by using the ion exclusion properties of the homogenous ion exchange membranes. These studies focused on the effects of different oxidants on the PANI deposition site and resultant membrane morphology. A systematic investigation of the effects of various *in situ* chemical polymerization techniques on PANI deposition on the base microporous membrane has not been presented so far. The special focus of this thesis is to deposit PANI on the pore walls of the base membrane by using the two-compartment cell technique. An earlier study showed PANI deposition in the pores of the ceramic discs using the same technique, however the effects of various polymerization conditions and the permeation of the oxidant and monomer controlled by the diffusional flow in the base membrane have not been discussed [105].

In this thesis, ME microporous membranes were modified with PANI that was deposited on the base membranes by using various chemical oxidative polymerization techniques. Each polymerization technique and the conditions in a single technique affected the PANI deposition site, deposition and doping levels. These parameters influence the permeability and selectivity of the composite membrane. The characterization of PANI deposition on ME membranes by using scanning electron microscopy (SEM), Fourier-transform infrared spectroscopy (FTIR) and x-ray photoelectron spectroscopy (XPS) has been discussed in the subsequent sections. XPS has been used to quantify PANI layering extent at the membrane

surface that affects the electrochemical performance of the composite membranes. The effects of PANI deposition site and extent on the electronic conductivity have been elaborated by measuring surface and trans-membrane conductivities. The possible mechanism of PANI deposition in the various employed techniques has been discussed in the last section of the chapter.

4.2 SEM Characterization of Composite Membranes

SEM micrographs of surface and cross section of unmodified mixed cellulose ester (ME) membrane are shown as Figures 4.1 (a) and (b), respectively. ME membranes used in this study are symmetric porous membranes with tortuous open pore structure. The structure of ME membranes can be imagined as a skeleton made of closely knitted cellulosic fibres forming micro-sized pores. Solution-phase polymerization of aniline was conducted by using, either, ammonium persulfate (APS) or $FeCl_3$ as an oxidant. The coated PANI layer, in the case of APS, was of dark green colour, initially, and turned blue afterwards. It turned blackish brown on prolonged polymerization (after ~ 20 minutes) due to PANI degradation by the over-oxidation at the employed concentrations. No degradation was observed in the case of $FeCl_3$ even after 72 hours of polymerization (Figure 4.1 c and d). Vapour-phase aniline polymerization yielded a compact, coherent but thin (< 10 μm) surface layer on the base membrane (Figure 4.1 e and f). During the polymerization in the two-compartment cell, PANI deposition initiated on aniline-facing side of the membrane and maintained its asymmetric growth in the bulk membrane throughout the polymerization. This particular polymerization technique demonstrated PANI deposition on the strands (fibres) of the base membrane network without blocking the pores (Figures 4.1 g-j), though the deposited PANI layer on membrane face grew with the polymerization time. The cross sectional views of membranes where the cellulose strands coating became intensified with polymerization time (Figures 4.1 h and j) also demonstrated the extent of 'in-pore' PANI deposition.

The solution-phase and vapour-phase polymerizations showed PANI surface layering whereas the bulk of the membrane remained unchanged. The two-compartment cell polymerization showed in-pore PANI deposition along with the surface layering. The surface coverage and in-bulk PANI deposition increased with the polymerization time. Two important aspects should be noted in this polymerization technique: the composite membranes remained porous even after a prolonged polymerization (> 6 h) and the PANI was deposited on the fibres of the membrane skeleton instead of the pore-filled deposition.

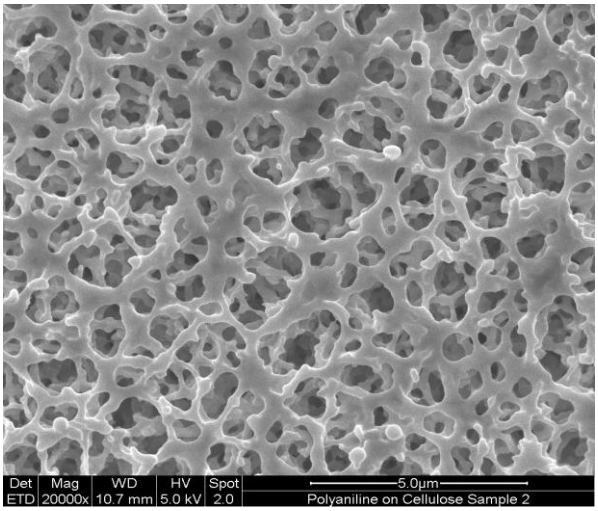
Det Mag WD HV Spot
ETD 20000x 10.7 mm 5.0 kV 2.0
5.0µm
Polyaniline on Cellulose Sample 2

(a)

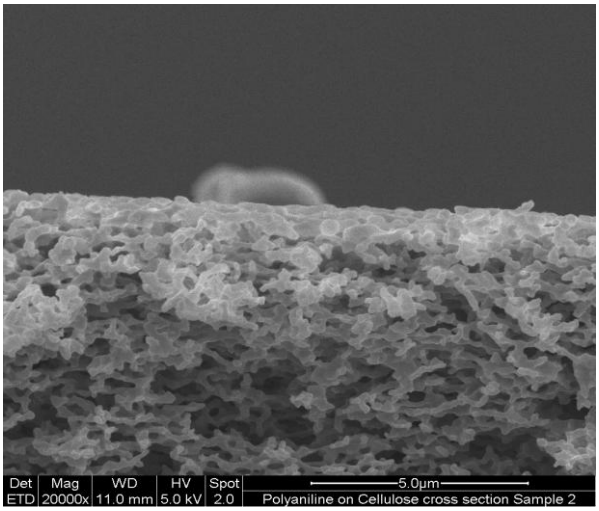
Det Mag WD HV Spot
ETD 20000x 11.0 mm 5.0 kV 2.0
5.0µm
Polyaniline on Cellulose cross section Sample 2

(b)

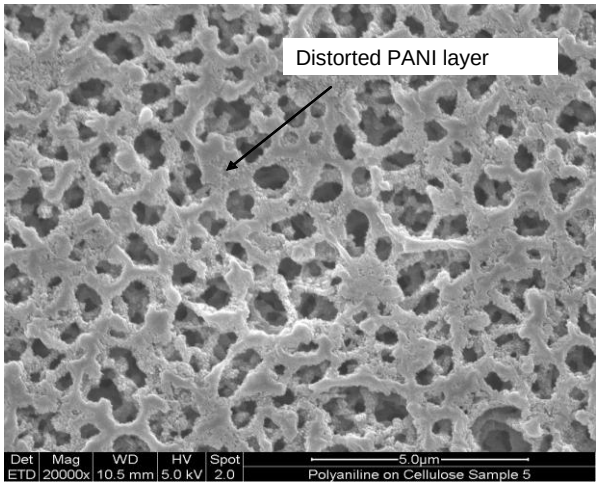
Distorted PANI layer
Det Mag WD HV Spot
ETD 20000x 10.5 mm 5.0 kV 2.0
5.0µm
Polyaniline on Cellulose Sample 5

(c)

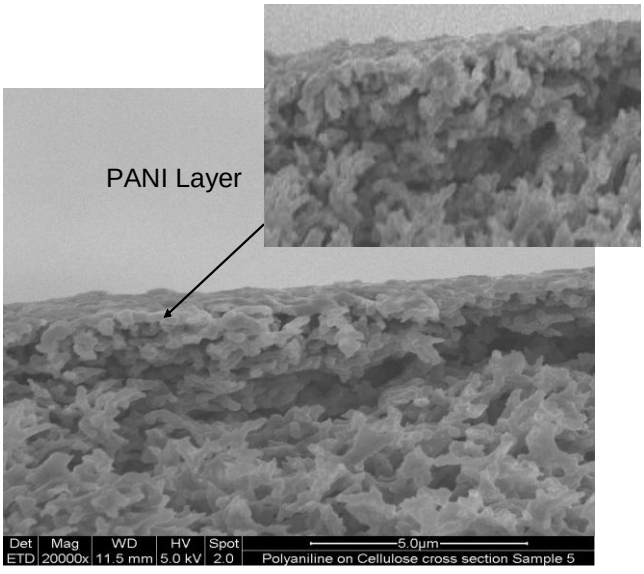
PANI Layer
Det Mag WD HV Spot
ETD 20000x 11.5 mm 5.0 kV 2.0
5.0µm
Polyaniline on Cellulose cross section Sample 5

(d)

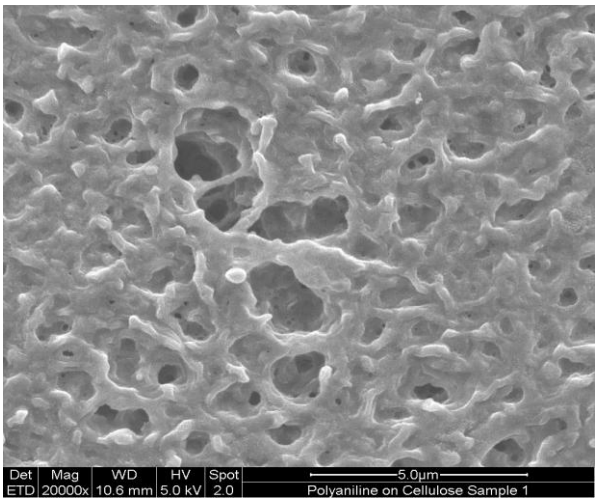
Det Mag WD HV Spot
ETD 20000x 10.6 mm 5.0 kV 2.0
5.0µm
Polyaniline on Cellulose Sample 1

(e)

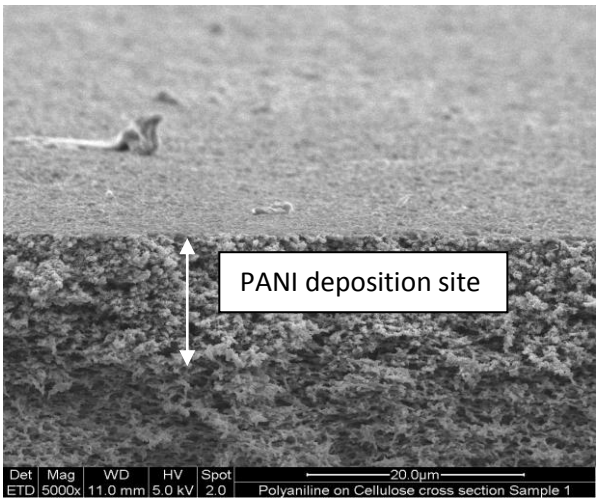
PANI deposition site
Det Mag WD HV Spot
ETD 5000x 11.0 mm 5.0 kV 2.0
20.0µm
Polyaniline on Cellulose cross section Sample 1

(f)

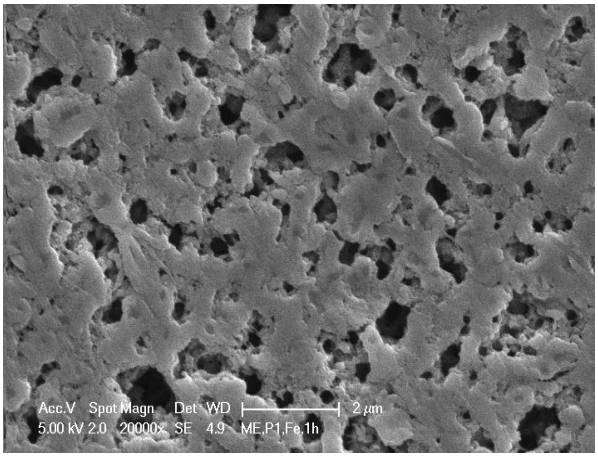
Acc.V Spot Magn Det WD 2 µm
5.00 kV 2.0 20000x SE 4.9 ME,P1,Fe,1h

(g)

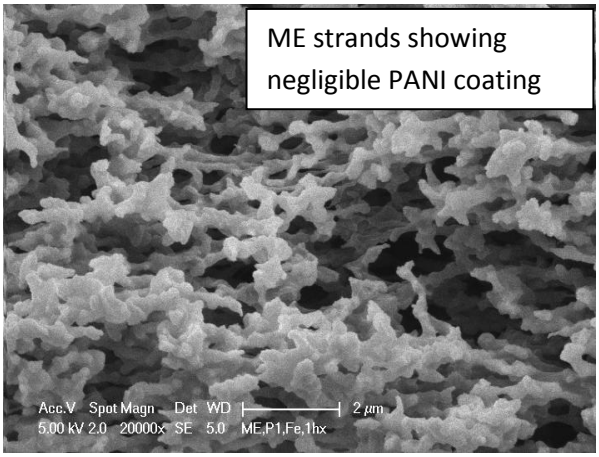
ME strands showing
negligible PANI coating
Acc.V Spot Magn Det WD 2 µm
5.00 kV 2.0 20000x SE 5.0 ME,P1,Fe,1hx

(h)

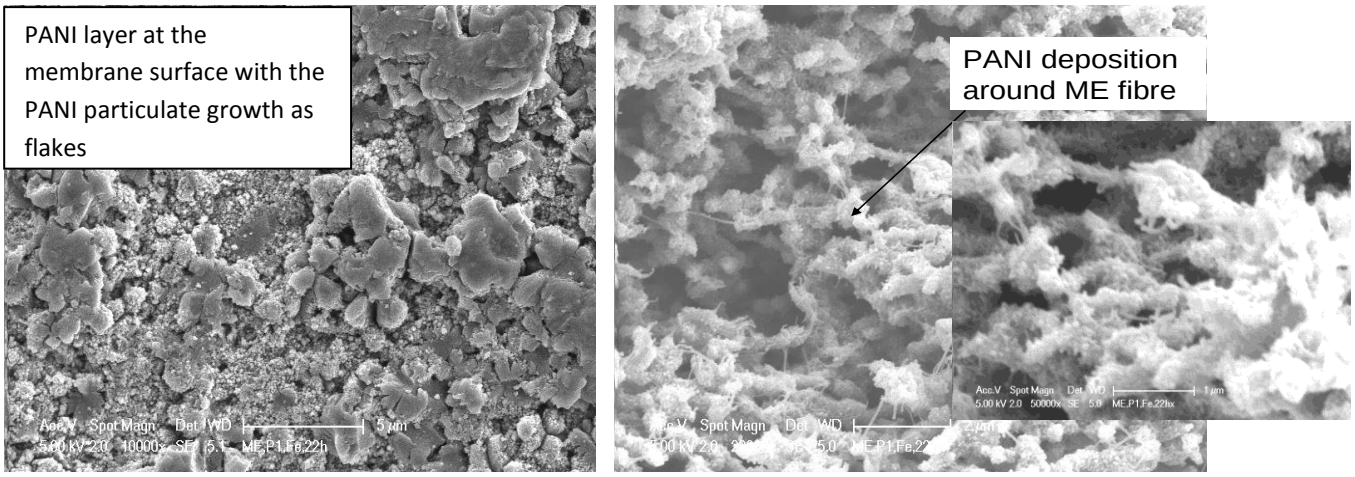

(i) (j)

***Figure 4.1**: SEM micrographs of membranes surface and cross section, respectively, (a) & (b) bare ME membrane; (c) & (d) ME,Poly,APS,15m; (e) & (f)ME,Vap,APS,15m; (g) & (h) ME,P1,Fe,1h; (i) and (j) ME,P1,Fe,22h (The inserts show higher magnification images).*

To confirm PANI deposition on the pore walls without blocking the membrane pores, cellulose nitrate (CN) filters with large-pore (0.45 μm) were modified by using two-compartment cell polymerization with both oxidants ($FeCl_3$ and APS), separately. The difference in PANI morphology with the two different oxidants is evident in SEM micrographs of the composite membranes. SEM image with $FeCl_3$ clearly shows PANI deposition as a thin layer on the cellulose fibres (Figures 4.2 a & b). PANI was deposited as more conventional nodular nanoparticles in the case of APS, stacked vertically on the membrane surface (Figures 4.2 c & d).

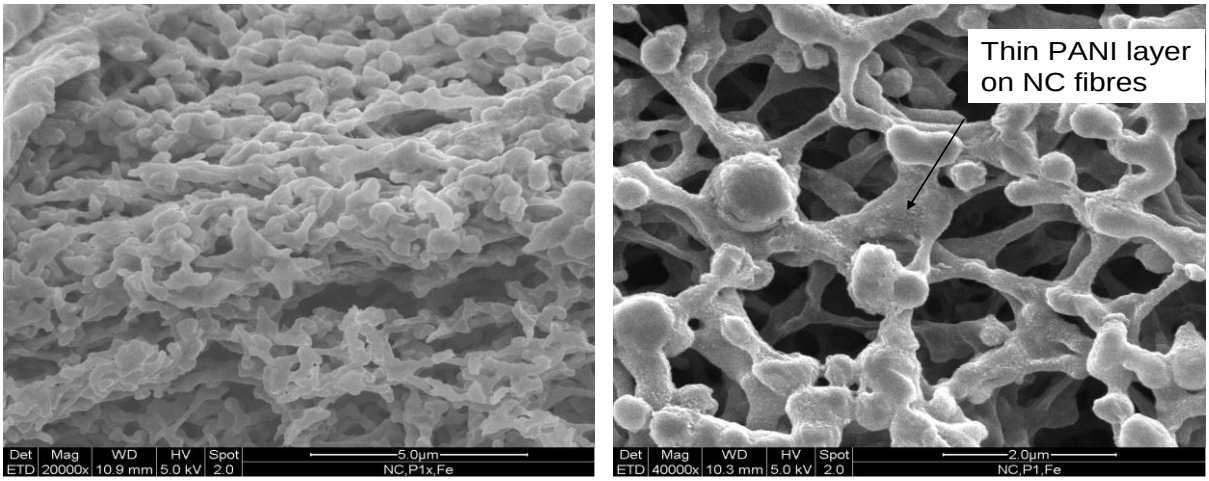

(a) (b)

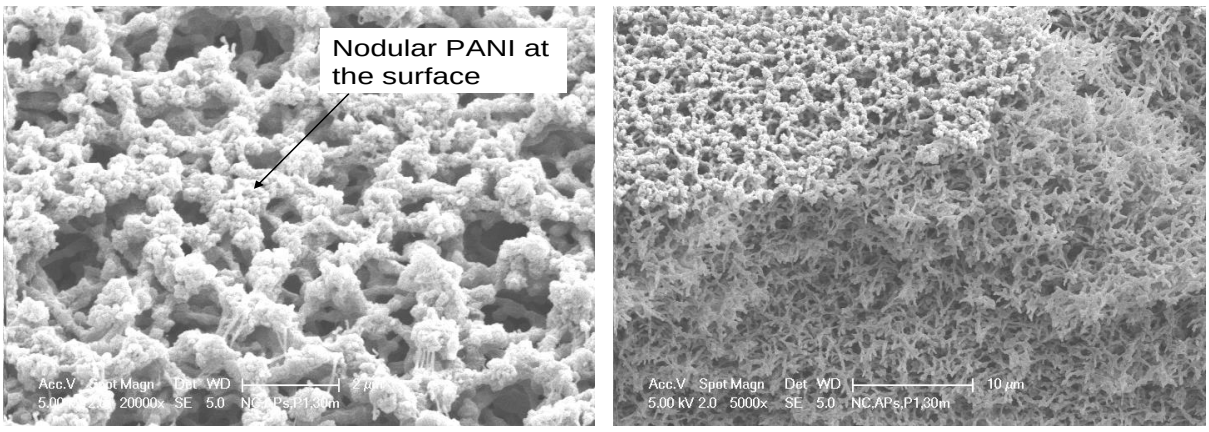

(c) (d)

Figure 4.2: *SEM micrographs of composite membranes, (a & b) NC (Nitrocellulose), P1, Fe,30min surface and cross section, respectively (c & d) NC,P1,APS,30min , surface and cross section, respectively.*

4.3 PANI Intercalation Levels in the Composite Membranes

The intercalation levels of PANI in the base ME membranes were measured by the gravimetric technique and these are shown in Table 4.1.

Table 4.1: PANI intercalation levels in the membranes

Membranes	PANI %
ME,Poly,Fe,6h	5.9
ME,Poly,Fe,22h	12.6
ME,P1,Fe,2h	1.9
ME,P1,Fe,6h	33.9
ME,P1,Fe,22h	50.1
ME,AN2.5,Vap	19.5

The values in Table 4.1 show PANI intercalation levels in the membranes as polymerization technique dependent. Solution-phase polymerization yielded the lowest values with respect to the polymerization times that indicate only surface deposition. Higher values from the two - compartment cell technique show PANI deposition inside the bulk of the membrane (i.e. in the pores) along with the surface deposition. Keeping in view the high porosity of the base membrane (~75%) and the maximum PANI deposition level from the solution-phase (12.6 % from 22h polymerization), it can be concluded that PANI was deposited inside the pores of the membrane from the two-compartment cell polymerization. SEM images show PANI deposition on the skeleton fibres and almost complete membrane surface coverage at prolonged polymerization (Figures 4.1 i and j). In this case, the high intercalation level may also be attributed to the PANI deposition as the growing flakes at the surface. Vapour-phase polymerization showed deposition level higher than that from 22h solution phase polymerization indicating more compact and dense PANI layering at the surface. However, it may also represent the entrapped electrolyte (anilinium ions) inside the pores due to very rapid surface layering which resulted from a very fast vapour-liquid phase polymerization

reaction. This aspect will be discussed in detail latter in this chapter and the effects on electronic and ionic conduction will be discussed in next chapter.

4.4 FTIR-ATR Spectroscopy of Composite Membranes

FTIR is a powerful technique to study the surface characteristics of a material up to a few micrometer depth. Infrared spectra of thee composite membranes were acquired using attenuated-total-reflectance (ATR) mode. The raw spectra were corrected for baseline and ATR shifts.

FTIR spectrum of unmodified ME membrane shows dominant cellulose nitrate peaks along with minor cellulose acetate bands (Figure 4.3). The wave number of the characteristic bands in mixed cellulose esters are given in Table 4.2 [139].

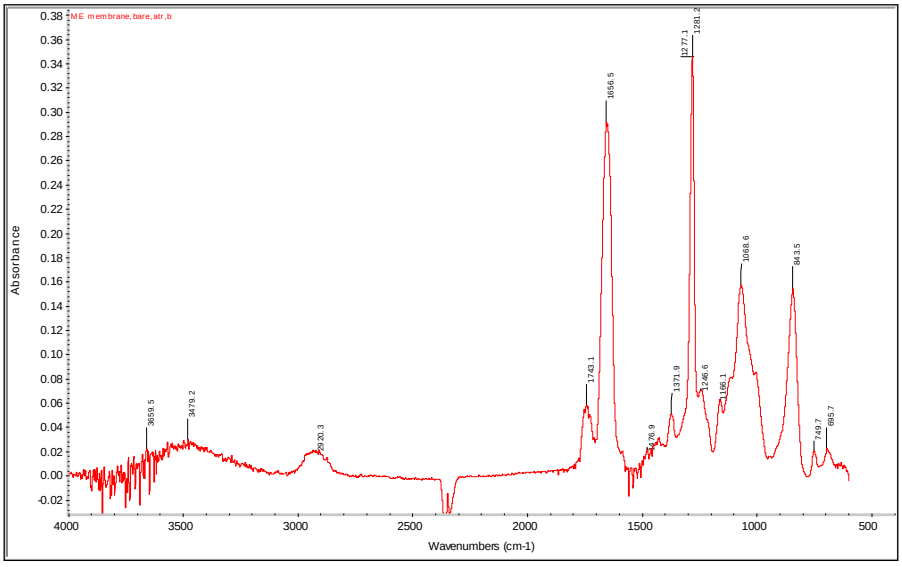

Figure 4.3: *FTIR-ATR spectrum of unmodified ME membrane.*

Table 4.2: Infrared peaks for ME membranes

Wave Number (cm^{-1})	**Assignment**
1745	C=O stretching
1655	NO_2 stretching (asym.)
1371	CH_3 bending
1280	NO_2 stretching (sym.)
1070	C-O-C (C-O)
845	O-NO_2 stretching

PANI deposition on the base membrane is evidenced by the appearance of various PANI bands at 1585 cm^{-1}(quinonoid), 1485 cm^{-1}(benzenoid) and 1150 cm^{-1}(polaron) in conjunction with the growth of peak at 1612 cm^{-1} arising from the benzene ring in PANI backbone chain (Figure 4.4) [14, 140, 141]. In addition to the confirmation of PANI deposition on the surface of the membrane, the effects of the polymerization techniques on PANI deposition can be studied qualitatively by analysing the FTIR spectra of the composite membranes. The extent of membrane surface coverage by PANI is indicated by the relative suppression of nitrate ester peaks at 1655 cm^{-1} and 1280 cm^{-1} and by the emergence of PANI peaks at the characteristic wave numbers given above. Additionally, the oxidation state of deposited PANI can be assessed by the relative intensity of quinonoid and benzenoid peaks.

Solution-phase aniline polymerization for prolonged times (i.e.ME,Poly,Fe,22h) shows very weak PANI bands indicating an incomplete surface coverage. However, almost complete coverage can be achieved for prolonged polymerization (i.e. for >72) where strong PANI peaks have been evidenced. Vapour-phase deposition (ME,Vap,APS,10m) shows PANI bands of intermediate strength, indicating a thin and incomplete PANI layer at the surface. Composite membranes synthesized by the two-compartment cell show PANI deposition extent improving with the polymerization time (comparing ME,P1,Fe,6h with ME, P1,Fe,22h). A complete surface coverage with PANI is evidenced from the presence of strong peaks in ME,P1,Fe,22h as compared to that in the membranes modified by solution-phase polymerization for the same time (ME,Poly,Fe,22h). An symmetric deposition of PANI in membrane bulk is also observed by recording less prominent PANI peaks on the oxidant-

facing side of the membrane (ME,P1,Fe,6h(o)) compared with that from the aniline-facing side (ME,P1,Fe,6h).

Although PANI deposition on ME membranes and the effects of various polymerization techniques and conditions have successfully been characterized by using FTIR-ATR spectroscopy, some ME characteristics bands might interfere with the PANI bands and hence limit the full potential of this technique in this case. Particularly ME bands for NO_2 (sym.) at 1280 cm^{-1} and NO_2 (asym.) at 1655 cm^{-1} can interfere with PANI characteristics bands such as π electron conjugation at 1305 cm^{-1} and aromatic stretching band around 1612 cm^{-1}. To study the PANI deposition characteristics more clearly, cellulose acetate microporous membranes have also been modified by using the same *in situ* PANI deposition techniques and conditions as used for ME membranes. Investigation of PANI deposition on cellulose acetate membranes yields two additional features: it confirms the characteristics effects of

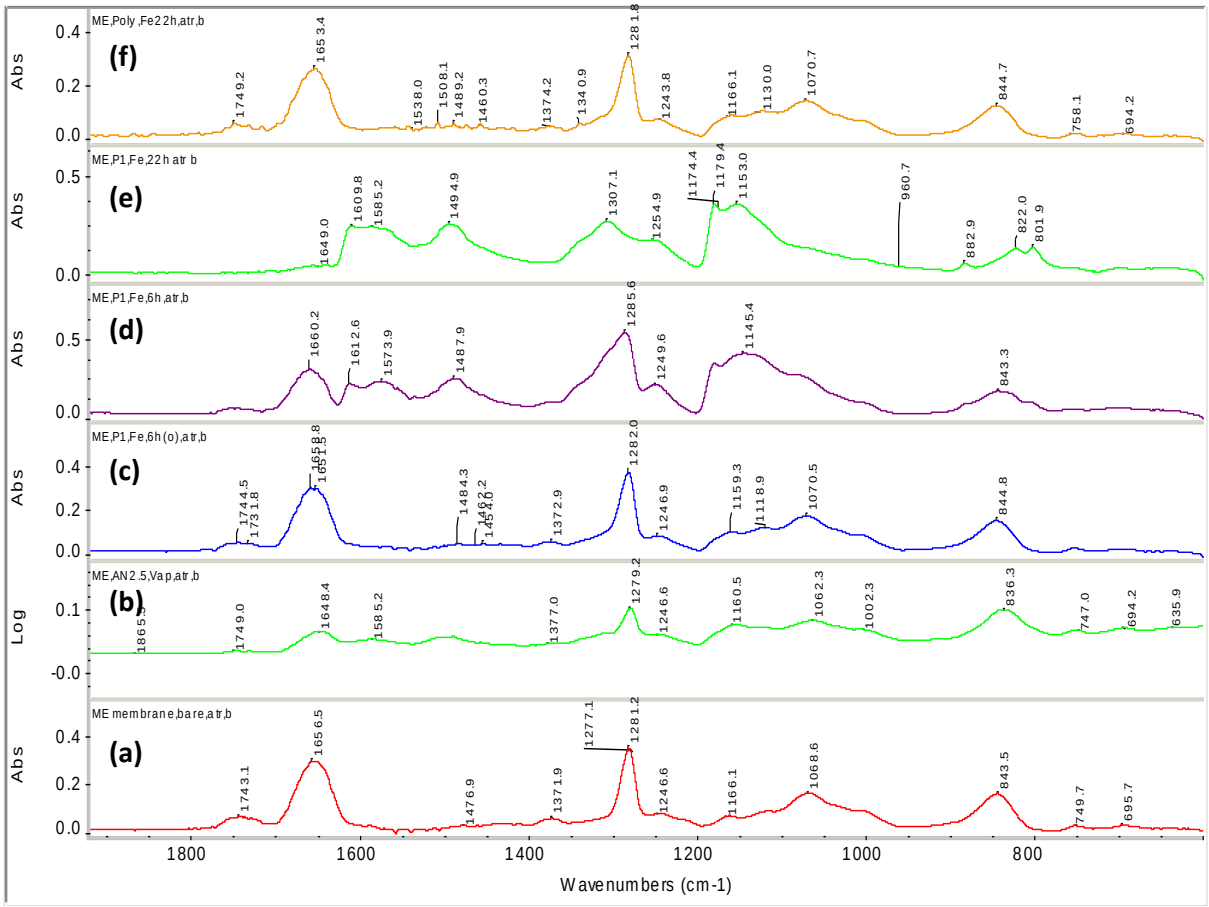

Figure 4.4: *FTIR-ATR spectra of PANI-ME composite membranes (a) bare ME membrane (b) ME,AN2.5,Vap (c) ME,P1,Fe, 6h(o) (d) ME,P1,Fe,6h (e) ME,P1,Fe,22h and (f) ME, Poly,Fe,22h.*

various polymerization techniques on PANI deposition levels and oxidation/doping states and also more clearly elaborates the effects of NO_2 group on PANI deposition site and extent as discussed in the last section of this chapter.

The FTIR-ATR spectra of unmodified cellulose acetate (CA) and CA-PANI composite membranes, synthesized by using various (but similar to that of PANI-ME membranes) polymerization techniques are shown in Figure 4.5.

The prominent IR bands characterizing various functionalities in cellulose acetate are identified at 1735 cm^{-1} (C=O stretching), 1368 cm^{-1} (C-H stretching), 1230 cm^{-1} (C-O stretching) and 1065 cm^{-1} (C-O-C stretching) [142]. The characteristic benzenoid (1485 cm-1) and quinonoid (1575 cm^{-1}) bands characterize PANI deposition on the membranes. The growth of these PANI bands in comparison with the cellulose acetate bands indicates PANI layering extent on the base membrane surface. The peaks at 1306 cm^{-1} and at 1150 cm^{-1} are attributed to π electron conjugation and $–NH^{+}=$, respectively, in doped conducting emeraldine [14, 141].

Various polymerization techniques showed trends for deposition levels similar to that observed in PANI-ME membrane syntheses. Two-compartment cell polymerization showed time-dependent surface layering comparable to the vapour-phase and prolonged solution-phase polymerizations. However, PANI layering at the surface as indicated by the suppression of cellulose acetate bands and growth of PANI bands is of lesser extent as compared to the layering on ME membranes (comparing with Figure 4.4). This may show the effects of pore size and presence of NO_2 on PANI deposition. CA membranes has a nominal pore size 0.45 μm compared to 0.22 μm of ME membranes. The larger pores in the former case also facilitate the flow of reactants by offering less diffusion resistance as compared to ME membrane. The smaller PANI deposition at the surface of CA-PANI membranes may be attributed to this fact. Secondly, NO_2 groups play important role in anchoring anilinium ions at the surface and also in the ion exchange process during the two-compartment cell polymerization which might increase the PANI deposition for the comparable time on ME base membrane. The mechanisms involved in the various polymerization techniques are discussed in the last section of this chapter.

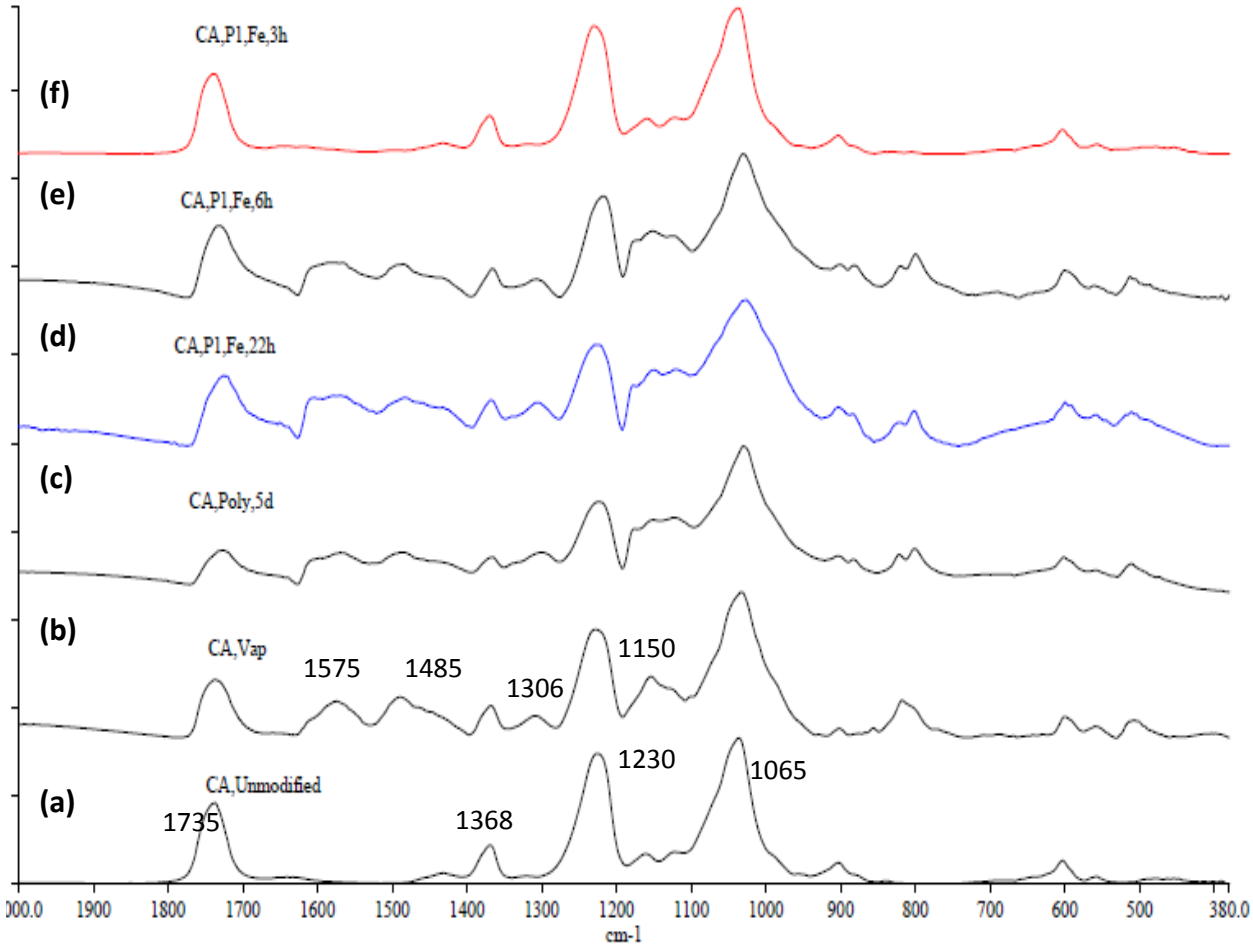

***Figure 4.5**: FTIR-ATR spectra of PANI-cellulose acetate composite membranes (a) bare CA membrane (b) CA,AN,Vap (c) CA,poly,Fe,5d (d) CA,P1,Fe,22h (e) CA,P1,Fe,6h and (f) CA,P1,Fe,3h.*

4.5 Electrical Conductivity Measurements

Electrical conductivity of the composite membranes measured by four-point probe technique are shown in Figures 4.6 a & b. The conductivity values of cellulose acetate membranes modified with PANI have also been included in these figures for comparison purpose. Similar levels of electrical conductivity have been recorded when the same polymerization methods were used with similar times on CA base membranes. This trend indicates that the composite membrane morphology resulted from the specific PANI deposition method is the dominant factor which controls the electrical conductivity of the membranes (see ME/CA,P1,Fe,6h, ME/CA Poly,Fe,48h, ME/CA APS (Vap) in Figure 4.6 a). Membrane prepared by the two-compartment cell technique at longer polymerization time (> 6 h) shows higher level of conductivity signifying the higher PANI fraction within the membrane bulk and extent of

PANI coating on the cellulosic strands of the membrane. Asymmetric PANI deposition is evidenced by the electrical conductivity measurement at the opposite faces of the composite membranes where the oxidant-facing surface shows significantly lower conductivity values as compared to the values from the opposite side (see ME,P1,Fe,1 h and ME,P1,Fe,1h(o) in Figure 4.6 a). Solution-phase polymerization shows higher levels of conductivity with APS as oxidant and lower values for $FeCl_3$, probably due to the higher extent of PANI deposition at the surface through a faster chemical reaction. Vapour-phase polymerization shows conductivity values in the range of 10^{-2} -10^{-1} $S.cm^{-1}$ owing to a continuous PANI layer at the surface. Conductivity values for the membranes synthesized by the two-compartment cell demonstrate strong dependence on the polymerization time that indicates the higher deposition extent at the surface. The higher conductivity values showing the uniformity of PANI surface layer as compared to that from other two techniques.

To investigate the effects of in-pore PANI deposition on the electrical properties of the composite membranes, trans-membrane conductivities measured from a two-point method are also shown (Figure 4.6 b). In the two-point conductivity measurement, electrical charge is forced to flow through the thickness of the composite membranes. Although these measurements are not as accurate as that from the four-point probe technique, yet these can be used for comparison purpose. Four-point technique yields sheet conductance where electrical conductivity (specific conductance) is calculated by assuming a uniform conductivity value throughout the membrane bulk (cross section). The composite membranes synthesized by the two-compartment cell polymerization show two to three orders of magnitude higher conductivity values because of the greater deposition of PANI inside the membrane bulk. Membranes modified either by the solution-phase or by vapour-phase polymerization show almost similar conductivity values due to nearly same PANI deposition at the surface and its oxidation and doping state. Time emerges as an important factor within a single polymerization technique. Higher conductivity values for longer polymerization times, for example in the two-compartment cell, signify greater in-bulk PANI deposition.

$FeCl_3$ and APS (both in HCl) were used as oxidant in the two-compartment cell and vapour-phase polymerizations, respectively. $FeCl_3$ was used, mainly, as the oxidant in the solution-phase polymerization. A few membranes were also modified using APS, initially. For APS + HCl case, $S_2O_8^{2-}$ and Cl^- both act as doping anions for PANI. However, the prolonged dipping in 1M HCl for more than 24 h (section 3.1.2) yielded dominant Cl^- doping and the

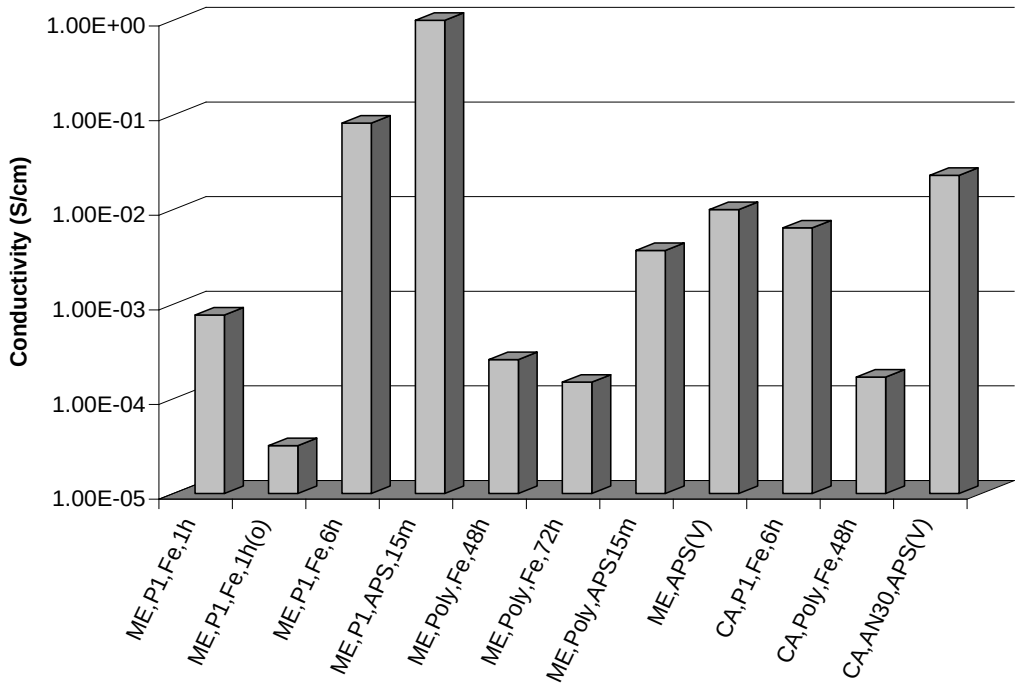

(a)

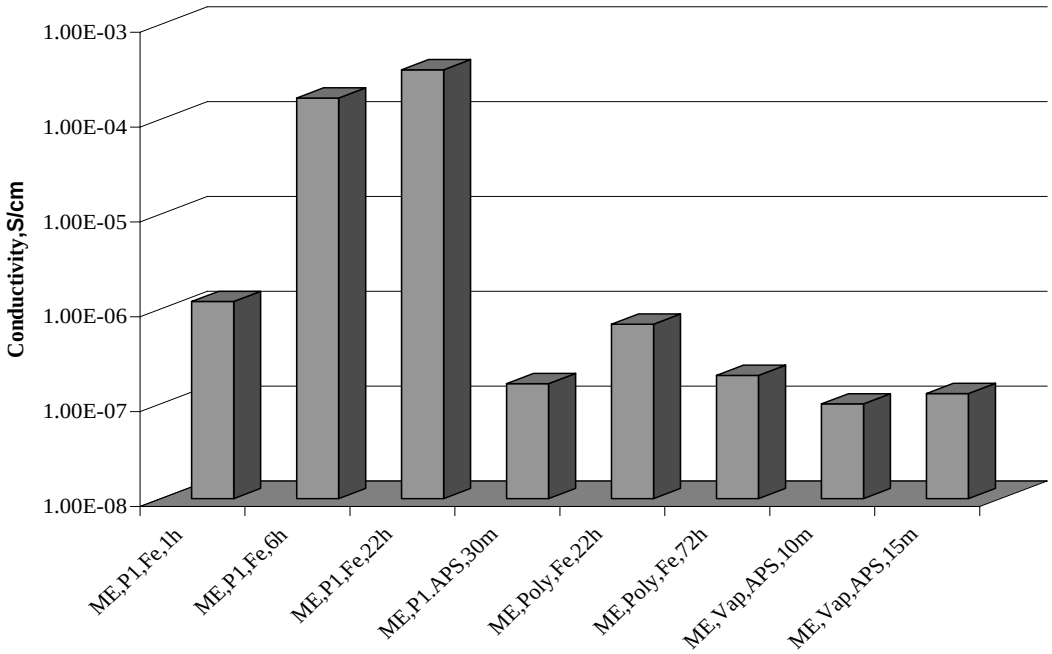

(b)

Figure 4.6: *Electrical conductivities of PANI-ME membranes (a) Surface conductivities by four-point technique (b) Trans-membrane conductivities by two-point method.*

conductivities only depend on PANI deposition site and levels in the membranes. The dependence of PANI formation rate on different oxidant is discussed in section 4.7.2.

4.6 Surface Characterization of PANI Composite Membranes

Under the employed conditions of solution- and vapour-phase polymerizations, PANI deposition began at the interface of ME membrane and the reaction mixture. In the two-compartment cell polymerization, PANI deposition started at the monomer-facing side of the base membrane and then progressed through the membrane bulk with comparatively smaller deposition on the oxidant-facing side of the membrane. PANI deposition levels and its oxidation and doping states were polymerization technique and time dependent in all the employed techniques. Hence, the effects of various contacting patterns of the monomer and oxidant in aniline polymerization and polymerization time were studied by characterizing PANI deposition on the surface of the base membrane. In addition, because these membranes are developed for electrochemical based applications, the surface properties play an important role in the permeation and selectivity performance of the membranes in these electrochemical processes. The ionic charge from electrolyte is transferred to the electronic charge in the membrane via a charge transfer reaction at the membrane/electrolyte interface. PANI deposition levels and its oxidation and doping states at the surface of PANI-ME composite membranes strongly affect the nature and extent of charge transfer processes at the interface.

In this thesis, X-ray photoelectron spectroscopy (XPS) was used to characterize PANI deposition at the surface of the base membrane. Identification of the oxidation state and PANI doping levels in pristine PANI and PANI composites [143-146] has been conducted by using XPS. Neoh et al. [147] discussed the limitations of XPS investigation on conducting polymers. Surface and bulk compositions were determined for PANI powder and films by using XPS. The effects of doping anion size and doping/undoping sequence on the doping level of PANI have been elaborated. In addition to the studies on pristine PANI powders and films, few studies have been conducted on the blends and composites of PANI with other polymers, especially in the powder form. These include polyurethane-PANI [148], polyimide-PANI [140] and PVC-PANI [149] composites. In these studies, PANI oxidation states have been identified and quantified in addition to the detailed XPS characterization of the base polymer. Loh et al. [150] characterized acrylic acid functionalized PANI by studying the N 1s and C 1s core level spectra of as-formed surfaces. It was shown that plasma assisted grafting of acrylic acid has decreased the intrinsic oxidation state of polyaniline significantly due to an oxidative degradation of polyaniline at the surface. Modification of PANI by sulfonation (“self-doped PANI”) has been characterized by XPS [151, 152]. XPS core level

spectra revealed substitution of $–SO_3H$ group in the phenyl ring yielding PANI in its doped emeraldine form. Sulfonated PANI showed unchanged protonation level under high vacuum in contrast to HCl doped PANI which lost doping anion under vacuum in XPS chamber.

To correlate the surface composition with the electrodialysis performance of a PANI-ion exchange membrane, surface chemical composition was characterized by XPS analysis [110]. In this study, PANI was deposited on the surface of a commercial sulfonated cation-exchange homogenous membrane by using the two-compartment cell polymerization technique. PANI deposition by ~1 h polymerization yielded the composite membrane with maximum cation blocking efficiency in electrodialysis. XPS analysis revealed that the polymerization reaction longer than 1 h degraded the deposited layer to quinone via PANI hydrolysis reaction that reduced the membrane selectivity from its maximum level at 1 h polymerization. In addition, PANI oxidation and doping states and its interaction with the matrix of base cation-exchange membrane were also discussed.

4.6.1 XPS Characterization of PANI-ME Composite Membranes

Mixed cellulose ester membrane contains cellulose nitrate and cellulose acetate as the constituting components in 75:25 ratio (Figure 4.7). XPS survey spectra of all the membranes showed the presence of C, N, O, Cl, Fe and S atomic species. Sulfur was found in the membranes prepared by using APS as oxidant whereas Cl was present as doping anion.

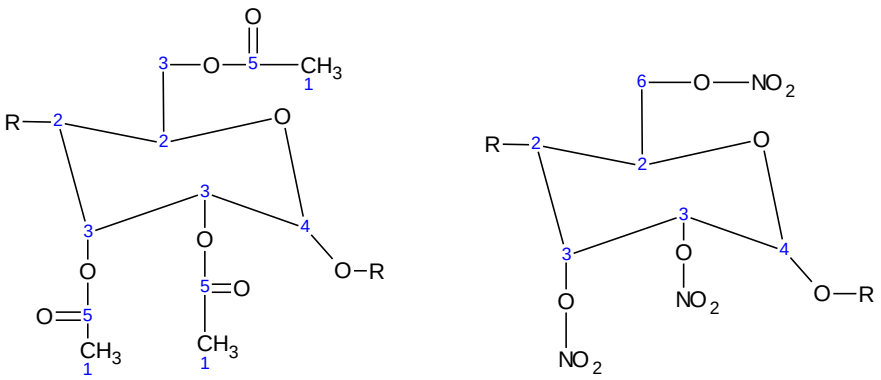

(a) (b)

Figure 4.7: *(a) Cellulose acetate and (b) cellulose nitrate structures (C# 1-6 indicates carbons of different functionalities).*

Survey level spectra of unmodified ME and a PANI-ME membrane are shown in Figure 4.8. Unmodified ME membrane shows C/O ratio ~ 1.3 and C/N ratio ~ 5.2 that signify an oxygen rich environment in cellulose ester structure. PANI coating on the membrane surface changed these ratios to C/O ~7.2 and C/N ~ 16 that show an increase in the carbon content arising from the benzene ring of PANI (C/H=1/6). Similarly the increase in C/N is attributed to C/N = 6 in PANI as compared to C/N =2 in cellulose nitrate (Figure 4.7).

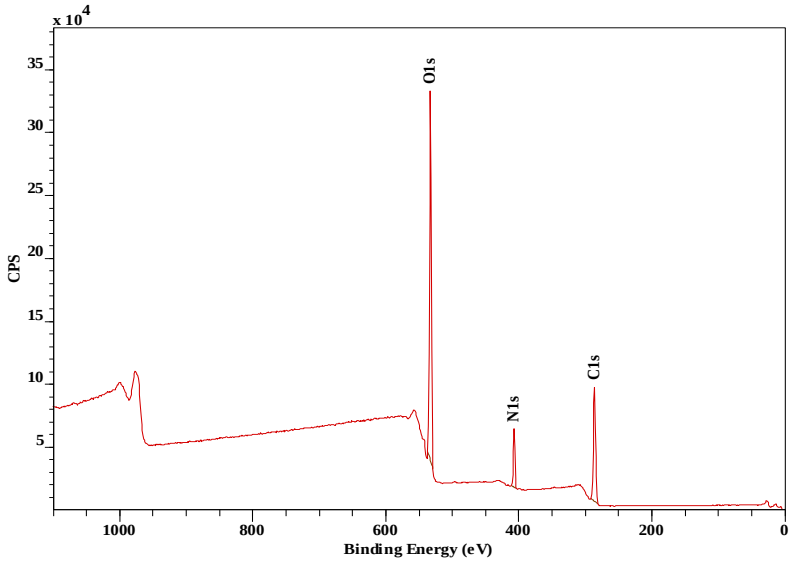

(a)

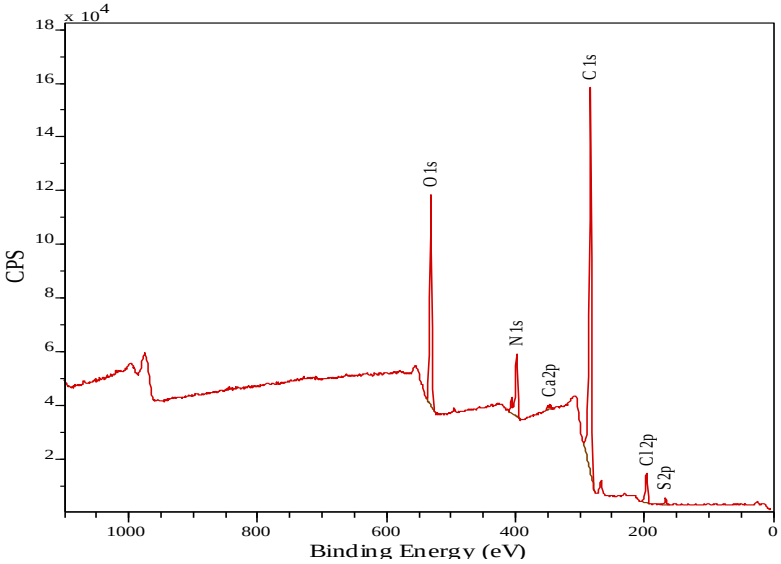

(b)

Figure 4.8: *Survey level spectra of (a) uncoated ME and (b) PANI-ME composite membranes.*

C 1s spectra of uncoated membranes were deconvoluted into five peaks as shown in Figure 4.9. These peaks are assigned to (referring to Figure 4.7), C-H (C1), C-C-O (C2) or C=N of oxime, C-ONO_2 (C6), O-C-O (C4) and C=O (C5) with respect to progressively positive shift from the lowest binding energy (285.4 eV of C-H) peak [153, 154]. N 1s composite peaks were decomposed into 401.3 eV (oxime nitrogen, see discussion in the following text), 405.7 eV (ONO) and nitrates at ≥ 408 eV (Figure 4.9 b). The quantification results are given in Table 4.3 (page 79).

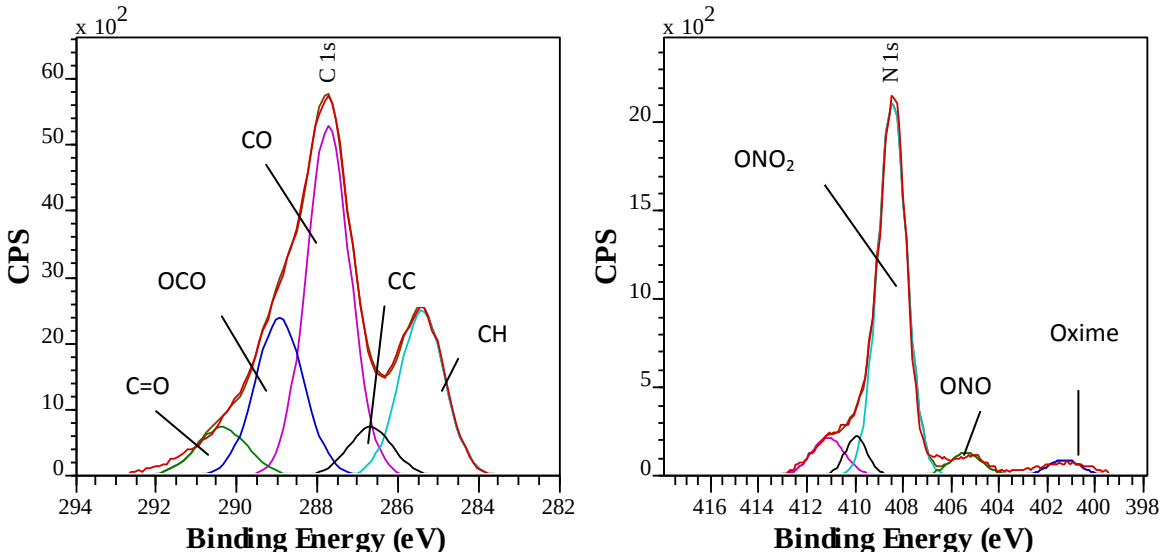

(a) (b)

Figure 4.9: *C 1s (a) and N 1s (b) spectra of unmodified ME membrane.*

For uncoated membranes, N 1s peak was centred on 408 eV characterizing nitrates in the mixed ester membranes. Another envelope appeared around 401 eV indicating the presence of organic nitrogen in the membranes. This N 1s envelope was supposed to arise from free radical cleavage of cellulose ring under x-ray irradiation (in XPS chamber) and subsequent formation of oxime (C=N-OH) functionality [155, 156]. This conversion depends on various parameters including x-ray irradiation time in XPS chamber (See appendix-A). The formation of oxime linkage was also indicated by the peak at 286.7 eV which might have originated from C=N functionality of oxime in addition to the C-C linkage in cellulose ring structure. A detailed account on the degradation of ME membranes under x-ray irradiation is given in Appendix-A.

C 1s core level composite peaks of PANI-ME membranes were deconvoluted into five peaks except for vapour phase polymerization that did not show as broad a shoulder as that of other composite membranes, indicating fewer high binding energy C 1s species (Figure 4.10, for assignment see Table 4.3). Deconvolution of the C 1s yields multiple peaks in the region of 284-290 eV for which the assignments are quite difficult due to the presence of multiple bonds with binding energies in close vicinity. In addition, the degradation of the surface PANI layer to hydroquinone and benzoquinone by the hydrolysis reaction makes the interpretation quite complex [145, 157]. Keeping in view the structure of mixed cellulose esters and extent of PANI layering at the surface, BE assignments for generated peaks are given in Table 4.4. Noticeably higher BE tail components may be attributed to the carbon bonding with oxygen at the surface.

N 1s spectra of PANI-ME membranes show two major distinctive envelopes centred at lower BE (~399.5 eV) and higher BE (~408 eV). These characterize PANI (or organic nitrogen) and nitrate ester (inorganic nitrogen), respectively (Figure 4.11). The first two peaks appeared in the N 1s spectra are assigned to imine (-N=) at ~398.4 eV and amine (-NH-) at ~ +1.2 eV shift to that of imine peak. Moreover, protonated nitrogen (N^+) emerges at >400 eV and yields multiple peaks depending on the localization or delocalization of the acquired positive charge depending on the association distance of doping anion (Cl^-, in this case) [146].

The quantification results obtained from the core level XPS spectra of PANI composite membranes are given in Table 4.4. PANI coating from the two-compartment cell with shorter polymerization time (ME,P1,Fe,30min) yields significant ONO_2 peak along with PANI characteristic peaks, indicating incomplete PANI coating on the base ME membrane surface. In the case of solution-phase polymerization (ME,Poly,Fe,48h), a small ONO_2 peak is observed which indicates better surface coverage with PANI layer at the longer polymer time. PANI coating in the two-compartment cell for comparatively longer time (ME, P1, Fe,6h) and from vapour-phase polymerization show minor nitrate peaks indicating almost complete PANI layering on the surface of ME membranes. This complete surface coating can also be confirmed by the relative suppression of C-O-NO_2 peak (287.2 eV) in the C 1s spectra. The relative amount of the three forms of PANI nitrogen i.e., imine (-N=), amine (-NH-) and protonated nitrogen (N^+), depends on the oxidation state and protonation level of the deposited PANI. Imine nitrogen is more prone to protonation as compared to amine nitrogen (Dissociation constant: pKa = 5.5 for $–HN^+=$ and 2.5 for $–NH_2^+$) [112].

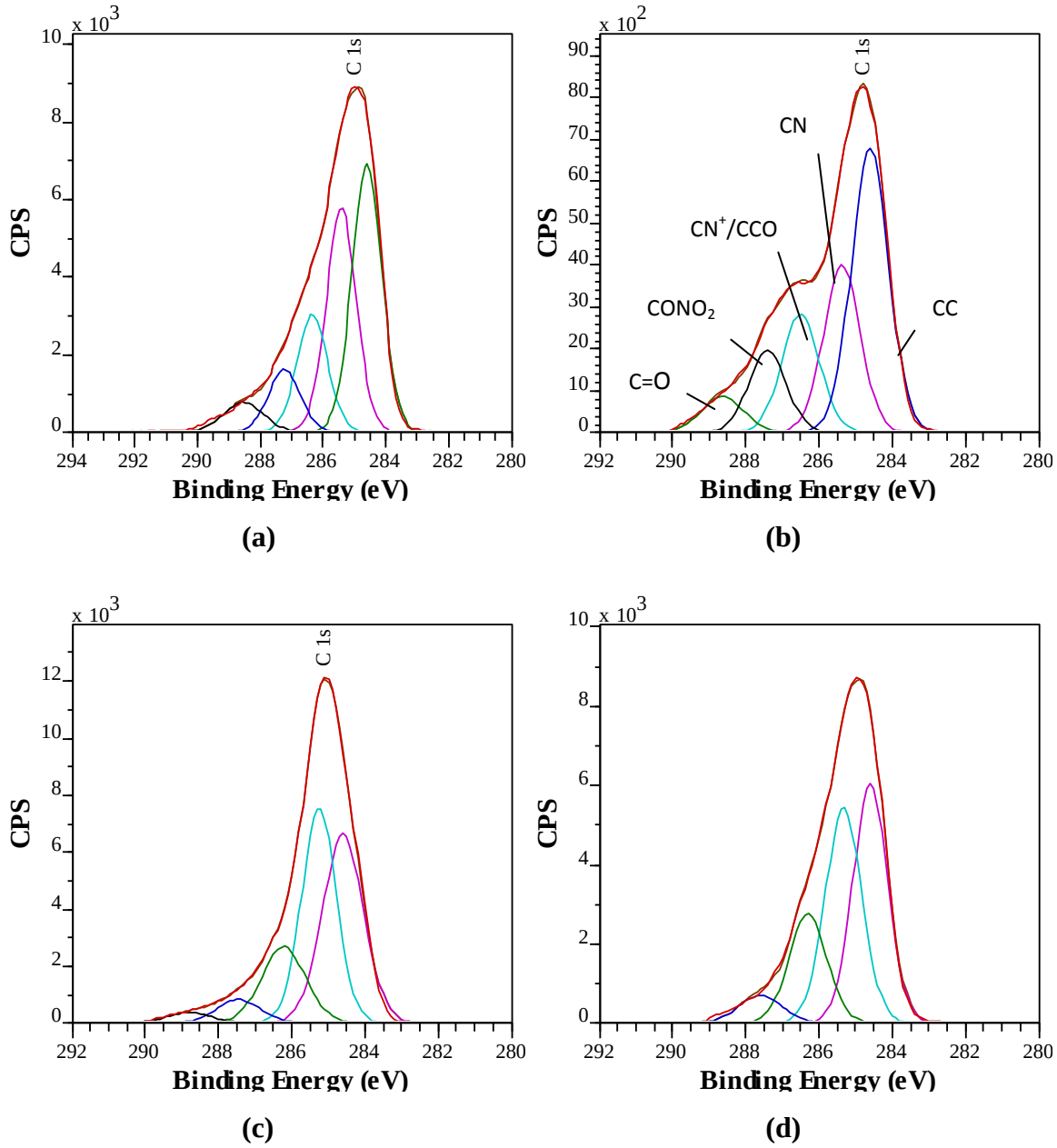

Figure 4.10: *C 1s spectra (a) ME,Poly,Fe,48h (b) ME,P1,30min (c) ME,P1,6h and (d) ME,Vap,APS,10min.*

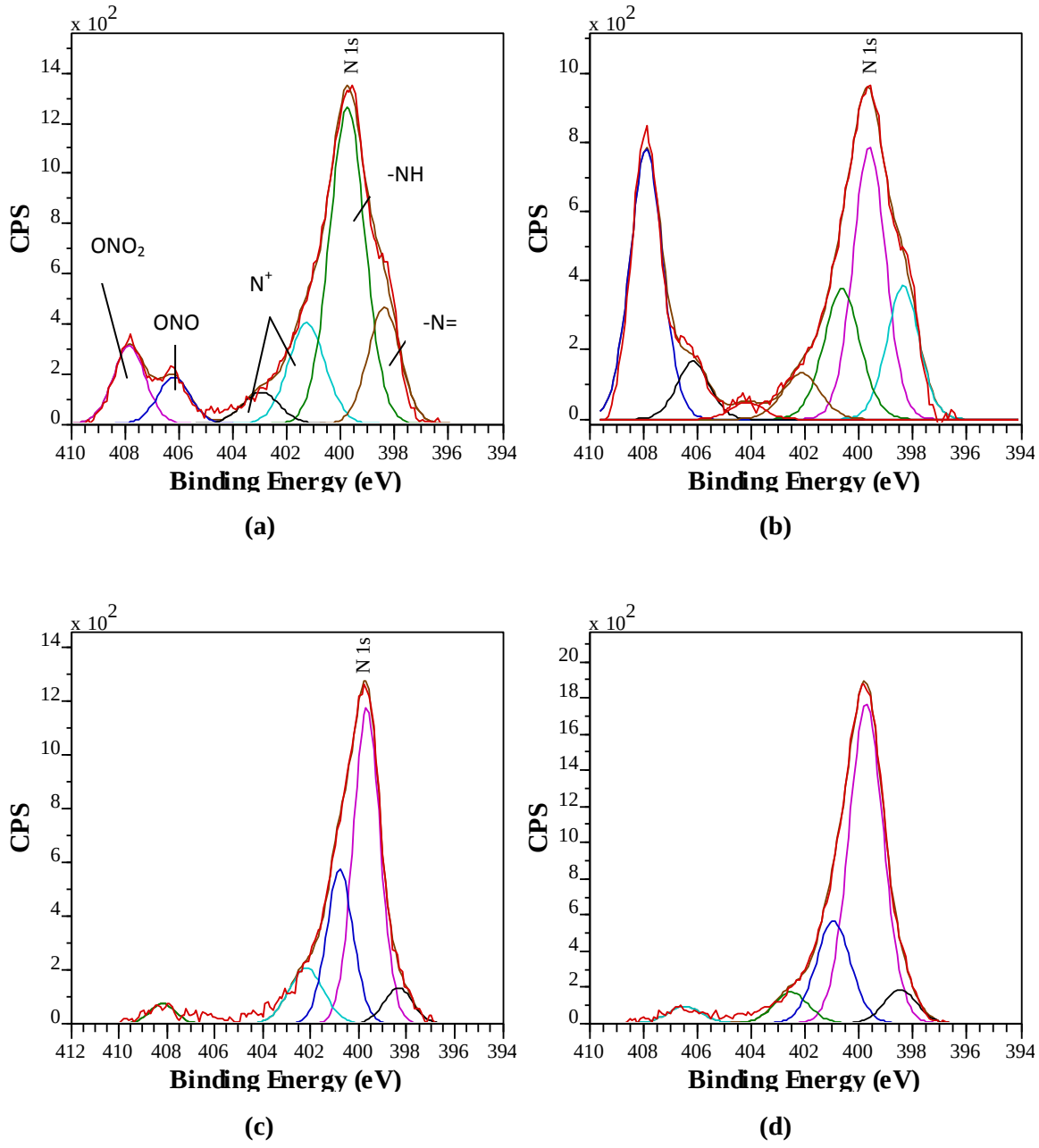

Figure 4.11: *N 1s spectra (a) ME,Poly,Fe,48h (b) ME,P1,30min (c) ME,P1,6h and (d) ME,Vap,APS,10min.*

Table 4.3: C 1s and N 1s deconvolution results of relative atomic % of the components in ME membrane

Membrane Identity/BE assignments (eV)	***C 1s***						***N 1s***	
	285.4	**286.7**	**287.7**	**288.8**	**290.4**	**401.3**	**405.7**	**>408**
	C-H	**C-C-O**	**C-ONO_2**	**O-C-O**	**C=O**	**Organic N**	**NO_2**	**(ONO_2)**
Relative Atomic %	21	6	44	22	7	4	5	91

Table 4.4: C 1s and N 1s deconvolution results of relative atomic % of the components in PANI-ME composite membranes

Membrane Identity	***C 1s***					***N 1s***			
	284.6 (C-C)	**285.4 (C-N)**	**286.3 ($C-N^+$) and/or C-O**	**287.2 (C-O-NO_2)**	**288.6 (O-C =O)**	**398.4 (-N=)**	**399.6 (-NH-)**	**400.5-402.5 (N^+)**	**406-408 (ONO_2)**
References for BE assignments	**140,146, 152**	**140,146**	**150**	**153**	**150**	**144,146-148**	**144,146-148**	**146,148, 150-152**	**155**
ME,Poly,Fe,48h	37	31	17	10	5	16	47	20	17
ME,P1,Fe,30min	41	24	17	12	6	14	29	22	35
ME,P1,Fe,6h	39	37	17	5	2	-	57	37	6
ME,Vap,APS,10min	39	37	19	5	-	6	64	26	4

Doping Levels of PANI in the Membranes

Composite membranes only with almost complete surface layering with PANI are included for the evaluation of the doping levels to avoid the interference of oxime nitrogen from the base membrane in the membranes that are incompletely covered by the PANI. The doping levels of the composite membranes can be estimated from the ratios of anion Cl to protonated nitrogen. To estimate anion Cl at the surface, Cl 2p peaks are fitted with a number of spin-orbit doublets (Cl $2p_{1/2}$ and Cl $2p_{3/2}$, area ratio ~ 1:2). The Cl $2p_{3/2}$ component at ~197.4 eV represents anion Cl whereas the peak around 200.1 eV emerges from the covalently bonded chlorine (Figure 4.12) [145, 151, 158, 159]. The + 1.5 eV shift in Cl $2p_{3/2}$ from the first doublet (197.4 eV) indicates the presence of Cl* species which appears during the charge transfer between Cl and protonated PANI nitrogen [159]. Based on the survey level spectra and the deconvolution of core level N 1s and Cl 2p spectra of the membranes, the total protonated PANI nitrogen and Cl^- are quantified and tabulated in Table 4.5. The ratios of the doping Cl (i.e. Cl^-+Cl*) to the total Cl are also mentioned in Table 4.5. The $(Cl^-+Cl^*)/N^+$ values from all the techniques are greater than unity which indicate the excessive chloride deposition at the surface in addition to the doping chloride. The solution-phase and the two-compartment cell polymerization (48 h and 6 h respectively) show almost equal ratios but at different N^+ contents. This emphasizes the association of anion chlorine only with the doped PANI nitrogen. In addition to the anion Cl, covalently bonded Cl has also been detected from the deconvolution results. The covalently bonded Cl might have resulted from the substitution of Cl with H in benzene ring of PANI probably due to the reaction with HCl [158] but the exact origin is not fully clear at the present.

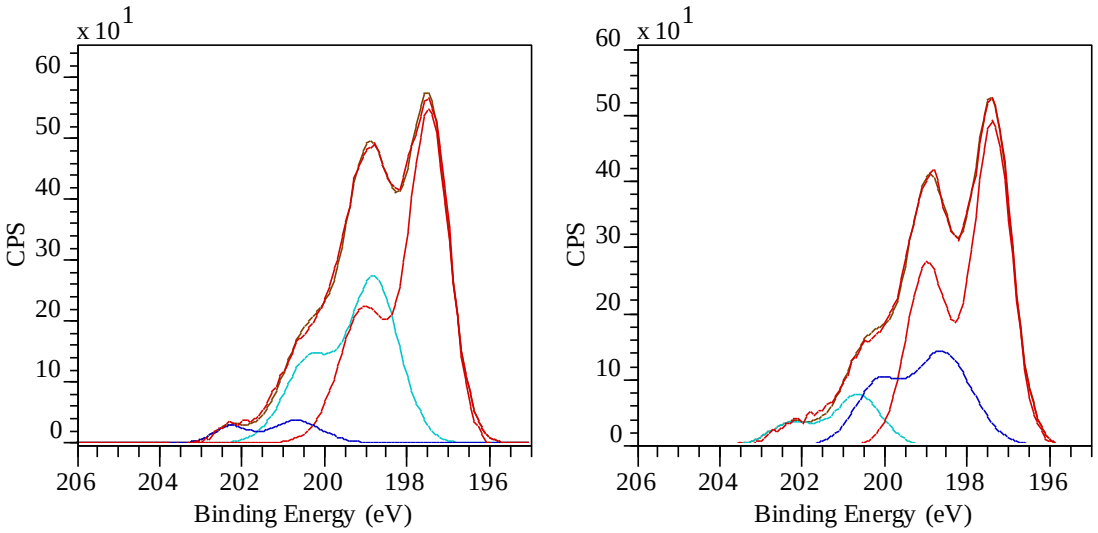

(a) **(b)**

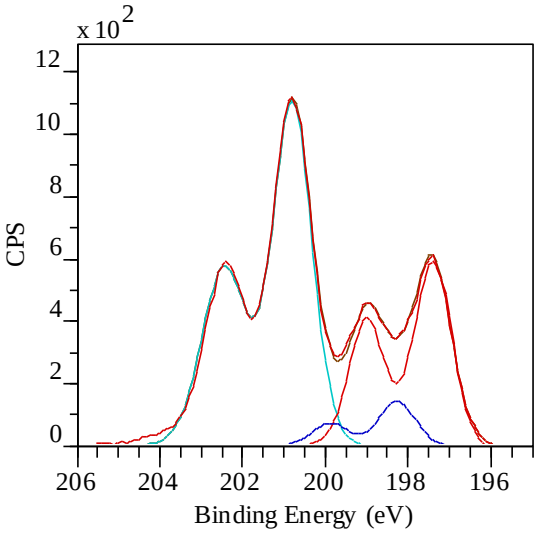

(c)

Figure 4.12: *Cl 2p core level spectra of (a) ME,P1,6h, (b) ME,Poly,Fe,48h and (c) ME,Vap,APS,10min.*

Table 4.5: Doping levels of PANI composite membranes

Membrane Identity	**At. %**			**$[Cl^- + Cl^*]/N^+$**	**$[Cl^- + Cl^*]$ %**
	-N=	**-NH-**	**$-N^+$**		
ME,P1,Fe,6h	-	57	37	1.8	90
Me,Poly,Fe,48h	16	47	20	1.9	91
ME,Vap,APS,10min	6	64	26	1.3	39

The Degradation of PANI at the Membrane Surface

Hydrolytic decomposition of PANI to benzoquinone and hydroquinone is a well established phenomenon which can be represented by the following simple chemical reaction equations [110, 160].

$$R\text{-}NH{=}Ph{=}NH\text{-}R + 2H_2O \rightarrow O{=}Ph{=}O + (2H^+) \rightarrow HO{=}Ph{=}OH$$

The degradation occurs due to the over-oxidation in the presence of an oxidant and it can be studied by deconvoluting O 1s spectra of the membranes. Core level O 1s spectra of unmodified ME and PANI-ME composite membranes synthesized by different polymerization techniques are shown in Figure 4.13. The deconvolution of O 1s spectrum of uncoated ME shows C-O-C/C-ONO_2 at 533.9 eV, NO_2 at 534.8 eV and higher BE energy species at ~535.4 eV [153]. Deposition of PANI on the surface of base membrane shifts the composite O 1s envelope to the lower BEs that indicates the disappearance of a comparatively higher BE NO_2 functionality and appearance of a low BE oxygen-bearing functionality. The deconvolution results for uncoated ME and PANI-ME composite membranes are given in Table 4.6.

The disappearance of NO_2 peaks in the O 1s spectra of the membranes synthesized by the two-compartment cell and vapour-phase polymerizations shows the surface coverage of the base ME membrane with PANI. However, the significant percentage of NO_2 in the membranes synthesized by the solution-phase polymerization (ME,Poly,Fe,48h) is consistent with the deconvolution results of N 1s peak (Figure 4.11 and Table 4.4). This indicates comparatively incomplete surface coverage with a thin PANI layer. The C-O functionality in the composite membranes might have arisen from the conversion of PANI to hydroquinone along with the formation of benzoquinone. The latter functionality dominates (C=O at 532.4 eV [160]) probably due to the prolonged contact with the oxidant and HCl solutions. This also explains the high C/O ratio calculated from the survey level spectra of the membranes. The C/O ratio increases from ~1 in ME membranes to ~7 for the membranes synthesized by solution phase and the two-compartment cell polymerizations. The high C % indicates PANI layering at the surface whereas the oxygen species arise mainly from the degradation reaction along with that from the cellulose ester functionality. Vapour-phase polymerization shows C/O value ~16 which indicates the lesser amount of oxygen at the surface. The peak at 532.4 eV may also be assigned to the sulphate oxygen from the oxidant (APS) [146].

The peak at 531.6 eV from the vapour-phase and the two-compartment cell polymerization may be attributed to -$NH_3^+HCO_3^-$- group which is formed by the adsorption of CO_2 by PANI at the surface [109].

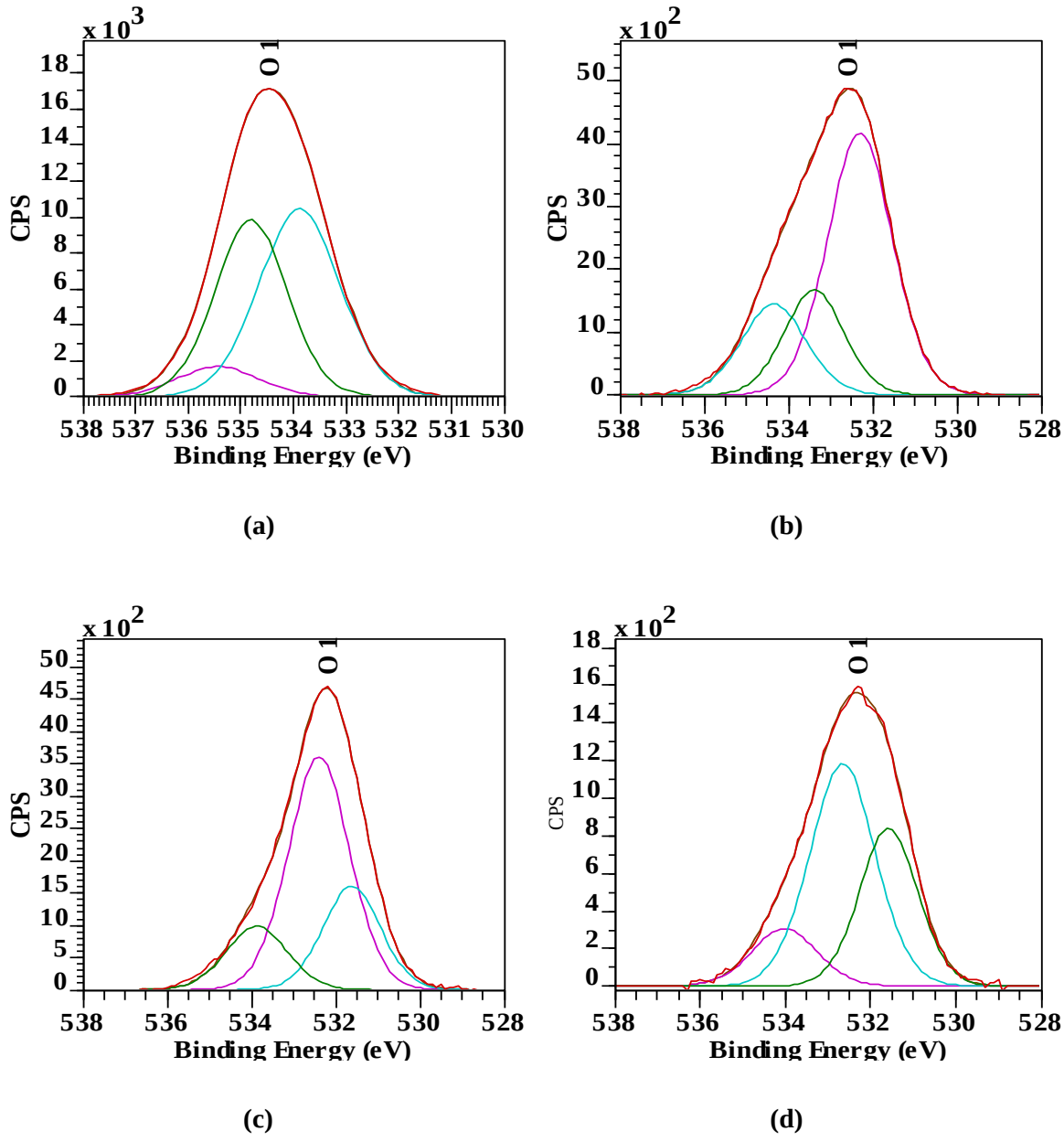

Figure 4.13: *O 1s core level spectra of (a) ME, bare (b) ME,Poly,Fe,48h, (c)ME,P1,Fe,6h and (d) ME,Vap,APS,10min.*

Table 4.6: O 1s deconvolution results of (relative atomic %) of ME and PANI-ME membranes

Membrane Identity/BE(eV)	531.6 (HCO_3^-)	532.4 (C=O)	533.9 (C-O)	534.8 (NO_2)	535.4 (H_2O)
ME, unmodified	-	-	50	42	8
ME,Poly,Fe,48h	-	58	22 (533.4 eV)	20 (534.3 eV)	-
ME,P1,Fe,6h	25	59	16	-	-
ME,Vap,APS,10m	33	53	14	-	-

4.7 Control of PANI Deposition under Various Techniques and Conditions

Aniline has been polymerized *in situ* in the presence of a substrate (ME membrane) by chemical oxidative polymerization. With the involvement of different substrates, the deposition does not depend on the chemical reaction only, but the physical processes and the chemistry of the substrate play an important role in determining the site and extent of PANI deposition. Based on the contacting pattern of reacting species, we adopted three distinctive PANI deposition techniques and manipulated the site and extent of PANI deposition.

4.7.1 PANI Deposition in Solution- and Vapour- phase Polymerizations

PANI deposition by solution-phase polymerization yielded only a surface layer that was well adhered to the base ME membrane. ME membranes swelled appreciably in aqueous aniline solution so Ph-NH_3^+ (anilinium) adsorbed on the surface of negatively charged (nitrate ester) ME membrane and subsequently polymerized to PANI. Because adsorption is a physical phenomenon that depends on the morphology and chemistry of the surface, PANI was deposited as a distorted surface layer. The depth of the deposited layer in the membrane cross section was not only limited but also it incompletely covered the surface, as shown by the SEM, FTIR-ATR and XPS results. FTIR and XPS spectra showed the presence of PANI and mixed cellulose ester at the surface with more pronounced PANI peaks at longer

polymerization times. As a result, the electrical conductivity increased with polymerization time for both $FeCl_3$ and APS as oxidants.

In vapour-phase polymerization, PANI layer was formed, presumably, by the reaction between soaked anilinium species on the membrane and the vaporized products of APS decomposition in a highly acidic aqueous solution at 60-70 ^oC. These decomposition products might include free radicals, hydrogen peroxide and peroxymonosulfate generated by the following reactions, respectively [161].

$$S_2O_8^{2-} = 2SO_4^{\cdot -}$$

$$S_2O_8^{2-} + H_3O^+ \longrightarrow 2HSO_4^- + H_2O_2$$

$$S_2O_8^{2-} + H_3O^+ \longrightarrow HSO_4^- + HSO_5^-$$

The generation of free radicals was the most probable as it might have lead the propagating frontal polymerization as it was observed under the similar polymerization conditions [162, 163]. The polymerization resulted in a full surface covering compact layer that hindered the further penetration of the propagating reaction front in the membrane bulk. It limited aniline polymerization only up to the a few micrometers in the bulk.

4.7.2 Effects of Oxidants

Aniline has limited solubility in water, i.e. 3.6 g/100 g water at 20 ^oC. It is almost fully converted to the corresponding anilinium salt when dissolved in dilute acid solutions. Polyaniline is deposited on the substrate membrane by oxidative polymerization of anilinium (acidulated aniline) reacting with the oxidizing species ($S_2O_8^{2-}$ in case of APS and Fe^{3+} for $FeCl_3$) as shown by the following equations [126].

$$4Ph\text{-}NH_3^+Cl^- + 5(NH_4)_2S_2O_8 \longrightarrow [\text{-}Ph\text{-}NH\text{-}Ph\text{-}NH^+Cl^-\text{-}Ph\text{-}NH\text{-}Ph\text{-}NH^+Cl^-\text{-}] + 10(NH_4)HSO_4 + 2HCl$$

$$4Ph\text{-}NH_3^+Cl^- + 10FeCl_3 \longrightarrow [\text{-}Ph\text{-}NH\text{-}Ph\text{-}NH^+Cl^-\text{-}Ph\text{-}NH\text{-}Ph\text{-}NH^+Cl^-\text{-}] + 10FeCl_2 + 12HCl$$

These reactions are characterized by the standard redox potentials of the oxidants (versus standard hydrogen electrode potential).

$$S_2O_8^{2-} + 2e^- \longrightarrow 2SO_4^{2-} \qquad E^o \text{ (Vs NHE)} = 2.01 \text{ V}$$

$$Fe^{3+} + e^- \longrightarrow Fe^{2+} \qquad E^o \text{ (Vs NHE)} = 0.77 \text{ V}$$

APS is more effective oxidant as compared to $FeCl_3$ so more PANI is formed using APS as compared to $FeCl_3$ under similar conditions [15, 138]. PANI formation (and deposition) reaction rate can be controlled by choosing among the commonly used oxidants (e.g. APS, $FeCl_3$, H_2O_2). Polymerization with different oxidants may result in different PANI morphology as depicted by the SEM pictures (Section 4.2).

4.7.3 Manipulation of PANI Deposition in the Two-Compartment Cell

In the chemical oxidative polymerization of aniline under diaphragmatic conditions (using two-compartment cell), various physical process are involved besides chemical kinetic step that may affect the overall rate of the heterogeneous reaction [109, 126, 138, 164]. Processes such as diffusion and migration, are more controlling being the slower in the succession of the heterogeneous reaction kinetics. Also, the exclusion of charged species due to a particular ion exchange character of the substrate is another controlling factor [138]. Polymerization site of aniline on the base membrane can be controlled by manipulating the diffusion and migration of the reacting species through the membrane. These manipulations can be achieved by carefully choosing the right functional substrate to provide the anchoring sites for aniline, reactants concentration, polymerization time and regulating the diffusion rates by ion exchange phenomena. Iyoda et al. [164] studied the diaphragmatic polymerization of pyrrole on and inside the Nafion® membrane by using both APS and $FeCl_3$ as oxidant and they concluded that Donnan exclusion plays controlling role in the determination of polypyrrole deposition site. Tan and Belanger also reached at the similar conclusions while studying the Nafion® - PANI composite membranes [109, 138]. Blinova et al. [126] showed that PANI was formed only at the aniline-facing side of the microporous cellulosic dialysis tubing during the diaphragmatic polymerization. FTIR characterization revealed formation of N-phenyl-1,4-benzoquinonediimine, an oxidized product of aniline and oxidant reaction, on the opposite side (oxidant-facing).

Mixed cellulose ester membranes, employed in the present research, are weak cation-exchange membranes owing to the fixed negative charge of mixed ester groups (Figure 4.7). ME base membranes are microporous with tortuous pore morphology. When these membranes are employed in the two-compartment cell polymerization, these act as both diffusion and ion exchange dialytic membranes. Ion exchange (and ion-exclusion) and diffusional flow phenomena control the permeation of various ions across the membranes.

Additionally, a kinetically fast and thermodynamically favoured chemical reaction (aniline polymerization) takes place being catalyzed strongly by the presence of an inorganic acid (HCl) according to well established mechanism of chemical oxidative polymerization of aniline [15, 135]. The presence of an acid enhanced the rate of aniline oxidation through the mechanism of proton transference which was auto-catalyzed by the already formed PANI in the base membrane [135]. The chemical reaction also promoted the diffusional flow due to the depletion of monomer (aniline) or oxidant at the reaction site.

To identify the factors affecting the polymerization site on ME membranes, a simple experimental scheme was executed. Initiation of PANI deposition and its asymmetric (or symmetric) growth inside the pores of membranes were investigated in the two-compartment cell polymerization by changing the oxidant (APS or $FeCl_3$) and adding HCl either in the monomer or in the oxidant compartment or in both (Table 4.6). Because microporous membranes do not hinder as effectively as a dense membranes does, the reactant species can flow freely through the membranes. In addition, due to the weak ion exchange character of ME membrane, the strong chemical reaction potential seems to be the determining factor in the selection of PANI deposition site (Table 4.7). PANI deposition was initiated and dominated on the side of ME membrane contained catalyzing H^+ ions (by adding HCl, see experiments 2-4). These results comply with the study of Tzou and Gregory [135] who modelled the chemical polymerization of aniline by a two-rate constant kinetic equation. The second rate constant accounts for an already formed PANI or nature of the substrate in aqueous solution and has values two to three orders of magnitude greater than the first rate constant that comes from the chemical reaction alone. Additionally, an auto-acceleration mechanism for aniline polymerization was proposed due to the presence of protonated PANI in the reaction mixture. This influencing factor was also confirmed by experiment No. 6 (Table 4.7) where high HCl concentration (twice as that of aniline compartment) drove the reaction to the oxidant side, only.

For comparatively balanced HCl cases (Experiments 1 and 5) and with slower reaction kinetics by using $FeCl_3$, the ion exchange character of ME membrane played its role because more Fe^{3+} ions were exchanged and transported through the membrane as compared to the relatively slower diffusion of bulky anilinium ions. In the experiment No.1, though, PANI deposition started at aniline-facing side of the membrane, the reaction front progressed towards the oxidant side through the membrane resulted in an asymmetric deposition. In

Table 4.7: Results of the experiments for PANI deposition site control

Experiment Number	Monomer Compartment	Oxidant Compartment	Observations
1	$C_6H_5NH_2$ + HCl	$FeCl_3$ + HCl	 PANI deposition started from aniline side and resulted in an asymmetric deposition.
2	$C_6H_5NH_2$ + HCl	$FeCl_3$	 PANI deposition started from aniline side and resulted in a highly asymmetric deposition.
3	$C_6H_5NH_2$	$(NH)_2S_2O_8$ + HCl	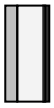 PANI deposition started from oxidant side.
4	$C_6H_5NH_2$ + HCl	$(NH)_2S_2O_8$	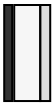 PANI deposition started from aniline side.
5	$C_6H_5NH_2$ + HCl	$(NH)_2S_2O_8$ + HCl	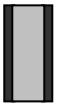 PANI deposition started from both sides and resulted in a symmetric deposition.
6	$C_6H_5NH_2$ + HCl	$FeCl_3$+ $(NH)_2S_2O_8$ + HCl	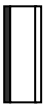 PANI deposition started from oxidant side and resulted in deposition only at the single face (oxidant side).

- The intensity of black colour in the given sketches indicates the extent of PANI deposition.
- Reactant concentrations: $FeCl_3.H_2O$ (0.3M); ammonium persulfate (0.3); aniline (0.8) and HCl (0.4). The volume of the reagents in the both compartment used was about 110 ml.

experiment No.5, because transportation of negatively charged $S_2O_8^{2-}$ ions was less favoured through the membrane, PANI deposition started at the both faces, simultaneously. For $FeCl_3$ case, PANI deposition started on the monomer-facing side of the membrane and subsequently it grew inside the pores of ME membranes towards the oxidant-facing side. The competitive PANI growth of already deposited PANI layer towards monomer-facing side due to the proposed trans-membrane proton transference was less favoured as compared to the more direct aniline polymerization in the pores on opposite side (Figure 4.14) [126]. This proposed mechanism was also confirmed by FTIR spectra which show an asymmetric PANI deposition and mixed (PANI and cellulosic) bands were detected on the aniline-facing membrane side as the function of time (Figure 4.15). The relative growth of PANI peaks with respect to polymerization time confirmed the asymmetric deposition in the membrane bulk. This deposition asymmetry was also shown in the electrical conductivity values of these membranes (Figures 4.6). All composite membranes, except those modified with the two-compartment permeation cell, showed order of magnitude lower two-point conductivities as compared to that of latter ones. This indicates higher levels of PANI deposition in the bulk of base membrane resulted by the pore wall coating of base membrane.

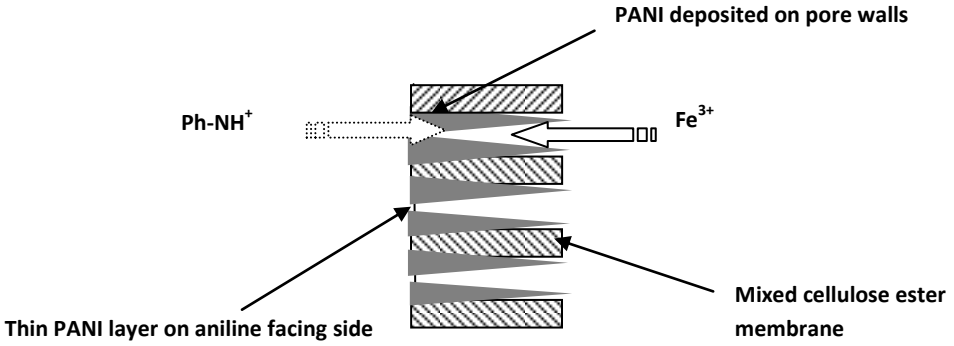

Figure 4.14: *Schematic representation of in-pore PANI deposition.*

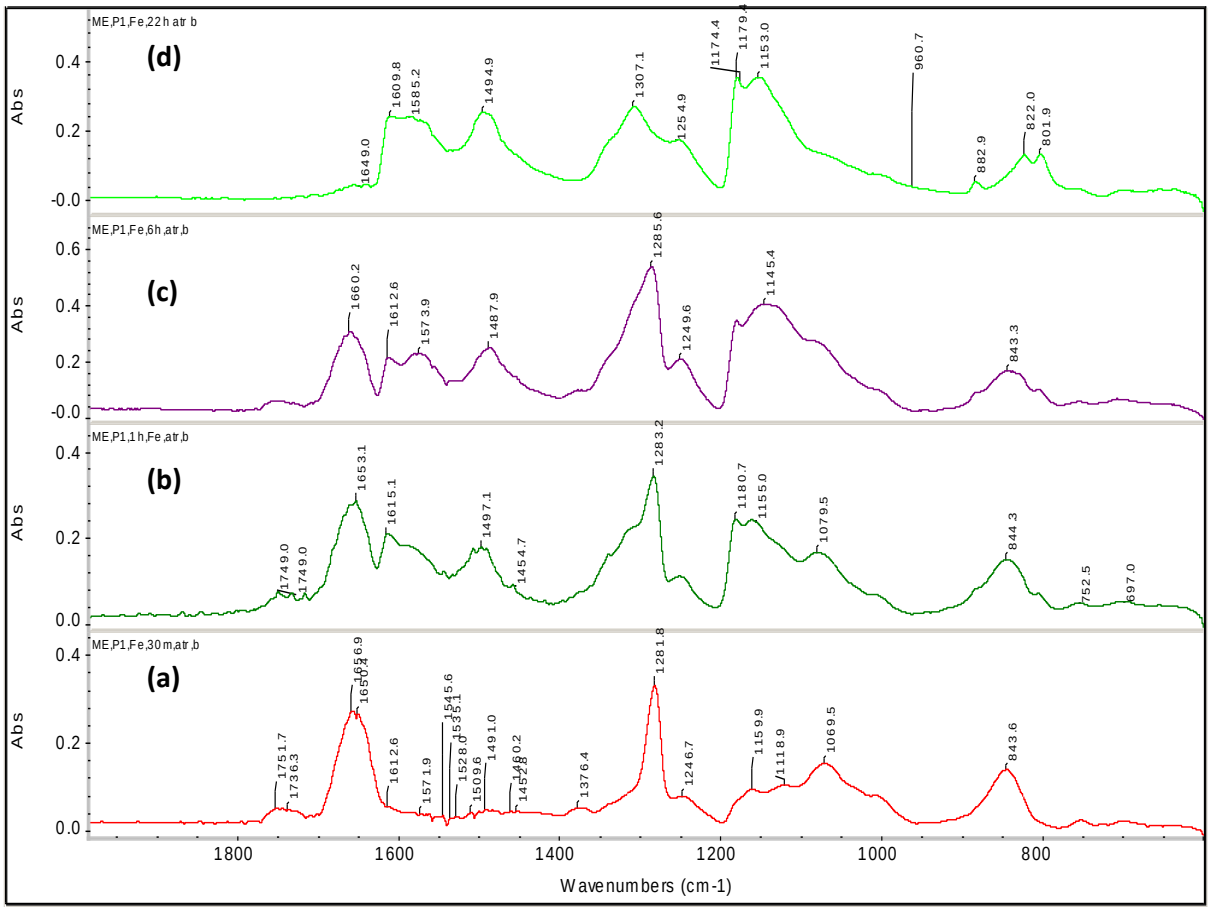

Figure 4.15: *FTIR-ATR spectra of PANI composite membranes synthesized from two-compartment cell polymerization at various polymerization times (a) 30 min (b) 1 h(c) 6 h and (d) 22 h.*

4.8 Summary

PANI deposition on base ME microporous membranes were studied and the effects of various chemical polymerization techniques on the PANI deposition site and extent on the base membrane have been discussed. SEM was used to observe the PANI deposition site whereas FTIR-ATR was used as a standard technique to characterize PANI layering extent and its oxidation/doping states on the surface of base membrane. To elucidate the effects of PANI deposition site on the electronic conductivity of the composite membranes, membrane surface and trans-membrane conductivities were measured. In addition to these qualitative characterizations of PANI deposition, PANI layering extent and the chemical state at the membrane surface were quantified by using XPS. The degradation of PANI by a hydrolysis reaction was also studied by analysing O 1s spectra. The membrane characterization presented in this chapter leads to the following significant conclusions regarding the effects

of various chemical polymerization techniques and parameters on PANI deposition on base ME membranes.

- PANI was deposited at the surface of the base membrane as an incomplete and non-uniform layer by the solution- and vapour-phase polymerizations. In contrast, the two-compartment cell polymerization deposited PANI on the pore walls of the base membrane without blocking the pores. Surface coverage with PANI improved with polymerization time in the solution- and vapour-phase polymerizations whereas in-bulk PANI deposition increased in the two-compartment cell polymerization.

- FTIR-ATR spectra showed mixed ME and PANI bands indicating incomplete surface coverage. From all the employed techniques, aniline was deposited as emeraldine salt. XPS spectra showed that the surface layering extent and doping levels of PANI increased by increasing polymerization time in a single technique. FTIR-ATR and XPS characterization revealed significantly increased surface layering extent in the two-compartment cell polymerization for the same times as compared to the solution-phase polymerization. Vapour-phase polymerization deposited comparatively thick and uniform surface PANI layer.

- Asymmetric PANI deposition in the bulk membrane was observed in the two-compartment cell polymerization with greater PANI deposition extent on the aniline-facing side of the membrane as compared to the oxidant ($FeCl_3$)-facing side. Ion exchange character of the base membrane controlled the initiation and progression of in-bulk PANI deposition in the two-compartment cell.

- PANI deposition site and levels, and oxidation/doping states influenced the electronic conductivity levels and orientation of the composite membranes as shown by surface and trans-membrane conductivity measurements. The conductivity values were dependent on the polymerization techniques and conditions (i.e. time, oxidant etc.) within a single technique.

Chapter Five

Electronic and Ionic Transport in the Composite Membranes: Effects of PANI Deposition Site, Extent and Doping

5.1 Electrochemical Characterization of PANI Composite Membranes

Membrane separation processes based on ion exchange membranes such as dialysis and electrodialysis depend on the electrochemical interactions of the permeating ions with the functional moieties of the membranes. Electronic charge from the electrodes is transferred to electrolyte ions via an electrochemical reaction governed by the Faraday's law [165]. The charge travels through the bulk of electrolyte by the bulk transportation of ions towards oppositely charged electrodes whereas only counter-ions (ions with the opposite charge to that of the membrane) pass through ion exchange membrane bearing either positively or negatively charged immobilized functionalities in anion- and cation-exchange membranes, respectively [165, 166]. The selective transportation of counter-ions and exclusion of co-ions (i.e. Donnan exclusion) in the membrane phase give rise to the depletion of ions on the dilute side of the membrane with the simultaneous increase in the concentration on the other side (concentrate side). This depletion and enrichment result in the polarization of the electrolyte layers adhering to the both faces of the membrane due to the interaction with the fixed charges on the membrane. This nanometer-sized layer is called diffusion boundary layer (DBL) or simply double layer [167].

Ionic transport in ion exchange membranes is conventionally studied by the current-voltage (I-V) curves that are obtained by increasing current density across the membrane and recording the resultant potential difference. Various regions of the I-V curve identify electrochemical processes that take place in the system including concentration polarization (Figure 5.1).

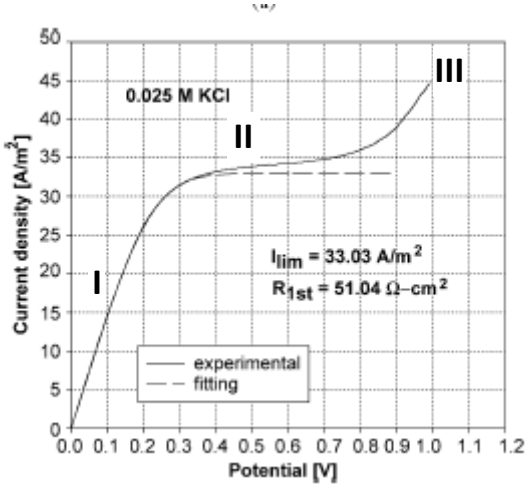

Figure 5.1*: I-V curve of ion exchange membrane (anion-exchange membrane in 0.01 M KCl [167].*

In Figure 5.1, the curve can be divided into three regions. The first linear part shows the polarization of the membrane system by the application of current on the electrodes. The membrane shows ohmic behaviour in this region from where the ionic conductivity can be calculated. The second plateau region indicates a limiting current density (LCD) which arises due to the concentration polarization and depletion of electrolyte on the dilute side of the cell. It follows a sharp increase in the current with voltage. This sharp rise in the current is difficult to explain exactly especially when dilute side has already been depleted with current carrying ions. Many phenomena have been attributed to this sharp rise in the current such as water dissociation and electro-convective flow but still the exact cause is not fully clear [165, 167].

In addition to the electrochemical characterization by I-V curves, determination of membrane transport number is another useful characterization parameter [166-168]. The transport number is defined as the fraction of the total current carried by the counter-ions through the membrane. For an ideal anion- or cation-exchange membrane, the transport number for counter-ions is 1. To determine the transport number, the ion exchange membrane is transposed between two halves of a two-compartment permeation cell. The potential difference across the membrane is measured by varying the concentration of the electrolyte in one compartment while keeping it constant in the other. Transport numbers are calculated by fitting the following equation to the data [165].

$$V = \left(t_{coun}^{m} - t_{co}^{m}\right)\frac{RT}{F}\ln\frac{a_s^1}{a_s^2} = \left(2t_{coun}^{m} - 1\right)\frac{RT}{F}\ln\frac{a_s^1}{a_s^2} \quad (5.1)$$

Here t^m is the transport number with subscripts *coun* and *co* for counter- and co-ions, respectively, *a* denotes activity constant where superscripts 1 and 2 specify the two compartments of the cell. R is the ideal gas law constant, T is absolute temperature and F is the Faraday's constant.

Although the above mentioned techniques have been successfully used to characterize ion exchange membranes, these techniques are static in nature and do not fully explain the complex transport phenomena taking place in the membranes. For example, the diffusion double layer is crucial in the performance of ion exchange membrane however, the study of the I-V curves does not distinguish the double layer polarization from the polarization of the bulk membrane. Dynamic, instead of a static electrochemical technique such as electrochemical impedance spectroscopy (EIS) is required to fully characterize ion exchange membranes [167].

In ICP based membranes, ion transport takes place coupled with electron transport. At the membrane/electrolyte interface, an electrochemical reaction takes place (by a Faradic process) and electrons are injected or ejected from the ICP films by the electrolyte. The kinetics of this electrochemical process in addition to the transport phenomena in the double layer at the interface can be studied by EIS. Such charge transfer studies at the interface, coupled with the transport processes in the bulk membrane give full characterization of an electrochemical system.

Electrochemical impedance spectroscopy (EIS) and membrane potential measurements have been used in this thesis to analyse the transport and interfacial transfer processes in PANI composite membranes. The effects of composite membrane morphology (i.e. PANI deposition site and extent) and oxidation/doping states on the electrochemical transport/transfer processes have been studied in various electrolytes. In the following, the relevant theory and results are discussed for the employed techniques.

5.2 Electrochemical Impedance Spectroscopy of PANI Composite Membranes

5.2.1 Equivalent Circuit Modelling of EIS Data

In EIS, an electrochemical system is excited by a sinusoidal function of either electrical potential (potentiostatic) or current (galvanostatic) and response in the corresponding form (voltage or current) is recorded [132, 169]. A sinusoidal voltage is represented mathematically as,

$$v(t) = V_o \sin(\omega t) \tag{5.2}$$

where v(t) is the frequency (ω) dependent voltage of amplitude V_o (r.m.s). The angular frequency is defined as $\omega = 2\pi f$ where f is the frequency in cycles. s^{-1}.

The response to the forcing function of Equation (5.2) is a sinusoidal current i(t) of the same frequency and of amplitude I_o. The response either lags or leads by a phase angle (Φ) with respect to v(t);

$$i(t) = I_o \sin(\omega t + \Phi) \tag{5.3}$$

Φ is a signed (+/-) quantity that depends on the characteristics of the system.

In EIS, the amplitude of the exciting function is kept small in order to maintain the linearity in the response that is also a simple function of ω. For nonlinear behaviour at the large amplitudes of the forcing function, the response is a periodic function of multiple of ω i.e. 2ω, 3ω, …..

If system behaves as a pure resistor, the response current is given by the Ohm's law i.e., $i = \frac{v}{R}$ where R is the resistance in ohm. In this case the phase angle (Φ) is zero and the current is totally in phase with the applied voltage and the amplitude of the current wave (I_o) is $\frac{V_o}{R}$.

For a pure capacitor, the stored charge (q) is related to the potential (v) across the capacitor plates by the following equation.

$$q = Cv \tag{5.4}$$

Where C is the capacitance in Faraday (F).

The current flowing through a capacitor is given by

$$i = \frac{dq}{dt} = C\frac{dv}{dt}\,. \tag{5.5}$$

The current in response to the sinusoidal applied voltage is given by,

$$i = \omega C V_o \cos(\omega t)$$

or

$$i = \frac{V_o}{X_c}\sin\left(\omega t + \frac{\pi}{2}\right) \tag{5.6}$$

where X_c is called capacitance reactance, $\frac{1}{\omega C}$. The current lags 90^o and the response is totally out of phase to the applied potential.

To analyse the dynamic response of complex elements such as a combination of resistors, capacitors and inductors, phasor (vector) notation of applied and response functions is very helpful. The expressions for the responses of a pure resistor and capacitor are shown, respectively, as follows:

$$\hat{V} = \hat{I}R \tag{5.7}$$

$$\hat{V} = -jX_c\hat{I} \tag{5.8}$$

where $j = \sqrt{-1}$, $\hat{I}$ and $\hat{V}$ are the phasor representation of the current and voltage, respectively.

Impedance (Z) is defined as the complex resistance arises from the combined resistance and reactance in an electrochemical system. If a sinusoidal voltage is applied to an electrical circuit comprising pure resistor and capacitor connected in series, the overall voltage drop is a sum of the individual voltage drops across the resistor and capacitor.

$$\hat{V} = \hat{V}_R + \hat{V}_C \tag{5.9}$$

or

$$\hat{V} = \hat{I}(R - jX_C) \tag{5.10}$$

or

$$\hat{V} = \hat{I}Z \tag{5.11}$$

where Z is defined as impedance and it can be written in terms of the resistance and reactance as

$$Z = R - jX_c \tag{5.12}$$

Because Z is a complex quantity depending on the frequency, it is usually represented as,

$$Z(\omega) = Z_{\mathrm{Re}} - jZ_{\mathrm{Im}} \tag{5.13}$$

where Z_{Re} and Z_{Im} are the real and imaginary components of the impedance. For an R-C series element, Z_{Re} = R and Z_{Im}= X_c=$\frac{1}{\omega C}$. The magnitude of the impedance ($|Z|$) and the phase angle (Φ) are given by, respectively,

$$|Z| = \sqrt{Z_{\mathrm{Re}}^2 + Z_{\mathrm{Im}}^2} \tag{5.14}$$

$$\phi = \tan^{-1}\frac{Z_{\mathrm{Im}}}{Z_{\mathrm{Re}}} = \tan^{-1}\left(\frac{1}{\omega RC}\right) \tag{5.15}$$

Equation (5.11) can be considered as the generalized Ohm's law with Z replacing R. The magnitude and phase angle of the impedance depend on the relative capacitive versus resistive characteristics of the system. For pure resistor, phase angle is zero whereas it is π/2 for a pure capacitor. Real systems never approach to an ideal behaviour so a mixed impedance results where phase angle varies between –π/2 to +π/2. For a pure inductor, phase angle is equal to +π/2 i.e., the response always leads the input.

EIS data are commonly represented as Bode and Nyquist plots. Bode representation comprises of two graphs; $|Z|$ and Φ versus log ω whereas Nyquist plot comprises Z_{Im} versus Z_{Re} with ω as a hidden parameter. Nyquist plot for a parallel R-C element with R=100 ohm and C=1 μF is shown in Figure 5.2. The impedance for this parallel R-C element is given by the following expression.

$$Z = \frac{R}{1+(\omega RC)^2} - j\frac{\omega R^2 C}{1+(\omega RC)^2} \tag{5.16}$$

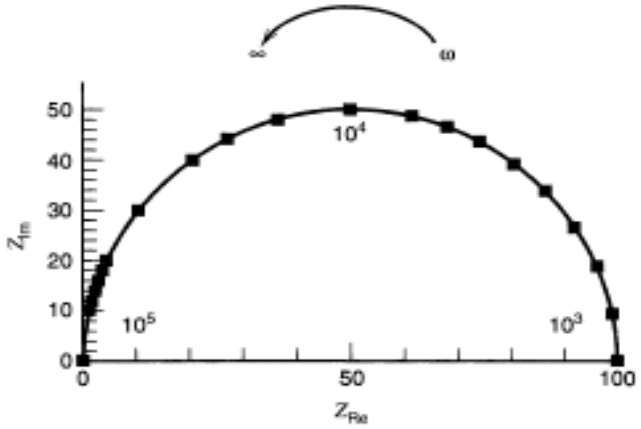

Figure 5.2*: Nyquist plot of a parallel R-C circuit [132].*

For this particular case, the Nyquist plot is a semicircle with Z=0 and R at ω→∞ and ω→0, respectively, the high and low frequency intercepts. The peak is observed at the characteristic frequency, $\omega^* = \frac{1}{\tau} = \frac{1}{RC}$, where τ is the characteristic relaxation time. To plot the magnitude and phase angle as a function of frequency (Bode plot), the expressions for the magnitude and the phase angle in this case are shown in the following (from Equation 5.14 and 5.15).

$$|Z| = \sqrt{\frac{R^2}{\left[1+(\omega RC)^2\right]}} \tag{5.17}$$

$$\phi = \tan^{-1}(-\omega RC) = \tan^{-1}(-\omega\tau) \tag{5.18}$$

The Bode plot of the same R-C circuit is shown in Figure 5.3.

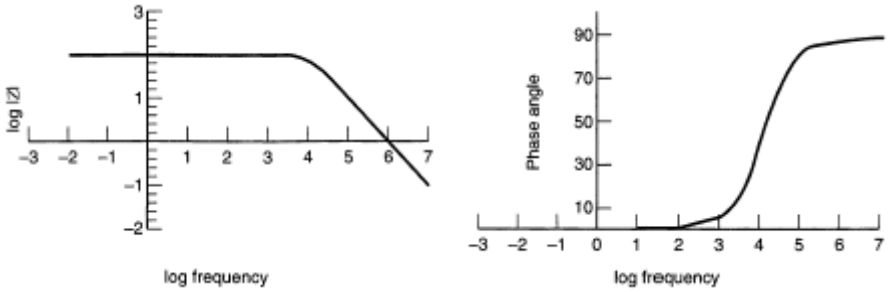

(a) **(b)**

Figure 5.3*: Bode plots for a parallel RC circuit (a) magnitude and (b) phase angle versus frequency [132].*

The magnitude of the impedance remains constant at 100 (Equation 5.17) over all frequencies up to the characteristic frequency (i.e., 10^4 radians.s^{-1} in this case) where it starts decreasing with a constant slope of -1. On the phase diagram, phase angle starts increasing (from 0^o) at low frequencies, reaches 45^o at the characteristic frequency and then reaches to its maximum value i.e., 90^o at high frequencies (Equation 5.18).

EIS data are analysed by using either analytical modelling based on the ion transport/transfer relationships (e.g., Nernst-Planck equation) or equivalent circuit analysis. In the latter methodology, physical processes that are taking place in an electrochemical cell are interpreted in terms of various electrical elements such as resistor, capacitor and inductor. The most common equivalent circuit that represents many of the electrochemical processes is Rundles circuit shown in Figure 5.4. The EIS data of a film-coated electrode in a three-electrode electrochemical cell (a film-coated working electrode and counter and reference electrodes in electrolyte) can be analysed by using Randles circuit. It consists of a parallel combination of a double-layer capacitance (C_d) which arises from the development of a double layer between working electrode and the adjacent electrolyte and a charge-transfer or polarization resistance (R_{ct}) which accounts for the interfacial charge transfer.

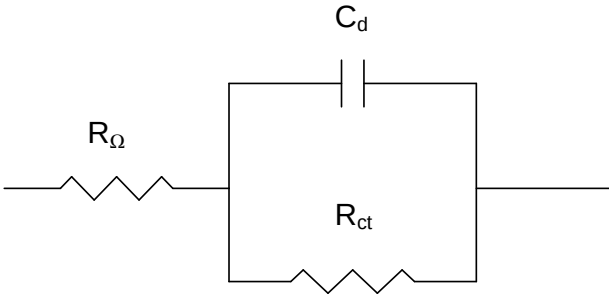

***Figure 5.4**: Randles equivalent circuit.*

R_Ω in this particular case represents film plus electrolyte resistance which is in series with the parallel C_d-R_{ct} combination. The total impedance of the system is represented by the following expression.

$$Z = R_\Omega + \frac{R_{ct}}{1+(\omega R_{ct} C_d)^2} - j\frac{\omega R_{ct}^2 C_d}{1+(\omega R_{ct} C_d)^2} \tag{5.19}$$

The Nyquist plot for the Randles circuit is shown in Figure 5.5.

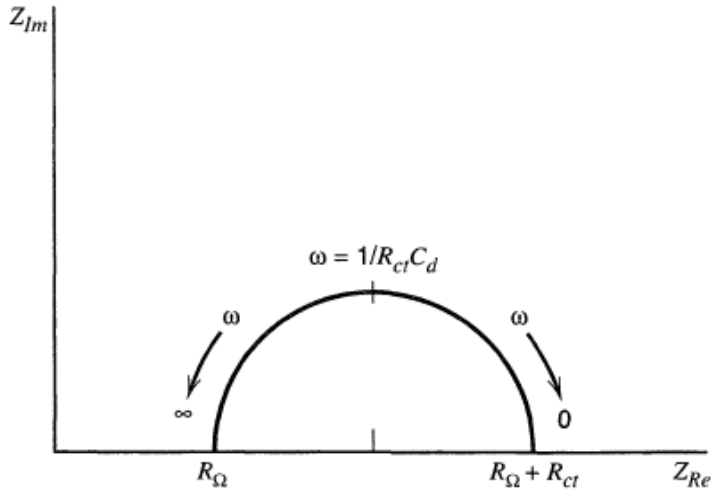

***Figure 5.5:** Nyquist plot for Randles circuit shown in Figure 5.4 [132].*

The Nyquist plot consists of a semicircle of diameter equals $\frac{R_{ct}}{2}$. As $\omega\rightarrow\infty$, the reactance of the capacitor becomes negligible (≈ 0) and it short-circuits the parallel R-C circuit. In this case $Z=R_\Omega$ (also from Equation 5.19). At very low frequencies i.e. $\omega\rightarrow 0$, the capacitance becomes infinitely large thus it is eliminated and the total impedance becomes $Z = R_\Omega + R_{ct}$. The imaginary part arises only from the capacitor so it contributes at the intermediate

frequencies with maximum Z_{Im} at $\omega^* = \frac{1}{\tau} = \frac{1}{R_{ct}C_d}$. Randles circuit also models the EIS data of the membranes where R_Ω gives combined resistance of the electrolyte and the membrane and C_d and R_{ct} show the double layer capacitance and charge transfer resistance at both membrane/electrolyte interfaces [111].

5.2.2 EIS Studies of ICP Films and Membranes

Intrinsically conducting polymers have drawn special attention of researchers due to their interesting electrochemical and charge conduction properties. Based on these properties, ICPs find applications in various technological fields such as charge storage, protective coatings, electrical displays, and electrochemical sensors. Charge conduction in ICPs takes place by the movement of both electronic (i.e. polarons) and ionic charge carriers. The involvement of ions in charge conduction process originates ICPs application as ion exchange films and membranes [51]. However, contrary to the conventional ion exchange membranes, ions transport in ICPs takes place coupled with the electronic charge transport. Due to their unique transport properties, the electrochemical impedance characterization of ICPs has remained the topic of special interest [170-173]. Mixed electronic-ionic conduction through the bulk of the film/membrane and various interfaces has been modelled by EIS. Various geometries of the electrochemical cells were used including modified electrodes and free-standing films/membranes [174, 175]. Modified electrode configuration has been used as the most common geometry in the electrochemical impedance studies due to the ease in the electrode coating by ICP using the electrochemical polymerization technique [70, 175, 176]. Electrochemical characterization by using free-standing membranes is comparatively rare due to the fabrication limitations of ICPs in free-standing films and membranes. However, the modified electrode configuration is not preferred over the free-standing membrane to study the electrochemical processes of the membranes. Interfacial phenomena are observed at the low frequency limits (i.e. dc characteristics) which in the case of modified electrodes, are given by the both metal/polymer and polymer/electrolyte interface due to the electronic and ionic conduction of the system. It makes the identification of the transfer processes at the both interfaces very difficult.

The charge transport and charge transfer processes involved in an ICP-coated electrode in the electrolyte solution is shown in Figure 5.6.

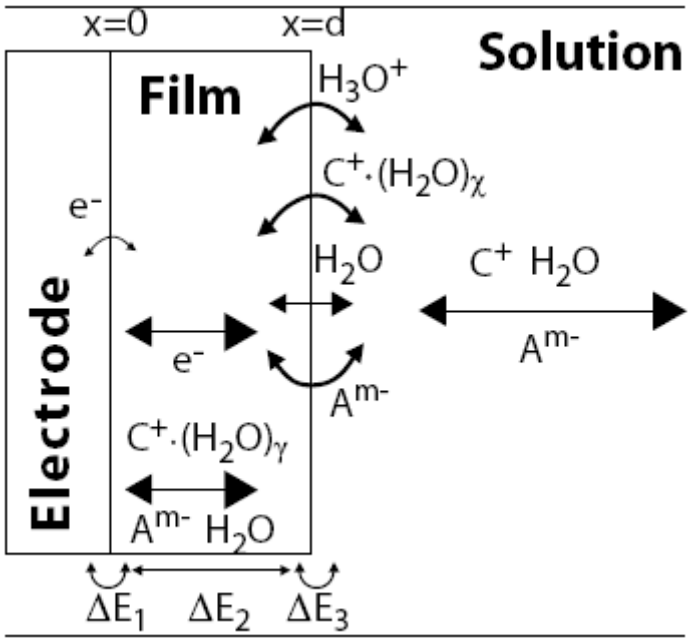

Figure 5.6: *Charge transport and interfacial transfer processes in an ICP-coated electrode [51, 177].*

Here an ICP film of thickness *d* (on a metal electrode) is shown that exchanges electrons and ions with metal electrode and electrolyte, respectively. Including the electrolyte in the system, the figure shows two bulk transport processes and the same number of interfacial transfer processes. Electrons are exchanged only at metal/polymer interface under ΔE_1 potential difference. The cations ($C^+.(H_2O)_\gamma$), anions (A^{m-}), protons and solvent (water) ingress/egress from polymer/electrolyte interface under ΔE_3. Electrons and ions move through the bulk membrane under a potential difference ΔE_2 whereas ions move freely in the electrolyte solution. Ions and electrons are completely blocked at metal/polymer and polymer/electrolyte interface, respectively. It implies that no net current whether electronic or ionic can pass through the system, completely, at low frequencies. This limits the complete understanding of the diffusional processes taking place in the system.

Contrary to ICP coated electrodes (also called asymmetric configuration), a symmetric configuration has been employed where a free-standing membrane is bathed with electrolyte on both sides so blocking the electronic charge transport through the interfaces but allowing ionic current to pass through the membrane. The interfacial phenomena observed in this case is attributed only to the ionic charge transfer at polymer/electrolyte interface [175, 176, 178].

To study the charge transport and interfacial charge transfer phenomena in ICPs (both in asymmetric and symmetric configurations), various models have been proposed. These models differ in the consideration of the nature of ICP film either as homogenous or heterogeneous, composed of nano-sized pores [179]. The heterogeneous models stem from the nodular or fibrillar morphology of ICP that gives rise to nanopores in the bulk film. Additional differences arise from different viewpoints on whether including or not the interfacial charge transfer in the model and the nature (Faradic versus non-Faradic double layer charging) of the process. Vorotynstev et al. [179] proposed a homogenous film model based on diffusion-migration phenomena representing the electron (polaron) and (counter) ion transport in ICP film coated on a metallic electrode. The model has some specific features that had not been considered in the previous homogenous film models. These features include the incorporation of interfacial double layer charging phenomenon and unequal diffusivities of electrons and ions in the film (i.e. $D_e \neq D_i$). The latter resulted in non-uniform electrical and concentration fields throughout the bulk of the film. This model was used in various subsequent studies to investigate the effects of the nature of cations and anions on the diffusivities and interfacial charging [69, 180, 181]. Deslouis et al. [175] have adopted the model of Vorotynsetev et al. for a free-standing membrane configuration and compared the response with that of the modified electrode geometry. The diffusion-migration fluxes in the membrane were based on Nernst-Planck equations;

$$J_e = -D_e \frac{\partial c_e}{\partial x} - D_e \frac{c_e e}{kT} \frac{\partial \Phi(x)}{\partial x} \tag{5.20}$$

$$J_i = -D_i \frac{\partial c_i}{\partial x} + D_i \frac{c_i e}{kT} \frac{\partial \Phi(x)}{\partial x} \tag{5.21}$$

where J, D and c denote flux, diffusivity and concentration, respectively. Subscripts e and i denote electronic and ionic entities, respectively, whereas e stands for the charge (+e for polaron and –e from anions). k denotes Faraday's law constant and T is absolute temperature. The model differentiates between the Faradic charge transfer and a double layer charging at metal/electrolyte interface. The final expression includes both the film polarization impedance and impedance of the interfacial double layer charging represented by a parallel R-C circuit.

$$Z_M = \frac{2Z_i}{1 + j\omega C_i Z_i} + R_p + R_p \frac{(D_e - D_i)}{2D_i} \frac{\tanh \upsilon}{\upsilon}. \tag{5.22}$$

Z_M is the impedance of the free-standing membrane, Z_i and C_i are the interfacial double layer impedance and capacitance, respectively. R_p is the film resistance defined as $\frac{kTd}{e^2c(D_e + D_i)}$ with d as the membrane thickness. Here ν is a dimensionless quantity defined as;

$$\upsilon^2 = d^2 j\omega \frac{(D_e^{-1} + D_i^{-1})}{8} \tag{5.23}$$

Equation (5.22) gives a response comprising two semicircles in Nyquist plot whereas the size and position of the semicircles depend on the relative values of the electronic and ionic diffusivities.

On the other hand, Albery et al. [174, 182, 183] developed a transmission line model for ICP coated electrodes by assuming two-phase heterogeneous film morphology. Electronic charge passes through the film whereas ions are transported through the electrolyte present in the nanopores of the film. Two different transmission lines represent both electronic and ionic resistances whereas these both lines are interconnected by a charge transfer capacitance that arises from the electrolyte in nanopores (Figure 5.7). The capacitance in this case is distributed i.e., it varies with the frequency. Many researches later used this model to study the electrochemical properties of ICP and their composites [70, 184, 185].

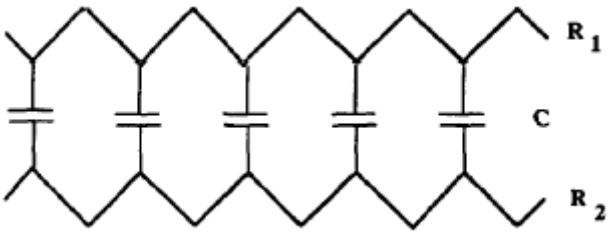

Figure 5.7: *Transmission line model for modified electrode, R_1 and R_2 represent two resistive paths whereas C is the capacitance[174].*

Albery's model does not include the interfacial phenomena that take place at the polymer/electrolyte interface. Deslouis et al. [70] adopted the model for a free-standing PANI membrane by changing the boundary conditions but they also neglected the interfacial charge transference.

Paasch et al. [186] developed an improved transmission line model for macroscopically homogenous porous modified electrodes. They extended their model by incorporating the

short-range diffusive resistances originating from the charge transfer reactions at the walls of the nanopores. Additionally, these charge transfer resistances have been considered distributed in nature in view of the spatially distributed oxidation-reduction transitions in the bulk of the film. Robberg et al. [71, 187] used the same model to study the PANI modified electrodes at various potentials and pH of the electrolyte.

Ehrenbeck et al. [176] extended model developed by Paasch et al.[186] and investigated the electrochemical processes in polypyrrole free-standing membranes by using EIS. In their earlier studies, Ehrenbeck and Juttner [188, 189] used an older version of the model for heterogeneous films to interpret the EIS response of free-standing polypyrrole membranes with mobile and immobilized dopants. The model was based on the two transmission lines, each for electronic and ionic conduction and both are linked with the interfacial capacitance and charge transfer resistance at the walls of the nanopores (Figure 5.8).

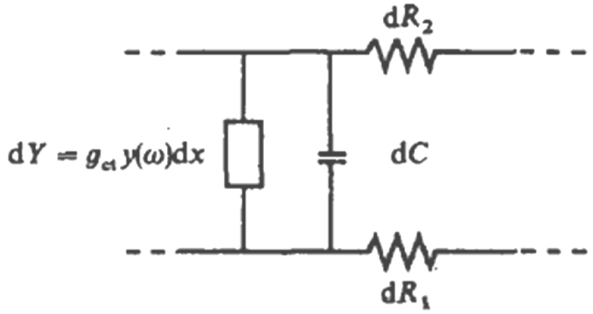

Figure 5.8: *Transmission lines model for ICP film modified electrode [186].*

In the above schematic figure, dR_1 and dR_2 represent two resistive lines for two types of charges, i.e., electronic and ionic, and dC is the interfacial capacitance developed at the pore walls. Here, g_{ct} represents charge transfer conductivity;

$$g_{ct} = i_0 SA\frac{F}{RT} \tag{5.24}$$

where i_0 is charge transfer current density, S is pore surface area per unit volume of the membrane, A is the surface area of the membrane, F is Faraday's law constant, R is general gas law constant and T is the absolute temperature.

The charge transport takes place by oxidation-reduction coupling of micro-domains of PPY film by the incorporation of doping anions from the solution. Since this oxidation front progresses gradually within the film, the charge transfer resistance is distributed in the bulk

film, instead of being a constant one across the cross section. The charge transfer conductivity is opposed by the diffusion hindrance so the local conductivity value is modified with a frequency-dependent admittance, as follows,

$$g_{ct} \rightarrow g_{ct} Y(j\omega) \tag{5.25}$$

where Y(jω) is admittance (reciprocal of impedance), defined as,

$$Z(\omega) = \frac{1}{Y} = 1 + \left(\frac{\omega_2}{j\omega}\right)^{\frac{1}{2}} \coth\left(\frac{j\omega}{\omega_3}\right)^{\frac{\alpha}{2}} \tag{5.26}$$

Here ω stands for the angular frequency (radians.s^{-1}), ω_2 and ω_3 are the characteristic frequencies representing (anions) diffusion hindrance and space limitations due to the available pore length. α denotes pore length distribution in the film. This leads to the final expression for the film impedance,

$$\left(Z - R_0\right)\frac{A}{d} = \frac{\rho_1\rho_2}{\rho_1 + \rho_2} + \frac{\rho_2^2}{\rho_1 + \rho_2}\frac{2\lambda}{d}\tanh\frac{d}{2\lambda} \tag{5.27}$$

Here R_0 is electrolyte resistance; ρ_1 and ρ_2 are the resistivities of ICP film and electrolyte, respectively; A and d are the area and thickness, respectively, whereas λ represents the decay length. The Nyquist plot of this equation consists of two successive semicircles representing the dielectric distribution and charge transfer resistance at the high and low frequency ranges. Impedance arising from the interfacial phenomenon between film and electrolyte was not observed in the experiments.

More recently, EIS has successfully been used to study the charge transport characteristics of pristine PANI and PANI composites membranes. Kocherginsky and Wang [76] employed EIS to elaborate the effects of interfacial capacitance of nanopores of apparently homogenous PANI film on the ionic transport along with the effects of membrane thickness. The equivalent circuit modelling was used to distinguish the high frequency bulk characteristics from the low frequency interfacial charge transfer effects. Super-capacitance (480 F. g^{-1}) of the self doped PANI nanofibres was measured by using the two-electrode EIS technique [190]. High values of capacitance of nanofibres were observed which were attributed to the highly porous structure due to the fibrillar and nodular morphology of PANI nanofibres.

Perflourinated cation-exchange membranes were modified with PANI using *in situ* chemical polymerization, and electrical and ionic conductivities were measured by using EIS to investigate the effects of PANI intercalation levels in the base membrane [111]. PANI inclusion in the base cation-exchange membrane did not affect the conductivity values as compared to the unmodified base membrane. Higher levels of PANI intercalation at prolonged aniline polymerization times reduced the ionic conduction that was attributed to the change in the microstructure of the composite membrane. The change in the dispersion levels of the PANI in the bulk membrane at prolonged polymerization from uniform distribution to the cluster formation decreased the protonic conductivity of the composite. In another study, Deka and Kumar [97] studied the effect of incorporation of undoped PANI nanofibres in a porous polymer electrolyte membrane for Li-ion batteries. The composite membrane was synthesized by using solution-casting method and ionic conductivity was measured by the fitting an equivalent circuit model on the EIS data. Ionic conductivity increased for up to 6% intercalation level of PANI and then decreased for higher levels. It was postulated that initially, PANI incorporation facilitated Li ion transport but upon the cluster formation at higher incorporation levels, the conduction path was blocked. Temperature dependence of conductivity was also elaborated.

5.2.3 EIS Characterization of PANI Composite Membranes

Selection of the Experimental Conditions

EIS results of PANI-mixed cellulose ester membranes synthesized by using various chemical oxidative polymerization techniques are presented in this section with the aim to evaluate the electronic and ionic charge transport properties of the composite membranes. Equivalent circuit (EC) approach has been used in which the physical processes taking place in the membrane and membrane/electrolyte interface are modelled by an equivalent circuit comprising common electrical elements such as resistor, capacitor, inductor etc. [191]. For EIS characterization of free-standing membranes, two-electrode and four-electrode electrochemical cell configurations have been employed. The four-electrode configuration is preferred over the two-electrode because of the elimination of electrode polarization effects in the former case [70, 175]. In the four-electrode configuration, current is supplied through the electrode pair and voltage is measured through another electrode pair. However for high impedance systems, these both configurations yield essentially same impedance results [70]. In the EIS of solid films/membranes with two charge carriers (e.g., ICPs with electrons or polarons, and ions as charge carriers), the conditions at the film/electrode and/or electrode/membrane interface define the boundary conditions for the transport equations. In addition, these interfacial conditions describe the low frequency response, which is termed as dc response of the system. For example, in metal/membrane/electrolyte electrochemical system (i.e. modified electrodes) at low frequencies, neither electrons nor ions can pass through the film so the semicircle in Nyquist plot does not intersect the real axis. In contrast, for metal/membrane/metal or electrolyte/membrane/electrolyte systems, low frequency response is always ohmic and the curve in the Nyquist plot intersects the real axis at low frequencies [178, 192]. In addition, for metal/membrane/electrolyte asymmetric systems, ions from the electrolyte move into the membrane to balance the net electronic charge imparted from the metal/membrane interface thus the system is non ‘conservative’ for ions. Symmetric systems are always conservative as the net ions ingress in a half cycle of the wave is balanced by the egress in another half cycle [178].

In view of the above discussion, a metal/membrane/metal configuration is selected in this thesis to characterize the free-standing membranes. This configuration has the advantages of being a conservative system with respect to anions, as they cannot leave the system. The electronic charge passes across the membrane through the electrodes so essentially the interfacial charge transfer can be identified as electronic charge transfer. EIS of PANI composite membranes was attempted by sandwiching the membrane between two inert gold electrodes. This configuration was adopted to minimize the interfacial effects arising from the various charge transfer phenomena (e.g. surface polarization) by ensuring a good electrode/membrane contact. To elucidate the effects of PANI doping state on the charge transport characteristics, EIS studies in both doped and undoped states were conducted with HCl (pH < 1) and water (pH~ 6) as electrolyte, respectively. To equilibrate the membrane with doping anion (Cl^-) or vice-versa, each membrane was soaked with respective solution (HCl or water) for longer than 12 hours prior to EIS measurements. Metal/membrane/metal configuration has been considered as ion-blocking which allows only electrons to pass through the interface hence depicting electronic dc characteristics at extremely low frequencies [181, 192]. However, because these membranes are electrolyte-soaked, a thin film might have formed at membrane/electrode interface so truly speaking this interface is not completely ion blocking [174, 181]. Although the membranes have been soaked for sufficiently long times, yet entrapped electrolyte may not fulfil the condition of being an anion reservoir to compensate all the electronic charge developed in the membrane [192]. To get the improved response, in addition to the conventional metal/membrane/metal configuration, Pt/membrane/Pt configuration was used where Pt wires were attached to the both faces of the membranes and these were bathed with the electrolyte from both sides in a two-compartment cell. This set-up yields mixed electronic-ionic transference at the interface but with the availability of anion in abundance. The EIS of bathed membrane in the two-compartment cell was conducted at different doping conditions by using either 1 M HCl (pH < 1) or 1M $CaCl_2$ (pH~12) as electrolyte. The experimental plan describing various employed combinations of membrane, electrolyte and electrochemical cell configuration is given in the Experimental Section (Table 3.1).

Electrochemical Modelling of EIS data

As discussed in section 5.2.2, the modelling of the electrochemical charge transport processes in pristine ICPs have been conducted under the framework of either homogenous film diffusion-migration model [179, 181] or macroscopically homogenous porous film model [174, 182]. The latter is based on a dual transmission line which connects electronic conductivity of the membrane phase with that of the ionic conductivity of the electrolyte in the pores through a double layer capacitance and charge transfer resistance at the pore surface [182]. These models mainly elucidate the charge transport characteristics of ICP coated electrodes. Later on, these models have also been applied to free-standing pristine ICP membranes [70, 175, 176, 188]. These models have inherent limitations such as the assumption of a homogenous film in the first model and macroscopically homogenous porous film in the second model. The migration/diffusion processes in the second model are represented by the volume-averaged parameters such as resistance, capacitance etc. Moreover, these models are based only on the electronic and ionic diffusion inside the membrane bulk and ignore interfacial charge transfer processes. To model the more general systems with heterogeneous morphologies and surfaces, other equivalent circuits comprising lumped parameters (resistors, capacitors etc.) have been used. In view of the above discussion, equivalent circuit modelling has been used in this thesis where electrochemical characteristics of the system are model as lumped parameters. However, the distribution of the capacitance has been considered by incorporating constant phase element (CPE) in the model to account for the spatially distributed properties of the system. In addition, the Warburg element has been included (wherever required) which models the semi-infinite restricted diffusion. The Warburg element gives rise to the same effects as that of a transmission line in a heterogeneous film model.

The equivalent circuit modelling has widely been used for EIS data of free-standing membranes. These include characterization of the transport and fouling properties of conventional ion exchange membranes [167, 168, 191], redox reactions at the surface of polyaniline membrane [193], ionic transport in polyaniline membrane at different pH [76] and effects of polyaniline intercalation on the charge transport characteristics of the conventional cation-exchange membrane [111]. In addition, the electrochemical transport in solid electrolyte membranes for Li-ion batteries has been also characterized by equivalent circuit modelling [194, 195].

In all these studies, charge transport processes in the bulk membrane and charge transfer at the electrode/membrane or electrolyte/membrane interface have been modelled by using various combinations of capacitors and resistors each representing a physical process in electrochemical cell. However, it should be emphasized here that sometimes this correspondence is not straightforward. Particularly in the case of conducting polymers, the controversy in the interpretation of various charge transport processes still prevails in the literature [51, 196]. Different resistor-capacitor (R-C) combinations have modelled interfacial charge transfer and bulk charge transport where ionic diffusion in the bulk membrane is represented by either another R-C element or a Warburg element (defined latter) for semi-infinite diffusion.

In an early study on the transport processes in a free-standing PANI membrane, the interfacial electronic and ionic transfer processes are modelled by a combination of a double layer capacitance and the electronic and ionic charge transfer impedances [193]. The bulk transport due to the ionic diffusion has been modelled by an additional impedance element. This multiple capacitance-impedance model is fitted well on the EIS data to study the surface reactions of the redox active species in the electrolyte.

Kocherginsky and Wang have modelled EIS data of a free-standing pristine polyaniline membrane by using a two R-C loop equivalent circuit where both loops are connected in parallel to represent the high and low frequency impedance behaviour [76]. The high frequency R-C loop represents bulk membrane transport processes whereas the low frequency R-C loop represents slow diffusionally controlled transport of ions trough the membrane. EIS modelling of both doped and undoped membranes was attempted. The high resistance ($\sim 10^{6}$ ohm) and low capacitance ($\sim 10^{-9}$ F) in undoped PANI represent charge transport in an insulating film. These values were increased around 3-4 orders of magnitude upon doping by HCl (up to 1.7 ohm and 0.5 F, respectively), representing the low electronic resistance and presence of the redox capacitance of PANI (pseudocapacitance).

In another study, a perflourinated cation-exchange membrane was modified by depositing PANI inside the base membrane [111]. The composite membranes were characterized by fitting an equivalent circuit model to the EIS data. In this equivalent circuit, a resistor and a series-connected R-C element model the protonic conductivity and interfacial charge transfer

processes, respectively. The protonic resistance decreases with acid doping whereas the charge transfer capacitance does not change much with the doping (~10^{-5} F). This indicates the presence of a double layer capacitance at the interface instead of a PANI redox capacitance.

In the present research, the composite membranes represent a complex electrochemical system comprising insulating ME phase, conducting PANI phase and the electrolyte in the pores. The exact interpretation of the electrochemical behaviour is very complex and involves a number of known and unknown parameters. Therefore, in the following discussion, the EIS interpretation mainly focuses on the effects of PANI deposition site, extent and doping state on the electrochemical behaviour.

EIS data of the composite membranes were analysed by using ZSinpWin$^{(R)}$ electrochemical impedance analysis software and the equivalent circuit models have been fitted by considering the following factors.

1. The fitted equivalent circuit should represent, at least, the important physical processes taking place in the bulk membrane and at the interfaces. It implies that equivalent circuit should be simple so that the components can easily be correlated to the physical processes in the electrochemical system [191].
2. The fitting process should yield a minimum statistical error. The software iterates to minimize chi-square (χ^2) values that remained in the range of ~10^{-4} for all the fitted models.

In the following discussion, EIS data and the modelling of the composite membranes conducted with two-point gold electrodes are presented first which follow the data and the modelling of the bathed membrane.

As mentioned in Table 3.1, the composite membranes covering a wide spectrum of the synthesis conditions have been tested by EIS. However, under the condition of ion-blocking electrodes (i.e. two gold electrodes), some of these membranes did not yield satisfactory EIS spectra. The composite membranes containing comparatively small amount of PANI showed

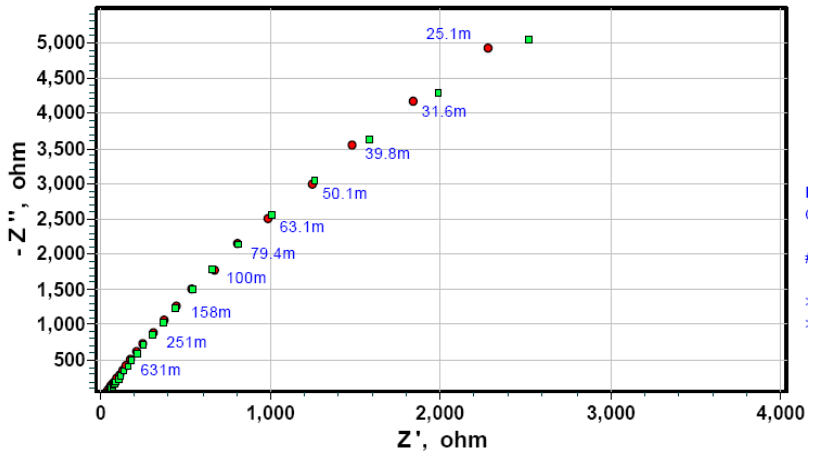

(a)

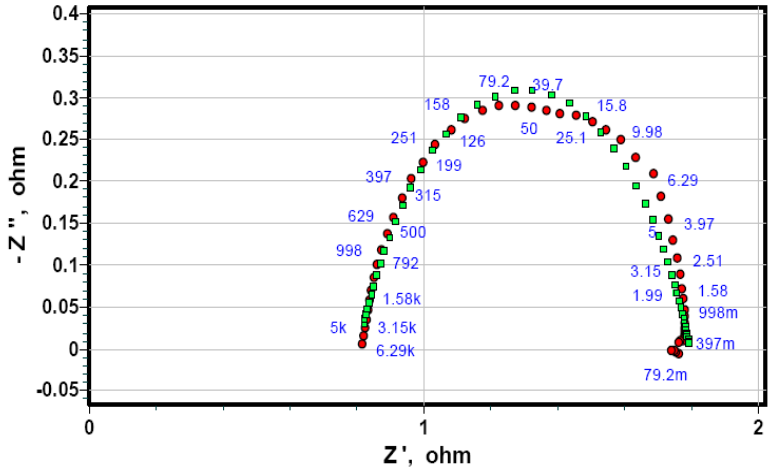

(b)

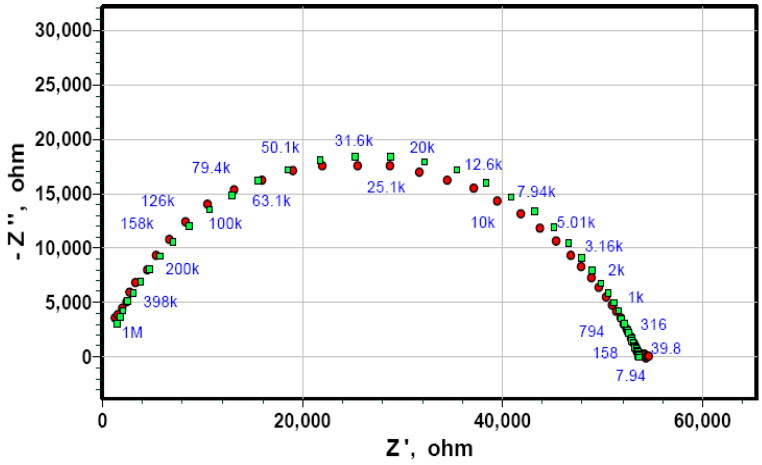

(c)

Figure 5.9*: The Nyquist plots of PANI composite membranes impregnated with 1M HCl (a) ME,Poly,Fe,22h (b) ME,P1,22h and (c) ME,Vap,APS.*

highly distorted spectra with very large impedance values (~10^{11} ohm). These include acid-soaked bare ME; ME, Poly, 6 h and ME, P1, 2 h.

On the other hand, HCl doped composite membrane synthesized by using the two-compartment cell polymerization for > 6 h showed low resistance value. The membranes with scattered EIS data were not included in the analysis due to uncertainty in the results.

The Nyquist plots of HCl-soaked membranes are shown in Figure 5.9 where the measured (red) and fitted (green) data points are shown to illustrate the quality of the model fitting (for the modelling detail, see the following discussion). The shape and impedance scale of these curves show the effects of PANI deposition from different polymerization techniques on the charge transport properties of the composite membrane. A quick qualitative analysis reveals the following trends.

1. The impedance on the real axis shows charge transport/transfer resistance whereas the charge holding capacity (capacitance) is inversely proportional to the imaginary component of the impedance [132]. ME membranes modified by the solution-phase and vapour-phase PANI deposition showed high levels of charge transport resistance (10^4-10^6 ohm) and low levels of charge storage capacitance(~10^{-4} F) as compared to the membranes synthesized by using the two-compartment permeation cell (< 3 ohm and up to 0.1 F, respectively).

2. The resolution of impedance with respect to the frequency i.e., appearance of a semicircle in a particular frequency range represents a relaxation process with a characteristic time (i.e., τ = RC). The impedance resolution at high and low frequencies represents kinetically and diffusionally controlled processes, respectively [197]. An inspection of the Figure 5.9 reveals diffusionally controlled charge transport for ME, Poly, 22 h whereas ME, Vap, APS and ME, P1, 22 h show charge transport hindered by the kinetically limiting step.

Because each polymerization technique deposited PANI at a distinctive site in the base membrane, the composite membranes were analysed by using different equivalent circuits representing membrane morphology and the electrochemical processes taking place within the composite membrane. Starting with the composite membrane synthesized by the solution-phase polymerization that has a thin PANI layer only at the surface and the most of the bulk

membrane remained unmodified; the various electrochemical processes are shown in Figure 5.10.

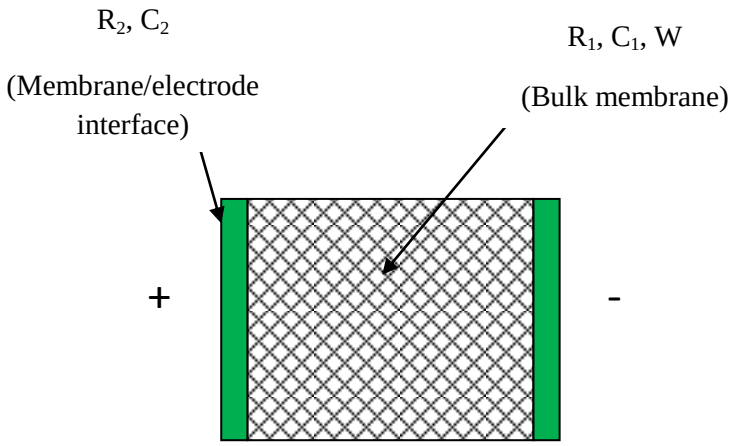

Figure 5.10: *Schematics of the electrochemical transport processes of PANI composite membrane synthesized by the solution phase polymerization (22h).*

The electrochemical system consists of a PANI layer at the membrane surface that is in contact with two inert (gold) electrodes. The electronic charge transfer from the electrodes to the membrane surface is a kinetically controlled process due to the involvement of the interfacial charge transfer process with a certain charge transfer resistance (R_2). Moreover, the surface polarization develops a charge separation at the surface that can be represented by a double layer capacitance (C_2). This double layer capacitance becomes a redox capacitance (pseudocapacitance) depending on the PANI deposition level and the doping state. For the bulk membrane, the charge transport through the membrane depends on the relative magnitudes of the electronic resistance of the polymer phase and ionic resistance of the electrolyte in the pores of the membrane. These two resistances are connected with each other through a double layer capacitance of the electrolyte in the pores (C_1). The equivalent circuit representing these electrochemical processes is shown in Figure 5.11. It consists of two R-C loops and a Warburg element (W). The first R-C element represents bulk membrane processes where R_1 represents the resistance of the membrane that comprises the polymer phase and the pore electrolyte. The second R-C loop coupled with the Warburg element represents kinetically slow processes in the membrane. These may arise from either the ionic diffusion through the bulk membrane or interfacial charge transfer from the electrodes (e.g. adsorption of the ionic species at the surface). In the latter case, the interfacial charge transfer is affected by the development of a polarization double layer at the surface. Here R_2 and C_2 represent the charge transfer resistance and capacitance at the surface, respectively. The

Warburg element (defined latter) represents the slow ionic diffusion of ions in the membrane bulk [192, 193, 198]. The slow interfacial charge transfer shifts to a swift charge transfer reaction in the presence of a PANI layer at the surface and in this case, the second loop may represent ionic diffusion through the membrane.

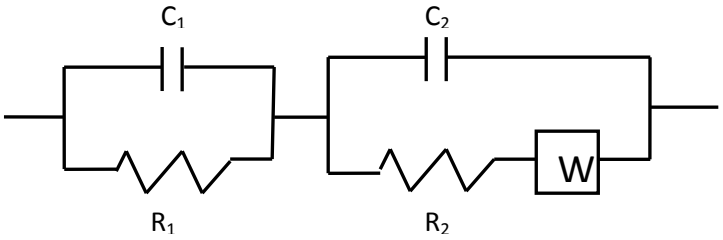

Figure 5.11: *The equivalent circuit representing the EIS behaviour of PANI composite membrane synthesized by the solution-phase polymerization (22 h).*

Depending on PANI deposition site and extent, and its doping state, one or more elements in this general equivalent circuit (Figure 5.11) can be eliminated and the electrochemical processes of the membranes can be fitted with a simpler equivalent circuit.

The distorted semicircles in the electrochemical spectra of Figure 5.9 are indicative of a frequency-dependent capacitance instead of a constant capacitance. Such variable capacitance is called distributed capacitance and it shows the heterogeneity of the system e.g., surface heterogeneity in the case of interfacial charge transfer process. Distorted semicircles in the Nyquist plots can be represented by a constant phase element (CPE) instead of a pure capacitor. The impedance of a CPE is given by,

$$Z(\omega) = \frac{1}{Y_0}(j\omega)^{-\alpha} \tag{5.28}$$

where $Z(\omega)$ is the impedance of CPE, ω is angular frequency and α is CPE index that varies as $-1 \leq \alpha \leq 1$ showing pure inductance, resistance and capacitance at α=-1,0 and 1, respectively. The value of α in the range $0.5 \leq \alpha \leq 1$ shows the scale of heterogeneity as it departs from the

ideal capacitance value of 1 [186, 191]. Y_0 represents admittance (i.e.1/Z) at ω=1 and α=1, which may be considered equivalent to the capacitance of an ideal capacitor [191].

The overall impedance of the equivalent circuit of Figure 5.11 is given by the following equation (using Equation 5.28 for CPE).

$$Z(\omega) = \frac{R_1}{1 + R_1 Y_0 (j\omega)^{\alpha}} + \frac{R_2 Z_W}{[R_2 + Z_W] + (R_2 Z_W) Y_o (j\omega)^{\alpha}} \tag{5.29}$$

where all the symbols have been defined above except Z_W which represents the impedance of a Warburg element and is defined as,

$$Z_W = \frac{1}{Y_W \sqrt{(j\omega)}} \tag{5.30}$$

Here Y_W is the admittance of Warburg element ($S.s^{0.5}$).

The values of the various electrochemical parameters obtained by fitting the model equation are shown in Table 5.1 along with chi-square value. The low chi-square values confirm the excellent quality of the fit that is also depicted by the good overlapping of the model curve in Figure 5.9. Because the resistance of ME phase is very high, the charge transport through the pore electrolyte may dominate in the bulk membrane as also shown by the comparatively lower R_1 values. The charge transfer resistance (R_2) at the surface is much higher as compared to that of a typical range for pristine polyaniline (3~6 $ohm.cm^{-2}$ [199]). This can be explained in terms of incomplete surface coverage with a non-uniform PANI layer as also indicated by the low CPE admittance value (Y_o) of the fitted equivalent circuit. The low value of Y_W indicates a slow charge transfer process that is due to mainly by the slow ionic diffusion in the polymer phase.

An inspection of Figure 5.9 (b) readily reveals a significant change in the shape and impedance scale of the membrane synthesized by the two-compartment cell polymerization. The small resistance value shows a fast charge transfer process through the PANI phase in the composite membrane. In this situation, there should be no charge transfer resistance (or negligibly small) and the bulk charge transport takes place through the electronic conduction in PANI coated ME strands linked with a double layer capacitance at the pore walls of the membrane [176, 186]. A modified Randles circuit as shown in Figure 5.12 can satisfactorily model these electrochemical processes.

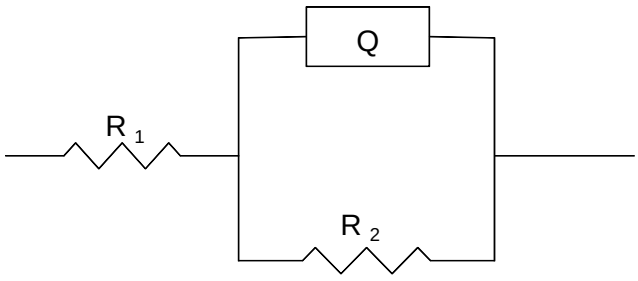

Figure 5.12: *Modified Randles circuit.*

Here R_1 shows uncompensated cell resistance (wires, connecters etc). In fact an inductive behaviour at high frequencies was observed in this case (not included in the curve)[191]. R_2 and Q represent the resistance and capacitance (distributed: CPE), respectively, of a bulk redox reaction taking place during the charge transport in the PANI phase. This capacitance is termed as pseudocapacitance that arises from the PANI redox reactions involving anion transport [76]. The impedance of this equivalent circuit is given by,

$$Z(\omega) = R_1 + \frac{R_2}{1 + R_2 Y_0 (j\omega)^{\alpha}} \tag{5.31}$$

One can deduce this equivalent circuit from that of Figure 5.11 by applying certain assumptions as stated above. The results are tabulated in Table 5.1. The low value of R_2 indicates resistance of the electronic path in the membranes that originates from a swift charge transfer reaction involving PANI layer at the surface of the pores. This conclusion is also supported by the high value of CPE admittance that could result from the redox transformation in PANI phase.

The Nyquist plot of the composite membrane synthesized by using vapour-phase polymerization shows an incomplete semicircle at high frequencies (i.e. small relaxation time) (Figure 5.9 c). The impedance resolution at high frequencies indicates the transport processes in the bulk membrane that can be modelled by a distributed capacitance (Q) in parallel with an ionic resistance (R) of the pores (Table 5.1). The kinetics of the interfacial charge transfer process is also neglected in this case. The high charge transportation resistance (~10^4 ohm) along with the low admittance value indicate charge transfer in the

bulk membrane involving high resistance. The low admittance value in this case represents an incompletely developed double layer at the pore walls. This can be attributed to the hydrophobic nature of the membrane surface that may not allow sufficient electrolyte to penetrate into the membrane. The absence of the low frequency impedance resolution indicative of bulk diffusion also supports this explanation.

Undoping of PANI composite membranes by soaking in water introduces significant changes in the electrochemical behaviour as shown in Figure 5.13. The comparatively higher resistance and low admittance values are attributable to undoped PANI in the composite membranes. Unmodified ME shows impedance resolution at low frequencies that indicates diffusionally controlled charge transport probably due to the low electronic conductivity of the polymer phase. In contrast, ME, Vap, APS, ME,P1,6 h and ME, P1,22 h show impedance resolution at high frequencies, characteristics of kinetically controlled processes exhibiting small relaxation times. However, the high resistance values indicate large charge transport resistances of the membrane phase. These kinetically controlled processes at high frequencies might have arisen from the combination of a double layer capacitance (in the pores) and resistance of the electronic path of the membrane phase.

In the case of unmodified ME membrane soaked in water, the impedance resolution at medium-to-low frequency range and shape of the impedance curve (Figure 5.13 a) suggest an equivalent circuit comprising two R-C element as shown in Figure 5.11. The assignment of different circuit elements to the various electrochemical processes remains same as that of the acid-soaked membrane (ME,Poly,Fe,22h). The model parameters are tabulated in Table 5.2. The high frequency R-C loop accounts for the bulk membrane processes mainly arising from the charge transport in the pore electrolyte. An R-C loop at the low frequency coupled with a Warburg resistance represents the interfacial charge transport and slow ionic diffusion in the bulk membrane, respectively. The membranes synthesized by using the two-compartment cell and vapour-phase polymerizations show semicircles at high frequencies indicative of the charge transport relaxation in the bulk membrane [192, 200]. The similar relaxation phenomena have also been observed for the corresponding acid-soaked membranes. This suggests that PANI deposition site strongly affects the impedance resolution at a specific frequency range characterizing either bulk membrane or interfacial charge transport processes. For these membranes, the data can be modelled by a single R-C parallel combination (Table 5.2). The resistor represents membrane phase resistance whereas the capacitor represents double layer capacitance of the electrolyte (water) in the pores. The

charge transfer resistance from the membranes synthesized by the two-compartment cell polymerization represents charge transfer of PANI coated structural strands of the bulk membrane. This is also supported by the low admittance values indicative of low levels of double layer polarization as compared to that of HCl-soaked membranes.

The higher resistance value in the case of vapour-phase synthesized membrane may represent the electronic resistance of polymer (ME) phase due to incomplete wetting of the membrane. The same trend has also been observed for HCl soaked membrane (discussed above) and may be attributed to the hydrophobic nature of the membrane surface.

The composite membrane synthesized by prolonged solution-phase polymerization shows a semicircle at the high frequencies representing the bulk membrane relaxation processes. A capacitive rise in the low frequency range shows slow diffusion of the electrolyte ions in the membrane phase. The equivalent circuit represents the electrochemical processes of the membrane is shown in Figure 5.14 and the results are given in Table 5.2.

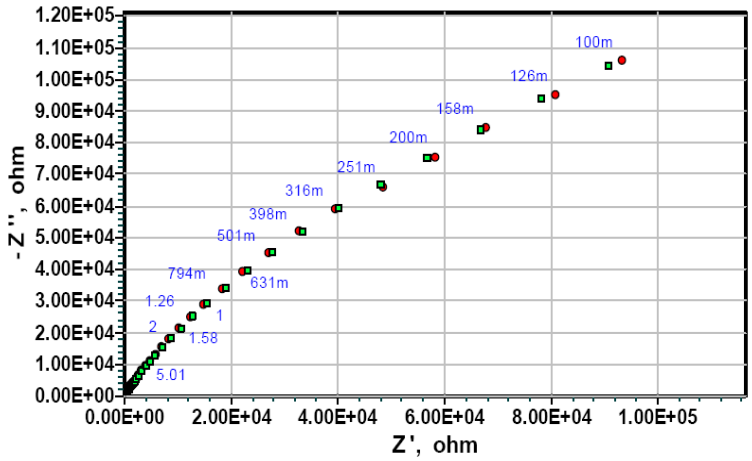
1.20E+05
1.10E+05
1.00E+05
9.00E+04
8.00E+04
7.00E+04
6.00E+04
5.00E+04
4.00E+04
3.00E+04
2.00E+04
1.00E+04
0.00E+00
- Z '', ohm
0.00E+00
2.00E+04
4.00E+04
6.00E+04
8.00E+04
1.00E+05
Z', ohm
100m
126m
158m
200m
251m
316m
398m
501m
631m
794m
1
1.26
1.58
2
5.01

(a)

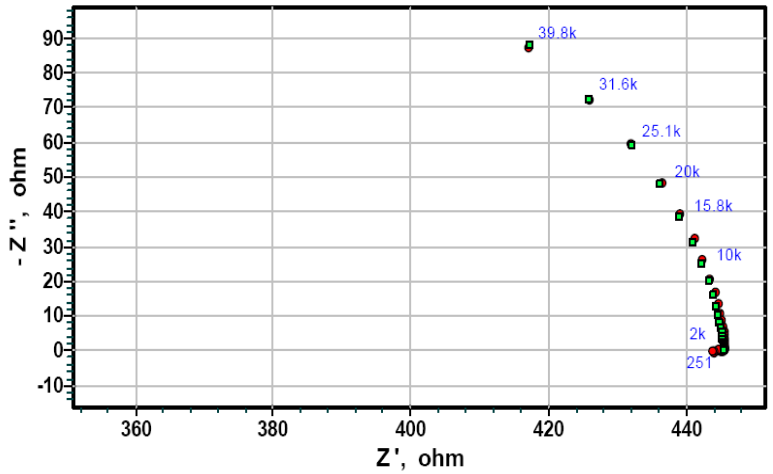
90
80
70
60
50
40
30
20
10
0
-10
- Z '', ohm
360
380
400
420
440
Z', ohm
39.8k
31.6k
25.1k
20k
15.8k
10k
2k
251

(b)

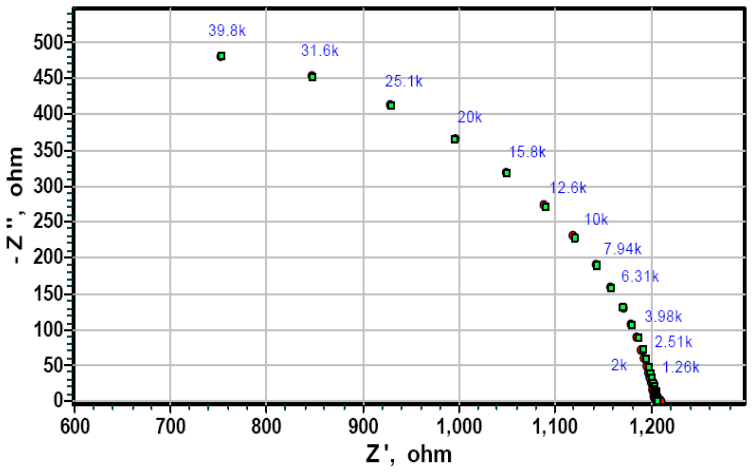
500
450
400
350
300
250
200
150
100
50
0
- Z '', ohm
600
700
800
900
1,000
1,100
1,200
Z', ohm
39.8k
31.6k
25.1k
20k
15.8k
12.6k
10k
7.94k
6.31k
3.98k
2.51k
2k
1.26k

(c)

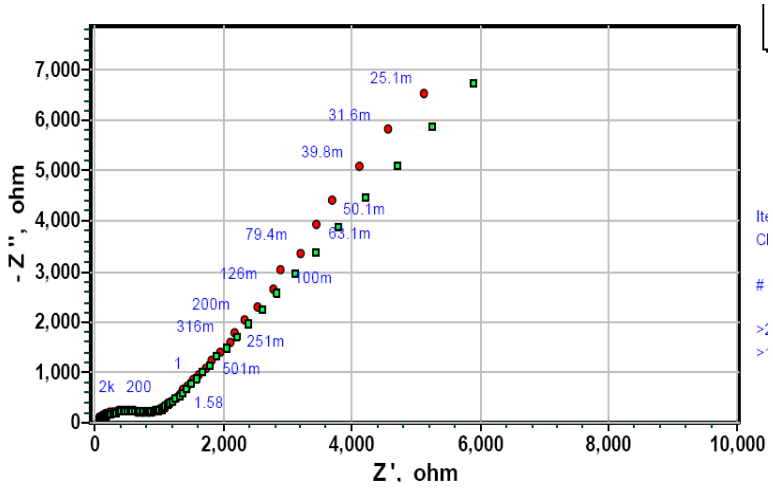

(d)

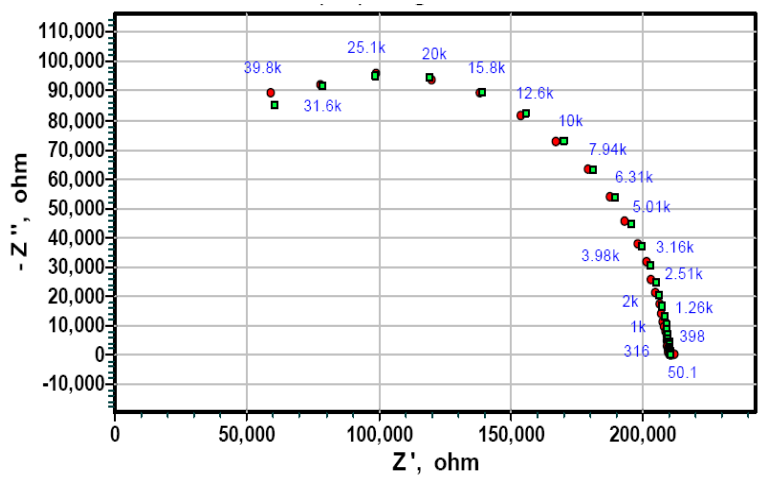

(e)

Figure 5.13: *EIS spectra of PANI-ME composite membranes soaked in water (a) bare ME (b) ME,P1,6h (c) ME,P1,22h (d) ME,Poly,22h and (e) ME,Vap,APS.*

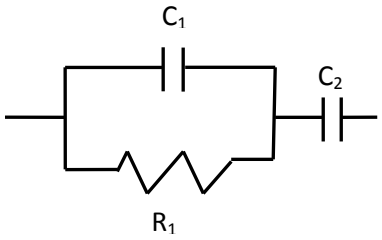

Figure 5.14: *The equivalent circuit representing the EIS behaviour of PANI water-soaked composite membrane synthesized by the solution-phase polymerization (22h).*

Table 5.1: The parameters of equivalent circuits fitted on EIS data of HCl soaked membranes

Membrane	**EC Model**	**R_o (ohm)**	**CPE_1 ($S.s^{\alpha}$)**	**R_1 (ohm)**	**CPE_2 ($S.s^{\alpha}$)**	**R_2 (ohm)**	**Y_W ($S.s^{0.5}$)**
ME,Poly,22h	(QR)(Q(RW)) χ^2:$6x10^{-5}$	-	Y_1= $7.6x10^{-4}$ α=0.5	42.6	Y_2= $7.3x10^{-4}$ α=0.84	$1.2x10^4$	$1.6x10^{-4}$
ME,P1,22h	R(QR) χ^2:$2.8x10^{-4}$	0.8	Y_2= $1.6x10^{-2}$ α=0.78	1.0	-	-	-
ME,Vap,APS	(QR) χ^2:$6x10^{-4}$	-	Y_2= $1.7x10^{-9}$ α=0.77	$5.4x10^4$			-

Table 5.2: The parameters of equivalent circuits fitted on EIS data of water soaked membranes

Membrane	EC Model	CPE_1 ($S.s^{\alpha}$)	R_1 (ohm)	CPE_2 ($S.s^{\alpha}$)	R_2 (ohm)	$\sigma(W)$ ($S.s^{0.5}$)
ME, unmodified	(QR)(Q(RW)) χ^2:$9x10^{-4}$	Y_1= $2.5x10^{-3}$ α=0.23	43.6	Y_2= $6.7x10^{-6}$ α=0.77	$1.9x10^{5}$	$9x10^{-6}$
ME,P1,6h	(QR) χ^2:$2.3x10^{-6}$	Y_1= $3.9x10^{-9}$ α=0.94	446	-	-	-
ME,P1,22h	(QR) χ^2:$5x10^{-6}$	Y_1= $9.7x10^{-9}$ α=0.89	1207	-	-	-
ME,Poly,22h	(QR)Q χ^2:$2.7x10^{-3}$	Y_1= $1.5x10^{-5}$ α=0.52	989	Y_2= $3.6x10^{-4}$ α=0.60	-	-
ME,Vap,APS	(QR) χ^2:$5.4x10^{-5}$	Y_1= $6.8x10^{-11}$ α=0.94	$2.1x10^{5}$	-	-	-

To ensure the abundant availability of doping anions from the electrolyte [192] and to investigate the effects of PANI deposition site on the charge transport processes of the composite membranes, EIS was also conducted in the electrolyte bathing condition. In this configuration, the membranes were interposed between the two compartments of a permeation cell. Two Pt wire electrodes were used for the supply of an electrical potential perturbation and simultaneously measuring the resultant current. The electrodes were directly attached to opposite sides of the membrane to minimize the effects of interfacial charge transfer polarization. Similar to the two gold electrodes configuration, these schematics also exchange electronic charge at the interface whereas electrolyte ions also ingress/outgress freely from both sides of the membranes.

The Nyquist plots of unmodified ME and PANI composite membranes bathed with 1M HCl are shown in Figure 5.15 along with the fitted curves of the appropriate equivalent circuits (discussed in the following).

The Nyquist plots of the various composite membranes show significant influence of PANI deposition site and extent on the charge transport properties of the membranes. Unmodified ME shows impedance resolution at the low frequency indicating a dominant diffusionally controlled transport process. The electrochemical processes can be modelled by an equivalent circuit comprises two R-C elements with an added Warburg resistance (Figure 5.11). A high frequency resistance (R_0) was added to the circuit of Figure 5.11 to account for the uncompensated resistance of the electrolyte. Furthermore, the composite membrane synthesized by the solution-phase polymerization for comparatively shorter time (i.e. 6 h) has been modelled by fitting the same equivalent circuit as fitted for unmodified ME membrane (Figure 5.11). The low level of PANI deposition in this case shows the similar electrochemical properties as that of the unmodified membrane. The results are given in Table 5.3. The comparatively lower resistances in the both cases (~12 ohm) represents ionic resistance in the pores with a typical double layer capacitance in the range of 10^{-4} F [76]. Similarly, the admittance of CPE_2 and high charge transfer resistance along with the low value of Warburg admittance (Y_W) indicate highly hindered electronic and ionic charge transfer at the interface and in the bulk membrane.

The increase in PANI deposition level by 22 h solution-phase deposition imparts significant changes to the electrochemical properties as compared to that of 6 h polymerization (Figure 5.15 and Table 5.3). The Nyquist plot shows a kinetic-diffusion type process that can be modelled by the same equivalent circuit as used for 6 h solution-phase polymerization. The similar resistance value of the bulk membrane (R_1) may be attributed to the ionic resistance in the pores. This explanation is also supported by the presence of a lower charge transfer resistance at the interface (R_2). This implies that the presence of a substantial amount of PANI in the composite membrane may change the resistance levels of the charge transport in the membranes.

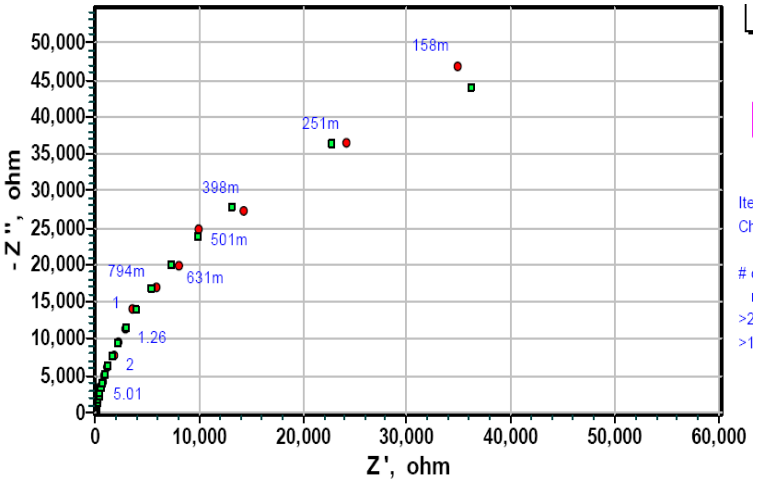
158m
251m
398m
501m
794m
631m
1
1.26
2
5.01
- Z '', ohm
Z', ohm

(a)

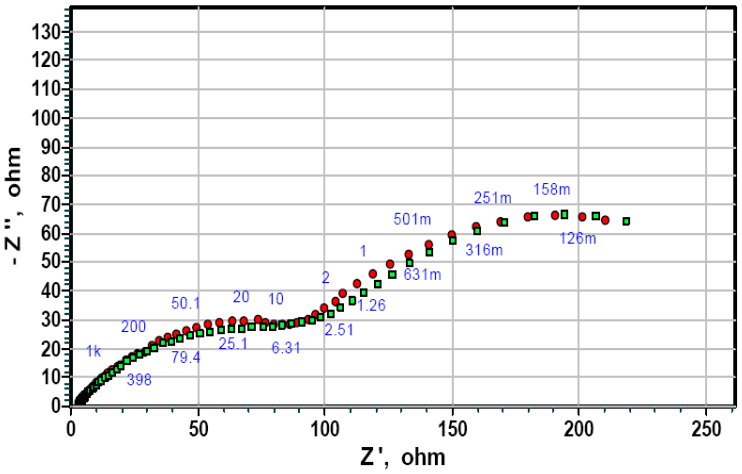
251m
158m
501m
316m
126m
1
631m
2
1.26
50.1
20
10
200
2.51
25.1
1k
79.4
6.31
398
- Z '', ohm
Z', ohm

(b)

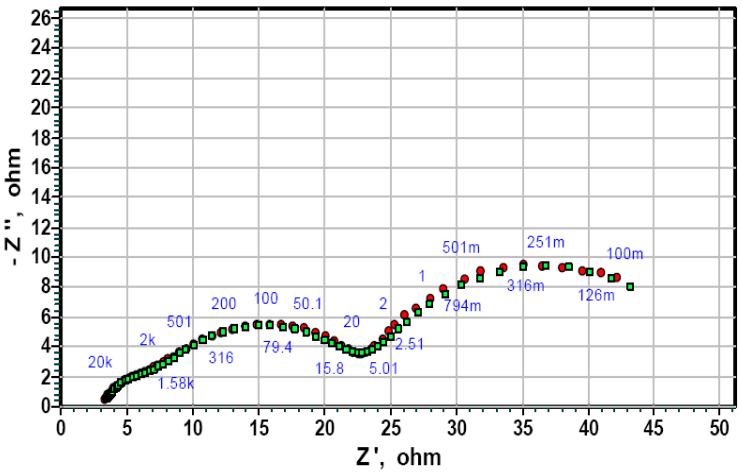
501m
251m
100m
316m
1
126m
794m
200
100
50.1
2
501
2k
20
316
79.4
2.51
20k
15.8
5.01
1.58k
- Z '', ohm
Z', ohm

(c)

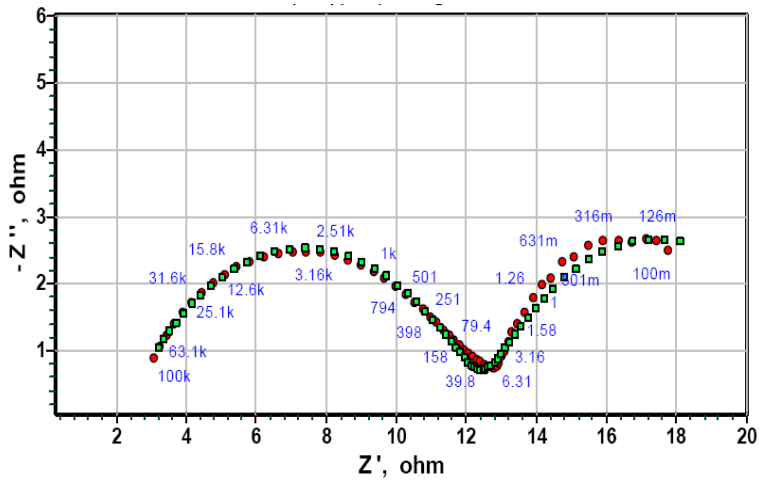
- Z '', ohm
Z', ohm
6.31k
2.51k
15.8k
1k
31.6k
3.16k
501
12.6k
1.26
316m
126m
631m
251
794
1
100m
398
79.4
1.58
25.1k
158
3.16
63.1k
39.8
6.31
100k

(d)

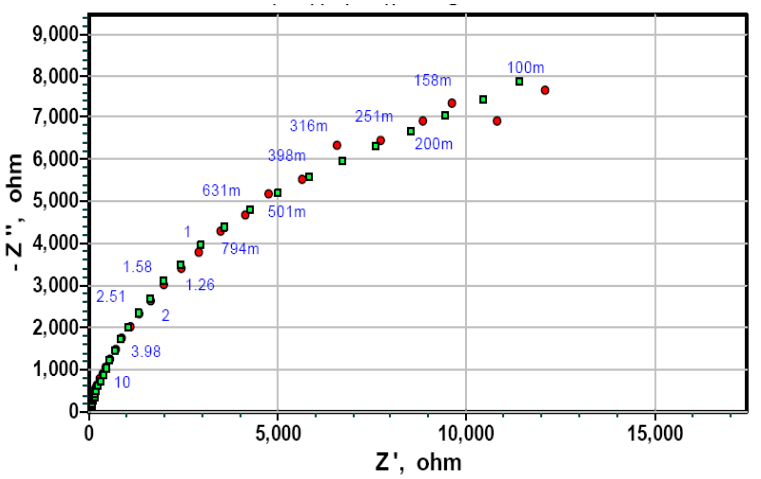
- Z '', ohm
Z', ohm
100m
158m
316m
251m
200m
398m
631m
501m
1
794m
1.58
1.26
2.51
2
3.98
10

(e)

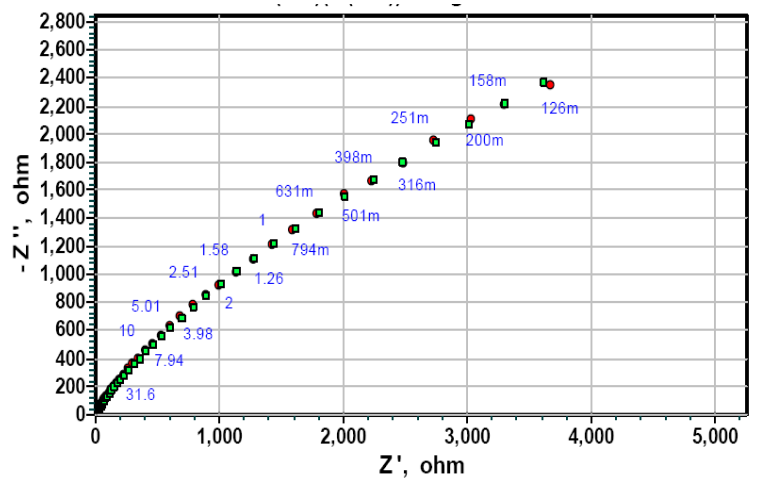
- Z '', ohm
Z', ohm
158m
126m
251m
200m
398m
316m
631m
501m
1
794m
1.58
2.51
1.26
5.01
2
10
3.98
7.94
31.6

(f)

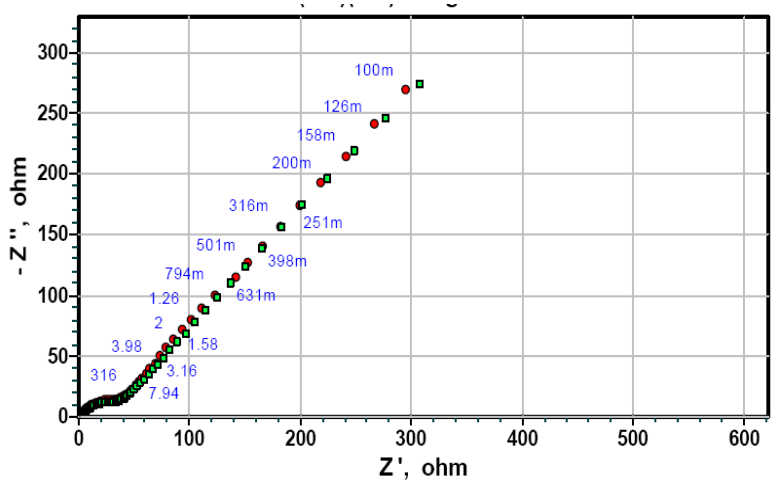

(g)

Figure 5.15: *EIS spectra of PANI-ME composite membranes bathed with 1M HCl (a) bare ME (b) ME,P1,2h (c) ME,P1,6h (d) ME,P1,22h (e) ME,Poly,6h (f) ME,Poly,22h and (g) ME,Vap,APS.*

Table 5.3: The parameters of equivalent circuits fitted on EIS data of HCl-bathed membranes in a two-compartment cell

Membrane/ Figure reference	EC Model	R_o ohm	CPE_1 ($S.s^{\alpha}$)	R_1 ohm	CPE_2 ($S.s^{\alpha}$)	R_2 ohm	σ(W) ($S.s^{0.5}$)
ME, unmodified (Figure 5.15a)	R(QR)(Q(RW)) χ^2:$9x10^{-4}$	2.5	Y_1= $3.1x10^{-4}$ α=0.62	14.8	Y_2= $1.2x10^{-5}$ α=0.92	$8.7x10^{4}$	$4.7x10^{-5}$
ME,P1,2h (Figure 5.15b)	R(QR)(QR) χ^2:$2.2x10^{-4}$	2.1	Y_1= $5.6x10^{-4}$ α=0.52	110	Y_2= $5.9x10^{-3}$ α=0.76	184	-
ME,P1,6h (Figure 5.15c)	R(QR)(QR) χ^2:$1.4x10^{-3}$	2.7	Y_1= $1.9x10^{-3}$ α=0.47	25.2	Y_2= 0.033 α=0.90	20.3	-
ME,P1,22h (Figure 5.15d)	R(QR)(QR) χ^2:$2.4x10^{-4}$	2.2	Y_1= $2.8x10^{-4}$ α=0.58	10.3	Y_2= 0.11 α=0.62	9.9	-
ME,Poly,6h (Figure 5.15 e)	R(QR)(Q(RW)) χ^2:$8x10^{-4}$	2.7	Y_1= $3.0x10^{-4}$ α=0.63	12.8	Y_2= $3.7x10^{-5}$ α=0.82	$1.2x10^{4}$	$1.6x10^{-4}$
ME,Poly,22h (Figure 5.15f)	R(QR)(Q(RW)) χ^2:$1.8x10^{-4}$	3.7	Y_1= $2.9x10^{-5}$ α=1.0	60.2	Y_2= $2.4x10^{-4}$ α=0.55	$3.8x10^{3}$	$5.2x10^{-4}$
ME,Vap,APS (Figure 5.15g)	R(QR)W χ^2:$7x10^{-4}$	2.4	Y_1= $1.1x10^{-4}$ α=0.68	27.2	-	-	$3.3x10^{-3}$

Intercalation of doped PANI in the base ME membrane by the two-compartment cell polymerization significantly changes the shape of the EIS curve. Two clearly resolved semicircles have emerged with about three orders of magnitude lower resistance compared to that of the unmodified membrane. The semicircle at high frequencies indicates that the charge transport in the bulk membrane that is mainly controlled by the charge transfer reaction in the pores. This process involves an electronic resistance of the charge transfer reaction at the pore walls and a double layer capacitance of the pore electrolyte. The high admittance values (e.g. 1.9×10^{-3} F for 6 h polymerization) support this interpretation in terms of the double layer charging inside the pores. However, this value is much higher than that of a simple flat plate capacitor [76]. The progressive decrease in the resistance values at prolonged polymerizations in the two-compartment cell also indicates a decrease in the charge transfer resistance of the bulk membrane. The low frequency semicircle shows diffusionally controlled processes but with low resistance and high admittance (up to 0.11 F for 22 h polymerization) values. The significantly higher admittance values as compared to that of the unmodified membranes indicate the contribution of charge transfer through PANI redox reactions in addition to the double layer charging. A several orders of magnitude decrease in the resistance by increasing the polymerization time also indicates the fast charge transfer reaction at the surface in the presence of PANI. Alternatively, this may represent highly conductive PANI phase in the membrane bulk. The charge transfer involves anion diffusion in the doped PANI either at the surface or inside the membrane bulk. As the polymerization time increased in the two-compartment cell polymerization, the charge transfer resistance decreased and admittance increased depending on PANI content in the membrane.

The composite membrane synthesized by the vapour-phase polymerization shows semicircles at high and low frequencies. An R-C element at high frequencies has been used to model the charge transport process in the bulk membrane. The low frequency process shows a 45^{o} rise that can be modelled by a Warburg resistance (Figure 5.16). The Warburg element shows a pure diffusive transport and in the case of a compact PANI layer at the surface, it can be attributed to the ionic diffusion in the membrane.

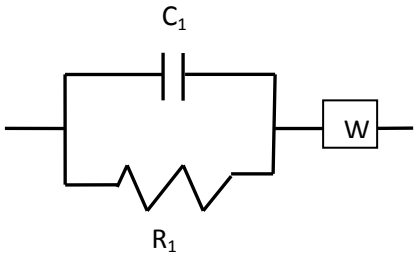

Figure 5.16: *The equivalent circuit representing the EIS behaviour of HCl bathed PANI composite membrane synthesized by the vapour phase polymerization.*

The Nyquist plots of undoped PANI composite membranes (Appendix B) show charge transport processes controlled by the ionic diffusion in the membrane phase irrespective of the employed polymerization techniques. These spectra can be interpreted in terms of a high electronic resistance that originates from the adsorption resistance at the membrane/electrode interface. The EIS data were fitted with R(QR) type modified Randles circuit and the parameters obtained by curve fitting are shown in Table 5.4. These membranes showed relaxation time ~0.6 s that is the characteristic of long-range diffusionally controlled processes in the bulk membrane. The admittance values in the range of 5-7 μF show double layer charging at the membrane/electrode interface [76].

Table 5.4: Equivalent circuit parameters for PANI composite membranes bathed with 1M $CaCl_2$ in the two-compartment cell

Membrane	R_0 **Ohm**	Y_1 $S\text{-}s^{\alpha}$	α	R_1 **Ohm**
ME, bare	16.1	$6.9\text{x}10^{-6}$	0.81	$9.1\text{x}10^{5}$
ME,P1,2h	7.3	$8.2\text{x}10^{-6}$	0.82	$5.0\text{x}10^{5}$
ME,P1,6h	23.2	$5.7\text{x}10^{-6}$	0.78	$1.9\text{x}10^{5}$
ME,P1,22h	11.3	$4.3\text{x}10^{-6}$	0.79	$1.9\text{x}10^{5}$
ME,Poly,6h	13.1	$6.9\text{x}10^{-6}$	0.85	$6.9\text{x}10^{5}$
ME,Poly,22h	19	$5.1\text{x}10^{-6}$	0.83	$5.1\text{x}10^{5}$
ME,Vap,APS	13.6	$6.8\text{x}10^{-6}$	0.81	$2.4\text{x}10^{5}$

5.2.4 Discussion

The earlier studies on the free-standing membranes comprising intrinsically conducting polymers focused on the charge transport mechanism mainly in pristine ICP films. The effects of various parameters such as membrane thickness, oxidation state and the nature of cations and anions on the electronic and ionic conductivities have been elaborated [69-71, 180]. The charge transport in the membranes takes place by both electronic (polarons) and ionic diffusion which increases with the oxidation state and decreases with the film thickness. The association of various cations (e.g. Zn^{2+}) with doped PANI by a complex formation reaction and size of the diffusing anion affect charge transfer in the membrane. The blending of polystyrene sulfonate with polypyrrole converts the latter to a cation-exchanger due to the introduction of sulfonate groups in the composite [201]. These composite membranes show similar trends of charge transport as that of a pristine polypyrrole film [176] but with cation-exchange behaviour. The charge transport resistance increased with the electrochemical reduction of polypyrrole at lower electrical potentials and increased by increasing the membrane thickness.

In addition to the above-mentioned studies pertaining to the charge transport mechanisms of ICP films, EIS studies of PANI aiming at the membrane applications have also been elaborated. To employ PANI membrane as a polymer electrolyte in fuel cell technology, the proton conductivity and diffusion of halide (Cl^-) ions were evaluated by EIS [78]. The diffusion coefficient of Cl^- was evaluated from a Warburg coefficient that models the low frequency impedance dispersion. These membranes showed higher values of halide diffusion coefficients (Warburg coefficient = 473 ohm.$s^{-0.5}$) as compared to that of Nafion®. However, the depletion of Cl^- in the membrane during the operation of the fuel cell remained a problem. Ionic diffusion of PANI membrane as the function of PANI doping state was studied by using EIS [76]. Many orders of magnitude high (~10^6 ohm) and low resistance (~3.0 ohm) values in doped and undoped PANI states, respectively, evidence the charge transport process controlled by the ionic diffusion in the membrane. The several orders of magnitude variation in the capacitance values of the membranes (10^{-9} F versus 0.5 F) also support this observation. The doping anion is transported through the redox reactions in doped PANI that results in a high capacitance value of the membrane. The effects of PANI intercalation in the conventional cation-exchange membrane on the protonic conductivity was elaborated [111]. Effects of PANI doping/undoping on the ionic transport were studied by fitting various

equivalent circuit models on the EIS data. Positively charged (doped) PANI decreased the protonic conductivity of the base ion exchange membrane significantly due to its interaction with the anionic fixed charges (sulfonate moieties) of the membrane. In another study, the effects of the incorporation of undoped PANI nanofibres on the ionic conduction of a polymer electrolyte membrane were investigated by using EIS [97]. These studies showed that PANI nanofibres modified the morphology of nanopores of the base membrane and hence enhanced the ionic diffusion through the membrane. However, beyond a certain threshold concentration of nanofibres, the opposite trends were observed due to the cluster formation of PANI nanofibres.

To the best of the author's knowledge, the effects of various *in situ* PANI deposition techniques on the charge transport characteristics of PANI composite membranes have not been presented so far in the literature. The equivalent circuit modelling of EIS data of the membranes synthesized using solution-phase, vapour-phase and two-compartment cell polymerizations (Table 5.1-5.4) revealed significant effects of PANI deposition site, extent and doping state on the charge transport properties of the composite membranes. PANI composite membranes synthesized by relatively shorter polymerization time (< 6 h) showed highly scattered EIS data with the large resistance values when soaked in HCl and tested without electrolyte bathing. This may be explained in terms of an inadequate retention of the electrolyte that increased the resistance of PANI in the membrane. In the case of water-soaked membranes, the probable swelling of cellulose ester at high pH could have retained sufficient electrolyte to give smooth EIS curves but with high resistance values [202]. To overcome the issue of electrolyte soaking, the membranes were also tested in a two-compartment cell bathing with the electrolyte. The metal/membrane/metal configuration was used to achieve a swift electronic charge transfer at the interface that helped in a better elaboration of the electronic and ionic transport processes in the bulk membrane [111, 192].

For HCl-soaked membranes in metal/membrane/metal configuration, ME,Poly,22h and ME, Vap, APS show high resistance levels (~10^4 ohm) due to small PANI deposition level mainly at the membrane surface. ME,Poly,22h show diffusionally controlled charge transfer processes. However, the higher capacitance value (~10^{-4} $S.s^{-0.5}$ versus ~10^{-9} $S.s^{-0.5}$ for vapour-phase modified membranes) for the surface charge transfer indicates an interfacial charge transfer through PANI redox transitions. ME,Vap,APS showed control of the charge transport in the bulk membrane but the high resistance (~10^4 ohm) and low admittance (10^{-9} $S.s^{-0.5}$) values that indicate a highly hindered charge transport. On contrary, ME,P1,22h shows bulk

membrane control in the charge transport with an order of magnitude higher capacitance (~10^{-4} $S.s^{-0.5}$) that emphasizes the involvement of PANI in the charge transport mechanism. The absence of the low frequency semicircle in the case of the two-compartment cell and vapour-phase polymerizations indicates a swift interfacial charge transfer due to almost complete PANI layering on the membrane surface.

Water-soaked PANI composite membranes show high resistance values due to the presence of undoped PANI inside the membranes. Vapour-phase (ME,Vap,APS) and the two-compartment cell polymerization (ME,P1,6h and ME,P1,22h) show the charge transport control in the bulk membrane that indicates a small charge transfer resistance at the membranes surface. Bare ME and the membranes synthesized by the solution-phase polymerization (ME,Poly,22h) show diffusionally controlled charge transfer at the membrane/electrode interface. Undoped PANI membranes show 3-4 orders of magnitude higher resistance as compared to that of doped PANI composite membranes. These values are significantly higher than that of undoped pristine PANI (~10^6 ohm [76]). The possible reason may be the dipping the membranes in Milli-Q water (pH 5-6) might not fully undope PANI inside the membranes.

Bathing the membranes with the electrolyte solution changes the conditions at the membrane/electrode interface and ensures the abundance of the doping anions in the membranes. The acid (HCl) doping clearly shows the effects of PANI deposition site on the electrochemical characteristics of the membranes. The unmodified ME and the composite membranes synthesized by the solution-phase and vapour-phase polymerizations showed diffusionally controlled transport processes [70, 167]. The high resistance (Table 5.3, 10^3-10^4 ohm) and low admittance (10^{-5}-10^{-4} $S.s^{\alpha}$) values showed that these membranes are in their insulating state (due to the low level of PANI deposition mainly at the surface) and dominant charge transport mechanism is ionic diffusion. In contrast, PANI deposition inside the pores of the base membrane from the two-compartment cell polymerization shifts the control from the ionic diffusion to the charge transfer reaction in the membrane bulk. PANI deposition inside the pores of the base membrane significantly decreases the resistance levels up to 3-4 orders of magnitude. It implies that not only the PANI intercalation level but also the deposition site (on the pore walls of the membrane) determines the mechanism and extent of the electrochemical charge transport processes.

The low resistance values represent electronic nature of the membranes whereas the high admittance (up to 0.11 $S.s^{\alpha}$) values represent a highly charged double layer involved in the bulk transport processes. The exceptionally high admittance values show pseudocapacitance of PANI in the membranes which results from the redox transition of PANI by the incorporation of doping anion (capacitance ≈ 0.5 F [76]). The progressive increase in the pseudocapacitance of the membranes and decrease in the charge transfer resistance with the polymerization time in the two-compartment cell clearly shows charge transport involving PANI-coated strands of the membrane along with the double layer charging of the pore electrolyte.

In view of the above-mentioned discussion, the composite membranes synthesized by using the two-compartment cell polymerization may be used for an effective permeation control in various membrane separation applications. By either applying an electrical potential or through doping/undoping switching, permeation of the electrolyte through PANI-coated pores can be effectively controlled. Because doping anions take part in redox transitions during the charge transport processes, the selectivity can be controlled by changing the polarity and/or the electrostatic charge density of the electrolyte ions. The porous nature of the membrane guarantees high permeation flux that is a major limitation of the conventional homogenous (dense) membranes.

5.3 Membrane Potential and Transport Numbers of PANI Composite Membranes

When an ion exchange membrane either containing embedded charged functionalities (i.e. conventional ion exchange membranes) or a charge on the polymeric chains (e.g. doped PANI) separates an electrolyte solution of different concentrations on both sides, an electrical potential is developed due to the passage of only counter-ions through the membrane. In fact, due to the passage of counter-ions and blockage of the co-ions, one side of the membrane (higher concentration side) becomes depleted in the counter-ions whereas the opposite side becomes richer in the counter-ions. This difference in the concentration of charged species on both sides generates a membrane potential [165]. This electrochemical potential is the result of three distinctive potentials in the system: two Donnan potentials (due to the exclusion of co-ions) at both interfaces and a diffusion potential through the membrane [203]. When the concentration of the fixed charges in the membrane is much smaller compared to the electrolyte concentration, the Donnan potential can be neglected and the electrochemical potential depends only on the concentration difference across the membrane [203]. In this case, the following mathematical expression for the potential difference across the membrane can be derived from Nernst equation,

$$V = \left[\frac{t^m_{coun}}{|z_{coun}|} - \frac{t^m_{co}}{|z_{co}|} \right] \frac{RT}{F} \ln \frac{c_1}{c_2} \tag{5.33}$$

where V is the electrochemical potential (V) and c_1 and c_2 are the electrolyte concentrations (mol/L) across the membrane, respectively; R,T,F are gas law constant, absolute temperature and Faraday's constant, respectively. z_{coun} and z_{co} are the valence numbers of the ions and t^m is the membrane transport number where subscripts *coun* and *co* specify the counter- and co-ions. The transport number obeys the electroneutrality principle i.e.,

$$t^m_{coun} + t^m_{co} = 1 \tag{5.34}$$

For a 1:1 electrolyte such as HCl, Equation (5.33) can be written as (by using Equation (5.34)).

$$V = (2t^m_{coun} - 1) \frac{RT}{F} \ln \frac{c_1}{c_2} \tag{5.35}$$

If the membrane potential (V) is plotted against ln c_1/c_2, the slope of a fitted straight line gives the transport number of the counter ions through the membrane.

Membrane potential and transport number measurements have been used for pristine ICP and ICP composite membranes to characterize the effects of ICP oxidation state or the intercalation levels on the transport of various ions through the membrane. Ehrenbeck and Juttner [188, 189] evaluated the transport numbers of K^+ and Cl^- for electrochemically synthesized polypyrrole membranes. For small molecule dopants, the positively charged membrane acted as an anion exchange membrane with t_{Cl^-}=0.92. Doping of the membrane with dodecylsulfonate originated cation-permselectivity with t_K=0.88. More recently, the transport number of NO_3^- through an oxidized polypyrrole was measured (t_{NO3}=0.94) [203]. The oxidized polypyrrole film behaved as an anion-exchange membrane due to the presence of positively charged molecular chains in the oxidized form. In addition to pristine ICP membranes, the transport numbers for ICP composite membranes were also studied. The transport number of proton (H^+) through a cation-exchange sulfonated poly(ether-ether ketone) (SPEEK) membrane was measured and the effect of PANI incorporation on the transport numbers was investigated [118]. Unmodified SPEEK showed H^+ transport number t_H=0.96 comparable to that of Nafion$^{(R)}$ indicating high permselectivity for the protons due to the presence of sulfonate fixed groups. Incorporation of positively charged PANI decreased the H^+ transport number due to the interaction of PANI with sulfonate groups hence decreasing the ion exchange capacity of the SPEEK membrane. Compan et al. [111] measured the membrane potential of perflourinated cation-exchange membranes with or without PANI. The base membrane was modified by *in situ* chemical polymerization where PANI was deposited mainly as a surface layer on the membrane. Three different electrolytes with common anion (HCl, NaCl and KCl) were employed to investigate the effect of cation size on the transport properties of the membranes. Transport number of Cl^- in polypyrrole-polyethylene composite membranes were determined where polypyrrole was layered on the surface of the microporous polyethylene membrane by *in situ* chemical polymerization of pyrrole [204]. The composite membranes showed a high transport number (0.903) at about 10% PPY content in the membrane and the transport numbers increased up to 0.985 with 48 % PPY content in the membranes.

In this thesis, membrane potentials have been measured by using a two-compartment cell where the membranes (area: 1.7 cm^2) were exposed to the ionic flux between the two

compartments of a permeation cell. The concentration of the electrolyte (either HCl or $CaCl_2$) was kept constant (1M) in one compartment whereas it was varied (1.0-0.001M) in the other compartment of the cell. Polarization curves were obtained by traversing the electrical potential between -1000 to +1000 mV and the resultant current density was recorded. The membrane potentials were obtained from the polarization curves at i (current density) = 0 A, i.e. at the zero current condition by fitting the straight line to the data points.

PANI composite membranes showed different behaviour in HCl and $CaCl_2$ due to the difference in the doping state. In HCl, the membranes showed negative potential in the range of 0-160 mV. However, in the case of $CaCl_2$ the potential was positive initially and then became negative but the values remained small (close to zero) even at the maximum concentration difference (~20 mV). This clearly shows the anion exchange behaviour of PANI composite membranes in HCl due to PANI doping state [72]. The membrane potentials as a function of $\ln(c_2/c_1)$ in are shown in Figure 5.17. As shown in the figure, the membrane potentials deviate from the linear relationship with $\ln(c_1/c_2)$ at higher concentration ratios. The same trend was also observed in the earlier studies [188, 189, 203]. Ariza and Otero [203] attributed this to the effect of a strong Donnan exclusion at the high concentration ratios. Hijnen and Smit [205] presented a detailed analysis of the membrane potential of a weak cation-exchange membranes prepared by the modification of porous cellulose acetate membranes with long-chain polyacids. The development of a stagnant film adjacent to the membrane surface in the unstirred electrolyte systems establishes a potential difference in addition to that arising from the diffusion in the membrane phase. This leads to the decreased concentration difference across the membrane as compared to that of the bulk electrolyte and results in decreased membrane potentials.

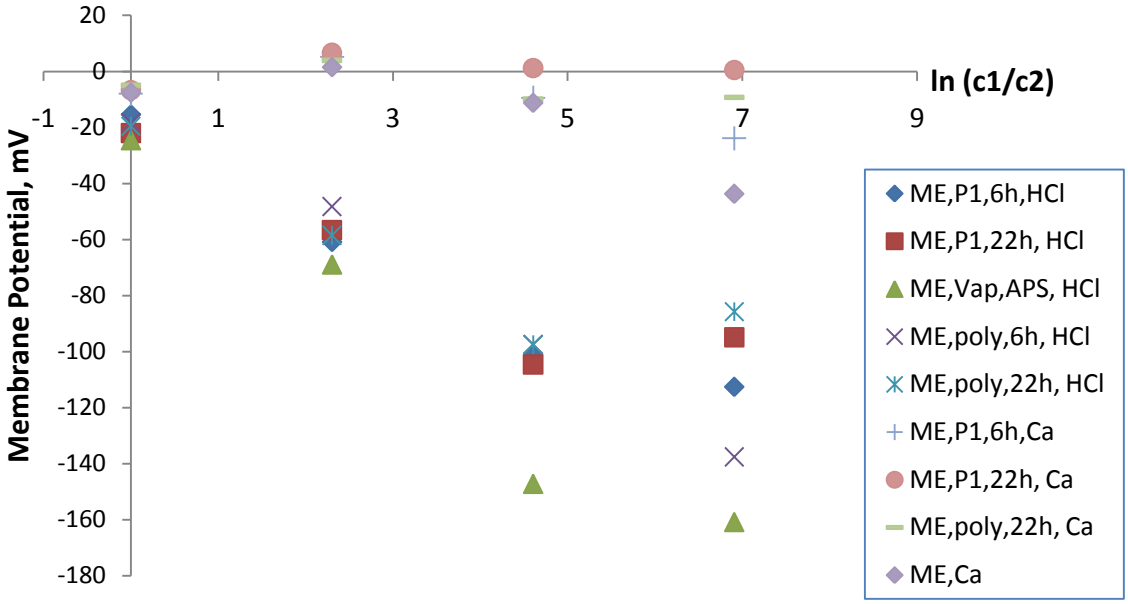

Figure 5.17: *Membrane potential versus ln(c_1/c_2)(legend shown in the figure).*

The transport numbers of HCl-soaked membranes were calculated from the linear part of the curves and the results are given in Table 5.5. The % permselectivities have also been shown (columns 3 & 4) which are defined as the following based on the transport numbers [204],

$$P(\%) = 100\frac{\left(t_{coun}^{m} - t^{m}\right)}{\left(1 - t^{m}\right)} \tag{5.36}$$

where t^m is the transport number of the counter-ion in the solution (or in bare ME).

Unmodified ME has a transport number 0.75 which can be attributed to the weak cation-exchangeability of the cellulose ester [206]. However this counter-ion transport number may be attributed to the porous nature of the membrane where a "leak' of the counter ion (H^+) is significantly high. The deposition of PANI in the base membrane increased transport number significantly which can be explained in terms of the strong ion exchange effects of doped PANI in the membrane. PANI has strong H^+ exchangeability coupled with anion transport in the same direction [72]. Various deposition techniques of PANI on the base membrane affect the transport number as slightly higher values have been shown for the composite membranes synthesized by the two-compartment cell polymerization as compared to the solution-phase synthesized membranes. This difference can be attributed to the PANI deposition inside the

pores of the base membrane that increased the PANI deposition content, as well. However, the transport numbers decreased slightly at the prolonged aniline polymerization in the both techniques probably due to the degradation of PANI layer at the surface. ME,Vap,APS shows higher transport number as compared to that of the other membranes. This may be explained in terms of a more uniform and compact surface PANI layer that screens co-ions more effectively as compared to the other composite membranes. The thick surface layer as indicated by 19.5 % PANI content compared to 12.6% from the solution-phase polymerization may also contribute towards the higher permselectivity. However, the exact explanation of this phenomenon requires further investigation.

The PANI composite membranes show higher H^+ selectivity as compared to the weak cation-exchangeability of cellulose ester membrane. In addition, the higher membrane potentials in HCl solution as compared to the lower values in $CaCl_2$ (pH~12) clearly indicate a strong proton permselectivity. However, this technique could not clearly measure the effects of various PANI deposition sites and extent on H^+ permselectivity of the membranes. This may be attributed to the pronounced H^+ selectivity of ICPs even at the comparatively smaller content within the membrane as also shown by the earlier studies on PPY-polyethylene membranes [204]. In addition, this technique itself may have the measurement limitations due to the strong polarization effects at the membrane surface and at the surface of Ag/AgCl electrodes.

Table 5.5: Transport numbers and permselectivities of PANI composite membranes in 1M HCl

Membrane	t_{H^+}	**Permselectivity (H^+) based on water solution ,%**	**Permselectivity (H^+) based on bare ME,%**
Unmodified ME	0.75	-	-
ME,P1,6h	0.86	22.2	44.0
ME,P1,22h	0.85	17.0	40.0
ME, Vap, APS	0.91	50.0	64.0
ME,Poly,6h	0.84	11.1	36.0
ME,Poly,22h	0.83	6.0	32.0

Chapter Six

Conclusions and Potential Applications of the Membranes

6.1 Conclusions

The Contemporary Research

Membranes based on intrinsically conducting polyaniline have been synthesized and employed in various separation processes such as gas separation, pervaporation, nanofiltration, electrodialysis and fuel cell technology (see section 2.4 for references). Polyaniline (PANI) composite membranes have been developed to overcome the poor mechanical properties and loss of short-chain doping anions due to their leach out from the pristine PANI membranes in pervaporation and nanofiltration processes [63, 82-87]. Improvements in the selectivity and permeation rate have been achieved in PANI composite membrane primarily due to:

- Increase in the hydrophilicity of the composite by the doped PANI that enhanced the water permeation in pervaporation.
- Utilization of the change in PANI morphology that results from the redox switching and/or doping/undoping. The void fraction of the composite membrane depends on the morphology of the PANI layer.
- Interaction of PANI with acids to improve the selectivity in pervaporation.

Ion exchange membranes have also been modified with PANI by *in situ* oxidative polymerization and permselectivity studies were conducted [e.g., 107-122]. PANI influenced the permselectivity of the base membrane by the exclusion of counter-ions and electrostatic interaction with the positively or negatively charged PANI (short- or long-chain immobilized dopants) depending on the charge of the permeating ions. PANI deposition site was varied by employing different contacting patterns in the *in situ* polymerization technique where PANI deposition was achieved either as the thin surface layer or in the bulk of the base homogenous membrane. PANI deposition site showed significant effects on the permselectivity of the composite ion exchange membranes.

Focus of the Thesis

As discussed in Introduction (Chapter One), microporous membranes have been modified to achieve high permeation rate at a reasonable selectivity among the permeating ions. Micro-sized pores of these membranes are modified by depositing long-chain amino acids that are ionizeable and assume different conformations depending on the surrounding pH. This in-pore deposition shows an effective control on the membrane selectivity. To achieve a highly permeable membrane for electrochemical based separation, electroactive PANI was deposited on the surface or inside the pores of the base microporous membranes in the present research. PANI deposition on the pore walls of the base membrane in such a manner that the deposition process should not block the ion transport through the pores yields a membrane with high permeability in the electrochemical separation process. The presence of positively charged PANI layers on the pore walls influences the charging extent of the electrolyte double layer inside the pores that controls the permselectivity of the permeated ions. Contrary to the polyaminoacids deposited membranes where selectivity was achieved through the steric hindrance in the pores, permselectivity in the present research is achieved by the electrochemical interactions with the permeated ions. In earlier studies [19, 20, 28], PANI layering at the surface of the base microporous membrane has been trialled for enhanced permeation and selectivity in diffusional flow processes. However, a detailed and systematic account on PANI deposition and permeation properties has not been given to date. In this thesis, a systematic study on the effects of the various *in situ* polymerization techniques on PANI deposition site, extent and oxidation/doping state in the base microporous cellulose ester membranes has been presented. Detailed SEM, FTIR and XPS studies on the effects of various polymerization techniques on PANI deposition site and extent in the microporous base membrane has been presented. These studies show a strong dependence of PANI layering at the surface and its extent on the polymerization techniques and conditions. Similarly, the effects of PANI deposition site and extent on charge transport processes of the composite membranes by electrochemical impedance spectroscopy (EIS) have been elaborated first time in the literature.

Effects of the Synthesis Techniques on PANI Deposition Site and Extent

Mixed cellulose ester (ME) microporous membranes were modified by depositing PANI by using various *in situ* chemical oxidative polymerization techniques. One of the major objectives of the research was to evaluate the effects of various techniques and conditions on

PANI deposition site, extent and oxidation/doping states in the base membrane. SEM micrographs of the composite membranes revealed that PANI was deposited on the surface of the base membranes in the solution-phase and vapour-phase polymerizations whereas in-pore deposition was achieved by the two-compartment cell polymerization. In the latter technique, PANI was layered on the skeleton strands of the base membrane without blocking the pores along with some surface deposition as well. PANI intercalation extent in the base membrane was measured by the gravimetric technique. The solution-phase and vapour-phase polymerization yielded lower intercalation levels as compared to the two-compartment cell polymerization. This also confirmed in-pore PANI deposition in the base membrane. FTIR-ATR characterization showed the presence of PANI in its emeraldine salt state from all the polymerization techniques. In addition to the FTIR characterization, PANI composite membranes were characterized by x-ray photoelectron spectroscopy (XPS) to quantify the PANI deposition extent and its oxidation and doping states. The characterization results showed that the solution-phase polymerization yielded composite membranes with incomplete PANI layering at the surface that improved at prolonged polymerization. Vapour-phase polymerization yielded compact PANI layer that almost completely covered the surface. The two-compartment cell polymerization also showed time-dependent surface coating and almost a complete surface coverage at prolonged polymerization. In addition, asymmetric deposition on the both faces of the base membrane was observed where PANI was deposited in the greater extent on the monomer (aniline) facing side of the membrane as compared to the oxidant ($FeCl_3$) facing side. An analysis of the diaphragmatic polymerization in the two-compartment cell revealed the role of weak cation-exchange mixed ester membrane that controlled PANI deposition site. The type of the oxidant also played important role due to the polarity of the oxidizing species ($S_2O_8^{2-}$ versus Fe^{3+}) and their effect on oxidation rate ($S_2O_8^{2-} >> Fe^{3+}$).

To elucidate the effects of PANI deposition site and extent on the electronic conductivity of the membranes, surface and trans-membrane (through) conductivity of dry composite membranes were measured by four-point micro probe and two-point probe techniques, respectively. The electrical conductivity values were orientation-dependent and clearly showed the effects of in-pore or surface deposition.

6.1.1 Surface Characterization of the Composite Membranes

Surface characterization of the composite membranes has been emphasized due to the role of the surface related phenomena in the electrochemical performance of the membranes. Ionic charge from the electrolyte solution is converted, partially in the case of PANI, to the electronic charge by the surface reaction. XPS was used to study the surface chemistry of the membranes. PANI deposition levels on the surface of the membrane, oxidation state, doping levels and PANI degradation (via hydrolysis reaction) were studied by analysing the core level C 1s, N 1s, Cl 2p and O 1s spectra, respectively. N 1s spectra of the composite membranes showed that PANI deposited in emeraldine state doped with Cl^- from the polymerization reaction. Surface deposition levels were polymerization technique and time dependent. XPS spectra showed same trends of PANI deposition as shown by FTIR spectroscopy and PANI intercalation levels by the gravimetric measurements. PANI deposition levels were evaluated by comparing the area of the component peaks representing organic nitrogen (i.e. PANI) to that arising from inorganic nitrogen (nitrate ester). Uniform PANI layering at the surface was evidenced in the two-compartment cell and vapour-phase polymerizations as compared to the solution-phase polymerization. Doping levels were evaluated in terms of Cl^-/N^+ ratio. Prolonged polymerizations in the various techniques yielded maximum doping level due to the longer contact with the acid (HCl) solution. In addition to doping chloride ions, organic chloride and entrapped HCl also contributed to the total chlorine on the membrane. In addition, hydrolytic degradation of PANI to hydroquinone and benzoquinone was also indicated for prolonged polymerizations in various techniques.

6.1.2 Electrochemical Transport Properties of the Membranes

Electronic and ionic charge transport properties of PANI composite membranes were studied by using various electrochemical characterization techniques, which include electrochemical impedance spectroscopy (EIS) and transport number measurements from membrane potentials. EIS was used for the composite membranes in different doping states and by changing electrolyte-bathing conditions. The prime objective of the EIS characterization was to investigate the effects of PANI deposition site and extent on charge transport properties of the composite membranes. The following conclusions were drawn from the EIS studies of PANI composite membranes.

1. The overall impedance levels of the membranes depend on PANI deposition levels and can be correlated with PANI intercalation percentages measured by the gravimetric method (Table 4.1). The charge storage capacitance arises from the charge transportation mechanism of PANI and thus the levels depend on the PANI intercalation levels, too.

2. The relaxation process that indicates the limiting step in the overall charge transport process of the membrane depends on PANI deposition site and doping state. In-pore PANI deposition from the two-compartment cell polymerization showed capacitive charging of the electrolyte double layer inside the pores in the case of doped PANI state. The charge transport resistance decreased and capacitance increased with the polymerization time showing highly electroactive membranes with higher polarisation of the pore electrolyte with the increase in the PANI intercalation level. The solution-phase and vapour-phase polymerization did not show the significant capacitance levels for the bulk membrane and the charge transportation mainly takes place in the insulating cellulose ester phase.

3. Surface layering of PANI enhanced anion adsorption at the surface. In the case of doped PANI, anion diffusion in the bulk membrane is facilitated by the presence of PANI inside the pores from the two-compartment cell polymerization. For the solution-phase and the vapour-phase polymerizations, higher diffusional resistances were observed. This can be attributed to PANI deposition as a non-uniform layer at the surface of the membrane. At high pH, the membrane behaved as a thick membrane where ion diffusion processes take place at a slower rate with the simultaneous swelling of the cellulose ester phase.

In addition to the EIS studies, membrane potentials were also measured and the transport numbers of counter-ions were evaluated. Doped PANI showed ion exchange behaviour with high Cl^-/H^+ selectivity. The positive charge on PANI molecular chains at low pH (in HCl) facilitates anion transport coupled with H^+ transport that result in higher transport numbers (~0.86). PANI composite membrane in high pH medium showed weak ion exchange behaviour due to the presence of undoped PANI chains in the membranes.

Based on the electrochemical behaviour of the membranes, it can be concluded that PANI deposition site, extent and doping states have significant effects on the electrochemical performance of the membranes. PANI deposition inside the pores from the two-compartment

cell technique yields composite membranes, which can affect the electrolyte permeation in the pores by double layer charging affects (electro-kinetic separation). The permeation rate and the selectivity can be controlled by changing the polarisation conditions of the electrolyte in the pores. This implies that the permselectivity can be adjusted either by changing the dopant anion (mobility, size and polarity) or by applying a direct electrical potential to the membrane by taking the advantage of the high electronic conductivity of the composite membranes.

6.2 Potential Applications of the Present Research as a New Membrane System

In this research, electroactive polyaniline was deposited either as a surface layer or in the pores of the base microporous membrane. The extent surface layering and site of PANI deposition depend on the various employed techniques of *in situ* polymerization of aniline. EIS characterization revealed the strong effects of PANI deposition site and extent on the charge transport properties of the composite membranes. PANI deposition either by solution-phase or vapour-phase polymerization yields composite membranes that show diffusionally-controlled charge transport processes. However, in-pore PANI deposition from the two-compartment cell polymerization yields highly electrochemically active composite membranes. The charge transport in these membranes takes place by a charge transfer reaction that involves the interaction of anions and PANI layer at the pore walls. The high capacitance and extremely low resistance of the membranes characterize this charge transfer process. The H^+ selectivity of the membranes over anions (and over cation in the case of unmodified ME) has been established by the transfer number measurements. This implies that the intercalated PANI interacts electrostatically and electrochemically with the permeating ions through the membranes. A high permselectivity between various ions can be expected in electrochemical-based applications of these membranes such as in Donnan dialysis and electrodialysis. Further, the permselectivity can be controlled by applying an electrical potential directly to the PANI composite membrane. Though electrochemically modulated transport in various homogenous (dense) ICP membrane has been reported in recent past [8, 9, 203], these membranes have certain limitations such as poor mechanical properties, low permeation rate due to the dense nature of the membranes etc. In this thesis, electroactive PANI was deposited in the base membrane matrix that had a high mechanical

integrity. Secondly, *in situ* chemical polymerization has been used which has a potential of scale up to the industrial scale. Thirdly, in spite of being a composite with an insulating polymer (ME), these membranes have such a high electrical conductivity that these can give an economical electrical current efficiency in electrochemical-based processes such as electrodialysis. Above all, the highly porous structure of these membranes ensures high permeation rate with a reasonable selectivity level that is controlled by the interaction of ions with electroactive PANI in the pores.

In the membrane separation processes, high selectivity is desirable at the economical permeation rate. High permeation rates can be achieved only, for example, by increasing the operating pressure in ultra-/nano-filtration processes. In addition to the high operating costs, membrane integrity issues may emerge in this case. In this thesis, highly porous membranes were developed that have high permeability where selectivity is achieved by the interaction of PANI layer with the permeating species in the pores of the membrane. This implies that if these membranes are employed in pressure diffusion processes, much lower operating pressures (< 1.0 bar) as compared to that of the conventional processes (up to ~200 bar) would be required. On the other hand, due to their high ionic and electronic conductivities, these composite membranes can also be employed in electrodialysis process. There are many aspects of the membrane processes involving functional membranes that can be investigated by using the composite membrane developed in this research. For example, due to anion exchangeability of doped PANI, heavy metal anions (e.g. chromates) can be separated from water or from a mixture of various anions. Similarly, the separation of various acid anions (Cl^-, HSO_4^{2-}) from an acid mixture (e.g. waster acid) can be studied. In another application, the recovery of metal cations (Cu^{2+}, Zn^{2+}, $Cr3^+$) from the waste water of chemical etching and electroplating industries can be trialled. Extending this cation rejection capability of PANI composite membrane, direct desalination studies of water or cheese whey can be conducted in an electrodialysis cell. In this context, another aspect of functional PANI that can be utilized in the membrane separation is the probable complex formation capability with metals. Novel metal scavengers (sorbents [207]) can be developed or existing absorbents can be modified to improve their sorption capability.

The PANI deposition by *in situ* chemical polymerization eliminates the need of special treatment step of a membrane template that is required in other polymerization techniques such as metal sputtering prior to electrochemical polymerization. This implies that PANI can be easily and economically deposited inside the various templates (polymeric and non-

polymeric, as well) up to any desired extent. Inert base membranes can be modified for the subsequent applications in organic solvent filtration. Because the separation in these membrane systems is based on the electrostatic and electrochemical interactions, only functional solvents can be separated.

Another exciting area particular to the membranes developed in this research is the application in the fuel cell technology. As mentioned earlier, this technology is currently facing some key challenges such as to achieve high proton conductivity of the polymer electrolyte, loss in proton conductivity at high temperature and low humidity conditions etc. PANI composite membranes can easily be converted to cation-exchange membranes by immobilizing a long-chain polymeric anion (e.g. polysulfonates). In the two-compartment cell polymerization, PANI deposition content higher than 50 % (w/w) could be achieved due to the in-pore deposition in the membrane. By carefully selecting the base membrane and the polymerization conditions, a highly proton conductive composite membrane can be developed and trialled as an electrolyte for various fuel cell applications.

Water-immiscible macromolecules (e.g. oils) are emulsified and filtered through the microporous membranes by cross-flow filtration operation. The developed porous membranes can be employed in these processes as well for the treatment of oil-water mixtures from industrial wastes.

References

[1] Strathmann H. Synthetic Membranes and Their Preparation. In: Porter MC, editor. Handbook of Industrial Membrane Technology. New Jersey, U.S.A.: Noyes Publications, 1990.
[2] Rijin CJMv. Nano and Micro Engineered Membrane Technology. Amsterdam: Elsevier B.V., 2004.
[3] Purchas DB, Sutherland K. Handbook of Filter Media. Oxford,UK: Elsevier Science Ltd., 2002.
[4] Hollman AM, Bhattacharyya D. Functionalized membranes for tunable separations and toxic metal capture. In: Bhattacharyya D, Butterfield DA, editors. New Insight into Membrane Science and Technology:Polymeric and Biofunctional Membranes. Amsterdam: Elsevier Science B.V, 2003.
[5] Asturias GE, Jang G-W, MacDiarmid AG, Doblhofer K, Zhong C. Membrane-properties of polymer films. The acid-doping reaction of polyaniline. Berichte der Bunsengesellschaft/Physical Chemistry Chemical Physics 1991;95:1381.
[6] Sairam M, Nataraj SK, Aminabhavi TM, Roy S, Madhusoodana CD. Polyaniline membranes for separation and purification of gases, liquids, and electrolyte solutions. Separation and Purification Reviews 2006;35:249.
[7] Price WE, Too CO, Wallace GG, Zhou D. Development of membrane systems based on conducting polymers. Synthetic Metals 1999;102:1338.
[8] Pile DL, Hillier AC. Electrochemically modulated transport through a conducting polymer membrane. Journal of Membrane Science 2002;208:119.
[9] Pile DL, Zhang Y, Hillier AC. Electrochemically modulated permeability of poly(aniline) and composite poly(aniline)-poly(styrenesulfonate) membranes. Langmuir 2006;22:5925.
[10] Piletsky SA, Kurys YI, Panasyuk TL, Goumenyuk A, Sergeeva TA, Karim K, Piletska EV, El'skaya AV, Turner APF. Preparation and use of membranes with potential-controlled functions. Instrumentation Science and Technology 2001;29:383.
[11] Skotheim TA, Elsenbaumer RL, Reynolds JR. Handbook of conducting polymers, Second Ed. . Marcel Dekker Inc., New York 1998.
[12] Schultze JW, Karabulut H. Application potential of conducting polymers. Electrochimica Acta 2005;50:1739.
[13] Pud A, Ogurtsov N, Korzhenko A, Shapoval G. Some aspects of preparation methods and properties of polyaniline blends and composites with organic polymers. Progress in Polymer Science (Oxford) 2003;28:1701.
[14] Al-Ahmed A, Mohammad F, Rahman MZA. Composites of polyaniline and cellulose acetate: Preparation, characterization, thermo-oxidative degradation and stability in terms of DC electrical conductivity retention. Synthetic Metals 2004;144:29.
[15] Wallace GG, Spinks GM, Kane-Maguire LAP, Teasdale PR. Conductive Electroactive Polymers: Intelligent Materials Systems. Florida: CRC Press, 2003.
[16] Illing G, Hellgardt K, Schonert M, Wakeman RJ, Jungbauer A. Towards ultrathin polyaniline films for gas separation. Journal of Membrane Science 2005;253:199.
[17] Hollman AM, Bhattacharyya D. Controlled permeability and ion exclusion in microporous membranes functionalized with poly(L-glutamic acid). Langmuir 2002;18:5946.
[18] Hollman AM, Scherrer NT, Cammers-Goodwin A, Bhattacharyya D. Separation of dilute electrolytes in poly(amino acid) functionalized microporous membranes: model evaluation and experimental results. Journal of Membrane Science 2004;239:65.

[19] Elyashevich GK, Kuryndin IS, Rosova EY. Composite membranes with conducting polymer microtubules as new electroactive and transport systems. Polymers for Advanced Technologies 2002;13:725.
[20] Tishchenko GA, Dybal J, Stejskal J, Kudela V, Bleha M, Rosova EY, Elyashevich GK. Electrical resistance and diffusion permeability of microporous polyethylene membranes modified with polypyrrole and polyaniline in solutions of electrolytes. Journal of Membrane Science 2002;196:279.
[21] Song L, Dong C, Li J. Application of the PAA-PVDF microfiltration composite membrane for municipal wastewater advanced treatment. Toxicological and Environmental Chemistry 2007;89:223.
[22] Guangqun Zhai SCT, W. L. Tan, E. T. Kang,* and K. G. Neoh. Poly(vinylidene fluoride) with Grafted ZwitterionicPolymer Side Chains for Electrolyte-Responsive Microfiltration Membranes. Langmuir 2003:7030.
[23] Yamada K, Gasparac R, Martin CR. Electrochemical and transport properties of templated gold/polypyrrole-composite microtube membranes. Journal of the Electrochemical Society 2004;151:E14.
[24] Nishizawa M, Menon VP, Martin CR. Metal nanotubule membranes with electrochemically switchable ion-transport selectivity. Science 1995;268:700.
[25] Miller SA, Young VY, Martin CR. Electroosmotic Flow in Template-Prepared Carbon Nanotube Membranes. Journal of American Chemical Society 2001;123:12335.
[26] Kim DW, Kun Ae N, Chun JH, Kim SH, Ko JM. Highly conductive polymer electrolytes supported by microporous membrane. Solid State Ionics 2001;144:329.
[27] Zhang SS, Ervin MH, Xu K, Jow TR. Li-ion battery with poly(aciylonitrile-methyl methacrylate)-based microporous gel electrolyte. Solid State Ionics 2005;176:41.
[28] Tishchenko G, Rosova E, Elyashevich GK, Bleha M. Porosity of microporous polyethylene membranes modified with polypyrrole and their diffusion permeability to low-molecular weight substances. Chemical Engineering Journal 2000;79:211.
[29] Shirakawa H, Louis EJ, Macdiarmid AG, Chiang CK, Heeger AJ. Synthesis of Electrically Conducting Organic Polymers : Halogen Derivatives of Polyacetylene, (CH)x. Journal of Chemical Society,Chemical Cummunications 1977:578.
[30] Chiang CK, Fincher CR, Park YW, Heeger AJ, Shirikawa H, Louis EJ, Gau SC, MacDiarmid AG. Electrical Conductivity in Doped Polyacetylene. Physical Review Letters 1977;39:1098.
[31] Naarmann H. Polymers to the Year 2000 and Beyond John Wiley & Sons 1993;Chapter 4.
[32] Khalkhali RA. Electrochemical synthesis and characterization of electroactive conducting polypyrrole polymers. Russian Journal of Electrochemistry 2005;41:950.
[33] Unsworth J, Conn C, Jin Z, Kaynak A, Ediriweera R, Innis P, Booth N. Conducting polymers: properties and applications. Journal of Intelligent Material Systems and Structures 1994;5:595.
[34] Kumar D, Sharma RC. Advances in conductive polymers. European Polymer Journal 1998;34:1053.
[35] Jagur-Grodzinski J. Electronically conductive polymers. Polymers for Advanced Technologies 2002;13:615.
[36] Negi YS, Adhyapak PV. Development in polyaniline conducting polymers. Journal of Macromolecular Science - Polymer Reviews 2002;42:35.
[37] Xu J-K, Hu X-J, Pu S-Z, Shen L, Chen P. Novel inherently conducting polymer acting as antistatics. Ganguang Kexue yu Guanghuaxue/Photographic Science and Photochemistry 2005;23:232.

[38] Wang Y, Jing X. Intrinsically conducting polymers for electromagnetic interference shielding. Polymers for Advanced Technologies 2005;16:344.
[39] Angelopoulos M. Conducting polymers in microelectronics. IBM Journal of Research and Development 2001;45:57.
[40] Guimard NK, Gomez N, Schmidt CE. Conducting polymers in biomedical engineering. Progress in Polymer Science (Oxford) 2007;32:876.
[41] Peng H, Zhang L, Soeller C, Travas-Sejdic J. Conducting polymers for electrochemical DNA sensing. Biomaterials 2009;30:2132.
[42] Ramanavicius A, Ramanaviciene A, Malinauskas A. Electrochemical sensors based on conducting polymer-polypyrrole. Electrochimica Acta 2006;51:6025.
[43] Dong X-M, Zhang S-T, Luo Y, Wang Z-H. Application of gas sensors based on conducting polymers. Gaofenzi Cailiao Kexue Yu Gongcheng/Polymeric Materials Science and Engineering 2007;23:6.
[44] Lange U, Roznyatovskaya NV, Mirsky VM. Conducting polymers in chemical sensors and arrays. Analytica Chimica Acta 2008;614:1.
[45] Bittihn R. Batteries using electrically conducting polymers. Kunststoffe, German plastics 1989;79:23.
[46] Scrosati B. Conducting polymers: Advanced materials for new design, rechargeable lithium batteries. Polymer International 1998;47:50.
[47] Armelin E, Oliver R, Liesa F, Iribarren JI, Estrany F, Aleman C. Marine paint fomulations: Conducting polymers as anticorrosive additives. Progress in Organic Coatings 2007;59:46.
[48] Entezami AA, Massoumi B. Artificial muscles, biosensors and drug delivery systems based on conducting polymers: A review. Iranian Polymer Journal (English Edition) 2006;15:13.
[49] Malhotra BD, Singhal R. Conducting polymer based biomolecular electronic devices. Pramana - Journal of Physics 2003;61:331.
[50] Lux F. Properties of electronically conductive polyaniline: a comparison between well-known literature data and some recent experimental findings. Polymer 1994;35:2915.
[51] Lvovich VF. A Perspective on Electrochemical Impedance Analysis of Polyaniline Films on Electrodes. The Electrochemical Society Interface 2009;Spring 2009:62.
[52] Baker RW. Membrane and Module Preparation. In: R.W.Baker, editor. Membrane Separation System:Recent Developments and Future Directions, vol. 2. New Jesry,U.S.A.: Noyes Data Coporation, 1991.
[53] Strathmann H. Ion exchange Membrane Separation Processes. Amsterdam: Elsevier B.V., 2004.
[54] Chang MJ, Liao YH, Myerson AS, Kwei TK. Gas transport properties of polyaniline membranes. Journal of Applied Polymer Science 1996;62:1427.
[55] Chang MJ, Myerson AS, Kwei TK. Gas transport in ring substituted polyanilines. Polymer Engineering and Science 1997;37:868.
[56] Jiping Y, Qiushi S, Xiaohuai H, Meixiang W. Gas separation properties of free-standing film of polyaniline. Chinese Journal of Polymer Science (English Edition) 1993;11:121.
[57] Anderson MR, Mattes BR, Reiss H, Kaner RB. Gas separation membranes. A novel application for conducting polymers. Synthetic Metals 1991;41:1151.
[58] Kang YS, Lee HJ, Namgoong J, Ko HC, Lee H, Jung B, Kim UY. Oxygen Transport Through Electronically Conductive Polyanilines. ACS Symposium Series 1998;710:383.
[59] Kang YS, Lee HJ, Namgoong J, Ko HC, Lee H, Jung B, Kim UY. Oxygen transport through electronically conductive polyanilines. ACS Symposium Series 1999;710:383.

[60] Conklin JA, Anderson MR, Reiss H, Kaner RB. Anhydrous halogen acid interaction with polyaniline membranes: A gas permeability study. Journal of physical chemistry 1996;100:8425.
[61] Rebattet L, Escoubes M, Genies E, Pineri M. Sorption and interactions of gases in polyaniline powders of different doping levels. Journal of Applied Polymer Science 1995;58:923.
[62] Wang HL, Mattes BR. Gas transport and sorption in polyaniline thin film. Synthetic Metals 1999;102:1333.
[63] Ball IJ, Huang S-C, Miller KJ, Wolf RA, Shimano JY, Kaner RB. Pervaporation of ethanol/water feeds with polyaniline membranes and blends. Synthetic Metals 1999;102:1311.
[64] Ball IJ, Huang S-C, Su TM, Kaner RB. Permselectivity and temperature-dependent permeability of polyaniline membranes. Synthetic Metals 1997;84:799.
[65] Ball IJ, Huang S-C, Wolf RA, Shimano JY, Kaner RB. Pervaporation studies with polyaniline membranes and blends. Journal of Membrane Science 2000;174:161.
[66] Kaner RB. Gas, liquid and enantiomeric separations using polyaniline. Synthetic Metals 2001;125:65.
[67] Loh XX, Sairam M, Bismarck A, Steinke JHG, Livingston AG, Li K. Crosslinked integrally skinned asymmetric polyaniline membranes for use in organic solvents. Journal of Membrane Science 2009;326:635.
[68] Sairam M, Loh XX, Li K, Bismarck A, Steinke JHG, Livingston AG. Nanoporous asymmetric polyaniline films for filtration of organic solvents. Journal of Membrane Science 2009;330:166.
[69] Deslouis C, El Moustafid T, Musiani MM, Orazem ME, Provost V, Tribollet B. Effect of cations on the diffusivity of the charge carriers in polyaniline membranes. Electrochimica Acta 1999;44:2087.
[70] Deslouis C, Musiani MM, Tribollet B. Ac impedance study of transport processes in polyaniline membranes. Journal of Physical Chemistry 1994;98:2936.
[71] Rossberg K, Dunsch L. Electrochemical impedance spectroscopy on conducting polymer membranes. Electrochimica Acta 1999;44:2061.
[72] Wen L, Kocherginsky NM. Doping-dependent ion selectivity of polyaniline membranes. Synthetic Metals 1999;106:19.
[73] Wen L, Kocherginsky NM. Coupled H+/anion transport through polyaniline membranes. Journal of Membrane Science 2000;167:135.
[74] Kocherginsky NM, Lei W, Wang Z. Redox reactions without direct contact of the reactants. Electron and ion coupled transport through polyaniline membrane. Journal of Physical Chemistry A 2005;109:4010.
[75] Kocherginsky NM, Wang Z. Transmembrane redox reactions through polyaniline membrane doped with fullerene C60. Synthetic Metals 2006;156:558.
[76] Kocherginsky NM, Wang Z. The role of ionic conductivity and interface in electrical resistance, ion transport and transmembrane redox reactions through polyaniline membranes. Synthetic Metals 2006;156:1065.
[77] Kocherginsky NM, Wang Z. Ion/electron coupled transport through polyaniline membrane: Fast transmembrane Redox reactions at neutral pH. Journal of Physical Chemistry B 2008;112:7016.
[78] Treptow F, Jungbauer A, Hellgardt K. Halide diffusion in polyaniline membranes. Journal of Membrane Science 2006;270:115.
[79] Yang Z, Coutinho DH, Sulfstede R, Balkus Jr KJ, Ferraris JP. Proton conductivity of acid-doped meta-polyaniline. Journal of Membrane Science 2008;313:86.

[80] Mirmohseni A, Price WE, Wallace GG, Zhao H. Adaptive membrane systems based on conductive electroactive polymers. Journal of Intelligent Material Systems and Structures 1993;4:43.
[81] Mirmohseni A, Saeedi A. Application of conducting polyaniline membranes (II) separation of H2SO4/H3PO4 and HNO3/H2SO4 using dialysis, electrodialysis and electrodynamic methods. Iranian Polymer Journal (English Edition) 1998;7:15.
[82] Lee MY, Nam YS, Ha YS. Pervaporation of water/isopropanol mixtures through polyaniline membranes doped with poly(acrylic acid). Journal of Membrane Science 1999;159:41.
[83] Naidu BVK, Sairam M, Raju KVSN, Aminabhavi TM. Pervaporation separation of water + isopropanol mixtures using novel nanocomposite membranes of poly(vinyl alcohol) and polyaniline. Journal of Membrane Science 2005;260:142.
[84] Fan Z, Wang Z, Duan M, Wang J, Wang S. Preparation and characterization of polyaniline/polysulfone nanocomposite ultrafiltration membrane. Journal of Membrane Science 2008;310:402.
[85] Chatzidaki EK, Favvas EP, Papageorgiou SK, Kanellopoulos NK, Theophilou NV. New polyimide-polyaniline hollow fibers: Synthesis, characterization and behavior in gas separation. European Polymer Journal 2007;43:5010.
[86] Su TM, Ball IJ, Conklin JA, Huang S-C, Larson RK, Nguyen SL, Lew BM, Kaner RB. Polyaniline/polyimide blends for pervaporation and gas separation studies. Synthetic Metals 1997;84:801.
[87] Valente AJM, Burrows HD, Polishchuk AY, Domingues CP, Borges OMF, Eusebio MES, Maria TMR, Lobo VMM, Monkman AP. Permeation of sodium dodecyl sulfate through polyaniline-modified cellulose acetate membranes. Polymer 2005;46:5918.
[88] Amado FDR, Gondran E, Ferreira JZ, Rodrigues MAS, Ferreira CA. Synthesis and characterisation of high impact polystyrene/polyaniline composite membranes for electrodialysis. Journal of Membrane Science 2004;234:139.
[89] Amado FDR, Rodrigues MAS, Morisso FDP, Bernardes AM, Ferreira JZ, Ferreira CA. High-impact polystyrene/polyaniline membranes for acid solution treatment by electrodialysis: Preparation, evaluation, and chemical calculation. Journal of Colloid and Interface Science 2008;320:52.
[90] Amado FDR, Rodrigues Jr LF, Forte MMC, Ferreira CA. Properties evaluation of the membranes synthesized with castor oil polyurethane and polyaniline. Polymer Engineering and Science 2006;46:1485.
[91] Amado FDR, Rodrigues Jr LF, Rodrigues MAS, Bernardes AM, Ferreira JZ, Ferreira CA. Development of polyurethane/polyaniline membranes for zinc recovery through electrodialysis. Desalination 2005;186:199.
[92] Amado FDR, Rodrigues MAS, Bernardes AM, Ferreira JZ, Ferreira CA. Membranes of polyurethane and polyaniline for recovery of wastewater of finishing metal industry. Madrid, Spain: Minerals, Metals and Materials Society, 2005. p.1833.
[93] Amado FDR, Rodrigues MAS, Bertuol DA, Bernardes AM, Ferreira JZ, Ferreira CA. The effect of production method on the properties of high impact polystyrene and polyaniline membranes. Journal of Membrane Science 2009;330:227.
[94] Cai Y-Q, Huang M-Y, Wang Y-X, Xu L. Sulfonated polyether ether ketone/polyaniline membranes for direct methanol fuel cells. Gaofenzi Cailiao Kexue Yu Gongcheng/Polymeric Materials Science and Engineering 2007;23:246.
[95] Li X, Chen D, Xu D, Zhao C, Wang Z, Lu H, Na H. SPEEKK/polyaniline (PANI) composite membranes for direct methanol fuel cell usages. Journal of Membrane Science 2006;275:134.

[96] Pei H, Hong L, Lee JY. Effects of polyaniline chain structures on proton conduction in a PEM host matrix. Journal of Membrane Science 2008;307:126.
[97] Deka M, Nath AK, Kumar A. Effect of undoped (insulating) polyaniline nanofibers on the ionic transport and interfacial stability of poly(vinylidene fluoride-hexafluoropropylene) based composite polymer electrolyte membranes. Journal of Membrane Science 2009;327:188.
[98] Orlov AV, Kiseleva SG, Karpacheva GP, Teplyakov VV, Syrtsova DA, Starannikova LE, Lebedeva TL. Structure and gas separation properties of composite films based on polyaniline. Journal of Applied Polymer Science 2003;89:1379.
[99] Stolarczyk A, Lapkowski M. Investigation of gas separation on polyaniline laminar composite membranes. Synthetic Metals 2001;121:1385.
[100] Gupta Y, Hellgardt K, Wakeman RJ. Enhanced permeability of polyaniline based nano-membranes for gas separation. Journal of Membrane Science 2006;282:60.
[101] Gupta Y, Wakeman R, Hellgardt K. High-productive, nanostructured polyaniline membranes for gas separation. Desalination 2006;199:474.
[102] Lee YM, Ha SY, Lee YK, Suh DH, Hong SY. Gas separation through conductive polymer membranes. 2. Polyaniline membranes with high oxygen selectivity. Industrial and Engineering Chemistry Research 1999;38:1917.
[103] Fan Z, Wang Z, Sun N, Wang J, Wang S. Performance improvement of polysulfone ultrafiltration membrane by blending with polyaniline nanofibers. Journal of Membrane Science 2008;320:363.
[104] Martin CR, Liang W, Menon V, Parthasarathy R, Parthasarathy A. Electronically conductive polymers as chemically-selective layers for membrane-based separations. Synthetic Metals 1993;57:3766.
[105] Huang S-C, Huang C-T, Lu S-Y, Chou K-S. Ceramic/polyaniline composite porous membranes. Journal of Porous Materials 1999;6:153.
[106] Piletsky S, Piletska E, Bossi A, Turner N, Turner A. Surface functionalization of porous polypropylene membranes with polyaniline for protein immobilization. Biotechnology and Bioengineering 2003;82:86.
[107] Sata T, Ishii Y, Kawamura K, Matsusaki K. Composite membranes prepared from cation-exchange membranes and polyaniline and their transport properties in electrodialysis. Journal of the Electrochemical Society 1999;146:585.
[108] Tan S, Viau V, Cugnod D, Belanger D. Chemical modification of a sulfonated membrane with a cationic polyaniline layer to improve its permselectivity. Electrochemical and Solid-State Letters 2002;5:55.
[109] Tan S, Belanger D. Characterization and transport properties of nafion/polyaniline composite membranes. Journal of Physical Chemistry B 2005;109:23480.
[110] Tan S, Laforgue A, Belanger D. Characterization of a cation-exchange/polyaniline composite membrane. Langmuir 2003;19:744.
[111] Compan V, Riande E, Fernandez-Carretero FJ, Berezina NP, Sytcheva AAR. Influence of polyaniline intercalations on the conductivity and permselectivity of perfluorinated cation-exchange membranes. Journal of Membrane Science 2008;318:255.
[112] Nagarale RK, Gohil GS, Shahi VK, Trivedi GS, Rangarajan R. Preparation and electrochemical characterization of cation- and anion exchange/polyaniline composite membranes. Journal of Colloid and Interface Science 2004;277:162.
[113] Berezina NP, Kononenko NA, Loza NV, Sycheva AAR. Electrochemical behavior of MF-4SK/polyaniline composites as investigated by membrane voltammetry. Russian Journal of Electrochemistry 2007;43:1340.

[114] Berezina NP, Kubaisi AA-R, Alpatova NM, Andreev VN, Griga EI. Composite Polyaniline/MF-4SK Membranes:A Chemical Template Synthesis and the Sorption and Conduction Properties. Russian Journal of Electrochemistry 2004;40:286.
[115] Berezina NP, Kubaisi AA-R. Peculiarities of Electrotransport Characteristics of Composite Membranes PANi/MF-4SK in Sulfuric Acid Solutions. Russian Journal of Electrochemistry 2006; 42, : 81.
[116] Berezina NP, Kubaisy AA, Timofeev SV, Karpenko LV. Template synthesis and electrotransport behavior of polymer composites based on perfluorinated membranes incorporating polyaniline. Journal of Solid State Electrochemistry 2007;11:378.
[117] Berezina NP, Kononenko NA, Sytcheva AAR, Loza NV, Shkirskaya SA, Hegman N, Pungor A. Perfluorinated nanocomposite membranes modified by polyaniline: Electrotransport phenomena and morphology. Electrochimica Acta 2009;54:2342.
[118] Nagarale RK, Gohil GS, Shahi VK. Sulfonated poly(ether ether ketone)/polyaniline composite proton-exchange membrane. Journal of Membrane Science 2006;280:389.
[119] Chen C-Y, Garnica-Rodriguez JI, Duke MC, Costa RFD, Dicks AL, da Costa JCD. Nafion/polyaniline/silica composite membranes for direct methanol fuel cell application. Journal of Power Sources 2007;166:324.
[120] Choi BG, Park H, Im HS, Kim YJ, Hong WH. Influence of oxidation state of polyaniline on physicochemical and transport properties of Nafion/polyaniline composite membrane for DMFC. Journal of Membrane Science 2008;324:102.
[121] Wang CH, Chen CC, Hsu HC, Du HY, Chen CP, Hwang JY, Chen LC, Shih HC, Stejskal J, Chen KH. Low methanol-permeable polyaniline/Nafion composite membrane for direct methanol fuel cells. Journal of Power Sources 2009;190:279.
[122] Yang J, Shen PK, Varcoe J, Wei Z. Nafion/polyaniline composite membranes specifically designed to allow proton exchange membrane fuel cells operation at low humidity. Journal of Power Sources 2009;189:1016.
[123] Sahin M, Gorcay H, Kir E, Sahin Y. Removal of calcium and magnesium using polyaniline and derivatives modified PVDF cation-exchange membranes by Donnan dialysis. Reactive and Functional Polymers 2009;69:673.
[124] Rodriguez F, Castillo-Ortega MM, Encinas JC, Grijalva H, Brown F, Sanchez-Corrales VM, Castano VM. Preparation, characterization, and adsorption properties of cellulose acetate-polyaniline membranes. Journal of Applied Polymer Science 2009;111:1216.
[125] Rodriguez F, Castillo-Ortega MM, Encinas JC, Sanchez-Corrales VM, Perez-Tello M, Munive GT. Adsorption of a gold-iodide complex (AuI2-) onto cellulose acetate-polyaniline membranes: Equilibrium experiments. Journal of Applied Polymer Science 2009;113:2670.
[126] Blinova NV, Stejskal J, Trchova M, Ciric-Marjanovic G, Sapurina I. Polymerization of aniline on polyaniline membranes. Journal of Physical Chemistry B 2007;111:2440.
[127] Sivaraman P, Chavan JG, Thakur AP, Hande VR, Samui AB. Electrochemical modification of cation-exchange membrane with polyaniline for improvement in permselectivity. Electrochimica Acta 2007;52:5046.
[128] Rojas AM, Maldonado YO, Rodriguez LMT. An easy method to modify the exchange membranes of electrodialysis with electrosynthetized polyaniline. Journal of Membrane Science 2007;300:2.
[129] Shimizu T, Naruhashi T, Momma T, Osaka T. Preparation and methanol permeability of polyaniline/Nafion composite membrane. Electrochemistry 2002;70:991.
[130] Sherman Hsu CP. Infrared Spectroscopy. In: Settle FA, editor. Handbook of Intrumental Techniques for Analytical Chemistry. NJ: Prentice-Hall, Inc., 1997.
[131] Watts JF, Wolstenholme J. An Introduction to Surface Analysis by XPS and AES. Chichester: John Wiley & Sons Ltd., 2003.

[132] Bard AJ, Faulkner LR. Electrochemical Methods : Fundamentals and Applications. New York: John Wiley & Sons, Inc., 2001.
[133] Gospodinova N, Terlemezyan L. Conducting polymers prepared by oxidative polymerization: polyaniline. Progress in Polymer Science (Oxford) 1998;23:1443.
[134] Cao Y, Andreatta A, Heeger AJ, Smith P. Influence of chemical polymerization conditions on the properties of polyaniline. Polymer 1989;30:2305.
[135] Tzou K, Gregory RV. Kinetic study of the chemical polymerization of aniline in aqueous solutions. Synthetic Metals 1992;47:267.
[136] Job AE, Herrmann Jr PSP, Vaz DO, Mattoso LHC. Comparison between different conditions of the chemical polymerization of polyaniline on top of PET films. Journal of Applied Polymer Science 2001;79:1220.
[137] Pud AA, Rogalsky SP, Shapoval GS, Korzhenko AA. Polyaniline/poly(ethylene terephthalate) composite. 1. Peculiarities of the matrix aniline redox polymerization. Synthetic Metals 1999;99:175.
[138] Tan S, Tieu JH, Belanger D. Chemical polymerization of aniline on a poly(styrene sulfonic acid) membrane: Controlling the polymerization site using different oxidants. Journal of Physical Chemistry B 2005;109:14085.
[139] Jutier J-J, Harrison Y, Premont S, Prud'homme RE. Nonisothermal Fourier Transform Infrared Degradation Study of Nitrocellulose derived from Wood and Cotton. Journal of Applied Polymer Science 1987;33:1359.
[140] Han MG, Im SS. X-ray photoelectron spectroscopy study of electrically conducting polyaniline/polyimide blends. Polymer 2000;41:3253.
[141] Trchova M, edenkova I, Stejskal J. In-situ polymerized polyaniline films 6. FTIR spectroscopic study of aniline polymerisation. vol. 154: Elsevier Ltd, 2005. p.1.
[142] Lee S-J, Altaner C, Puls Jr, Saake B. Determination of the substituent distribution along cellulose acetate chains as revealed by enzymatic and chemical methods. Carbohydrate Polymers 2003;54:353.
[143] Kang ET, Li ZF, Neoh KG, Dong YQ, Tan KL. Protonation and deprotonation of polyaniline films and powders: Effects of acid and base concentrations on the surface intrinsic oxidation states. Synthetic Metals 1998;92:167.
[144] Kang ET, Neoh KG, Huang SW, Lim SL, Tan KL. Surface-functionalized polyaniline films. Journal of Physical Chemistry B 1997;101:10744.
[145] Kang ET, Neoh KG, Tan KL. Polyaniline with high intrinsic oxidation state. Surface and Interface Analysis 1993;20:833.
[146] Kumar SN, Gaillard F, Bouyssoux G, Sartre A. High-resolution XPS studies of electrochemically synthesized conducting polyaniline films. Synthetic Metals 1990;36:111.
[147] Neoh KG, Kang ET, Tan KL. Limitations of the x-ray photoelectron spectroscopy technique in the study of electroactive polymers. Journal of Physical Chemistry B 1997;101:726.
[148] Rodrigues PC, Lisboa-Filho PN, Mangrich AS, Akcelrud L. Polyaniline/polyurethane networks. II. A spectroscopic study. Polymer 2005;46:2285.
[149] Suzer S, Birer O, Sevil UA, Guven O. XPS Investigations on Conducting Polymers. Turkish Journal of Chemistry 1998 22 59.
[150] Loh FC, Tan KL, Kang ET, Kato K, Uyama Y, Ikada Y. XPS characterization of surface functionalized electroactive polymers. Surface and Interface Analysis 1996;24:597.
[151] Yue J, Epstein AJ. XPS study of self-doped conducting polyaniline and parent systems. Macromolecules 1991;24:4441.
[152] Wei XL, Fahlman M, Epstein AJ. XPS study of highly sulfonated polyaniline. Macromolecules 1999;32:3114.

[153] Beamson G, Briggs D. High Resolution XPS of Polymers: The Scienta ESCA300 Database. Chichester: John Wiley & Sons 1992.
[154] Beverly S, Seal S, Hong S. Identification of surface chemical functional groups correlated to failure of reverse osmosis polymeric membranes. Journal of Vacuum Science and Technology A: Vacuum, Surfaces and Films 2000;18:1107.
[155] Fowler AHK, Munro HS, Clark DT. ESCA Studies of the Thermal and X-ray induced Degradation of Cellulose Nitrates. Polymer Degradation and Stability 1985;11:287.
[156] Ng FMF, Yu KN. X-ray irradiation induced degradation of cellulose nitrate. Materials Chemistry and Physics 2006;100:38.
[157] Golczak S, Kanciurzewska A, Fahlman M, Langer K, Langer JJ. Comparative XPS surface study of polyaniline thin films. Solid State Ionics 2008;179:2234.
[158] Kang ET, Neoh KG, Khor SH, Tan KL, Tan BTG. Structural Determination of Polyaniline by X-Ray Photoelectron Spectroscopy. Journal of Chemical Sciety,Chemical Communication 1989.
[159] Tan KL, Kang ET, Neoh KG. X-ray photoelectron spectroscopic studies of charge transfer interactions in electroactive polyaniline. Polymers for Advanced Technologies 1994;5:171.
[160] Chen W-C, Wen T-C, Gopalan A. The inductive behavior derived from hydrolysis of polyaniline. Electrochimica Acta 2002;47:4195.
[161] Gall JF, Church GL, Brown RL. Solubility of ammonium persulfate in water and in solutions of sulfuric acid and ammonium sulfate. Journal of Physical Chemistry 1943;47:645.
[162] Kim J-Y, Lee J-H, Kwon S-J. The manufacture and properties of polyaniline nano-films prepared through vapor-phase polymerization. Synthetic Metals 2007;157:336.
[163] Huang M-R, Li X-G, Duan W. Effect of polymerization conditions on o-phenylenediamine and o-phenetidine oxidative copolymers. Polymer International 2005;54:70.
[164] Iyoda T, Ohtani A, Honda K, Shimidzu T. Diaphragmatic chemical polymerization of pyrrole in the Nafion film. Macromolecules 1990;23:1971.
[165] Tanaka Y. Ion exchange Membranes:Fundamentals and Application. Amsterdam: Elsevier B.V., 2007.
[166] Sata T. Ion Exchange Membranes:Preparation,Characterization,Modification and application. Tyne and Wear,UK: The Royal Society of Chemistry, 2004.
[167] Park J-S, Choi J-H, Woo J-J, Moon S-H. An electrical impedance spectroscopic (EIS) study on transport characteristics of ion exchange membrane systems. Journal of Colloid and Interface Science 2006;300:655.
[168] Park J-S, Choi J-H, Yeon K-H, Moon S-H. An approach to fouling characterization of an ion exchange membrane using current-voltage relation and electrical impedance spectroscopy. Journal of Colloid and Interface Science 2006;294:129.
[169] Inzelt G. Conducting Polymers:A New Era in Electrochemistry. Springer-Verlag Berlin Heidelberg 2008.
[170] Rubinstein I, Sabatani E, Rishpon J. Electrochemical Impedance Analysis of Polyaniline Films on Electrodes. Journal of the Electrochemical Society 1987;134:3078.
[171] Penner RM, Van Dyke LS, Martin CR. Electrochemical evaluation of charge-transport rates in electronically conductive polymers. Solid State Ionics 1989;32-33:553.
[172] Penner RM, Martin CR. Electrochemical investigations of electronically conductive polymers. 2. Evaluation of charge-transport rates in polypyrrole using an alternating current impedance method. Journal of physical chemistry 1989;93:984.
[173] Bull RA, Fan FRF, Bard AJ. Polymer Films Electrodes-7. Electrochemical behaviour at Polypyrrole-coated Platinum and Tantalum Electrodes. Journal of the Electrochemical Society 1982;129:1009.

[174] Albery WJ, Elliott CM, Mount AR. Transmission line model for modified electrodes and thin layer cells. Journal of electroanalytical chemistry and interfacial electrochemistry 1990;288:15.
[175] Deslouis C, Musiani MM, Tribollet B, Vorotyntsev MA. Comparison of the AC impedance of conducting polymer films studied as electrode-supported and freestanding membranes. Journal of the Electrochemical Society 1995;142:1902.
[176] Ehrenbeck C, Juettner K, Ludwig S, Paasch G. Electrochemical impedance of a free-standing polypyrrole membrane. Electrochimica Acta 1998;43:2781.
[177] García-Jareño JJ, Giménez-Romero D, Vicente F, Gabrielli C, Keddam M, Perrot H. EIS and Ac-electrogravimetry study of PB films in KCl, NaCl, and CsCl aqueous solutions. Journal of Physical Chemistry B 2003;107:11321.
[178] Buck RP. Diffusion-Migration Modelling for Finite, One-dimensional Transport in Thin-layer and Membrane Cells.Part II. Mixed Conduction cases:(III)/OS(II)CLO4 Polymers including steady-state I-V responses. Journal of Electroanalytical Chemistry 1987;219:23.
[179] Vorotyntsev MA, L.I. Daikhin LI, Levi MD. Modelling the impedance properties of electrodes coated with electroactive polymer films. Journal of Electroanalytical Chemistry 1994;364:37.
[180] Benyaich A, Deslouis C, El Moustafid T, Musiani MM, Tribollet B. Electrochemical properties of PANI films for different counter-ions in acidic pH analyzed by impedance techniques. Electrochimica Acta 1996;41:1781.
[181] Vorotyntsev MA, Badiali J-P, Inzelt G. Electrochemical impedance spectroscopy of thin films with two mobile charge carriers: effects of the interfacial charging. Journal of Electroanalytical Chemistry 1999;472:7.
[182] Albery WJ, Mount AR. Dual transmission line with charge-transfer resistance for conducting polymers. Journal of the Chemical Society, Faraday Transactions 1994;90:1115.
[183] Albery WJ, Mount AR. Second transmission line model for conducting polymers. Journal of electroanalytical chemistry and interfacial electrochemistry 1991;305:3.
[184] Ren X, Pickup PG. Impedance spectroscopy of polypyrrole/poly(styrenesulphonate) composites. Simultaneous anion and cation transport. Electrochimica Acta 1996;41:1877.
[185] Li G, Pickup PG. Ion Transport in a Chemically Prepared Polypyrrole/Poly(styrene-4-sulfonate) Composite. Journal of Physical Chemistry B 1999;103:10143.
[186] Paasch G, Micka K, Gersdorf P. Theory of the electrochemical impedance of macrohomogeneous porous electrodes. Electrochimica Acta 1993;38:2653.
[187] Rossberg K, Paasch G, Dunsch L, Ludwig S. Influence of porosity and the nature of the charge storage capacitance on the impedance behaviour of electropolymerized polyaniline films. Journal of Electroanalytical Chemistry 1998;443:49.
[188] Ehrenbeck C, Juttner K. Development of an anion/cation permeable free-standing membrane based on electrochemical switching of polypyrrole. Electrochimica Acta 1996;41:511.
[189] Ehrenbeck C, Juettner K. Ion conductivity and permselectivity measurements of polypyrrole membranes at variable states of oxidation. Electrochimica Acta 1996;41:1815.
[190] Ghenaatian HR, Mousavi MF, Kazemi SH, Shamsipur M. Electrochemical investigations of self-doped polyaniline nanofibers as a new electroactive material for high performance redox supercapacitor. Synthetic Metals 2009;159:1717.
[191] Soboleva T, Xie Z, Shi Z, Tsang E, Navessin T, Holdcroft S. Investigation of the through-plane impedance technique for evaluation of anisotropy of proton conducting polymer membranes. Journal of Electroanalytical Chemistry 2008;622:145.
[192] Johnson BW, Read DC, Christensen P, Hamnett A, Armstrong RD. Impedance characteristics of conducting polythiophene films. Journal of Electroanalytical Chemistry 1994;364:103.

[193] Deslouis C, Musiani MM, Tribollet B. Free-Standing Membranes for the Study of Electrochemical Reactions Occurring at Conducting Polymer/Electrolyte Interfaces. Journal of Physical Chemistry 1996;100:8994.
[194] Xu W, Siow KS, Gao Z, Lee SY. Ionic Conductivity and Electrochemical Characterization of Novel Microporous Composite Polymer Electrolytes. Journal of the Electrochemical Society 1999;146:4410.
[195] Subramania A, Kalyana Sundaram NT, Sathiya Priya AR, Vijaya Kumar G. Preparation of a novel composite micro-porous polymer electrolyte membrane for high performance Li-ion battery. Journal of Membrane Science 2007;294:8.
[196] Rubinson JF, Kayinamura YP. Charge transport in conducting polymers: insights from impedance spectroscopy. Chemical Society Reviews 2009;38:3339.
[197] MacDonald JR. Impedance Spectroscopy. Annals of Biomedical Engineering 1992;20.
[198] Grzeszczukz M, Poks P. The Double Layer and Redox Capacitances of Polyaniline Electrodes in Aqueous Trichloroacetic Acid. Journal of The Electrochemical Society 1999;146:642.
[199] Hu C-C, Chu C-H. Electrochemical impedance characterization of polyaniline-coated graphite electrodes for electrochemical capacitors — effects of film coverage:thickness and anions. Journal of Electroanalytical Chemistry 2001;503:105.
[200] Memet JB, Girault P, Sabot R, Compere C, Deslouis C. Electrochemical impedance spectroscopy of a free-standing oxide film. Electrochimica Acta 2002;47:1043.
[201] Komura T, Goisihara S, Yamaguti T, Takahasi K. Electron and ion transport in polypyrrole:polystyrenesulfonate composite films. Journal of Electroanalytical Chemistry 1998;456:121.
[202] das Neves S, De Paoli MA. Photoelectrochemistry of polyaniline supported in a microporous cellulose acetate membrane. Synthetic Metals 1998;96:49.
[203] Ariza MJ, Otero TF. Nitrate and chloride transport through a smart membrane. Journal of Membrane Science 2007;290:241.
[204] Bleha M, Kudela V, Rosova EY, Polotskaay GA, Kozlov AG, Elyashevich GK. Synthesis and characterization of thin polypyrrole layers on polyethylene microporous films. European Polymer Journal 1999;35:613.
[205] Hijnen HJM, Smit JAM. An analysis of partially film-controlled membrane potentials of weak cation-exchange membranes using the space–charge model. Journal of Membrane Science 2000;168:259.
[206] Thomas KC, Ramachandhran V, Misra BM. Electrochemical and Electrokinetic Characterization of Cellulose Acetate Polymeric Membranes. Journal of Applied Polymer Science 1987;34:2527.
[207] Ritchie SMC, Bachas LG, Olin T, Sikdar SK, Bhattacharyya D. Surface Modification of Silica- and Cellulose-Based Microfiltration Membranes with Functional Polyamino Acids for Heavy Metal Sorption. Langmuir 15:6346.
[208] Clark DT, Stephenson PJ. E.s.c.a. studies of the nitration and denitration of cellulosic materials. Polymer 1982;23:1034.

Appendix A

Degradation of Cellulose ester Membranes under X-ray Irradiation and Effects of HCl Treatment on the Structure

C 1s and N 1s spectra of mixed cellulose ester (ME) membranes are deconvoluted according to the structure of the membranes (Figure A1).

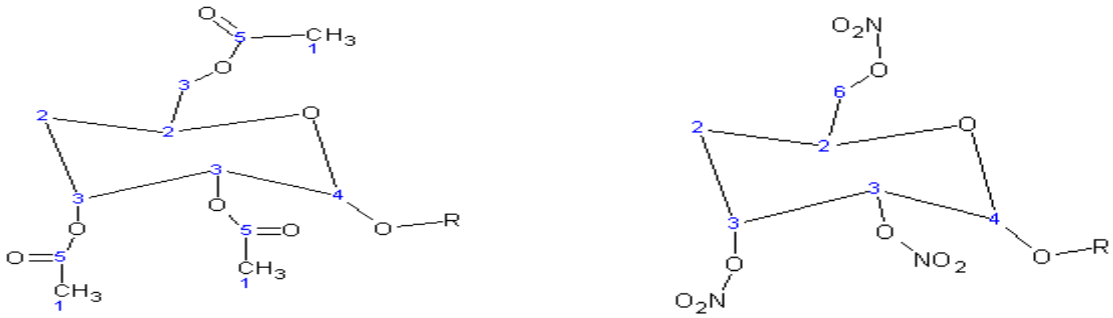

(a) (b)

Figure A1. (a) Cellulose acetate and (b) cellulose nitrate structures.

The C 1s composite peak of the bare membrane was resolved into five sub-peaks (Figure A2.a), namely, 285.4 eV (C1, Figure A1.a), 286.7 eV (C2, Figure A1.b), 287.7 eV (C3, Figure A1.b), 288.9eV(C4, Figure A1.a and b) and 290.4 (C5, Figure A1.a). The N 1s spectrum was resolved into ~ 401 eV (organic nitrogen, see the subsequent discussion), 405.7 eV (NO_2) and ≥ 408 eV (ONO_2) (Figure A2.a) [208]. High BE peaks in N 1s spectra indicate the presence of radical species which might result from x-ray induced degradation effects, Fowler and Munro [155]. The appearance of an organic peak at ~ 401 eV may be interpreted in the light of well known degradation phenomena of cellulose nitrate under x-rays irradiation [160, 208]. It was proposed that under the action of x-rays, the nitrate ester groups might be transformed into an oxime (C=NOH) functionality via a free radical initiated process [155]. To investigate this transformation, ME membrane which had been scanned once under XPS, was scanned a second time for survey and core level spectra. The deconvoluted spectra are shown in Figure A2.b. The C 1s composite peak shows a more pronounced low BE peak and broadening at higher BE as compared to the single scanned C 1s peak (Figure A2.a). The component peak at 286.7 eV arises probably due to C-N bonds in addition to the (O-)C-C bonds in the ME compound and becomes more pronounced in the case of the second XPS

scan (Table A1). The decrease in the C-ONO_2 peak shows loss of nitrate functionality whereas an increase in C=O groups (appearance of additional 289.8 eV peak) suggests cellulose ring scission and formation of an oxime functionality [155]. The N 1s shows more pronounced organic nitrogen peaks around 401-404 eV as compared to N 1s of single scanned membrane. The quantification results are shown in Table A1 with the relevant peak assignments.

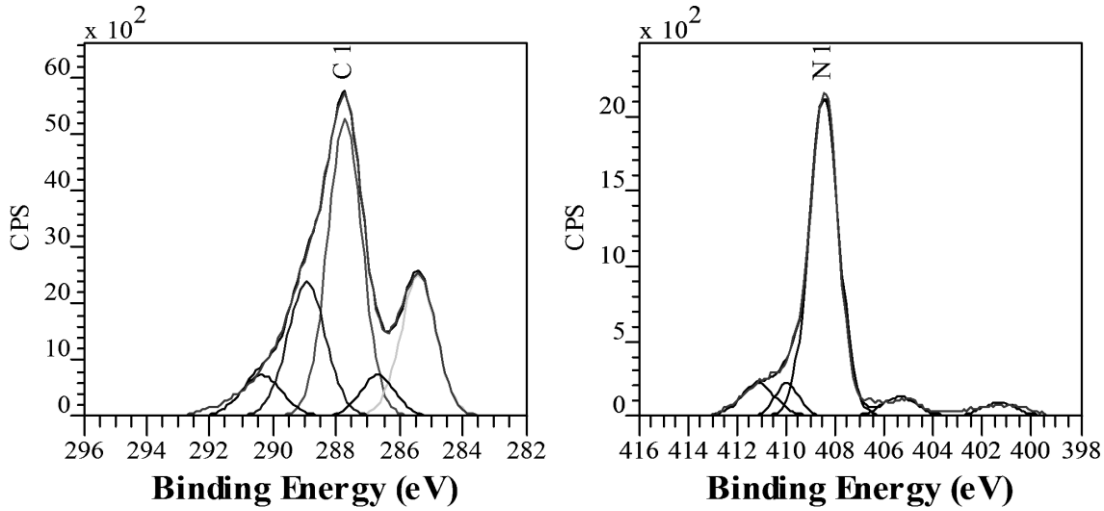

(a)

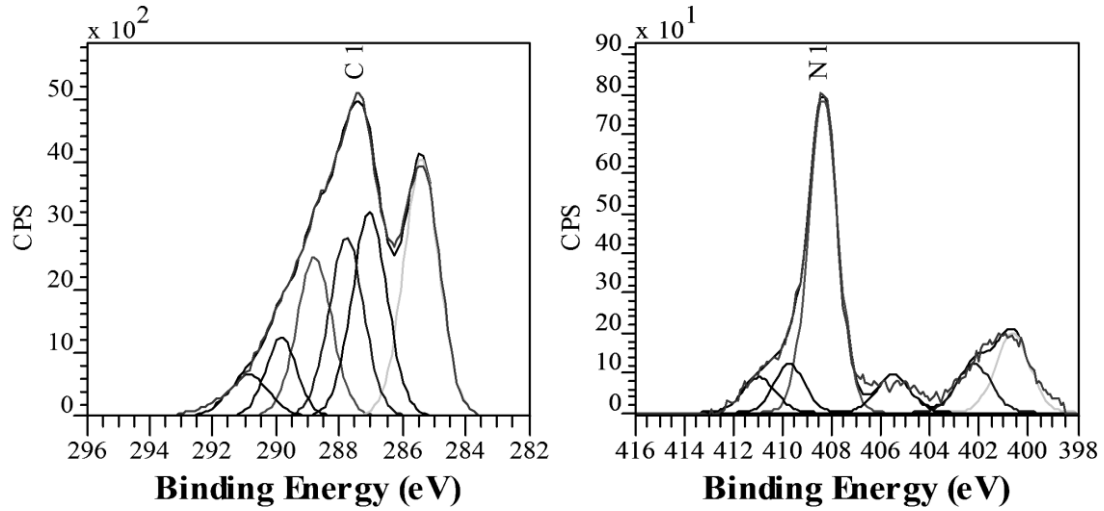

(b)

Figure A2: *C 1s and N 1s spectra of ME membranes (a) first scan and (b) second scan.*

Table A1. Quantification results of C 1s and N 1s of unmodified ME membrane (At.%)

Membrane Identity	C 1s							N 1s	
	285.4 C-H	286.7 O-C-C / C-N	287.7 C-O-NO_2	288.8 O-C-O	289.8 C=O	290.4 O-C=O	401.3 Organic N	405.7 NO_2	>408 (ONO_2)
ME, 1st scan	21	6	44	22	-	7	4	5	91
ME, 2nd scan	28	23	19	17	8	5	25	7	68

In the present study, because aniline polymerization has been conducted in HCl solution, it was important to determine the effects of acid treatment on bare ME membrane. The core level XPS spectra of ME membrane treated with 0.3 M HCl for 6 hours and their deconvolution are shown in Figure A3. The C 1s and N 1s spectra appear quite similar to those of untreated ME membrane (Figure 2A.a) except for the high BE broadening in the both spectra. This may be considered as an unavoidable feature of acid treatment of cellulose esters that results from the increased charging content of the ring. Various phenomena such as ester hydrolysis and residual entrapment of acid in the bulk (swelling) and pores of ME membrane may be taking place in this case without damaging membrane structure significantly.

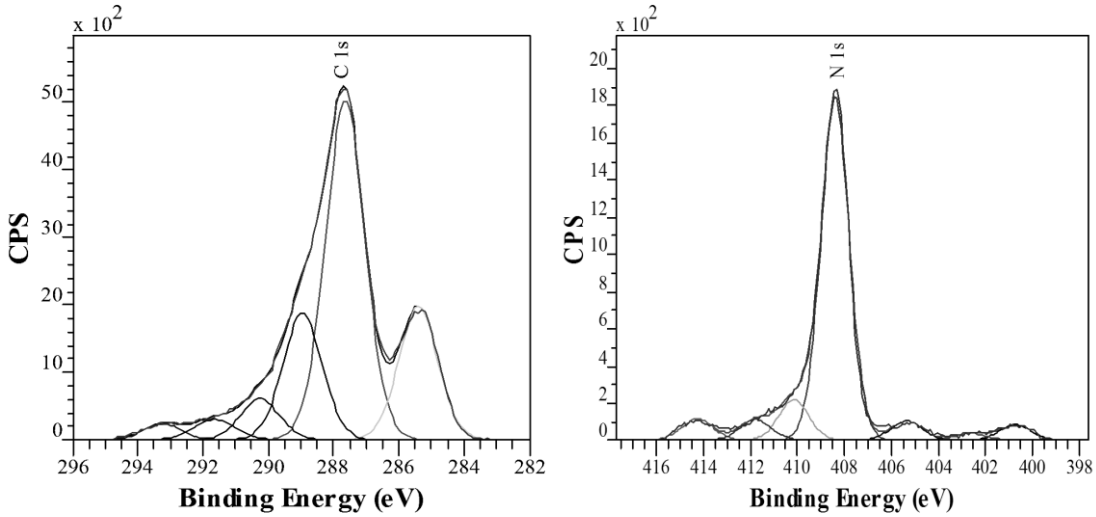

Figure A3. *C 1s and N 1s spectra of HCl treated ME membrane.*

Appendix B

Electrochemical Impedance Spectroscopy Spectra of PANI Composite Membranes bathed with $CaCl_2$ in the Two-compartment Cell

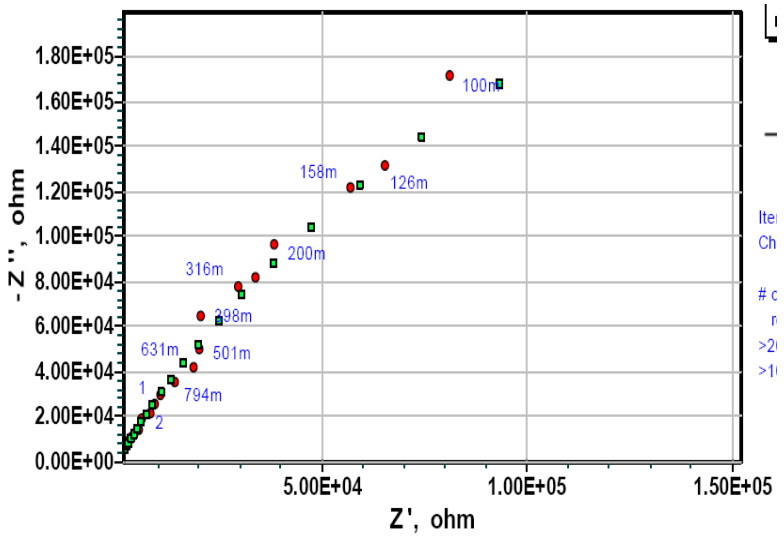

(ME uncoated)

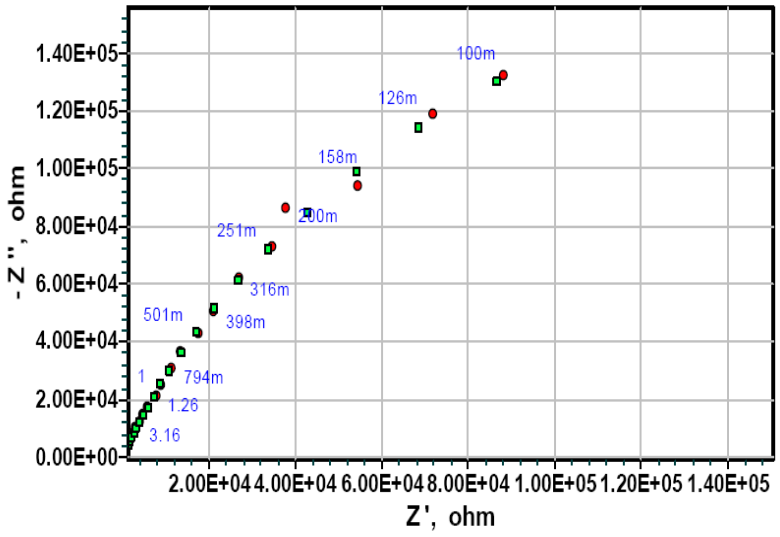

(ME,P1,2h)

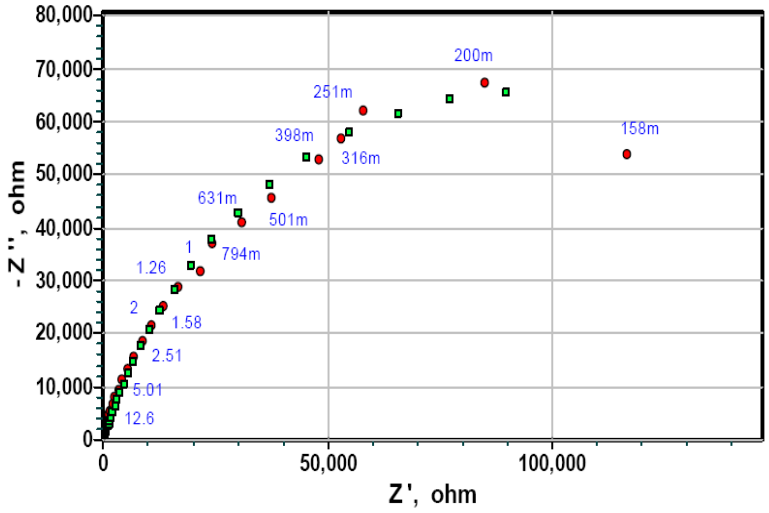

(ME,P1,6h)

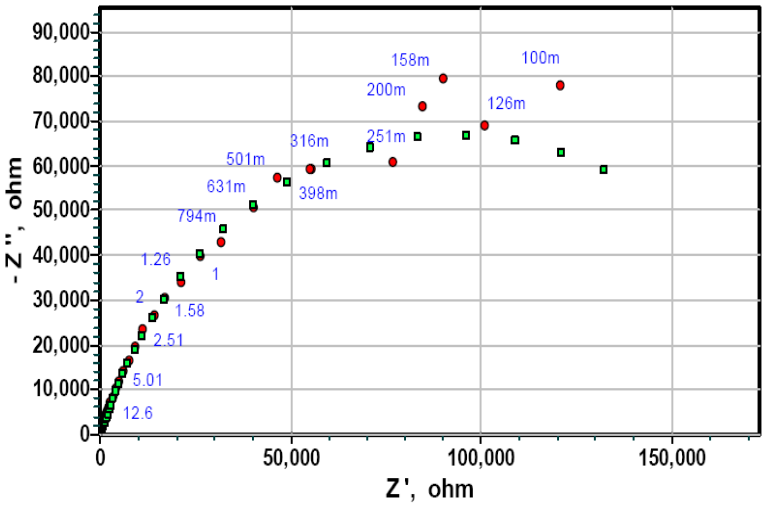

(ME,P1,22h)

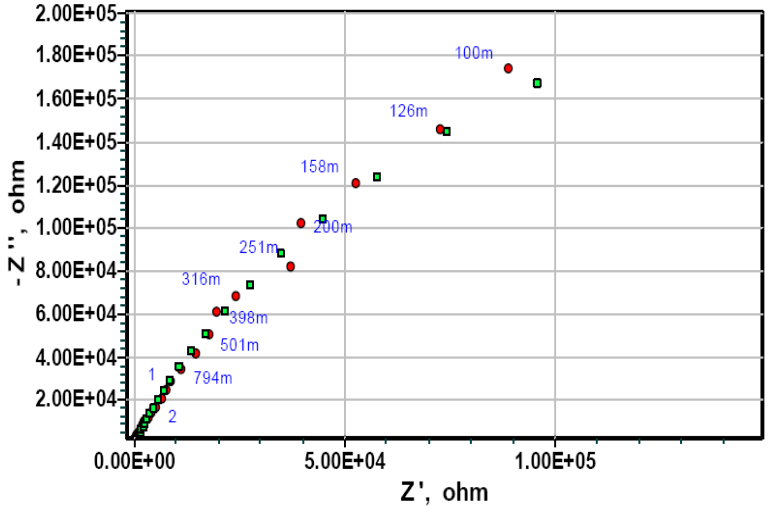

(ME,Poly,6h)

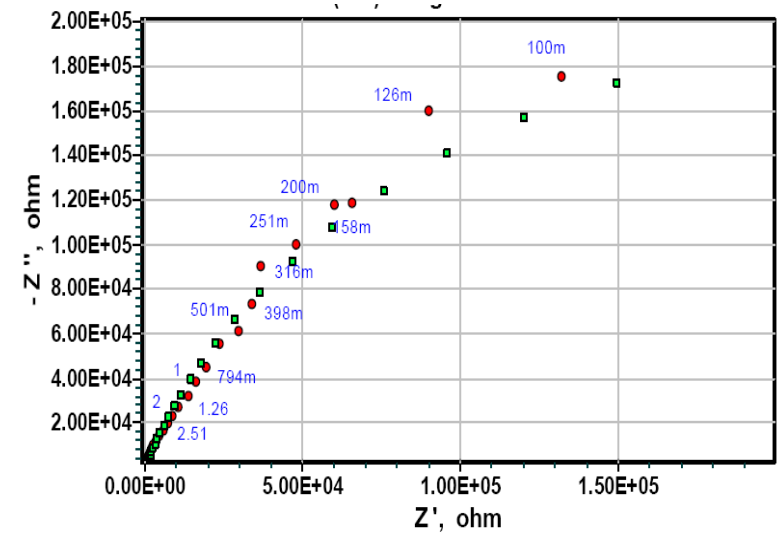

(ME,Poly,22h)

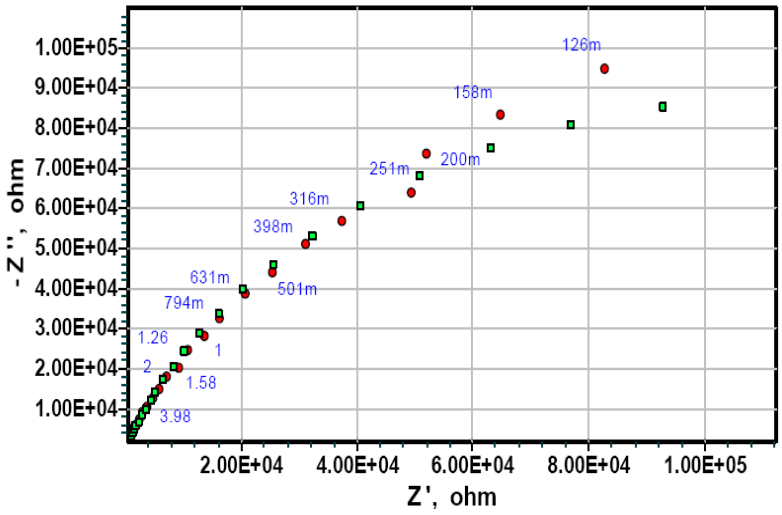

(ME,VAP,APS)

List of Publications

- **Qaiser, A. A**., Hyland, M. M. and D. A. Patterson, Polyaniline deposition site control on microporous mixed cellulose ester membranes: Surface and in-pore polymerization, *IOP Conf. Series: Materials Science and Engineering*, 4,012009, 2009

- **Qaiser, A. A**., Hyland, M. M. and D. A. Patterson, Control of polyaniline deposition on microporous cellulose ester membranes by in situ chemical polymerization, *J. Phys. Chem. B, 113,* 14986, 2009

- **Qaiser, A.A.** and M. M. Hyland, XPS Characterization of Polyaniline Composite Membranes, 2010, Materials Science Forum, 657, 35, 2010

- **Qaiser, A. A**., Hyland, M. M. and D.A. Patterson, Surface and Charge Transport Characterization of Polyaniline-Cellulose acetate Composite Membranes, *J. Phys. Chem. B*, (In Press)